Strathclyde Institute of Pharmacy and Biomedical Sciences

Development of tumour-targeted delivery systems entrapping plumbagin for cancer therapy

By

Intouch Sakpakdeejaroen

A thesis presented in fulfilment of the requirements for the degree of

Doctor of Philosophy

2019

Acknowledgements

First and foremost, I would like to express my deepest gratitude to my supervisor Dr Christine Dufès for her invaluable instruction, intellectual guidance, excellent suggestions and kindness, together with constant encouragement throughout my PhD study which are more than I can describe here.

I also would like to express my sincere appreciation to the Thammasat University for a scholarship and funding this project. My special thanks are extended to all the member in the Faculty of Medicine, Thammasat University and the Office of Educational Affairs, the Royal Thai Embassy in London, for their help and continuous support.

Without a great cooperation from several individuals, this thesis study could not have been completed. I would like to thank Mrs Margaret Mullin from University of Glasgow for her help with TEM. Many thanks to Mr Craig Irving for his help with NMR. Special thanks to my colleagues, Dr Sukrut Somani and Dr Partha Laskar for their kind advice and enormous help throughout my years of study, not to mention all my colleagues in Lab 224: Najla, Joan, Jitkasem and Jamal. My appreciation also goes to my friends in SIPBS, Kanidta and Thidarat, for their kindness and friendship.

Finally, this thesis is dedicated to my family. To my parents, I would not be where I am today without your unconditional love. Special thanks to my wife Itsaree for your patience, understanding and always supporting me no matter what decisions I make. To my precious daughter Venita, thank you for being such a wonderful girl, you've brought lights and colours into my life.

Contents

Table of contents

List of figures

List of tables

List of abbreviations

Akt	Protein kinase B
AMPK	Adenosine monophosphate-activated protein kinase
ATP	Adenosine triphosphate
BLI	Bioluminescence imaging
Blank LIP	Blank liposomes
Blank LPN	Blank lipid-polymer hybrid nanoparticles
Blank PN	Blank polymeric nanoparticles
BSA	Bovine serum albumin
C_{max}	Maximum serum concentration
CMC	Critical micelle concentration
Control LIP	Control liposomes
Control LPN	Control lipid-polymer hybrid nanoparticles
Control PN	Control polymeric nanoparticles
COX	Cyclooxygenase
CYP	Cytochrome P450
DMEM	Dulbecco's modified Eagle's medium
DMSO	Dimethyl sulfoxide
DNA	Deoxyribonucleic acid
ECM	Extracellular matrix
EGCG	Epigallocatechin gallate
EGF	Epidermal growth factor
EGFR	Epidermal growth factor receptor
EMA	European Medicines Agency

EPR	Enhanced permeability and retention
ERK	Extracellular signal-regulated kinases
FACS	Fluorescence-activated cell sorting
FBS	Foetal bovine serum
FDA	Food and Drug Administration
FOXM1	Forkhead box protein M1
GSH	Reduced glutathione
IC$_{50}$	Growth inhibitory concentration
IFN	Interferon
IFP	Interstitial fluid pressure
IKK	IκB kinase complex
IL	Interleukin
iNOS	Inducible nitric oxide synthase
IV	Intravenous injection
IκB	Inhibitor of NF-κB
JNK	c-Jun N-terminal kinase
LD$_{50}$	Lethal dose
LIP	Liposomes
LPN	Lipid-polymer hybrid nanoparticles
LUV	Large unilamellar vesicles
MAPK	Mitogen-activated protein kinase
MBC	Minimum bactericidal concentration
MDR	Multidrug resistance
MEK	Mitogen-activated protein kinase kinase
MFI	Mean fluorescence intensity

MIC	Minimum inhibitory concentration
MLV	Multilamellar vesicles
MMP	Matrix metalloproteinase
MPS	Mononuclear phagocyte system
mTOR	Mammalian target of rapamycin
MWCO	Molecular weight cut-off
NADPH	Nicotinamide adenine dinucleotide phosphate
NF-κB	Nuclear factor-kappa B
NMR	Nuclear magnetic resonance
PBG	Plumbagin
PBS	Phosphate buffer saline
PEG	Polyethylene glycol
P-gp	P-glycoprotein
PI3K	Phosphatidylinositol-3-kinase
PLA	Poly(lactic acid)
PLGA	Poly(lactic-co-glycolic acid)
PN	Polymeric nanoparticles (PLGA-PEG nanoparticles)
PTEN	Tensin homolog
RES	Reticuloendothelial system
ROS	Reactive oxygen species
RPMI-1640	Roswell Park Memorial Institute medium
SEM	Standard error of the mean
SLN	Solid lipid nanoparticles
Span 60	Sorbitan monostearate
STAT3	Signal transducer and activator of transcription 3

SUV	Small unilamellar vesicles
$t_{1/2}$	Elimination half-life
TEM	Transmission electron microscopy
Tf	Transferrin
Tf-LIP	Tf-bearing liposomes
Tf-LPN	Tf-bearing lipid-polymer hybrid nanoparticles
Tf-PN	Tf-bearing polymeric nanoparticles
TfR	Transferrin receptor
T_{max}	Time to reach the maximum serum concentration
TME	Tumour microenvironment
TNF-α	Tumour necrosis factor alpha
TPGS	d-α-Tocopheryl polyethylene glycol 1000 succinate
TRF	Tocotrienol-rich fraction
Tween 80	Sorbitan monooleate
VEGF	Vascular endothelial growth factor
VEGFR	Vascular endothelial growth factor receptor

Abstract

Plumbagin, a naphthoquinone mainly extracted from Plumbaginaceae plants, has been shown to have promising anti-cancer properties. However, its therapeutic potential is hampered by its failure to specifically reach tumours at a therapeutic concentration after intravenous administration, without secondary effects on normal tissues. Its use is further limited by its poor aqueous solubility and its rapid elimination *in vivo*. To overcome this limitation, we hypothesised that the entrapment of plumbagin within a delivery system conjugated to transferrin, whose receptors are overexpressed on many cancer cells, would result in a selective delivery to tumours after intravenous administration and a subsequently enhanced therapeutic efficacy. The aim of this study was to prepare and characterise transferrin-targeted delivery systems entrapping plumbagin.

In this work, we demonstrated that plumbagin could be formulated in transferrin-bearing liposomes, PLGA-PEG nanoparticles and lipid-polymer hybrid nanoparticles. The entrapment of plumbagin in these tumour-targeted nanomedicines led to an increase in plumbagin uptake by cancer cells, and improved its anti-proliferative and apoptosis activity in B16-F10, A431 and T98G cell lines compared to that observed with the drug solution. The intravenous injection of transferrin-bearing lipid-polymer hybrid nanoparticles entrapping plumbagin led to the complete tumour suppression for 40% of B16-F10 tumours. In addition, the intravenous treatment of B16-F10 tumours with transferrin-bearing liposomes and polymeric nanoparticles led to 10% tumour suppression. By contrast, all the tumours treated with plumbagin solution or left untreated were progressive. The animals did not show any visible signs of toxicity.

In conclusion, plumbagin entrapped in these transferrin-bearing nanomedicines are therefore highly promising therapeutic systems that should be further optimised as therapeutic tools for cancer treatment.

CHAPTER 1

Introduction

1.1 Natural derived compounds for cancer chemotherapy

Cancer is a group of diseases that arise from uncontrolled growth of abnormal cells. These malfunctioning cells have the potential to invade surrounding tissues and other organs, and can be life-threatening (Senapati *et al*., 2018). The development of cancer is a multi-step process, involving the accumulation and acquisition of oncogenic signals through genetic and epigenetic mutations that enable normal cells to become tumorigenic and ultimately malignant. Most cancers acquire six essential functional capabilities during their development, called 'the hallmarks of cancer': self-sufficiency in growth signals, insensitivity to anti-growth signals, evasion of programmed cell death, limitless replicative potential, sustained angiogenesis, and tissue invasion and metastasis (Hanahan and Weinberg, 2000). Two emerging hallmarks of cancer (reprogrammation of energy metabolism and evasion of immune destruction) and two enabling characteristics (genomic instability and mutation, and tumour-promoting inflammation) were later added to this list (Hanahan and Weinberg, 2011) **(Figure 1-1)**.
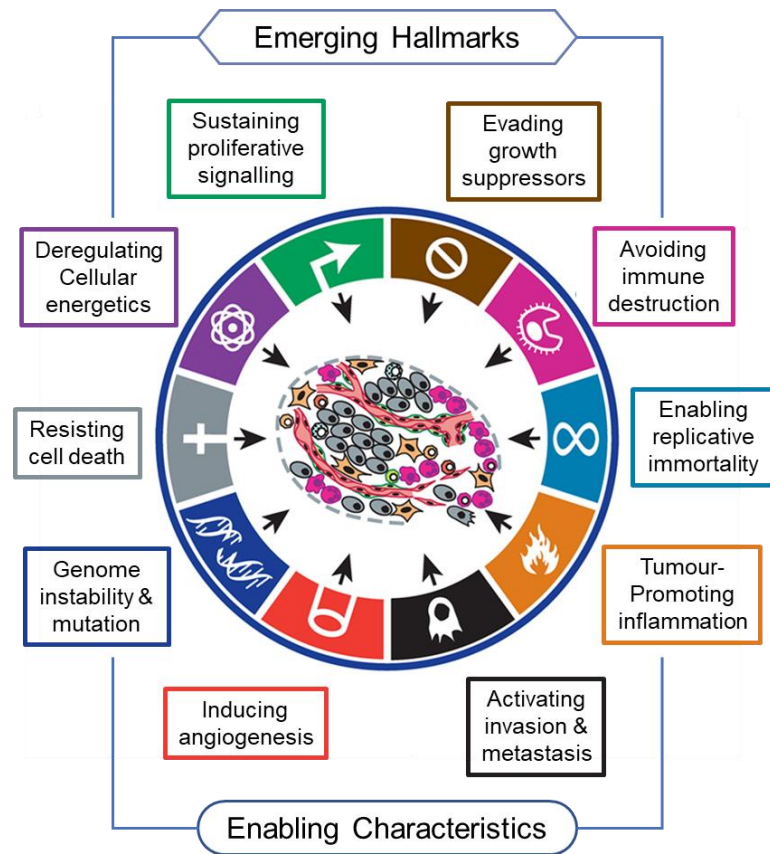
Figure 1-1: Schematic representation of the hallmarks and key features of cancer (adapted from Hanahan and Weinberg, 2011)

Recently, it has been reported that cancer is the second leading cause of death in the world, following heart disease (Bray *et al*., 2018). Cancer accounted for 9.6 million deaths in 2018 and continues rising worldwide, with an estimated 16.4 million deaths in 2040. The treatment of cancer requires close cooperation from a team of experts (e.g. oncologist, pathologist and radiologist) and usually involves various types of treatments. Although local therapies (e.g. surgery and radiotherapy) can be efficacious against localised cancers, chemotherapy remains the most common method for treatment of metastatic and blood cancers. It may also be used alone or in combination with surgery and/or radiotherapy, depending upon the specific tumour situation (Palumbo *et al*., 2013).

Natural derived compounds have gained a considerable interest among cancer researchers for the potential to affect multiple cancer hallmarks. A recent survey by Newman and colleagues (2016) indicated that approximately 55% of the approved anti-cancer drugs (from the late 1930s to 2014) were derived from natural sources. For example, paclitaxel (from the Pacific yew tree), doxorubicin (from *Streptomyces peucetius* bacterium), vincristine (from the periwinkle plant), topotecan (from the "happy tree" *Camptotheca acuminate*) and etoposide (from the mayapple plant *Podophyllum peltatum*) are well-established drugs commercially available for cancer treatment (Newman *et al*., 2016). In addition, several nature-derived compounds, such as isoflavones (from soy bean), curcuminoids (from turmeric) and resveratrol (from grape seed), are currently being investigated in clinical trials (Cragg *et al*., 2016). **Table 1-1** shows a list of some nature-derived chemotherapeutic agents used in cancer treatment or under development.

Table 1-1: List of the main anti-cancer compounds that are derived from natural sources

Compound	Natural source	Common name	Oncology indication
Doxorubicin	*Streptomyces peucetius*	-	Breast, lung, gastric and ovarian cancer, non-Hodgkin's and Hodgkin's lymphoma, multiple myeloma, sarcoma (Thorn *et al*., 2011)
Cytarabine	*Cryptotheca crypta*	Caribbean sponge	Leukaemia and lymphoma (Schwartsmann *et al*., 2001)
Gemcitabine	*Cryptotheca crypta*	Caribbean sponge	Pancreatic, breast, bladder and non-small-cell lung cancer (Schwartsmann *et al*., 2001)
Irinotecan	*Camptotheca acuminate*	"Happy tree"	Colorectal cancer (Iqbal *et al*., 2017)
Topotecan	*Camptotheca acuminate*	"Happy tree"	Ovarian and lung cancer (Iqbal *et al*., 2017)
Docetaxel	*Taxus brevifolia*	Pacific yew	Breast, ovarian, prostate and non-small-cell lung cancer (Seca and Pinto, 2018)
Paclitaxel	*Taxus brevifolia*	Pacific yew	Breast, ovarian and lung cancer (Seca and Pinto, 2018)

Table 1-1: List of the main anti-cancer compounds that are derived from natural sources (Continued)

Compounds	Natural source	Common name	Oncology indication
Vinblastine	*Catharanthus roseus*	Madagascar periwinkle	Breast cancer, testicular cancer and non-Hodgkin lymphoma (Hait *et al*., 2015)
Vincristine	*Catharanthus roseus*	Madagascar periwinkle	Acute lymphoblastic leukaemia, Hodgkin's and non-Hodgkin lymphoma and rhabdomyosarcoma (Hait *et al*., 2015)
Etoposide	*Podophyllum peltatum*	Mayapple	Small cell lung cancer and testicular cancer (Kwok *et al*., 2017)
Combretastatin A-4	*Combretum caffrum*	Bushwillow tree	Ovarian cancer (Grisham *et al*., 2018)
Flavopiridol	*Dysoxylum binectariferum*	White cedar	Leukaemia, lymphoma, multiple myeloma, breast, oesophageal, pancreatic, prostate and liver cancer (Peyressatre *et al*., 2015)
Ingenol mebutate	*Euphorbia peplus*	Petty spurge	Melanoma (Seca and Pinto, 2018)
Homoharringtonine	*Cephalotaxus harringtonii*	Plum yew	Chronic myeloid leukaemia (Seca and Pinto, 2018)

1.2 Plumbagin

Plumbagin (5-hydroxy-2-methyl-1,4-naphthoquinone) is a natural naphthoquinone mainly found in three families of plants, Plumbaginaceae, Droseraceae, and Ebenaceae (Panichayupakaranant and Ahmad, 2016). It has a wide spectrum of pharmacological properties, for example anti-inflammatory, antibacterial and antifungal activities (Padhye *et al.*, 2012). Moreover, plumbagin has recently gained considerable attention for its chemopreventive and therapeutic efficacies *in vitro* against many types of cancer, including breast (Yan *et al.*, 2013), lung (Li *et al.*, 2014), prostate (Zhou *et al.*, 2015), ovarian (Sinha *et al.*, 2013) cervical (Srinivas *et al.*, 2004b), liver (Wei *et al.*, 2017), pancreatic (Wang *et al.*, 2015), brain (Niu *et al.*, 2015), colon (Eldhose *et al.*, 2014), oesophageal (Cao *et al.*, 2018) and melanoma (Wang *et al.*, 2008).

The history of the medical use of plumbagin stretches back for several hundred years with the oldest reference to a Plumbago plant called "Chitraka" found in the ancient Indian Ayurvedic texts of Charaka (second century B.C.). The medical usage of the Plumbago root has been recognised as a treatment of dyspepsia, piles, diarrhoea and skin diseases (Checker *et al.*, 2018). The plant extract was also used to treat tuberculosis and leprosy (Padhye *et al.*, 2012). In Thai traditional medicine, the root of *Plumbago indica* (known as Chettamun-phloeng-daeng (Thailand) or official leadwort (English)) (**Figure 1-2**) can be used as carminative drug, appetite stimulant and for the treatment of haemorrhoids. However, this plant must be used cautiously in pregnant women, as plumbagin can stimulate uterus contraction, leading to abortion (Saralamp *et al.*, 1996).
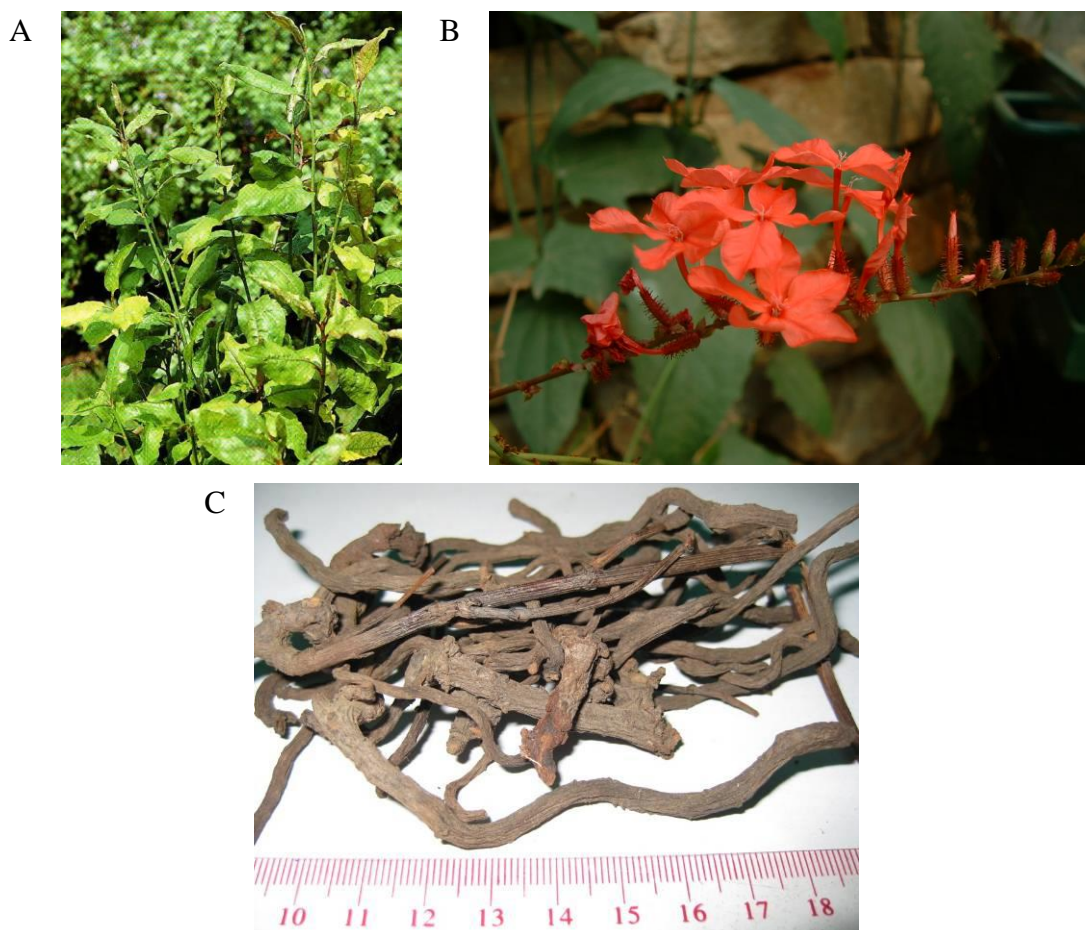
Figure 1-2: *Plumbago indica* (Plumbaginaceae): (A) Stem, (B) Flower, (C) Dried root

1.2.1 Physico-chemical properties of plumbagin

Chemically, plumbagin is one of the simplest hydroxy-naphthoquinones isolated from the root of Plumbago species where its name derived from. It usually appears as yellow-orange, needle-shaped crystalline powder with a molecular formula of $C_{11}H_8O_3$ and a molecular weight of 188.18 g/mol. It is a lipophilic compound (log *P* 3.04) with poor solubility in water (79 μg/mL), but good solubility in organic solvents such as alcohols, acetone, chloroform, dimethyl sulfoxide (Panichayupakaranant and Ahmad, 2016; Pawar *et al*., 2016). The chemical structure of plumbagin and its physico-chemical properties are shown in **Table 1-2**.

Table 1-2: Physico-chemical properties of plumbagin

| Chemical structure |
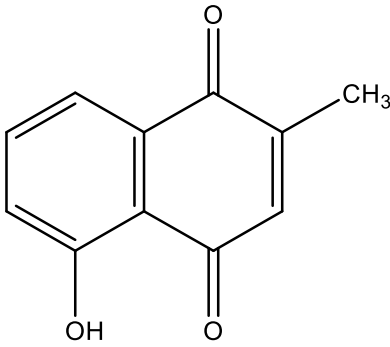
plumbagin |
|---|---|
| **Chemical name** | 5-hydroxy-2-methyl-1,4-naphthoquinone |
| **Chemical class** | 1,4-naphthoquinone |
| **Molecular formula** | $C_{11}H_8O_3$ |
| **Molecular weight** | 188.18 g/mol |
| **Appearance** | yellow-orange, needle-shaped crystalline powder with irritating odour |
| **Purity** | > 95% |
| **Melting point** | 78-79 °C |
| **log P** | 3.04 |
| **pKa** | 9.48 |
| **Solubility** | Poorly soluble in water (79 μg/mL)

Slightly soluble in hot water

Soluble in methanol, ethanol, isopropanol, acetone, chloroform, DMSO, pyridine and acetic acid |

(adapted from Rajalakshmi *et al.*, 2018)

1.2.2 Pharmacology of plumbagin

1.2.2.1 Pharmacokinetic and pharmacodynamic properties

Due to the promising pharmacological activities of plumbagin, especially its anti-cancer property, its pharmacokinetic and pharmacodynamic properties have been extensively investigated in different models. Sumsakul and Na-Bangchang (2016) have demonstrated that plumbagin has a moderate permeability across Caco-2 human epithelial colorectal adenocarcinoma cell monolayer via a passive transport mechanism. In addition, plumbagin did not interfere with the function of the P-glycoprotein drug transporter and the expression of multidrug resistance protein 1 (MDR-1) gene (Sumsakul and Na-Bangchang, 2016). A study by Hsieh and colleagues (2006) reported that the bioavailability of plumbagin after a single oral dose (100 mg/kg body weight) in Sprague–Dawley rat was $38 \pm 5\%$, with 49 % of drug excreted through feces. Plumbagin reached a maximum serum concentration (C_{max}) of 0.35 ± 0.10 mg/mL at the time to maximum concentration (T_{max}) of 150 ± 46 min (2.5 ± 0.8 h), then its serum concentration declined rapidly with an elimination half-life ($t_{1/2}$) of 1028 ± 323 min (17.1 ± 5.4 h). The authors also suggested that plumbagin is metabolised through phase Ⅰ aliphatic hydroxylation and phase Ⅱ glucuronidation pathways, as the metabolites of plumbagin were also detected in rat urine. However, different pharmacokinetics of plumbagin given by oral administration were also observed when using other rat species. A single oral administration of plumbagin (100 mg/kg body weight) in a Wistar rat model found that the drug absorption was delayed (T_{max} of 5 h), and the elimination half-life ($t_{1/2}$ of 9.63 h) was relatively short compared with that previously reported in Sprague–Dawley rats (Sumsakul *et al*., 2016). In addition, Kumar and colleagues (2011) reported that the plasma levels of plumbagin decreased rapidly after the intravenous injection of plumbagin at the dose of 6 mg/kg body weight (solubilised in PBS containing 25% PEG-

200 at a final concentration of 1.2 mg/mL) in C57BL/6J mice bearing B16F1 melanoma with the elimination half-life of 35.89 ± 7.95 min and a plasma clearance of 0.03 ± 0.01 L/min. The ability of plumbagin to modulate the activities of human and rat hepatic metabolising cytochrome P450 (CYP) enzyme was also investigated. Plumbagin was found to be an inhibitor of human hepatic microsomal enzymes CYP2B6, CYP2C9, CYP2D6, CYP2E1 and CYP3A4, with the inhibitor constant (Ki) values (the concentration required to produce half maximum inhibition; a small Ki means that the inhibitor is more potent) about 2.16 µM. Plumbagin was also found to be an inhibitor of rat hepatic microsomal enzymes CYP1A2 and CYP2D1, CYP2B1, CYP2C11 and CYP2E1 enzymes, with Ki values less than 9.93 µM. Based on these findings, the authors concluded that plumbagin would be highly likely to cause toxicity and drug interactions due to its impact on these cytochrome P450 enzymes (Chen *et al*., 2016).

1.2.2.2 Plumbagin toxicity

The toxicity of plumbagin has been studied by several research groups. Sumsakul and colleagues (2014) reported that plumbagin has relatively low toxicity at the dose levels up to 100 (single oral dose) and 25 (daily doses for 14 days) mg/kg body weight for acute and sub-acute toxicity testing in mice. The same research group also studied the toxicity of plumbagin in Wistar rats and found that the maximum tolerated doses in acute and sub-acute toxicity studies were 150 (single oral dose) and 25 (daily doses for 28 days) mg/kg body weight. The 50 % lethal dose (LD_{50}) of plumbagin was 250 mg/kg body weight for acute toxicity and 50–100 mg/kg body weight for sub-acute toxicity. In addition, a daily oral administration of plumbagin (25 mg/kg body weight) for 28 days did not change the haematological and blood biochemistry profiles of animals (Sumsakul *et al*., 2016). In other studies, however, oral administration of plumbagin has been

reported to cause diarrhoea, skin rashes, drowsiness, lethargy, increased white blood cell and neutrophil counts (Singh *et al*., 1997), cardiotoxicity (Shimada *et al*., 2012) and hepatotoxicity (Sukkasem *et al*., 2016). The increased systemic toxicity was further evidenced in an intravenous administration of plumbagin. Pawar and colleagues (2016) reported that the intravenous injection of plumbagin (2 mg/kg body weight for 15 days) caused abnormal tissue toxicity such as myocardial necrosis and degeneration, hepatocellular inflammation and necrosis as well as severe necrosis of tubules and glomeruli. Furthermore, plumbagin was found to prolong bleeding time in Wistar rats (daily doses of 2 mg/kg body weight for 31 days) by decreasing platelet adhesion and coagulation. This may be due to the structure of plumbagin, which has been reported to closely resemble the vitamin K3 (menadione or 2-methyl-1,4-naphthoquinone) (Vijayakumar *et al*., 2006).

1.2.2.3 Anti-inflammatory activity

Inflammation is the response of cellular and humoral defence mechanisms to injury or infection. The symptom of acute inflammation is characterised by five symptoms: pain, swelling, redness, heat and tissue injury (Ricciotti and FitzGerald, 2011). These symptoms occurred from the interaction between granulocytes, macrophages, lymphocytes as well as cell- and tissue-derived mediators (e.g. histamine, prostaglandins and leukotrienes). An increase in temperature is caused by cytokines derived from leukocytes, while pain indicates an inflammation of injured tissues (Schrör, 2009). If acute inflammation cannot resolve, it may lead to chronic inflammation which is involved in almost all chronic diseases such as cancer, cardiovascular diseases and autoimmune diseases (Ricciotti and FitzGerald, 2011).

A study by Checker and colleagues (2009) revealed that plumbagin inhibited mitogen-induced T-cell activation and proliferation, and secretion of pro-inflammatory cytokines such as interleukins (IL)-2, IL-4, IL-6 and interferon (IFN)-γ. In addition, it also prevented translocation of Nuclear factor-kappa B (NF-κB) by inhibiting the degradation of an inhibitor of NF-κB transcription factor (IκBα) *in vitro*. The anti-inflammatory activity of plumbagin was further confirmed by Luo and colleagues (2010). In their study, the oral dosing of plumbagin (10 to 20 mg/kg body weight) reduced the rat paw oedema caused by carrageenan and various pro-inflammatory cytokines, including histamine, serotonin, bradykinin and prostaglandin E_2. It also reduced the number of writhing episodes induced by the intraperitoneal injection of acetic acid in animals. Further examination demonstrated that plumbagin significantly decreased the production of IL-1β, IL-6 and Tumour necrosis factor alpha (TNF-α), and inhibited the expression of inducible nitric oxide synthase (iNOS) and cyclooxygenase-2 (COX-2).

1.2.2.4 Antimicrobial activity

Numerous studies have found that plumbagin exhibited antimicrobial activities against many types of human pathogenic microorganisms, including Gram-positive and Gram-negative bacteria, antibiotic-resistant bacteria, fungi and yeast. A study by Paiva and colleagues (2003) revealed that plumbagin showed antimicrobial activity against *Staphylococcus aureus* with a minimum inhibitory concentration (MIC) of 1.56 µg/mL and minimum bactericidal concentration (MBC) of 25 µg/mL, as well as against *Candida albicans* with a MIC of 0.78 µg/mL and a minimum fungicidal concentration (MFC) of 1.56 µg/mL. In another study, plumbagin exerted an inhibitory effect against nine strains of *S. aureus,* including methicillin- and multidrug-resistant strains with MICs ranging from 4 to 10.67 µg/mL. Further studies demonstrated that a combination of plumbagin at

2 µg/mL with oxacillin exhibited a synergistic effect against two epidemic methicillin resistant strains of *S. aureus*, EMRSA15 and MRSA1, resulting in a reduction of oxacillin MICs by 32-fold and 42-fold respectively (Rondevaldova *et al.*, 2015). Dzoyem and colleagues (2007) evaluated the antifungal activity of plumbagin against 5 strains of yeast pathogens (*Candida albicans*, *Candida glabrata*, *Candida krusei*, *Candida tropicalis* and *Cryptococcus neoformans*) and 7 strains of filamentous fungi (*Aspergillus flavus*, *Aspergillus niger*, *Alternaria* sp., *Cladosporium* sp., *Geotrichum candidum*, *Fusarium* sp., and *Penicillium* sp.). They found that plumbagin inhibited the growth of these fungi with MICs ranging from 0.78 to 6.25 µg/mL, which are close to the MICs of ketoconazole (0.25 to 5 µg/mL) used as a control antifungal treatment.

1.2.2.5 Anti-cancer activity

Plumbagin has demonstrated its anti-cancer potential against many types of cancer both *in vitro* and *in vivo*. Several studies suggested that plumbagin exerted its chemopreventive and anti-cancer properties by alteration of various signalling pathways which play a crucial role in cancer cell proliferation, survival, invasion, metastasis and angiogenesis. It is well established that these underlying activities of plumbagin are mainly due to the ability to modulate cellular redox cycle, resulting in the generation of reactive oxygen species (ROS) (Liu *et al.*, 2017; Checker *et al.*, 2018; Jaiswal *et al.*, 2018). The potential of plumbagin as a therapeutic agent for cancer treatment will be further studied in this thesis.

1.2.2.6 Other pharmacological activity of plumbagin

Other pharmacological activities of plumbagin have been investigated by several research groups as summarised in **Table 1-3**.

Table 1-3: Other pharmacological activities of plumbagin

Pharmacological activity	Assay method	Result
Antioxidant	Comet assay	Plumbagin (at non-DNA damaging concentrations of 0.25 ng/mL) significantly reduced the catechol-induced oxidative DNA damage in mouse lymphoma L5178Y cells (Demma *et al*., 2009)
	In vitro assay in the nucleus pulposus (NP) cells	Plumbagin exhibited a protective effect in NP cells by decreasing the generation of ROS and lipid peroxidation induced by hydrogen peroxide (Chu *et al*., 2016)
	In vivo assay in C57BL6/J mice with myocardial injury	ROS and lipid peroxide levels were found to be decreased in mice treated with plumbagin (5 mg/kg, i.p.) (Wang *et al*., 2016)
Antimalarial	*In vitro* assay using SYBR Green I assay	Plumbagin inhibited 3D7 chloroquine-sensitive and K1 chloroquine-resistant *Plasmodium falciparum* with IC_{50} of 580 and 370 nM, respectively (Sumsakul *et al*., 2014)

Table 1-3: Other pharmacological activities of plumbagin (Continued)

Pharmacological activity	Assay method	Result
Antimalarial	*In vivo* assay in Swiss albino mice infected with *Plasmodium berghei*	Oral dosing of plumbagin (30 mg/kg for 4 days) significant reduced parasitaemia and increased in mean survival time compared with untreated group (Gupta *et al*., 2018)
Hepatoprotection	*In vivo* assay in carbon tetrachloride-induced liver fibrosis in Sprague Dawley rats	Oral dosing of plumbagin (4 and 8 mg/kg three times a week for 8 weeks) significantly decreased liver functional enzymes (ALT, AST, ALP, TBIL) and inflammatory cytokines (IL-6, TNF-α), and improved hepatocellular impairments (Wei *et al*., 2015)
Hepatoprotection	*In vivo* assay in Wistar rats induced with obesity and non-alcoholic fatty liver disease (NAFLD) by chronic consumption of fructose	Oral administration of plumbagin (1 mg/kg from Weeks 9 to 16) exhibited anti-fibrotic effects, reduced the hepatic lipids and the hypertrophy of adipocytes (Pai *et al*., 2019)

Table 1-3: Other pharmacological activity of plumbagin (Continued)

Pharmacological activity	Assay method	Result
Antidepressant	*In vivo* assay in depression-like behaviour induced Swiss albino mice, by using tail suspension and sucrose preference tests	Mice treated with high dose of plumbagin (16 mg/kg, p.o.) significantly decreased the immobility of stressed mice and restored their normal sucrose preference. Plumbagin was found to inhibit brain MAO-A activity, decreased plasma nitrite, brain malondialdehyde and catalase levels while increasing reduced glutathione levels in stressed mice. It also reversed stress-induced increase in plasma corticosterone levels. These results were comparable with imipramine used as standard treatment in this study (Dhingra and Bansal, 2015)

1.2.3 Plumbagin and cancer

The first evidence for the anti-cancer effect of plumbagin was reported by Melo and colleagues (1974), when it was used to treat patients with skin cancer. However, the authors found that plumbagin also caused high skin irritation. In 1980, Santhakumari and colleagues (1980) have demonstrated that plumbagin at lower concentrations slowed the growth of chick embryo fibroblasts by inhibiting entry of cells into mitosis, while the compound at high concentration exhibited cytotoxic effects to the cells. Furthermore, Krishnaswamy and Purushothaman have shown that plumbagin could inhibit chemically-induced fibrosarcoma in rats as well as P388 leukemia in mice (Krishnaswamy and Purushothaman, 1980). Since then, plumbagin has gained much attention for its anti-cancer properties. Numerous studies have shown that plumbagin exhibited *in vitro* anti-proliferative effects on several types of cancer cell lines, as summarised in **Table 1-4.**

Table 1-4: Overview of *in vitro* anti-proliferative effects of plumbagin in various types of cancer

Types of cancer	Cell lines	References
Brain cancer	A172, KNS60, U251-MG, U251 and ONS76	Khaw *et al*., 2015
Breast cancer	MCF-7, MDA-MB-231 and MDA-MB-436	Ahmad *et al*., 2008; Lee *et al*., 2012; Yan *et al*., 2013; Somasundaram *et al*., 2016
Cervical cancer	ME-180, SiHa and HeLa	Srinivas *et al*., 2004b; Jaiswal *et al*., 2018

Table 1-4: Overview of *in vitro* anti-proliferative effects of plumbagin in various types of cancer (Continued)

Colorectal cancer	HT29, HCT15, HCT116, SW480 and SW620	Subramaniya *et al*., 2011; Eldhose *et al*., 2014; Raghu *et al*., 2014
Liver cancer	HepG2, SMMC-7721 and Hep3B	Shih *et al*., 2009; Wei *et al*., 2017
Lung cancer	A549, H460, H23, L9981 and NL9980	Gomathinayagam *et al*., 2008; Li *et al*., 2014; Yu *et al*., 2018
Melanoma	A431, A375.S2 and SK-MEL 28	Wang *et al*., 2008; Duraipandy *et al*., 2014
Oesophageal cancer	ESCC, KYSE-150 and KYSE-450	Cao *et al*., 2018
Ovarian cancer	BG-1, OVCAR-3, OVCAR-5 and SKOV-3	Srinivas *et al*., 2004a; Kapur *et al*., 2018
Pancreatic cancer	PANC-1 and BxPC-3	Wang *et al*., 2015
Prostate cancer	PC-3, LNCaP, C4-2 and DU145	Powolny *et al*., 2008; Zhou *et al*., 2015

In vivo, intravenous administration of plumbagin (2-6 mg/kg of body weight, dissolved in alcohol then in buffer saline) was found to delay the growth of Ehrlich ascites tumours and increase the lifespan of BALB/c mice by 10.0 to 47.8%. However, a progressive loss of body weight was observed in the animals treated with a dose of plumbagin higher than 3 mg/kg of body weight, which is a sign of severe toxicity (Naresh *et al.*, 1996). A study

by Singh and colleagues (1996) showed that the intratumoral injection of plumbagin (6 mg/kg of body weight/ day for 14 days) to BALB/c mice showed limited efficacy in slowing down the growth of sarcoma-180 tumours compared to the untreated group (volume-doubling times (VDT) of 7.2 ± 0.9 days for plumbagin and 3.5 ± 0.5 days for the untreated group). Lai and colleagues (2012) investigated the anti-tumour effect of plumbagin on human colon carcinoma (HCT116) and prostate cancer (PC-3) xenograft mouse models. They found that, following intratumoral injection of plumbagin (dissolved in DMSO) at the dose of 6 mg/kg (for HCT116 group) and 10 mg/kg (for PC-3 group) to mice for 20 days, the tumour volume significantly decreased in both treated groups in comparison with the control group. In another study, Hsu and colleagues (2006) demonstrated that plumbagin (2 mg/kg of body weight/day for 60 days, prepared in 25% polyethylene glycol, intraperitoneal injection) inhibited tumour growth and induced the apoptosis of A549 mouse xenograft model compared with the control group. The intraperitoneal administration of plumbagin (1 mg/kg of body weight/day for 26 days, dissolved in DMSO then in polyethylene glycol 30% w/v to reach a final DMSO concentration of 0.05% v/v) has been reported to slow down the growth of PTEN-P2 mouse prostate tumours compared to the untreated group, but did not cause regression (Abedinpour *et al*., 2013). In addition, intraperitoneal injection of plumbagin (2 mg/kg of body weight, 5 times a week for 24 days) to mice bearing subcutaneous U87 glioma tumours, was found to inhibit the growth of glioma by 54.5%, compared with the control group (Niu *et al*., 2015).

Although some studies have demonstrated the promising anti-cancer properties of plumbagin *in vitro*, its therapeutic potential *in vivo* has been limited so far, even after intratumoral administration. This is because plumbagin has a short half-life with rapid elimination, resulting in a decreased plasma concentration and a shortened duration of

action. Another obstacle to the widespread development of plumbagin is its high lipophilicity. Poor water solubility of plumbagin is a major problem encountered with the design of formulation, which often requires the use of vehicles containing organic solvents or excipients that may cause toxicity by themselves. Moreover, the chronic or high dose administration of plumbagin also has a tendency to cause systemic toxicity such as cardiotoxicity and hepatotoxicity. In this context, the introduction of nanotechnology could provide a novel approach to overcome the crucial hurdle of plumbagin's limitations to enhance its therapeutic efficacy.

1.2.4 Mechanisms of action

Several *in vitro* and *in vivo* experiments have supported the hypothesis that plumbagin could be a promising chemotherapeutic agent for cancer treatment. Various mechanisms and cell signalling pathways have been proposed for the anti-cancer properties of plumbagin, such as generation of reactive oxygen species (ROS), induction of cell cycle arrest, apoptosis and autophagy, and inhibition of cell invasion, metastasis and angiogenesis (**Figure 1-3**) (Lai *et al*., 2012; Sinha *et al*., 2013; Checker *et al*., 2018; Jaiswal *et al*., 2018; Liu *et al*., 2017; Zhou *et al*., 2015).
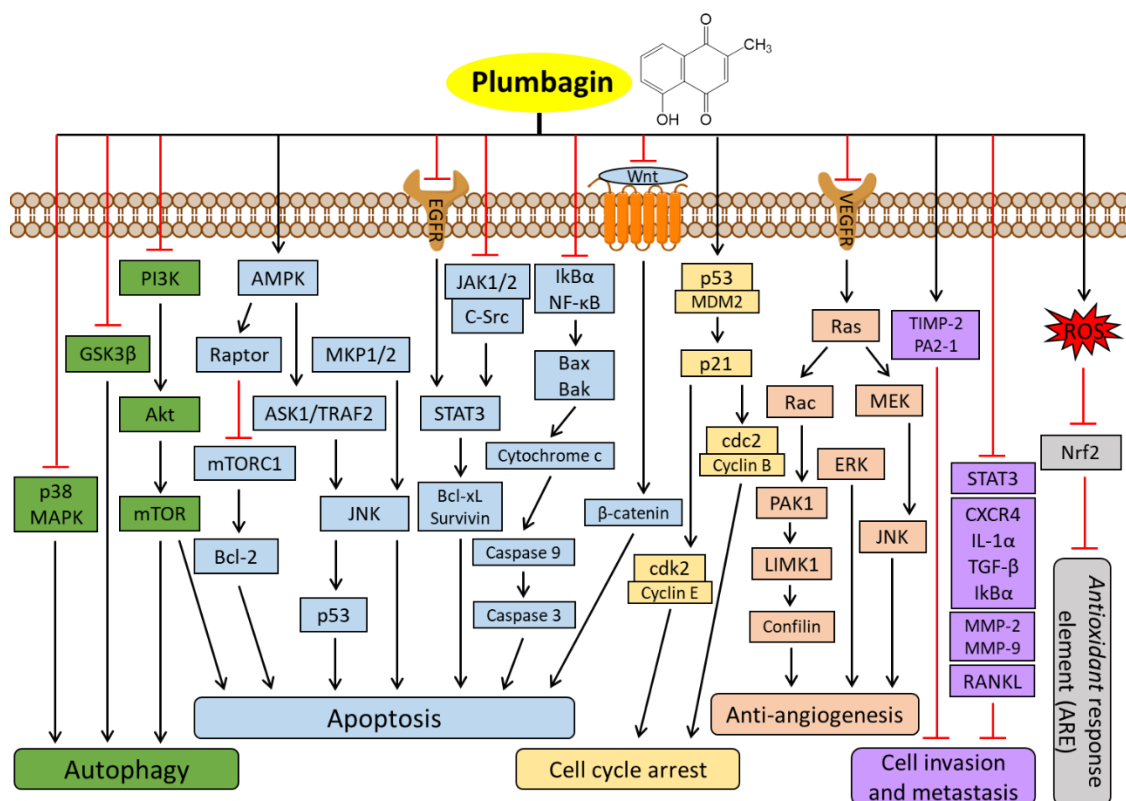
Figure 1-3: A summary of mechanisms and cell signalling pathways associated with the anti-cancer activities of plumbagin (adapted from Liu *et al*., 2017)

1.2.4.1 Generation of reactive oxygen species

Plumbagin has been reported to exert its anti-cancer effects primarily by promoting generation of ROS, such as hydroxyl radical (HO•), superoxide anion ($O_2^{•-}$) and hydrogen peroxide (H_2O_2), as well as causing alkylation reactions that disrupt the structure and/or the function of lipids, proteins and DNA (Powolny *et al*., 2008; Seshadri *et al*., 2011; Klotz et al., 2014; Jaiswal *et al*., 2018).

In mammalian cells, one-electron reduction (mediated by NADPH-cytochrome P450 reductase) and two-electron reduction (mediated by NAD(P)H: quinone oxidoreductase-1 (NQO-1 or DT-diaphorase)) convert plumbagin to a semi-quinone radical or quinol (also known as hydroquinone), respectively. These reactions lead to the auto-oxidation of the semi-quinone radical and quinol by molecular oxygen (O_2) to generate superoxide

anion ($O_2^{\bullet-}$) which subsequently undergo disproportionation to oxygen (O_2) and hydrogen peroxide (H_2O_2), causing oxidation of lipids, proteins and DNA. Alternatively, quinones may cause the alkylation (also termed arylation) of reduced glutathione (GSH) as well as cysteine residue of proteins, resulting in the depletion of GSH levels and modification of protein structure and function (**Figure 1-4**) (Inbaraj and Chignell, 2004; Klotz et al., 2014; Widhalm and Rhodes, 2016).
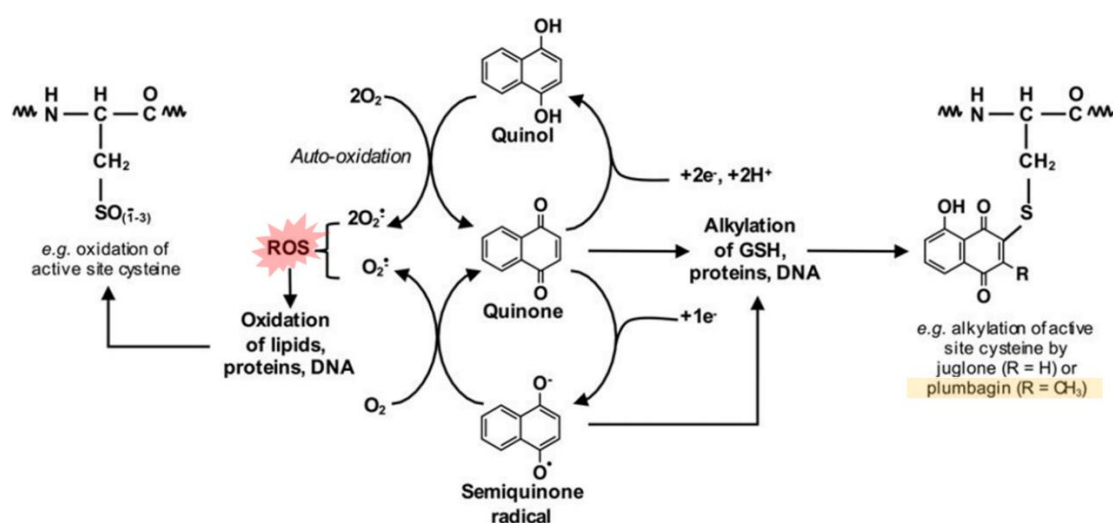
Figure 1-4: Potential mechanisms of plumbagin and other quinones by modulation of cellular redox, generation of reactive oxygen species and alkylation reaction with cysteine-rich proteins and DNA (adapted from Widhalm and Rhodes, 2016)

1.2.4.2 Modulation of cell signalling pathways

Plumbagin has been reported to inhibit cell proliferation and induce apoptosis by targeting multiple cell signalling pathways such as NF-κB, adenosine monophosphate-activated protein kinase (AMPK), phosphatidylinositol-3-kinase (PI3K)/protein kinase B (Akt)/mechanistic target of rapamycin (mTOR), Mitogen-activated protein kinase (MAPK)/ Extracellular signal-regulated kinases (ERK), Wnt/β-catenin including caspase-3, -8 and -9 (Liu *et al*., 2017).

A study by Li and colleagues (2012a) revealed that plumbagin can inhibit cell growth and induce apoptosis through downregulation of the nuclear factor-kappa B (NF-κB) regulated gene products expression. The role of NF-κB, a family of cellular transcription factors, is involved in inflammatory responses and regulation of anti-apoptotic genes expression in various types of cancers (Lee *et al.*, 2007). Generally, translocation of NF-κB to the nucleus occurs due to its sequestration in cell cytoplasm mediated by inhibitory kappa B (IκB) proteins that are phosphorylated by IκB kinase complex (IKK; consisting of two highly homologous catalytic subunits, IKKα and IKKβ) and then degraded by the 26S proteosome. In cancer, the activation of NF-κB activity leads to aberrant IKK activity and a shorter half-life of IκB proteins (Lee *et al.*, 2007). Plumbagin-inhibited NF-κB activity was further supported by Kawiak and Domachowska (2016), which demonstrated that plumbagin suppressed IKKα activity in HER2-overexpressing breast cancer cells and inhibited IκBα phosphorylation and degradation (Kawiak and Domachowska, 2016). In addition, an *in vitro* study by Khaw *et al.* (2015) showed that plumbagin can induce DNA damage and apoptosis in human brain tumour cells by upregulation of phosphatase and tensin homolog (PTEN), a tumour suppressor gene. As the activation of NF-κB can suppress PTEN expression and prevent apoptosis (Vasudevan *et al.*, 2004), the inhibition of NF-κB activity and upregulation of PTEN gene by plumbagin may improve apoptosis and reduce tumorigenesis (**Figure 1-5**).

In addition, the AMPK and mTOR kinase signalling pathways which played critical roles in controlling cell growth and proliferation, regulating metabolism, apoptosis and autophagy, are considered to be defective signalling pathways in cancer. Indeed, the activation of AMPK leads to the mTOR suppression (Shaw *et al.*, 2009; Li *et al.*, 2015). An *in vitro* study in colorectal cancer cells showed that plumbagin can induce

apoptosis through activation of AMPK, which directly leads to phosphorylation of Raptor protein, and then inhibition of mTOR complex 1 (mTORC1) activation (Chen *et al.*, 2013). Plumbagin was also found to inhibit PI3K/Akt/mTOR signalling pathways, a key regulator of cell survival under stress condition, which eventually promoted apoptosis and autophagy in cancer cells (Li et al., 2014; Wang et al., 2015; Zhou et al., 2015) (**Figure 1-5**).
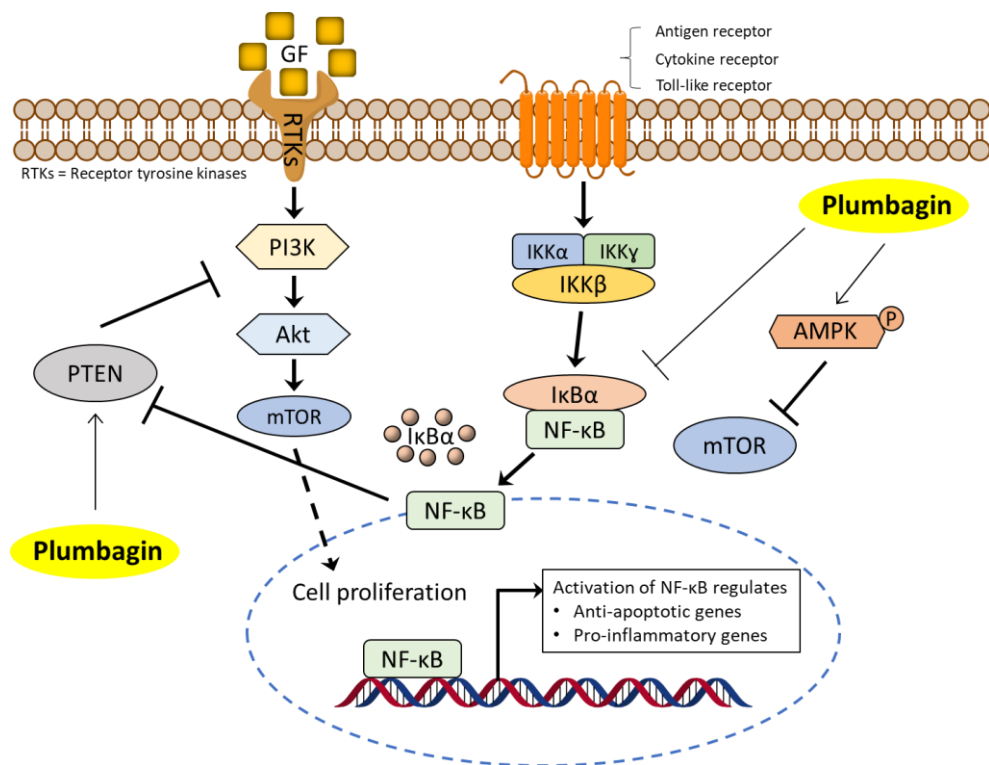
Figure 1-5: Effect of plumbagin on NF-κB and PI3K/Akt/mTOR signalling pathways

Furthermore, it was reported that plumbagin can inhibit the activation of ERK pathway (also known as the Ras-Raf-MEK-ERK pathway) (Lai *et al.*, 2012). This pathway is one of the MAPK pathways that control diverse cellular processes such as growth, proliferation, differentiation, migration and apoptosis (Dhillon *et al.*, 2007; Kohno *et al.*, 2011; Dovizio *et al.*, 2012). Particularly, upregulation of ERK pathway is associated with mutation or overexpression of Ras and Raf proteins, as well as the epidermal growth

factor (EGF), vascular endothelial growth factor (VEGF) and their receptors (Lai *et al.*, 2012; Ding *et al.*, 2016). This led to the stimulation of MEK and ERK, resulting in angiogenesis and cancer cells survival (Roberts and Der, 2007). Lai and colleagues (2012) have demonstrated that plumbagin inhibited proliferation of human umbilical vein endothelial cells (HUVEC) by blocking VEGF-stimulated Ras activation and phosphorylation of MEK, ERK. In addition, an *in vitro* study by Gomathinayagam *et al.* (2008) showed that plumbagin downregulated the expression of EGFR in non-small cell lung cancer (H460 cells). This result was similar to that previously reported by Hafeez and colleagues (2012). In their study, plumbagin was able to inhibit the growth of pancreatic cancer cells both *in vitro* and *in vivo* via the suppression of EGFR (**Figure 1-6**).
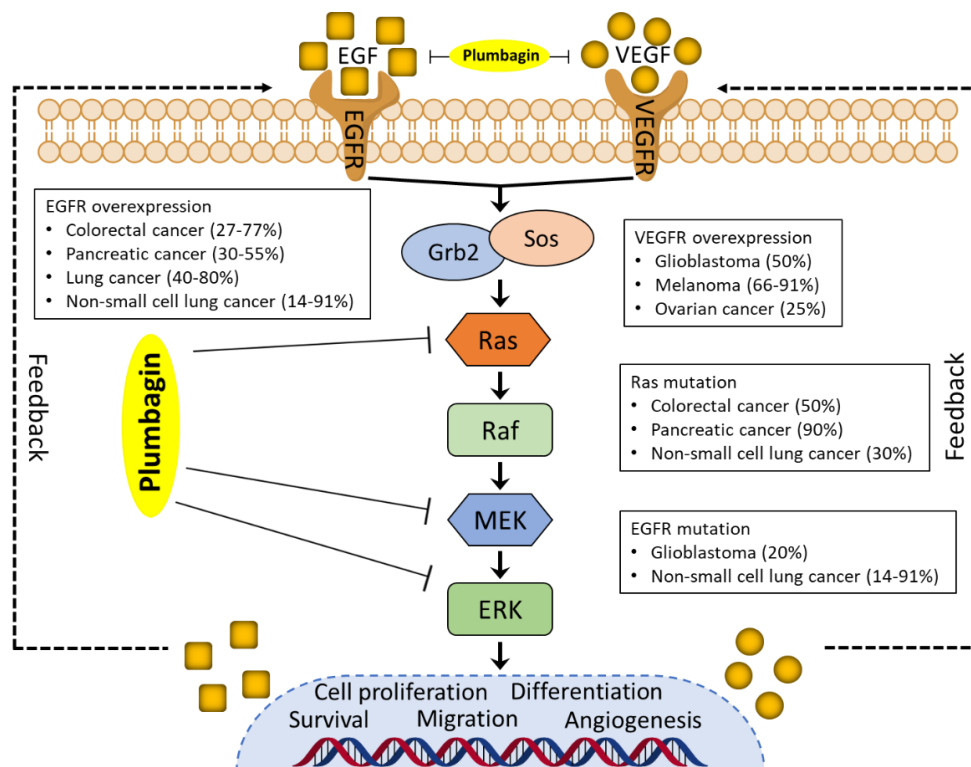
Figure 1-6: The ERK signalling pathway which is suppressed by plumbagin (adapted from Roberts and Der, 2007)

The Wnt/β-catenin signalling pathway which normally plays a role in various stages of cell division and growth, is another aberrant pathway established in some cancers such as colon, lung, breast, prostate cancer, melanoma, glioblastoma and osteosarcoma. An abnormal stimulation of Wnt signalling in this pathway leads to an accumulation of β-catenin in cytoplasm. It is then translocated into the nucleus and forms a complex with T-cell factor (TCF)/lymphoid enhancing factor (LEF), causing upregulation of some proto-oncogene transcriptions such as c-Myc and cyclin D1 and enhancing cell proliferation (Lin *et al*., 2014). Plumbagin was found to downregulate Wnt/β-catenin signalling and decrease the expression of c-Myc and cyclin D1 in human colorectal cancer cells (Subramaniya *et al*., 2011; Raghu and Karunagaran, 2014; Yan *et al*., 2015). In addition, an *in vivo* study by Niu and colleagues (2015) have demonstrated that plumbagin also inhibited the growth of gliomas via the suppression of forkhead box M1 (FOXM1) transcription factor and downstream its target genes including cyclin D1 (**Figure 1-7**).
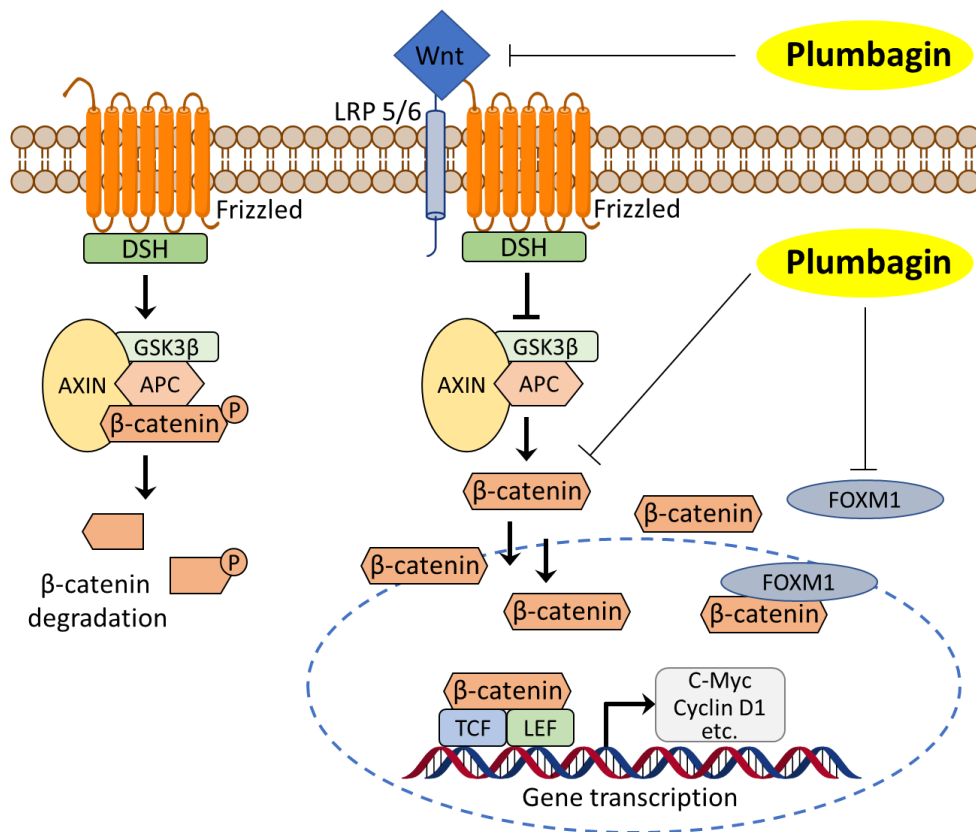
Figure 1-7: Effect of plumbagin on Wnt/β-catenin signalling pathway

Several studies have reported that plumbagin inhibited tumorigenesis by induction of apoptosis via caspase-activation pathways. An experiment by Chen and colleagues (2009) indicated that plumbagin triggers the mitochondrial apoptotic pathway by upregulation of Bax pro-apoptotic protein, increasing the release of cytochrome c from mitochondria to cytosol and cleaving procaspase-9. As a result, the release of cytochrome *c* associated with caspase-9 and apoptotic protease activating factor-1 (Apaf-1) can form the apoptosome, leading to the activation of caspase-3 (**Figure 1-8**). This outcome shows similarities with a study by Reshma *et al.* (2016) which demonstrated that plumbagin induced apoptosis through the activation of caspase-3, caspase-8 and caspase-9. In addition, plumbagin has been demonstrated to downregulate anti-apoptotic protein Bcl-2 expression (Seshadri *et al.*, 2011) and to activate apoptosis inducing factor (AIF), a caspase-independent apoptotic pathway (Srinivas *et al.*, 2004b).
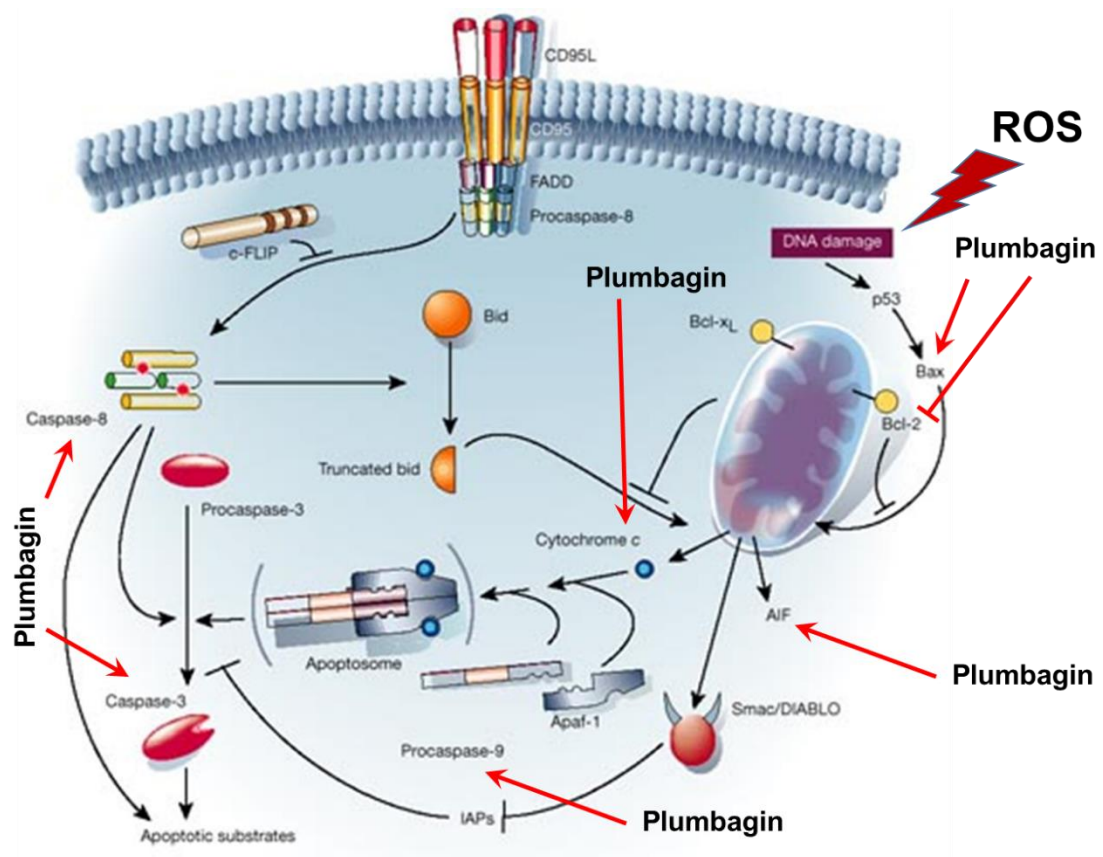
Figure 1-8: A summary of caspase-dependent and caspase-independent apoptotic pathways associated with the anti-cancer activities of plumbagin (adapted from Hengartner, 2000)

1.3 Nanomedicines in cancer therapy

The aim in cancer treatment is to completely remove the tumour from the body, while maintaining a good quality of life for the patient (Brundage, 2013). In early state disease, although almost all types of solid and localised tumours can be treated with surgery and/or radiation, these treatments cannot cure cancer patients who have haematological cancers (leukaemia, lymphoma and multiple myeloma) or metastases (Arruebo, *et al*., 2011). Systemic chemotherapy then becomes a crucial therapeutic modality, as a chemotherapeutic agent can reach all tumour sites through blood circulation system (Bhosle and Hall, 2009; Fernando and Jones, 2015). Unfortunately, the chemotherapeutic agents also lack specificity in their action, are associated with significant cytotoxicity to normal cells, particularly among high growth rate cells such as bone marrow cells (Caley and Jones, 2012). This issue was also the case with plumbagin, as it failed to specifically reach tumours after intravenous administration, thus resulting in a lack of efficacy on tumours and secondary effects on healthy tissues (skin rashes, cardiotoxicity, hepatotoxicity, increased risk of bleeding) (Singh *et al*., 1997; Vijayakumar *et al*., 2006; Shimada *et al*., 2012; Sukkasem *et al*., 2016). Furthermore, as a result of its rapid metabolism and elimination, plumbagin has a short half-life of 35.89 ± 7.95 min in the blood (Kumar *et al*., 2011), leading to plasma plumbagin concentrations much lower than those necessary to exert effective anti-cancer activity (Sagnella *et al.*, 2014).

To overcome these drawbacks, the use of nanotechnology along with tumour targeting would be a promising strategy (Lammers *et al.*, 2008; Bertrand *et al.*, 2014; Sagnella *et al.*, 2014). Nanomedicines are mostly referred to structures with a size range of 1-1000 nm (Hartman *et al.*, 2008; Alexis *et al.*, 2010; Grobmyer *et al.*, 2010; Egusquiaguirre *et al.*, 2012). The size of nanomedicines is an important parameter that drives several biological phenomena with discrete cut-off size ranges, including circulation half-life,

extravasation through leaky vasculature and macrophage uptake. It is suggested that nanomedicines in the range of 100–200 nm have the ability to effectively extravasate through the leaky vasculature of tumours, escape recognition by macrophages, as well as avoiding filtration by liver and spleen. Nanomedicines with a diameter less than 5 nm are rapidly cleared by renal clearance upon intravenous administration, while particles ranging from 50–100 nm may accumulate in a non-specific manner in the liver. Moreover, nanoparticles larger than 200 nm have been shown to accumulate in the spleen and are rapidly recognised by macrophages (Blanco *et al*., 2015).

Nanomedicines have the ability to carry one or more drugs and to release them at specific locations, thus enhancing drug accumulation. They also improve the solubility of drugs, reduce biodegradation, prolong blood circulation, enhance the bioavailability and reduce toxicity (Peer *et al.*, 2007; Bertrand *et al.*, 2014; Wicki *et al.*, 2015). The characteristics of an ideal tumour-targeted nanomedicine are shown in **Table 1-5**.

Table 1-5: Characteristics of an ideal tumour-targeted nanomedicine (Lammers *et al.*, 2008)

(1)   Increase drug localisation in the tumour through:
(a) passive targeting
(b) active targeting
(2)   Decrease drug localisation in sensitive or non-target tissues
(3)   Ensure minimal drug leakage during transit to target
(4)   Protect the drug from degradation and from premature clearance
(5)   Retain the drug at the target site for the desired period of time
(6)   Facilitate cellular uptake and intracellular trafficking
(7)   Have good biocompatibility and biodegradability

Note that not all characteristics apply to all types of nanomedicines

1.3.1 Nanomedicines in clinical practice

Doxil® (PEGylated liposomal doxorubicin, **Figure 1-9**) was the first nanomedicine approved by the FDA in 1995 for the treatment of AIDS-related Kaposi's sarcoma and then for the treatment of recurrent ovarian cancer in 1998 (Anselmo and Mitragotri, 2014). The development of Doxil® was based on various aspects of liposome technology to overcome limitations of doxorubicin, such as increase of drug stability, prolongation of blood circulation time and controlled drug release, as well as targeted delivery of doxorubicin to cancer cells. *In vivo*, Doxil® administration resulted in an increase of circulation time as well as a decrease of murine macrophage uptake. In clinical trials, Doxil® exhibited a longer half-life (2-3 days) compared to free doxorubicin (around 10 hours), and 4- to 16-fold increase of doxorubicin accumulation in tumours (Wang *et al.*, 2013; Anselmo and Mitragotri, 2014; Weissig *et al.*, 2014). Importantly, Doxil® also has a better toxicity profile, with reduced alopecia, nausea, vomiting, myelosuppression, mucocutaneous toxicity, and more importantly, decreased cardiotoxicity, compared to that of doxorubicin solution (Cagel *et al.*, 2017; Zhao *et al.*, 2018). The successful translation from research to clinical use of Doxil® led to the rapid development of traditional anti-cancer drugs into liposomal systems. Some of them are available in the market, such as Myocet® (non-PEGylated liposomal doxorubicin), DaunoXome® (liposomal daunorubicin), DepoCyt® (liposomal cytarabine) and AmBisome® (liposomal amphotericin B) (Slingerland *et al.*, 2012; Weissig *et al.*, 2014).
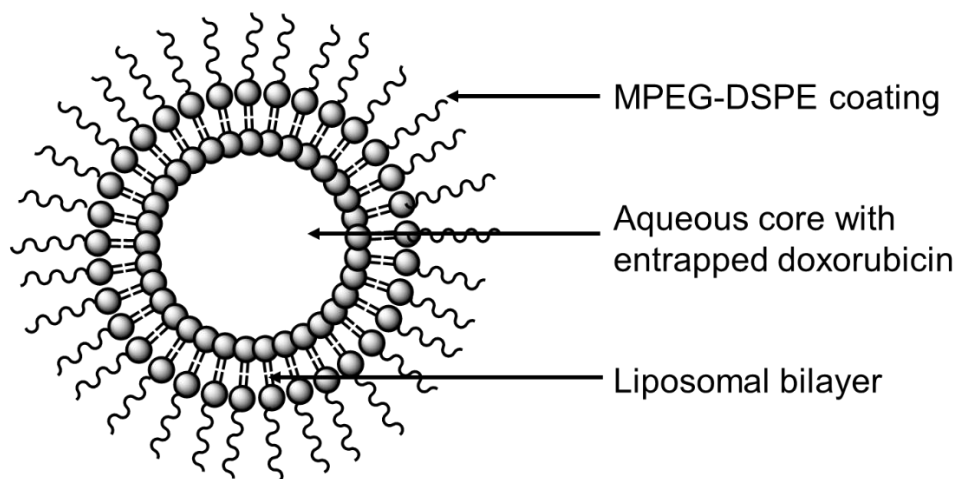
Figure 1-9: Liposome structure of Doxil[®]

However, some problems still exist regarding the clinical translation of nanomedicines. For instance, two adverse reactions that were rarely found with doxorubicin solution were observed in Doxil[®]. The first one is a grade 2 or 3 radiation dermatitis called palmar-plantar erythrodysesthesia, or hand-foot syndrome, which corresponds to redness, tenderness and peeling of the skin. This toxicity resulted from the accumulation of Doxil[®] in the skin due to its long circulation property (Solomon and Gabizon, 2008; Barenholz, 2012). The second one is an infusion-related reaction, such as flushing and shortness of breath. This acute hypersensitivity immune reaction is called complement activation-related pseudo-allergy, and results from the treatment with several cancer nanomedicines, including Doxil[®]. However, this issue can be solved by reducing the infusion rate and by premedication with antihistamines and corticosteroids (Barenholz, 2012; Doessegger and Banholzer, 2015).

To improve the performance while minimising the side effects and distribution of nanocarriers to healthy tissues, several strategies and advanced functionalities of nanomedicine platforms (i.e. use of targeted ligands and triggered release of the drug) have been used to modify the physico-chemical properties of nanomedicines and their

interactions with the human body (**Figure 1-10**) (Wicki *et al.*, 2015). Some of these nanomedicines have been commercialised, such as lipid-based nanocarriers (Marqibo® and Mepact®), polymer-based nanocarriers (Eligard® and Genexol®), protein–drug conjugates (Abraxane®, Kadcyla® Mylotarg® and Ontak®) and inorganic nanoparticles (NanoTherm®) (Weissig *et al.*, 2014; Wicki *et al.*, 2015). To date, 50 nanomedicines have been approved by the FDA and are available on the market for a wide range of indications (Ventola, 2017) (**Figure 1-11**). So far, 2,723 nanomedicine formulations are currently registered for clinical trials on ClinicalTrials.gov (search terms 'liposome'/ 'nanoparticle'/ 'micelle') (ClinicalTrials.gov, 2019).
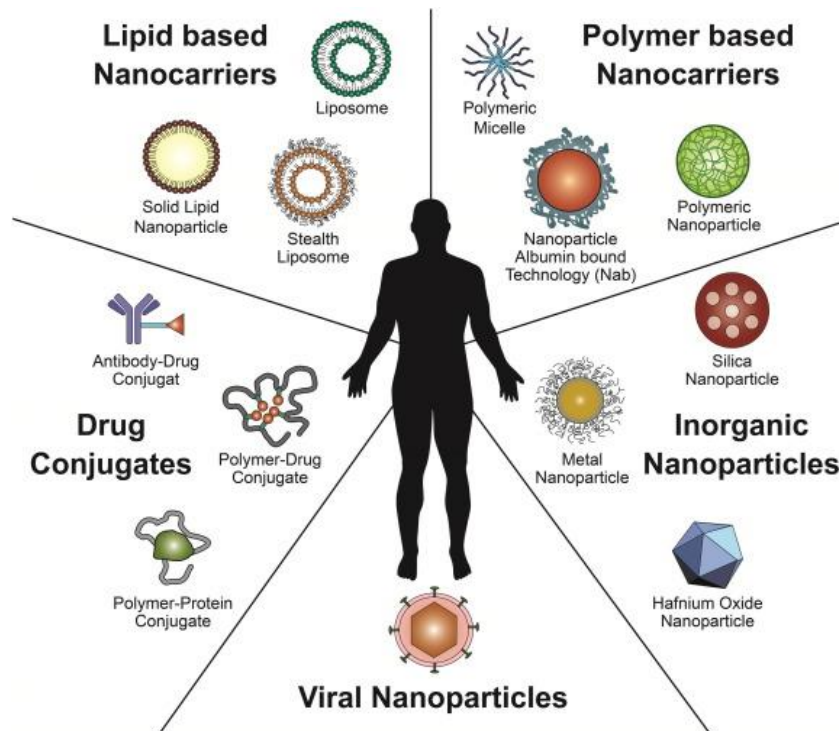
Figure 1-10: Schematic illustration of nanomedicine-based delivery systems (adapted from Wicki *et al.*, 2015)
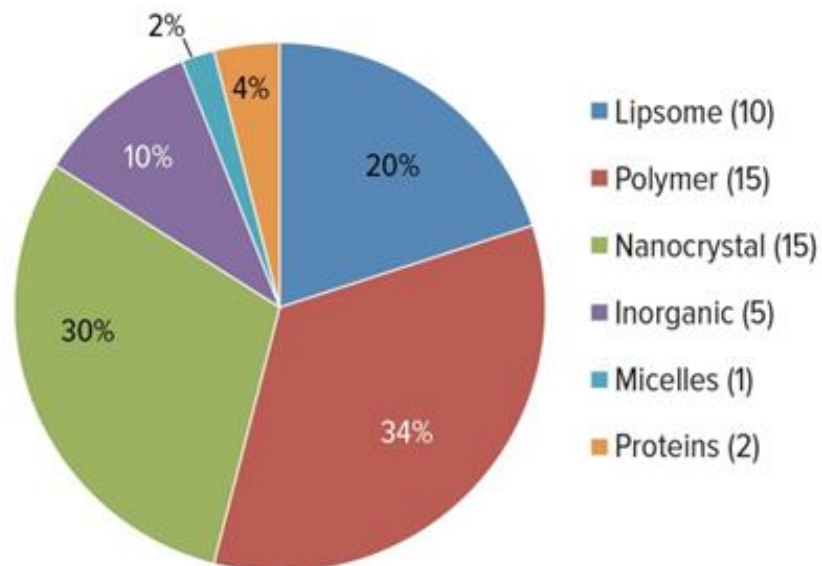
Figure 1-11: Types of nanomedicines approved by the FDA for clinical use (adapted from Ventola, 2017)

1.3.2 Biological barriers to nanomedicines

Nanomedicines have emerged as a promising strategy to overcome the limitations of conventional chemotherapy, such as poor water solubility, non-specific tissue distribution, systemic toxicity, rapid clearance and low therapeutic index (Sun *et al.*, 2014). However, the nanocarriers have to overcome numerous biological barriers before they can specifically reach tumour sites and achieve their therapeutic effects. These complex obstacles include opsonisation and recognition by the mononuclear phagocyte system (MPS), non-specific distribution, haemorheological limitations, intratumoral pressure, cell membrane internalisation/endosomal escape and multiple drug resistance via drug efflux pumps (**Figure 1-12**) (Barua and Mitragotri, 2014; Sriraman *et al.*, 2014; Blanco *et al.*, 2015).
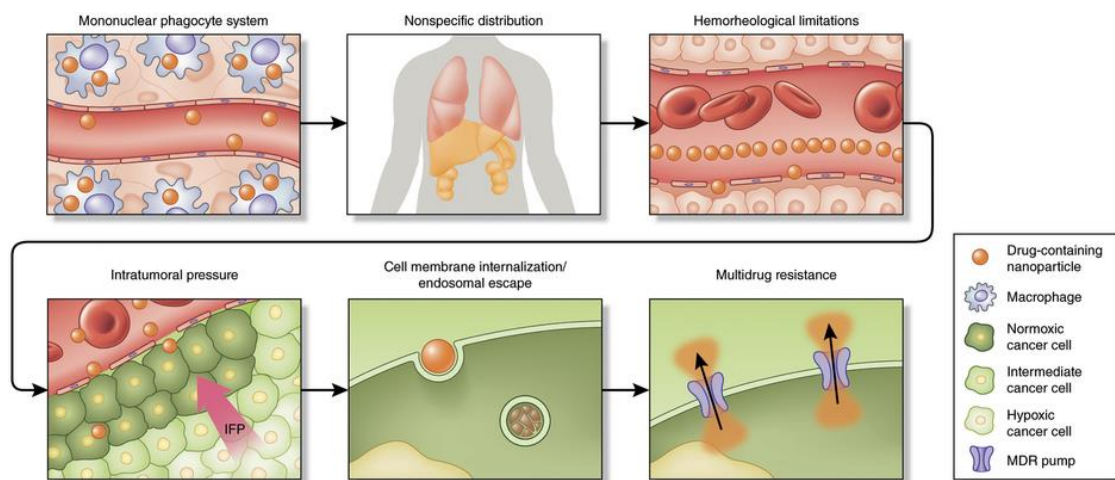
Figure 1-12: Framework of sequential biological barriers to nanomedicine-based drug delivery (adapted from Blanco *et al.,* 2015)

Generally, nanomedicines for cancer treatment are administrated by intravenous injection (Sriraman *et al.*, 2014; Sun *et al.*, 2014). Once they have reached the systemic circulation, they are subjected to rapid sequestration by the MPS. The sequestration process begins

36

with opsonisation of nanocarriers by adsorption of plasma proteins (opsonins), such as albumin, fibrinogen, apolipoproteins, immunoglobulins, as well as complement components, onto their surface to form the protein corona. After opsonisation, the protein corona may trigger recognition of nanomedicines by the MPS, and readily undergo phagocytosis by phagocytic cells as well as predominantly resident macrophages in the spleen, lymph nodes and liver (Sriraman *et al.*, 2014; Blanco *et al.*, 2015). Several studies have demonstrated that the formation of nanocarrier-protein corona complex depended on the size, shape, charge and surface properties of nanocarriers, and the MPS is responsible for the clearance of most nanoparticles larger than 10 nm (Sun *et al.*, 2014). Another significant barrier is the vascular endothelial layer, along with the glycocalyx coat, which represents a semi-permeable layer to control solutes and macromolecules across the blood vessels. Generally, particles larger than 5 nm cannot cross tight inter-endothelial junctions of the normal vasculature. Moreover, the negative charge of glycocalyx coat layer can interact with cationic particles, resulting in preventing them from extravasation into tissues (Sriraman *et al.*, 2014).

Following extravasation, the nanoparticles have to navigate through the tumour microenvironment (TME) to reach cancer cells. The main characteristics of TME, such as abnormal tumour vasculature, abnormal extracellular matrix (ECM) and high interstitial fluid pressure (IFP), have been recognised as the key features for cancer progression, invasion, metastasis and drug resistance (Tsai *et al.*, 2014; Khawar *et al.*, 2015). Although the enhanced permeability and retention (EPR) effect is associated with leaky vasculature and leads to accumulation of nanomedicines, it can be negated by the irregularity of tumour vessels (Sriraman *et al.*, 2014). The diameter, length, shape and networks of tumour vessels are highly heterogeneous, which results in turbulence flow, decreased blood flow, and subsequently hypoxia and acidic pH (~6.8) in tumours (Tozer

et al., 2005; Blanco *et al.*, 2015; Klemm and Joyce, 2015). It has been demonstrated that hypoxia contributed to chemoresistance to anti-cancer drugs such as etoposide, cisplatin, anthracyclines, paclitaxel, mitoxantrone and topotecan (Shannon *et al.*, 2005; Sriraman *et al.*, 2014). In addition, nanomedicines are able to cross the ECM, which is composed of a cross-linked network of collagen, fibronectin, elastin fibres and proteoglycans. A highly developed ECM may result in high tumour rigidity and high IFP (Sriraman *et al.*, 2014). These characteristics counteract the transportation of nanomedicines and substantially decrease the delivery of chemotherapeutic drugs to target regions (Blanco *et al.*, 2015).

For tumour target cells, nanocarriers are expected to deliver drugs upon cellular internalisation (Sriraman *et al.*, 2014). Normally, small or hydrophobic drugs can enter the cells by simple diffusion (Blanco *et al.*, 2015), while nanomedicines require active transport via endocytosis, which is classified into two major pathways: phagocytosis and pinocytosis (**Figure 1-13**) (Kou *et al.*, 2013). However, the endocytosis of nanomedicines may result in trafficking to a non-target organelle. For example, the nanomedicines entrapped in intracellular vesicles (phagosomes, macropinosomes and endosomes) can fuse with lysosomes that can degrade their payloads due to their highly acidic environment and lysosomal enzymes (Sriraman *et al.*, 2014; Blanco *et al.*, 2015).
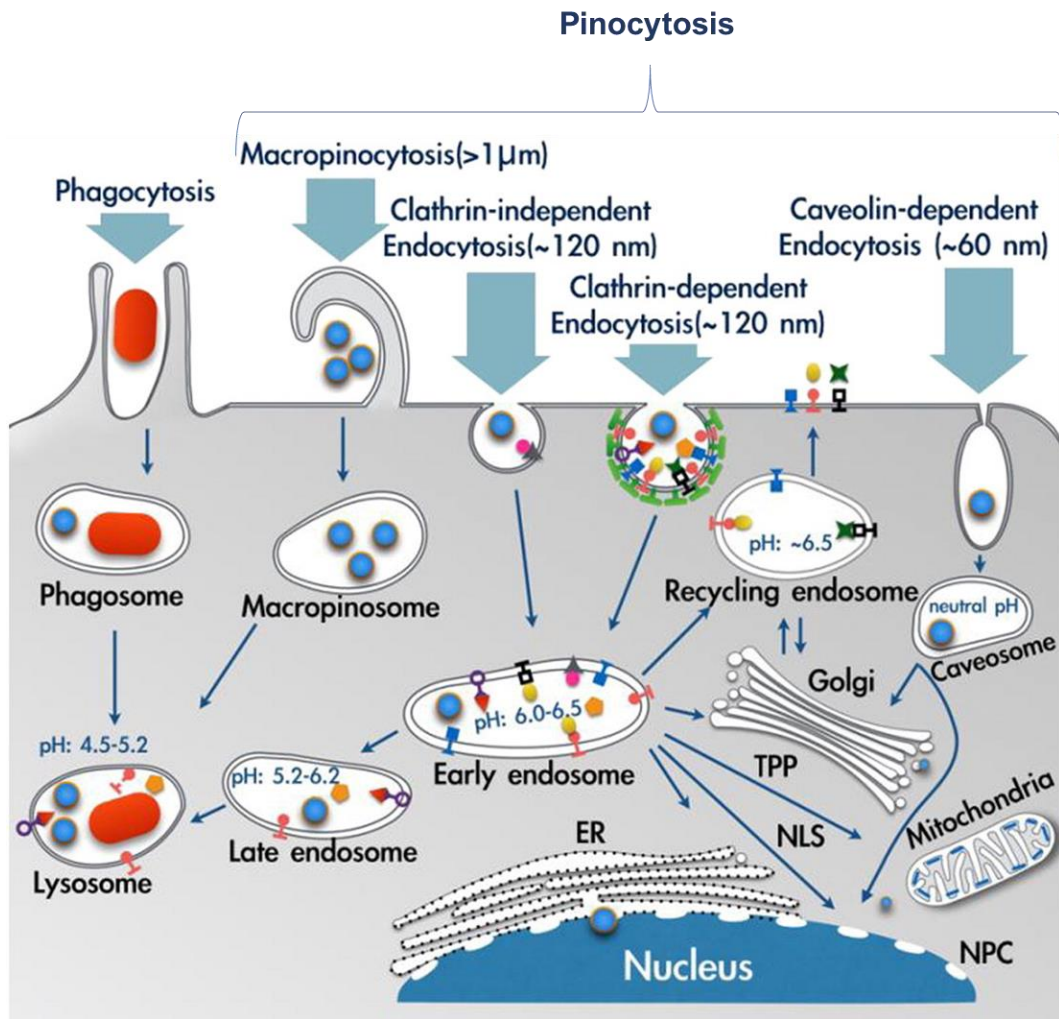
Figure 1-13: Summary of cellular internalisation pathways of nanocarriers (adapted from Yameen *et al.*, 2014)

Although nanocarriers can enter the tumour cells and release the chemotherapeutic agents they carry, they may be eliminated from the cells by the efflux action of ATP-dependent transporters, such as P-glycoprotein (P-gp) and multidrug resistance-associated protein 1 (MRP1). These transporters are members of the superfamily of ATP-binding cassette transporters that are overexpressed on cancer cells and are involved in MDR. One key consequence from MDR is the failure of treatment as well as the toxicity to healthy cells (Blanco *et al.*, 2015).

1.3.3 Types of nanocarriers

1.3.3.1 Liposomes (Lipid-based vesicles)

Liposomes are lipid bilayer-based nanovesicles formed by self-assembly of amphiphilic lipids (such as phospholipids) by continuous parallel packing of hydrophobic tails, with hydrophilic head groups pointing towards the aqueous phase (**Figure 1-14**). This bilayer structure allowed hydrophilic solutes to be encapsulated in the inner cavity while hydrophobic solutes can be incorporated into the hydrophobic layer (Alexis *et al.*, 2010; Kalra and Bally, 2013). Liposomes can range from 50 nm to larger than 1 µm, depending on the types of vesicles: multilamellar vesicles (MLVs, ranging from 500 to 5 000 nm), large unilamellar vesicles (LUVs, ranging from 200 to 800 nm) and small unilamellar vesicles (SUVs, around 100 nm or smaller). In addition, the encapsulation efficacy and release of drugs from vesicles rely on lipid composition, preparation methods and size and surface charge characteristics (Torchilin, 2010). Liposomes have become important delivery systems in drug development since their discovery by Alec Bangham in 1965 (Bangham *et al.*, 1964; Bangham *et al.*, 1965; Barenholz and Peer, 2012). They are biocompatible, biodegradable, cause no or very little allergic and toxic reactions, while protecting encapsulated drugs from physiological environments (Torchilin, 2010). Liposomes have already been studied for the entrapment of plumbagin. For example, Tiwari and co-workers (2002) prepared temperature-sensitive liposomes loaded with plumbagin for the treatment of melanoma. These liposomes encapsulated about 19% of plumbagin, with particle size ranging from 62 nm to 192 nm. *In vitro*, 51% of plumbagin was released from these liposomes at 42°C, while only 9% was released at 37°C. Moreover, the intravenous administration of these liposomes combined with localised hyperthermia (43°C for 30 min or 1 h) has been shown to slow down the growth of subcutaneous B16F1 tumours in mice, compared to that observed in animals treated with

free plumbagin solution (with or without hyperthermia). In another study, Kumar and colleagues (2011) have prepared PEGylated liposomes entrapping plumbagin, which showed sustained release of the drug (with a cumulative drug release of 58.27 ± 3.42 % in 24 h). Following intravenous administration, these liposomes significantly delayed tumour growth of B16F1 melanoma without any sign of tissue toxicity, unlike free plumbagin.

Although liposomes have many advantages, some problems still exist. For example, they are less stable, due to hydrolysis of their fatty acids and peroxidation of their unsaturated lipids, and have therefore a limited half-life and high leakage of encapsulated drugs. Adding cholesterol as a stabiliser in liposomes formulation has been shown to improve their stability (Anderson and Omri, 2004). Upon intravenous administration, liposomes are rapidly opsonised and sequestered by the reticuloendothelial system (RES), mainly from Kupffer cells in liver within 15–30 min, which decreases their circulation half-life and accumulation of drugs in the target cells (Torchilin, 2010; Briuglia *et al.*, 2015). One key strategy to increase the efficacy of liposomes is targeting, by modifying their surface with targeting moieties such as small ligands, peptides and monoclonal antibodies. These can improve systemic circulation, enhance drug accumulation at specific sites, and increase specific cellular internalisation (Deshpande *et al.*, 2013).
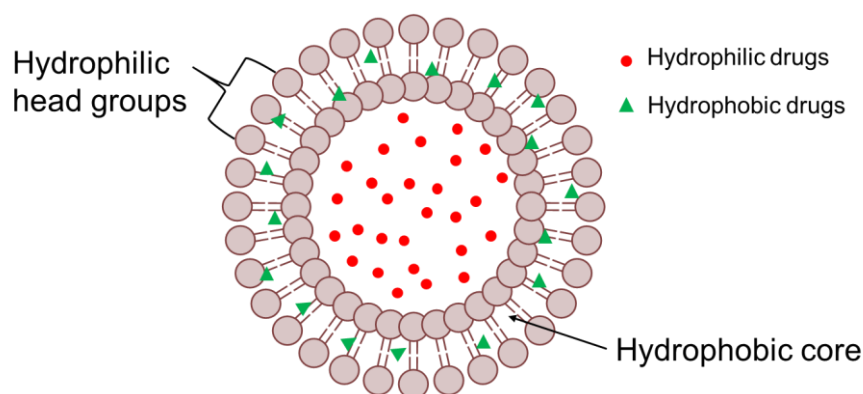
Figure 1-14: Structure of liposomes

1.3.3.2 Niosomes (Non-ionic surfactant-based vesicles)

Niosomes have been developed as an alternative vesicular delivery system analogue to liposomes, by using non-ionic surfactants instead of phospholipids (**Figure 1-15**). They offer several advantages over liposomes, for example higher stability, longer shelf-life, cost-effectiveness and large-scale production (Uchegbu and Vyas, 1998; Sahin, 2007). They are formed by self-assembly of non-ionic amphiphilic surfactants with some input of energy, such as physical agitation or heat (Uchegbu and Vyas, 1998; Sahin, 2007; Marianecci *et al.*, 2013). Several categories of non-ionic surfactants, such as alkyl esters, alkyl amides, alkyl ethers (Brij®) and fatty acid esters (Tween® and Span®), can be used to prepare niosomes (Marianecci *et al.*, 2013).

Niosomes have attracted a lot of attention for delivering drugs, due to their biocompatibility, biodegradability, low immunogenicity and low toxicity. Moreover, they can encapsulate a wide range of hydrophilic and hydrophobic drugs, including genes, proteins and vaccines, to treat many diseases (Moghassemi and Hadjizadeh, 2014). For example, transferrin-bearing niosomes encapsulating tocotrienol-rich fraction (TRF) improved cellular uptake (~3-fold) and *in vitro* cytotoxicity (more than 100-fold) against A431 epidermoid carcinoma, T98G glioblastoma and A2780 ovarian carcinoma, compared to TRF solution (Fu *et al.*, 2009). Shaker and colleagues (2015) developed niosomes loaded with tamoxifen, that exhibited high cytotoxicity against MCF-7 breast cancer cells, both *in vitro* and *in vivo*. In case of plumbagin, Naresh and colleagues (1996) developed niosomes loaded with plumbagin, which slowed the growth rate of sarcoma-180 and Ehrlich ascites tumours in BALB/c mice as compared with the drug solution. Oommen and co-workers (1999) prepared niosomes encapsulating plumbagin-beta cyclodextrin complex, with high entrapment efficiency of the drug complex (74%). The subcutaneous injection of niosomes loaded with plumbagin-beta cyclodextrin complex

was able to delay the tumour growth of B16F1 compared with free plumbagin or plumbagin complex in mice. These indicated that niosomes can be used as promising nanocarriers for delivery of plumbagin.
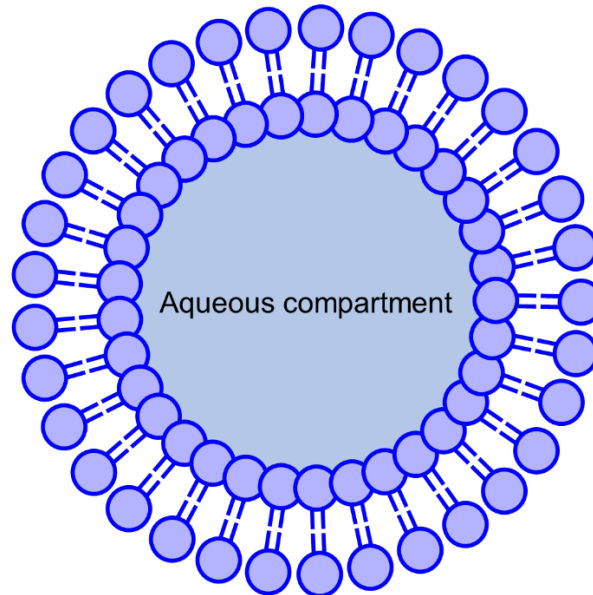
Figure 1-15: Structure of niosomes

1.3.3.3 Polymeric nanoparticles

Polymeric nanoparticles are one of the most extensively explored nanocarriers for cancer diagnosis and treatment, because of their biodegradability and biocompatibility (Faraji and Wipf, 2009; Patravale *et al.*, 2012). Generally, the structure of polymeric nanoparticles can be categorised as nanospheres (matrix particles), for which the payload is adsorbed on the surface or encapsulated inside the particle, and nanocapsules, for which drugs are entrapped into the cavity (**Figure 1-16**) (Rao and Geckeler, 2011). Such nanoparticles can be derived from both natural and synthetic polymers such as chitosan, gelatine, collagen, dextran, poly(lactic acid) (PLA) and poly(lactic *co*-glycolic acid) PLGA, poly(alkylcyanoacrylate), poly(methylmethacrylate), and poly(butyl)-cyanoacrylate (Peer *et al.*, 2007; Faraji and Wipf, 2009; Uchegbu *et al.*, 2013).

Furthermore, the physico-chemical properties of these polymers (molecular weight, dispersity index or hydrophobicity), as well as size and shape of the polymeric nanoparticles, also play an important role in their efficacy (Alexis *et al.*, 2010; Patravale *et al.*, 2012). Currently, several polymeric nanoparticles are in pre-clinical and clinical trial phases (Alexis *et al.*, 2010). Plumbagin has already been formulated as polymeric nanoparticles. For example, Pan and colleagues (2017) developed aptamer-targeted PLGA-PEG nanoparticles entrapping plumbagin. This formulation increased the anti-proliferative activity of plumbagin *in vitro*, with a drug concentration needed for growth inhibition of 50% of cell population (IC_{50}) of 4.8± 0.8 μM, which is lower than that of non-targeted nanoparticles (IC_{50} of 10.3 ± 2.5 μM).

Unfortunately, polymeric nanoparticles generally have some pitfalls, such as poor drug loading, high particle size variation (due to inherent structural heterogeneity of polymers), aggregation and toxicity (related to an increase in molecular weight of polymers) (Peer *et al.*, 2007; Danhier *et al.*, 2012).
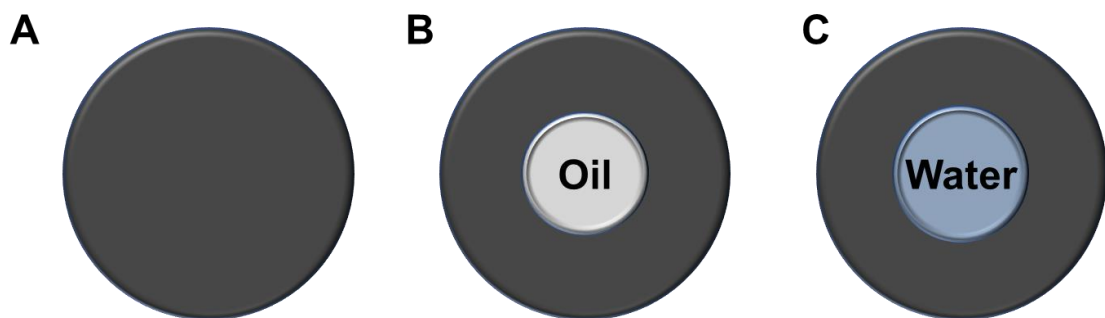
Figure 1-16: Various categories of polymeric nanoparticles: (A) nanospheres, (B) nanocapsules containing oil and (C) nanocapsules containing water

1.3.3.4 Micelles

Micelles are supramolecular core-shell nanostructures (10-100 nm) that are composed of surfactants or amphiphilic block copolymers. They can spontaneously self-assemble as lipid monolayers with a hydrophobic core and a hydrophilic shell (**Figure 1-17**) (Peer *et al.*, 2007; Jhaveri and Torchilin, 2014). Such self-assembly occurs by hydrophobic interactions between the amphiphilic molecules above their critical micelle concentration (CMC) and critical micelle temperature (CMT) in aqueous solution (Patravale *et al.*, 2012). The micelle structure allows non-polar drugs to be encapsulated in the hydrophobic core, polar drugs to be adsorbed on the surface of hydrophilic micelles, while drugs with intermediate polarity distribute along amphiphilic molecules (Jhaveri and Torchilin, 2014). Micelles possess several advantages for drug delivery applications in cancer, such as increased solubility, enhanced drug bioavailability and reduced side effects. For example, Pawar and colleagues (2016) developed folic acid-conjugated D-α-tocopheryl polyethylene glycol 1000 succinate nanomicelles entrappig plumbagin, which enhanced bioavailability, stability and cytotoxic activity of the drug compared with the solution. In addition, Bothiraja and colleagues (2013) prepared plumbagin-loaded phospholipid–Tween® 80 mixed micelles, which demonstrated a sustained release of the drug and resulted in a 2.1-fold enhancement of its cytotoxic activity against MCF-7 breast cancer cells *in vitro*.

However, upon intravenous injection, one of the major drawbacks of micelles is that the concentration of micelles is often diluted below their CMC, resulting in their disruption and loss of efficacy (Moghimi *et al.*, 2001).

(A) Micelles   (B) Polymeric micelles
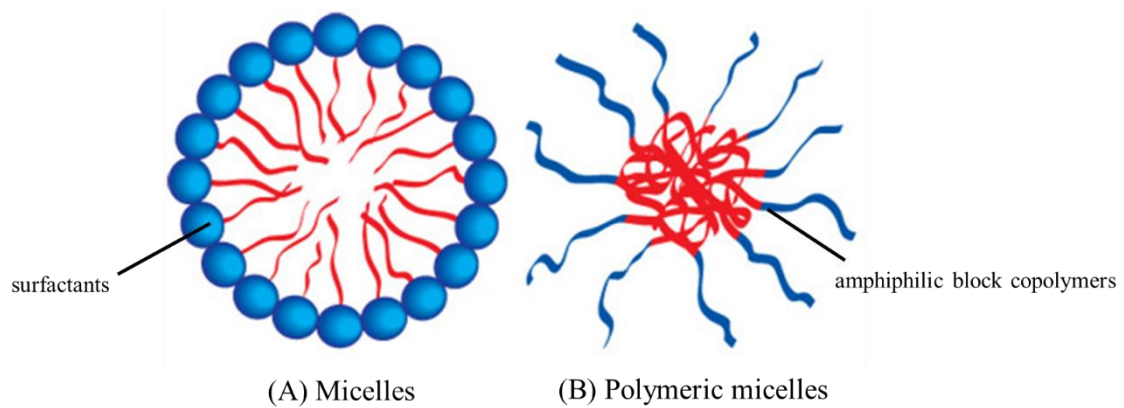
Figure 1-17: Self-assembled structures of (A) micelles (composed of surfactants) and (B) polymeric micelles (composed of amphiphilic block copolymers) in aqueous solution (adapted from Husseini and Pitt, 2008)

1.3.3.5 Solid lipid nanoparticles

Solid lipid nanoparticles (SLN) are particles ranging in size from 50 to 1000 nm. They are generally composed of surfactants (i.e. lecithin, polysorbate 80, poloxamer 188, sodium glycocholate) and physiological/biodegradable lipids that are solid at body and room temperatures (i.e. glycerides, fatty acids, PEGylated lipids, steroids and waxes) (Müller *et al.*, 2000; Souto *et al.*, 2013). In the literature, three models for drug incorporation within SLN are described, depending on the presence of surfactants, solubility of drugs, miscibility of drug-lipid and drugs-lipids ratio (**Figure 1-18**) (Müller *et al.*, 2000). SLN have been developed since 1990s to overcome the main drawbacks of polymeric nanoparticles and liposomes (Torchilin, 2006; Souto *et al.*, 2013). Compared to liposomes, SLN are more stable due to the solid structure of their lipid matrix (Faraji and Wipf, 2009). The main characteristics of SLN are their excellent physical stability, protection of incorporated drugs from degradation, controlled release of the drug (depending on the incorporation model), low toxicity and site-specific targeting (Wissing *et al.*, 2004). SLN can be used for various administration routes such as oral, dermal,

ocular, pulmonary, rectal and intravenous administration (Souto *et al.*, 2013). For example, Videira and co-workers (2012) developed solid lipid nanoparticles entrapping paclitaxel which showed anti-tumour effect in preclinical study towards the decrease of the number and size of lung metastases. It also reduced the systemic toxicity and increased the therapeutic index of paclitaxel.

However, SLN face limitations, such as low drug loading capacity and drug expulsion during storage due to lipid phase transitions (Kaur and Slavcev, 2013; Souto *et al.*, 2013). Such problems led to development of second-generation lipid nanoparticles, called nanostructured lipid carriers (NLC), which are thermodynamically stable with low lipid crystallinity (Tamjidi *et al.*, 2013).
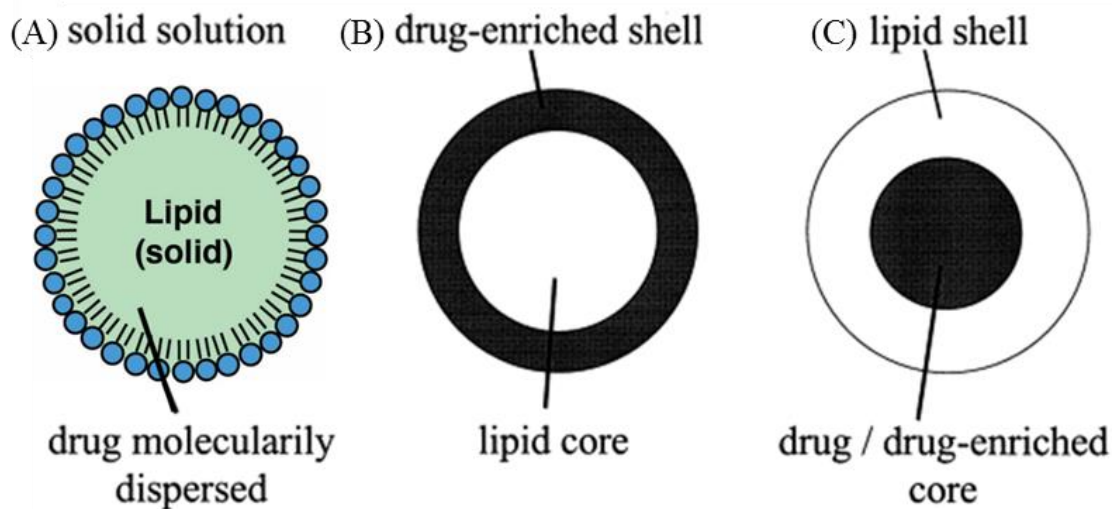
Figure 1-18: Different morphological types of SLNs: (A) solid solution model (homogenous matrix), (B) drug-enriched shell model and (C) drug-enriched core model (adapted from Müller *et al.*, 2000; Kakadia and Conway, 2014)

1.4 Drug targeting

In general, the specificity and activity of drugs towards disease depend on their ability to interfere with local pathological processes or defective biological pathways. Once intravenously administered, drugs are distributed throughout the whole body, proportionally to the regional blood flow (Torchilin, 2010). Moreover, they have to cross many biological barriers, such as the mononuclear phagocyte system and tumour microenvironment, which often result in drug inactivation and elimination or cause side effects, not to mention the need of high dose administration to achieve the therapeutic concentration (Torchilin, 2010).

Over a century ago, the concept of drug targeting, which was referred to as a "magic bullet", was introduced by Paul Ehrlich (Strebhardt and Ullrich, 2008). He postulated that "if a compound could be made that selectively targets a disease-causing organism, then a toxin for that organism (in patients) could be delivered along with the agent of selectivity" (Ho and Chien, 2014). This concept led to the development of targeting therapy in many diseases, including cancer. Drug targeting can be described as "passive" or "active" (**Figure 1-19**). Passive targeting is based on intrinsic factors, such as physico-chemical properties of drugs and drug carriers, and physiological characteristics of the target area. Active targeting relies on the intrinsic factors of the targeting moiety or ligand (Schätzlein, 2003).
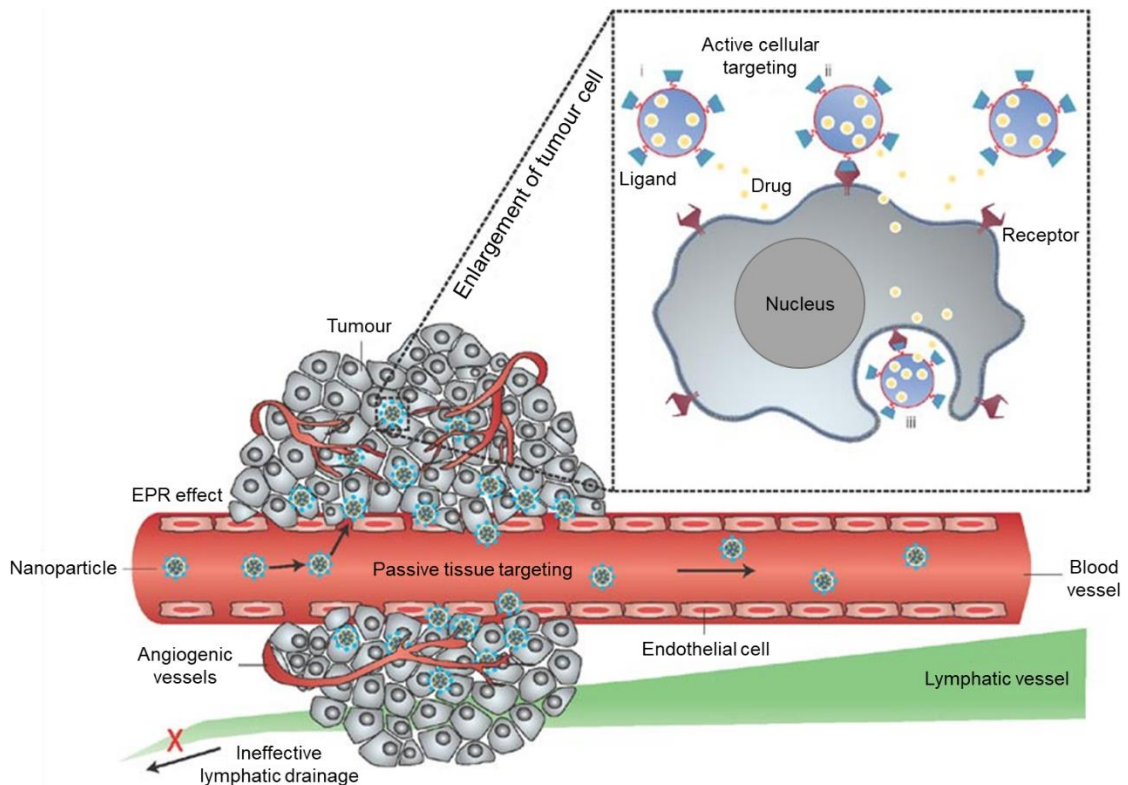
Figure 1-19: Delivery of passive and active targeting nanocarriers to tumours (adapted from Peer *et al.*, 2007)

1.4.1 Passive targeting

The theory of passive targeting is based on the pathophysiological properties and microenvironment of the tumour, as well as the physico-chemical properties of the drug delivery systems (Bazak *et al.*, 2014; Wicki *et al.*, 2015). Under pathological conditions such as infection, inflammation and cancer, the vascular endothelium tends to become more permeable due to fenestrations in its vasculature. This leaky vascular endothelium allows the extravasation and accumulation of nanocarriers (usually less than 400 nm in size) in tumours by convection and diffusion processes without specific targeting moieties. This unique phenomenon, called the enhanced permeability and retention (EPR) effect, was discovered by Matsumura and Maeda in 1986 (Matsumura and Maeda, 1986; Maeda *et al.*, 2000). However, the EPR effect does not apply to low molecular

weight drugs due to their rapid diffusion back into circulating blood and their elimination from the circulation by renal clearance (Maeda *et al.*, 2000).

In order to achieve optimal tissue accumulation via the EPR effect, nanocarriers should demonstrate the long-circulating ability in the bloodstream to provide a sufficient time for target accumulation (Deshpande *et al.*, 2013). They should have the ability to hide from the recognition of the MPS, which is largely determined by their physico-chemical properties such as particle size and surface charge. Nanoparticles with a size less than 200 nm are demonstrated to be less susceptible to MPS recognition (Hoshyar *et al.*, 2016). Moreover, the surface charge of nanoparticles should be neutral or anionic for efficient evasion from the renal clearance (Danhier e*t al.*, 2010). One of the key strategies to prolong blood circulating of nanoparticles is the surface modification by conjugating their surface with water-soluble polymers such as polyethylene glycol (PEG) (Torchilin, 2010).

However, even when passively targeted, anti-cancer drugs can still lead to side effects on healthy tissues. These side effects are caused by non-selective accumulation of nanoparticles in healthy organs with fenestrated endothelium, such as the liver and spleen (Wicki *et al.*, 2015). To overcome this limitation, the conjugation of active targeting to nanoparticles is a promising strategy to improve selectivity and increase efficacy while reducing toxicity of the drugs (Peer *et al.*, 2007; Wicki *et al.*, 2015).

1.4.2 Active targeting

Active targeting strategy is performed by conjugating the surface of nanoparticles with targeting ligands able to recognise their receptors on the target cells. The targeting ligands can be antibodies, proteins, peptides, sugars, lipoproteins and nucleic acids (Bertrand *et al.*, 2014; Pattni and Torchilin, 2015). The aim of active targeting is not only to increase

tumour accumulation of nanoparticles but also to enhance their cellular internalisation via receptor-mediated endocytosis. The efficiency of active targeting nanoparticles is dependent upon a variety of factors, such as the overexpression of specific receptors on the surface of target cells compared to non-target cells, the binding affinity of targeting ligands to receptors as well as the uptake of the nanoparticles (Danhier e*t al.*, 2010). For effective active targeting, Yeo (2013) suggested that the density of target receptors should be in the range of 10^4 or 10^5 copies per cell. Moreover, multivalence ligands can further enhance the binding affinity and specificity of the ligand to the receptor of target cells (Chittasupho, 2012).

Although the active targeting strategy has the potential to improve the delivery of payloads to target cells, some problems still remain. For example, ligand-bearing nanoparticles may lose their specificity after entering in biological fluids as a result of the corona formation with serum proteins (Durymanov *et al.*, 2015). Furthermore, in solid tumours, high affinity binding of the ligands to the receptors can decrease the internalisation of nanoparticles due to the "binding site barrier" effect (molecules with high affinities have restricted penetration inside the tumour mass) (Peer *et al.*, 2007; Yeo, 2013). To date, several targeting ligands have been investigated as a promising strategy to deliver therapeutic compounds to cancer cells such as folic acid, albumin, aptamer, biotin, hyaluronic acid, monoclonal antibodies, peptides and proteins, including transferrin which was selected as a targeting ligand in this study (Pérez-Herrero and Fernández-Medarde, 2015).

1.4.2.1 Transferrin

Transferrin (Tf) is a family of iron-binding proteins with a primary function of serum iron transportation. Tf monomer comprises of 678-800 amino acid residues with molecular weight about 78-80 kDa. Tf molecule is divided into two homologous domains known as the N-lobe and the C-lobe linked by a short spacer sequence (MacGillivray *et al.*, 1982; Daniels *et al.*, 2006b; Tortorella and Karagiannis, 2014). Free Tf molecule (apo-Tf) is capable of binding one or two iron atoms (monoferric Tf or diferric Tf). Diferric Tf (holo-Tf) exhibits higher binding affinity to the receptor compared to monoferric Tf (~30-fold higher) and apo-Tf (up to 500-fold higher) (Daniels *et al.*, 2006b). There are two types of Tf receptors (TfR), Tf receptors 1 (TfR1) and Tf receptors 2 (TfR2). The first one is Tf receptors 1 (TfR1), which is ubiquitously expressed in most proliferating cells. The second is Tf receptors 2 (TfR2) (45–66 % similarity to TfR1), which is overexpressed in hepatocytes but has 25-fold lower affinity to Tf compared with TfR1. The cellular uptake of iron mediated by Tf-TfR complex depends on clathrin-mediated endocytosis, which recycles TfR back to the cell surface (Tortorella and Karagiannis, 2014) (**Figure 1-20**).
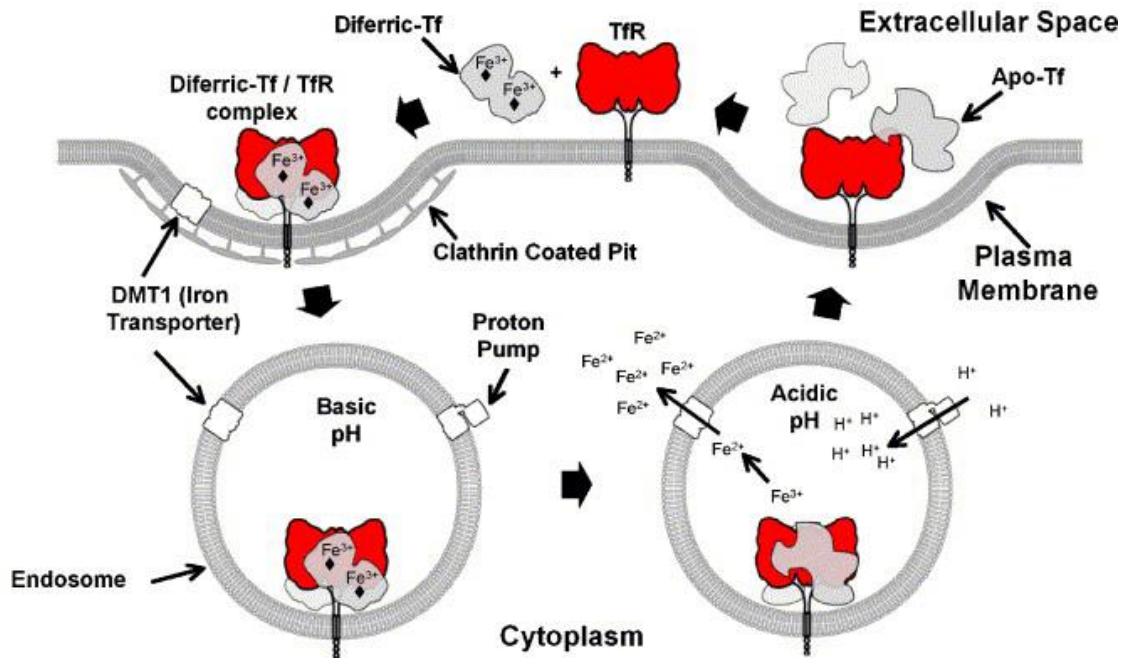
Figure 1-20: Mechanism of cellular uptake of iron via Tf- TfR complex upon clathrin-mediated endocytosis (adapted from Daniels *et al.*, 2006b)

The Tf-TfR complex pathway has been exploited as an active targeting strategy to deliver chemotherapeutic agents into cancer cells due to the overexpression of TfR (up to 100-fold) (Daniels *et al.*, 2006a) on various types of tumours such as pancreatic, colon, lung, bladder (Peer *et al.*, 2007), lymphomas and breast cancer (Thanki *et al.*, 2015). Direct conjugation of Tf to liposomes and niosomes improved drug internalisation and therapeutic outcome both *in vitro* and *in vivo* while reducing adverse effects (Peer *et al.*, 2007). For example, Li and colleagues (2009) developed Tf-bearing stealth liposomes loading doxorubicin, which enhanced cellular uptake, improved pharmacokinetic, biodistribution and therapeutic effects of the drug in HepG2 cancer cells. Zhai *et al.* (2010) reported a 3.6-fold increase in the cytotoxicity of the Tf-conjugated liposomes loading docetaxel against KB cells compared to non-targeted liposomes. An increase in anti-tumour activity of oxaliplatin was also found when encapsulated in Tf-bearing PEGylated liposomes compared to non-targeted liposomes and drug solution (Suzuki *et*

al., 2008). When using Tf-bearing niosomes, Dufès *et al.* (2000) showed an increased intracellular uptake of FITC-dextran in A431 cells compared with plain niosomes (90% versus 74%). Tf-conjugated pluronic niosomes loading doxorubicin also achieved cellular uptake and anti-cancer activity against MCF-7 and MDA-MB-231 human breast cancer cell lines (Tavano *et al.* 2013). Similar results were recently obtained with Tf-targeted niosomes entrapping tocotrienol, with 2.5-fold increment in drug uptake and 2-fold enhancement in cytotoxic effect in human breast cancer cells (Fu *et al.* 2016).

Our research group have previously prepared transferrin-conjugated vesicles entrapping the green tea polyphenol epigallocatechin gallate (EGCG) and tocotrienol that shared the same delivery issues as plumbagin. These targeted vesicles significantly increased the cellular uptake and anti-proliferative activity of the drugs in comparison with control vesicles and drug solution for all the tested cancer cell lines. This resulted in complete tumour suppression of respectively 40% and 60% of B16-F10 melanoma following intravenous injection of EGCG-loaded and tocotrienol-loaded vesicles over one month (Fu *et al*., 2009; Fu *et al*., 2011; Lemarié *et al*., 2013; Fu *et al*., 2014; Karim *et al*., 2017), thus highlighting the need of a tumour-targeted delivery system for delivering these compounds to their site of action.

However, it should be emphasised that the efficiency of active targeting of nanomedicines depends on several factors. Three major parameters have to be considered when designing optimally active targeting nanomedicines: (1) the target, (2) the nanocarrier, and (3) the targeting ligand (**Figure 1-21**) (Lopez and Lalatsa, 2013).
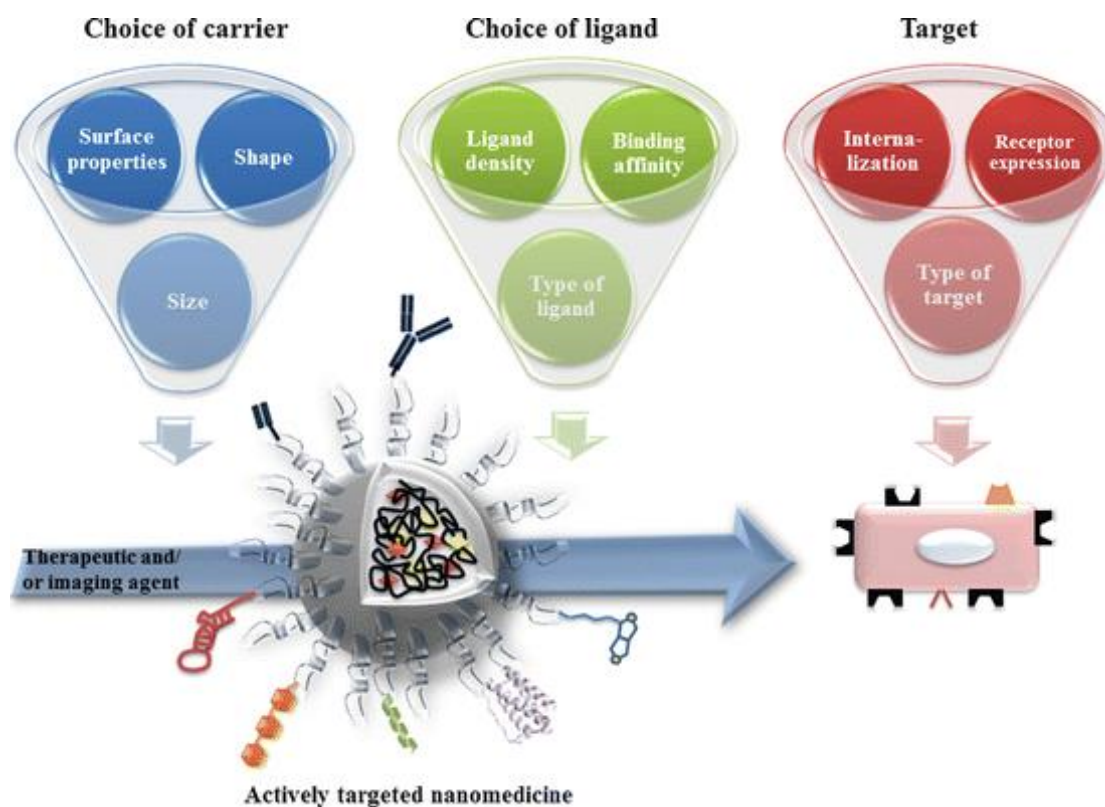
Figure 1-21: Parameters needed to optimise the active targeting of nanomedicines (adapted from Lopez and Lalatsa, 2013)

1.5 Aim and Objectives

Plumbagin, a naphthoquinone extracted from the official leadwort, has been shown to have promising anti-cancer properties *in vitro*. However, its therapeutic potential is hampered by its failure to specifically reach tumours at a therapeutic concentration after intravenous administration, without secondary effects on normal tissues. Its use is further limited by its poor aqueous solubility and its rapid elimination *in vivo*.

This drawback could be overcome by loading plumbagin within delivery systems that have the ability to entrap this lipophilic drug, improve its water solubility, prolong its blood circulation time and sustain its release over a period of time, thus lowering the frequency of administration and reducing the adverse effect of the drug. Moreover, conjugating the nanocarriers with transferrin as an active targeting ligand resulted in an enhanced cellular internalisation and improved therapeutic efficacy of the drugs.

The aim of this study is the development of various nanocarriers entrapping plumbagin and able to target cancers. We hypothesise that the entrapment of plumbagin within these novel nanocarriers conjugated with transferrin, whose receptors are overexpressed on many cancer cells, will significantly improve the therapeutic efficacy of plumbagin on cancer cells *in vitro* and *in vivo*.

The objectives of this study are therefore:

1. to develop and characterise novel transferrin-targeted nanocarriers entrapping plumbagin

2. to assess their cellular uptake, anti-proliferative and apoptosis efficacy on cancer cells *in vitro*

3. to evaluate their therapeutic efficacy *in vivo*, following intravenous administration to mice bearing tumours

CHAPTER 2

Preparation and characterisation of tumour-targeted nanomedicines entrapping plumbagin

2.1 Introduction

Plumbagin, a natural naphthoquinone mainly found in Plumbaginaceae plants, has been shown to have promising therapeutic efficacy against many types of cancer, including lung, liver, breast, prostate, colon cancers and melanoma (Checker *et al.*, 2018). It is well established that plumbagin exerts its anti-cancer effect through mechanisms such as generation of reactive oxygen species and depletion of intracellular glutathione, activation of p53, through suppression of AMPK, NF-kB, PI3K/Akt/mTOR, Ras, MAPK/ERK, VEGFR2, FOXM1, Wnt/β-catenin, Caspase 3, MMP2/9, STAT3 and JNK (Sandur *et al.*, 2006; Seshadri *et al.*, 2011; Lai *et al.*, 2012; Niu *et al.*, 2015; Pan *et al.*, 2015; Wang *et al.*, 2015; Xue *et al.*, 2016). This wide range of anti-cancer effects therefore makes plumbagin a very promising therapeutic molecule.

However, the therapeutic potential of plumbagin has been limited so far due to its poor solubility in water (79 μg/mL), high lipophilicity (log *P* 3.04), lack of stability (spontaneous sublimation in solid phase) and low oral bioavailability (less than 40%) (Hsieh *et al.*, 2006; Pawar *et al.*, 2016), which limited its biopharmaceutical applications. Furthermore, plumbagin failed to specifically reach tumours at a therapeutic concentration due to its lack of tumour specificity and rapid elimination, with a short biological half-life of 35.89 ± 7.95 min (Kumar *et al.*, 2011).

This drawback could be overcome by loading the drug within delivery systems that have the ability to entrap this lipophilic drug, improve its water solubility, prolong its blood circulation time and sustain its release over a period of time, thus lowering the frequency of administration and reducing the adverse effects of the drug. Moreover, nanocarriers can enhance plumbagin delivery to tumours via passive targeting using the EPR effect (Peer *et al.*, 2007; Bertrand *et al.*, 2014; Wicki *et al.*, 2015).

Liposomes have been extensively investigated and utilised as carriers for the delivery of pharmaceutically active agents since their discovery in mid-1960s (Marasini *et al*., 2017). They have been used to entrap many chemotherapeutic agents, owing to the advantages they confer to their cargo, such as increased drug solubility, stability and bioavailability, prolonged blood circulation time as well as enhanced therapeutic efficacy of drugs (Wakaskar, 2017). In addition, they are naturally non-toxic, non-immunogenic, biocompatible and biodegradable (Torchilin, 2010; Olusanya *et al*., 2018). Based on these properties, we hypothesise that liposomes would be suitable nanomedicines for the effective delivery of plumbagin to cancer cells.

Polymeric nanoparticles have become extensively used drug delivery systems for various substances such as vaccines, proteins, peptides and anti-cancer drugs (Dinarvand *et al*., 2011; Fredenberg *et al*., 2011; Sharma *et al*., 2016), due to the improvement of the physico-chemical properties of the drug they carry, such as increased solubility, bioavailability, protection from degradation and interaction with the biological environment, and controlled release (Kumari *et al*., 2010; Li *et al*., 2018). Among various polymers for nanoparticles preparation, polylactide-co-glycolide (PLGA) appears to be a particularly promising biomaterial, owing to its biocompatibility and biodegradability properties (Makadia and Siegel, 2011). This polymer has also been approved by the United States Food and Drug Administration (US FDA) and the European Medicines Agency (EMA) for application in humans due to its safety (Sharma *et al*., 2016). In addition, PEGylation of PLGA nanoparticles has been shown to increase drug payload, stability and circulation time, while escaping from the MPS (Sharma *et al*., 2016). It has been reported that incorporation of anti-cancer drugs in PLGA-PEG nanoparticles, for example paclitaxel, docetaxel, cisplatin, doxorubicin and curcumin, enhanced their therapeutic efficacy and reduced their side effects (Dinarvand *et al*., 2011). These results

therefore suggested that the PEGylated PLGA nanoparticles would be promising nanocarriers for an efficient delivery of plumbagin to cancer cells.

Lipid-polymer hybrid nanoparticles, a new generation of drug delivery systems, have been developed to exhibit complementary characteristics of both liposomes and polymeric nanoparticles: (i) a hydrophobic polymer core that is biocompatible, biodegradable and capable of carrying a poorly water-soluble drug and control its release; (ii) a lipid layer that can reduce water penetration into the nanoparticles, while at the same time prevents the entrapped drug from freely diffusing out of the nanoparticles; (iii) a hydrophilic PEG shell that can prevent a rapid clearance of the delivery system by MPS, thereby increasing the blood circulation half-life of the drug (Zhang *et al*., 2008). Based on these properties, lipid-polymer hybrid nanoparticles have been chosen as versatile and robust delivery systems for plumbagin.

Although nanocarriers have the potential to improve the delivery of chemotherapeutic agents to target cancer cells, some side effects related to non-selective accumulation of nanocarriers in other organs (e.g. liver and spleen) still exist. This problem can be overcome by using active targeting (Peer *et al.*, 2007; Wicki *et al.*, 2015). On the basis that iron is essential for cancer cell growth and can be effectively carried to tumours by transferrin (Tf), whose receptors are overexpressed on many cancer cells (Daniels *et al*., 2012), we hypothesise that conjugating nanomedicines with transferrin would enhance the specific delivery of the carried plumbagin to cancer cells, resulting in an improved therapeutic efficacy of the drug. The combination of active targeting, resulting from the conjugation of transferrin ligands to the nanomedicines, with the passive accumulation of delivery systems in tumours due to the enhanced permeability and retention (EPR) effect (Maeda, 1992), should provide tumour-selective targeting of plumbagin to the

cancer cells (Anabousi *et al*., 2006; Chang *et al*., 2009; Zheng *et al*., 2010; Gou *et al*., 2013; Gou *et al*., 2015; Sun *et al*., 2016; Jhaveri *et al*., 2018).

2.2 Aim and Objectives

The main objective of this chapter is to develop novel transferrin-targeted nanomedicines for the delivery of plumbagin to cancer cells. Three delivery systems have been chosen, as follows:

- Liposomes

- Polymeric nanoparticles

- Lipid-polymer hybrid nanoparticles

Thereafter, the synthesised nanomedicines entrapping plumbagin will be investigated for their physico-chemical characteristics such as morphology, drug entrapment efficiency, transferrin conjugation efficiency, size and zeta potential. Their stability will be assessed under storage conditions at 4 °C for 4 weeks by determining potential changes of particle size and zeta potential, as well as any eventual drug leakage. Finally, in order to ensure that plumbagin can be released from the delivery systems, drug release will be assessed using dialysis at three different pHs (7.4, 6.5 and 5.5) respectively mimicking physiological pH in normal tissue and blood, pH in the tumour extracellular environment and pH in the subcellular endosome.

2.3 Materials and methods

2.3.1 Materials

Materials	Supplier
1,2-distearoyl-*sn*-glycero-3-phosphoethanolamine-N-(Carbonyl-methoxypolyethyleneglycol 2000), sodium salt (DSPE-PEG2K)	NOF Corporation, Japan
1,2-distearoyl-sn-glycero-3-phosphoethanolamine-N-[maleimide(polyethylene glycol)-2000] (DSPE-PEG2K-MAL)	JenKem, USA
2-Iminothiolane hydrochloride (Traut's reagent)	Sigma-Aldrich, UK
3-(4,5-dimethylthiazol-2-yl)-2,5-diphenyl-tetrazolium bromide (MTT)	Sigma-Aldrich, UK
Acetone	Sigma-Aldrich, UK
Cholesterol	Sigma-Aldrich, UK
Cholesterol-PEG5K-maleimide (CLS-PEG5K-MAL)	Nanocs, USA
Chloroform ($CHCl_3$)	Sigma-Aldrich, UK
Cupric sulphate (pentahydrate) ($CuSO_4.5H_2O$)	Sigma-Aldrich, UK
Diethyl ether	Sigma-Aldrich, UK
Dimethyl sulfoxide (DMSO)	Sigma-Aldrich, UK
Folin & Ciocalteu's phenol reagent	Sigma-Aldrich, UK
Holo-transferrin, human (Tf)	Sigma-Aldrich, UK
Hydrochloric acid (HCl)	Sigma-Aldrich, UK
Hydrogenated soy phosphatidylcholine (HSPC)	Sigma-Aldrich, UK
Isopropanol	Sigma-Aldrich, UK

Maleimide-PEG5K-amine, TFA salt (MAL-PEG5K-NH$_2$)	JenKem, USA
Methanol	Sigma-Aldrich, UK
N-(3-Dimethylaminopropyl)-N'-ethylcarbodiimide (EDC)	Sigma-Aldrich, UK
N-Hydroxysuccinimide (NHS)	Sigma-Aldrich, UK
N,N-Diisopropylethylamine (DIEA)	Sigma-Aldrich, UK
Phosphate buffer saline (PBS)	Sigma-Aldrich, UK
Plumbagin (from *Plumbago indica*, purity > 95%)	Sigma-Aldrich, UK
Resomer® RG 503 H (poly(D,L-lactide-co-glycolide, acid terminated) (PLGA-COOH), lactide: glycolide 50:50, MW 24000-38000 Da, viscosity 0.32-0.44 dL/g	Sigma-Aldrich, UK
SnakeSkin® dialysis tubes (3.5K MWCO)	Thermo Fisher Scientific, USA
Sodium carbonate (anhydrous) (Na$_2$CO$_3$)	Sigma-Aldrich, UK
Sodium hydroxide (NaOH)	Sigma-Aldrich, UK
Sodium phosphate dibasic (anhydrous) (Na$_2$HPO$_4$)	Sigma-Aldrich, UK
Sodium phosphate monobasic (anhydrous) (NaH$_2$PO$_4$)	Sigma-Aldrich, UK
Sodium potassium tartrate (C$_4$H$_4$KNaO$_6$)	Sigma-Aldrich, UK
Vivaspin® 6 centrifuge tubes (3.5K and 100K MWCO)	Sartorius Ltd., UK
Vivaspin® 20 centrifuge tubes (100K MWCO)	Sartorius Ltd., UK

2.3.2 Determination of the maximum absorption wavelength of plumbagin

In order to identify the wavelength of maximum absorbance (λ_{max}) associated with plumbagin, a wavelength scanning was carried out using an Agilent Varian Cary® 50 UV-Vis Spectrophotometer (Agilent Technologies, Santa Clara, CA). Plumbagin stock solution of 10 mg/mL was prepared in isopropanol, then was further diluted to give a

final concentration of 25 µg/mL using the same solvent. Plumbagin solution was then scanned by spectrophotometry between 200 to 800 nm to obtain the specific λ_{max} wavelength. A standard calibration curve of plumbagin was then prepared at this wavelength, by measuring absorbance of plumbagin solutions at a starting concentration of 50 µg/mL in isopropanol, in triplicate. The absorbance obtained was then linearly correlated with plumbagin concentration, using OriginPro 9.0 software (OriginLab Corporation, Northampton, MA).

2.3.3 Preparation of transferrin-bearing liposomes

Due to poor water solubility of plumbagin (~100 µg/mL at 25°C), a highly concentrated plumbagin stock solution of 100 mg/mL was prepared in DMSO. To prepare control liposomes entrapping plumbagin, a mixture of HSPC (19.2 mg), DSPE-PEG2K (6.4 mg), cholesterol (5.3 mg) and cholesterol-PEG5K-maleimide (1.1 mg) (molar ratios: 60: 6: 34: 0.5), in 3.96 mL PBS (pH 7.4) was shaken at 75 °C for 1 hour. Plumbagin solution (40 µL, equivalent to 4 mg of plumbagin, measured from a stock solution of 100 mg/mL prepared in DMSO) was then added to the mixture, followed by probe sonication using Sonics Vibracell® VCX 500 (Sonics®, Newtown, CT) for 5 x 2 minutes. Blank liposomes were prepared in the same manner but without plumbagin.

In order to conjugate transferrin (Tf) to liposomes, 2-iminothiolane (Traut's reagent) was used as a cross-linking reagent to produce a thiolated Tf which can interact with thiol-reactive maleimide group of cholesterol-PEG-maleimide. To do so, 10 mg of transferrin were dissolved in 1 mL of 50 mM sodium phosphate containing 150 mM sodium chloride buffer (pH 8) and reacted with 10-fold molar excess of Traut's reagent (85 µL, 2 mg/mL in distilled water) under continuous stirring at 25 °C for 2 hours. The thiolated Tf was then isolated from unreacted Traut's reagent using Vivaspin® 6 centrifuge tubes with a

molecular weight cut-off of 5,000 Daltons (Sartorius Ltd., Epsom, UK), after centrifugation at 9,500 rpm (10,500 g) for 15 min at 20 °C (Hermle® Z323K centrifuge, Wehingen, Germany).

The freshly synthesised thiolated Tf was immediately conjugated to the control liposomes under continuous stirring at 25 °C for 2 hours. Free plumbagin and/or unreacted Tf were removed from both Tf-bearing liposomes and control liposomes using Vivaspin® 6 centrifuge tubes with a molecular weight cut-off of 100,000 Daltons (Sartorius Ltd., Epsom, UK) by centrifugation at 7,500 rpm (6,600 g) for 15 min at 20 °C.

2.3.4 Preparation of transferrin-bearing polymeric nanoparticles

2.3.4.1 Synthesis of PLGA-PEG-MAL

Poly(lactide-co-glycolide)-b-poly(ethylene glycol)-maleimide (PLGA-PEG-MAL) used in the experiments was synthesised according to a previous method described by Vasconcelos and colleagues (2015), with some modifications. To do so, PLGA-COOH (1.5 g, 48.4 µmoles) was dissolved in 3 mL of dichloromethane. PLGA-NHS was then synthesised by reacting PLGA-COOH with excess EDC (40 mg, 257.7 µmoles, 5-fold molar excess compared to PLGA-COOH) and NHS (23 mg, 199.8 µmoles, 4-fold molar excess compared to PLGA-COOH) under continuous stirring at 25 °C for 6 hours to achieve a complete reaction. PLGA-NHS was precipitated with 6 mL of diethyl ether: methanol (1:1) washing solvent and centrifuged at 7,500 rpm (6,600 g) for 5 min at 25 °C (Hermle® Z323K centrifuge, Wehingen, Germany). The supernatant was then discarded, and these washing/centrifugation steps were repeated twice. The polymer obtained from this step was dried overnight at 25 °C. To obtain PLGA-PEG-MAL, PLGA-NHS (1 g, 32.4 µmoles) was dissolved in chloroform (3 mL). MAL-PEG5K-NH$_2$ (210 mg, 41.2 µmoles, 1.2-fold molar excess compared to PLGA-NHS) and DIEA (30

µL, 176.4 µmoles, 5-fold molar excess compared to PLGA-NHS) were then added. The mixture was reacted overnight under continuous stirring at 25 °C. The polymer was precipitated with 6 mL of ice-cold diethyl ether and centrifuged at 7,500 rpm (6,600 g) for 5 min at 25 °C. After removing the supernatant, the product was further purified by washing with 6 mL of ice-cold diethyl ether followed by centrifugation as described above, and these steps were repeated twice. The resulting PLGA-PEG-MAL was dried overnight at 25 °C and stored at -20 °C until further experiments. Its synthesis was confirmed by ^{1}H NMR spectroscopy, using a Bruker Avance™ III HD 500 MHz spectrometer (Bruker BioSpin Corporation, Billerica, MA).

2.3.4.2 Nanoparticles preparation

The polymeric nanoparticles were prepared by nanoprecipitation method. Briefly, PLGA-PEG-MAL (35 mg) was dissolved in acetone (3.5 mL). Plumbagin solution (35 µL, equivalent to 3.5 mg of plumbagin, measured from a stock solution of 100 mg/mL prepared in DMSO) was then added to the polymer solution. The mixture was subsequently added dropwise into deionised water (7 mL) under moderate stirring. The product was stirred overnight at 25 °C in a chemical fume hood to evaporate all acetone. The nanoparticles were then collected by centrifugation at 7,500 rpm (6,600 g) for 30 min at 20 °C (Hermle® Z323K centrifuge, Wehingen, Germany), using Vivaspin® 6 centrifuge tubes with a molecular weight cut-off of 100,000 Daltons (Sartorius Ltd., Epsom, UK). They were washed twice with deionised water (2 mL) to remove exceed plumbagin, before being resuspended in deionised water (1 mL) and stored at 4 °C for further experiments.

Given the fact that particle size, zeta potential and drug entrapment efficiency of PLGA-PEG nanoparticles prepared by nanoprecipitation method can be affected by several

factors such as polymer concentration, water miscibility of organic solvent, ratio of water to organic solvent and theoretical drug loading (Cheng *et al*., 2007), the nanoparticles were optimised in this study by varying the volume ratio of water to acetone (1:1, 2:1, 3:1. 5:1 and 10:1) while fixing the concentration of polymer in acetone at 10 mg/mL and plumbagin loading at 10% w/w of polymer.

Transferrin was conjugated to PLGA-PEG nanoparticles in the same manner as described in **section 2.3.3**.

2.3.5 Preparation of transferrin-bearing lipid-polymer hybrid nanoparticles

Lipid–polymer hybrid nanoparticles were prepared by using one-step nanoprecipitation method. To do so, a mixture of HSPC (2 mg) and DSPE-PEG2K-MAL (3 mg) in 5 mL of deionised water was shaken at 75 °C for 1 hour. PLGA-COOH (25 mg) was dissolved in acetone (2.5 mL) and plumbagin solution (25 μL, equivalent to 2.5 mg of plumbagin, measured from a stock solution of 100 mg/mL prepared in DMSO) was then added to the polymer solution. It was subsequently added dropwise into the lipid mixture under moderate stirring. The product was stirred overnight at 25 °C under a chemical fume hood to evaporate all acetone. The resulting nanoparticles were then collected by centrifugation at 7,500 rpm (6,600 g) for 30 min at 20 °C (Hermle® Z323K centrifuge, Wehingen, Germany), using Vivaspin® 6 centrifuge tubes with a molecular weight cut-off of 100,000 Daltons (Sartorius Ltd., Epsom, UK). They were washed twice with deionised water (2 mL) to remove exceed plumbagin, before being resuspended in deionised water (1 mL) and stored at 4 °C for further experiments.

In order to obtain the lipid-polymer hybrid nanoparticles with desirable size, zeta potential and high drug entrapment efficiency, the nanoparticles were optimised by varying two factors: (1) weight ratio of lipids (HSPC and DSPE-PEG2K-MAL) to

PLGA-COOH polymer (1:10, 1:5, 1:2.5, 1:1.67, 1:1.25 and 1:1) and (2) the molar ratio of hydrogenated phosphatidylcholine to DSPE-PEG2K-MAL (90:10, 85:15, 80:20, 70:30, 60:40 and 50:50), while fixing the theoretical drug loading at 10% of polymer weight, the concentration of polymer in organic solvent at 10 mg/mL and the volume ratio of water to acetone at 2:1.

Lipid-polymer hybrid nanoparticles were conjugated with Tf in the same manner as described in **section 2.3.3.**

2.3.6 Transmission electron microscopy

The morphology of nanoparticles was visualised using transmission electron microscopy (TEM). Formvar/Carbon-coated copper grids (400 mesh) were glow discharged. A 3-5 μL drop of each sample (diluted to 1:10 with deionised water) was then added to the hydrophilic support film. Dried samples were imaged using a JEOL 1200 transmission electron microscope (JEOL USA, Inc., Peabody, MA) operating at 80 kv fitted with a Gatan 794 MultiScan® camera (Gatan, Pleasanton, CA).

2.3.7 Transferrin conjugation efficiency

The amount of Tf conjugated to the nanoparticles was quantified by Lowry assay (Lowry *et al*., 1951), as previously reported (Dufès *et al*., 2000; Fu *et al*., 2009). Briefly, 1 mL of sodium potassium tartrate solution (2% w/v in distilled water) and 1 mL of cupric sulphate solution (1% w/v in distilled water) were added dropwise (under continuous stirring to avoid precipitation) into 25 mL of sodium carbonate anhydrous solution (2% w/v in 0.1 M NaOH) to make up Solution A. The bovine serum albumin (BSA) was prepared as a standard protein solution (concentration ranging from 0 to 500 μg/mL). One hundred microliters of Tf-bearing nanoparticles or control nanoparticles (diluted 1:20 in

PBS) or BSA standard solution, was mixed with 1 mL of Solution A and incubated at 25 °C for 10 min. Subsequently, 100 µL of 1N Folin-Ciocalteu's phenol reagent was added to these samples (with immediate vortexing), followed by incubation at 25 °C for 30 min (protected from light). The absorbance of each sample was determined at a wavelength of 750 nm using an Agilent Varian Cary® 50 UV-Vis Spectrophotometer (Agilent Technologies, Santa Clara, CA). Blank nanoparticles were used as the reference cell to set zero. The experiment was done in quadruplicates. The amount of Tf was calculated by correlating the absorbance of each sample with the standard curve of BSA. The results were expressed as percentage of Tf conjugated to nanoparticles compared to the initial amount of Tf added.

2.3.8 Entrapment efficiency

To assess the entrapment efficiency of plumbagin, 10 µL of nanoparticles were mixed with 990 µL of isopropanol, followed by centrifugation at 10,000 rpm (9,300 g) at 25 °C for 10 min using an IEC Micromax® centrifuge (ThermoFisher Scientific, Waltham, MA). The absorbance of plumbagin dissolved in supernatant was measured by spectrophotometry (λ_{max}: 420 nm) using an Agilent Varian Cary® 50 UV-Vis Spectrophotometer (Agilent Technologies, Santa Clara, CA). The amount of plumbagin was calculated by correlating absorbance with standard calibration curve of plumbagin. The results were expressed as percentage of entrapment efficiency (% EE) and drug loading capacity (% LC) according to the equation (1) and (2) indicated below:

$$\% \text{ EE} = \frac{\text{amount of plumbagin in sample}}{\text{amount of plumbagin added}} \times 100 \qquad (1)$$

$$\% \text{ LC} = \frac{\text{amount of plumbagin in sample}}{\text{nanoparticles weight}} \times 100 \qquad (2)$$

2.3.9 Size and zeta potential measurement

Size and zeta potential of Tf-bearing nanoparticles and control nanoparticles entrapping plumbagin were measured by photon correlation spectroscopy and laser Doppler electrophoresis, using a Zetasizer Nano-ZS® (Malvern Instruments, Malvern, UK). All samples were prepared at a dilution of 1:100 in 5% w/v glucose solution (for liposomes) or deionised water (for PLGA-PEG and lipid-polymer hybrid nanoparticles) to make up 1 mL and vortexed before being transferred into a folded capillary cell for measurement. The experiment was done in triplicates.

2.3.10 Stability study

The stability of the formulations was assessed using 3 different batches of liposomes and nanoparticles. All samples were placed in glass vials protected from light and were kept under storage condition at 4°C for 4 weeks. The size and zeta potential of the samples were respectively measured by photon correlation spectroscopy and laser Doppler electrophoresis at specific time points (on Days 0, 7, 14, 21 and 28). The amount of plumbagin remaining in formulations was quantified by spectrophotometry compared to the initially entrapped amount.

2.3.11 Drug release study

To confirm that plumbagin could be released from the liposomes and the nanoparticles, the release profile of the drug was performed using a dialysis technique under three different pHs (5.5, 6.5 and 7.4). Briefly, plumbagin either formulated as Tf-bearing formulation, control formulation or in solution (500 μg of plumbagin in 1 mL phosphate buffer) was placed into a SnakeSkin® dialysis tube with a molecular weight cut-off of 3,500 Daltons (ThermoFisher Scientific, Waltham, MA) and was dialysed against 50 mL of phosphate buffer (pH 5.5, 6.5 and 7.4) at 37°C under gentle stirring. At specific time intervals (30 minutes, then every hour for the first six hours (1 h, 2 h, 3 h, 4 h, 5 h, 6 h), then every 2 hours for the next 6 hours (8 h, 10 h, 12 h), and 24 hours), 1 mL of the dialysate was withdrawn in triplicates and then replaced with an equal volume of fresh buffer. The amount of plumbagin in the samples was quantified by spectrophotometry and reported as a percentage cumulative drug release.

2.3.12 Statistical analysis

Results were expressed as means ± standard error of the mean. Statistical significance was assessed by one-way analysis of variance and Tukey multiple comparison post-test using OriginPro 9.0® software (OriginLab Corporation, Northampton, MA). Differences were considered statistically significant for p-values lower than 0.05.

2.4 Results

2.4.1 Plumbagin quantification

The spectrum of plumbagin obtained from UV-Vis scanning displayed the wavelength of maximum absorbance (λ_{max}) at 420 nm (**Figure 2-1**). This finding was similar to previous reports that plumbagin had a maximum absorbance at 420 nm (Chairungsi *et al*., 2006; Srinivas *et al*., 2011; Vasudevarao *et al*., 2011). As a result, further quantification of plumbagin was performed at this wavelength.

For plumbagin quantification, a standard calibration curve of plumbagin was first prepared at 8 concentrations in isopropanol (with two-fold dilutions, starting at 50 µg/mL) and analysed by UV-Vis quantification at 420 nm. As shown in **Figure 2-2**, the standard calibration of plumbagin was linear over the concentrations range used, which could be described by the regression equation: $Y = 0.02204X + 0.00068$ with a coefficient of determination (R-square, R^2) of 0.9983.
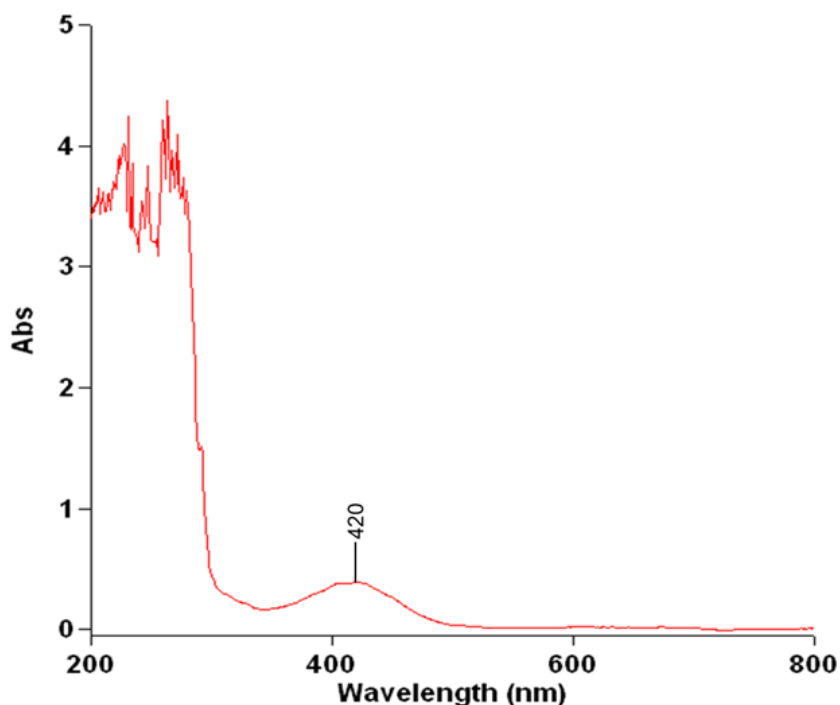
Figure 2-1: Absorption spectrum of plumbagin obtained using spectrophotometry, indicating the wavelength of maximum absorbance (λ_{max}) at 420 nm

Figure 2-2: Standard calibration curve of plumbagin for quantitative determination. The absorbance (optical density, O.D.) was obtained from serial two-fold dilution of plumbagin in isopropanol (*n*=3)

2.4.2 Preparation of tumour-targeted nanomedicines entrapping plumbagin

Three different delivery systems were prepared. The list of their abbreviated names is indicated in **Table 2-1**.

Table 2-1: Abbreviated names of tumour-targeted nanomedicines entrapping plumbagin and blank formulations of the delivery systems used in this study

Nanomedicine formulations entrapping plumbagin	Abbreviated names		
	Tf-bearing	**Control**	**Blank**
Liposomes (LIP)	Tf-LIP	Control LIP	Blank LIP
Polymeric nanoparticles (PN)	Tf-PN	Control PN	Blank PN
Lipid-polymer hybrid nanoparticles (LPN)	Tf-LPN	Control LPN	Blank LPN

Tf-bearing: Transferrin-bearing nanomedicine formulations entrapping plumbagin, Control: nanomedicine formulations entrapping plumbagin but not conjugated to Tf, Blank: empty nanomedicine formulations not conjugated to Tf

2.4.2.1 Transferrin-bearing liposomes

Tf-bearing and control small unilamellar liposomes entrapping plumbagin were successfully prepared by probe sonication, as confirmed by TEM images (**Figure 2-3**).

A

B
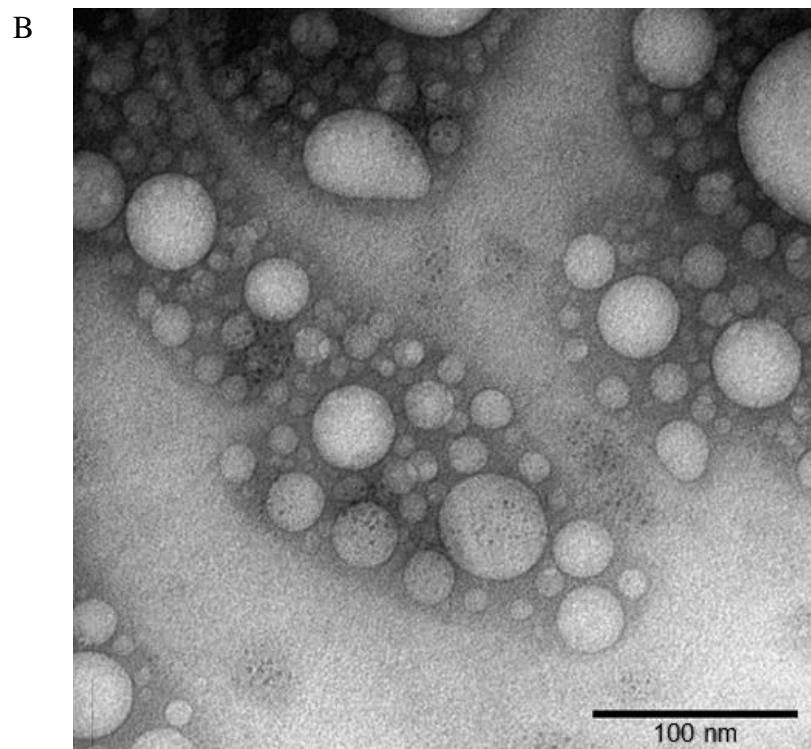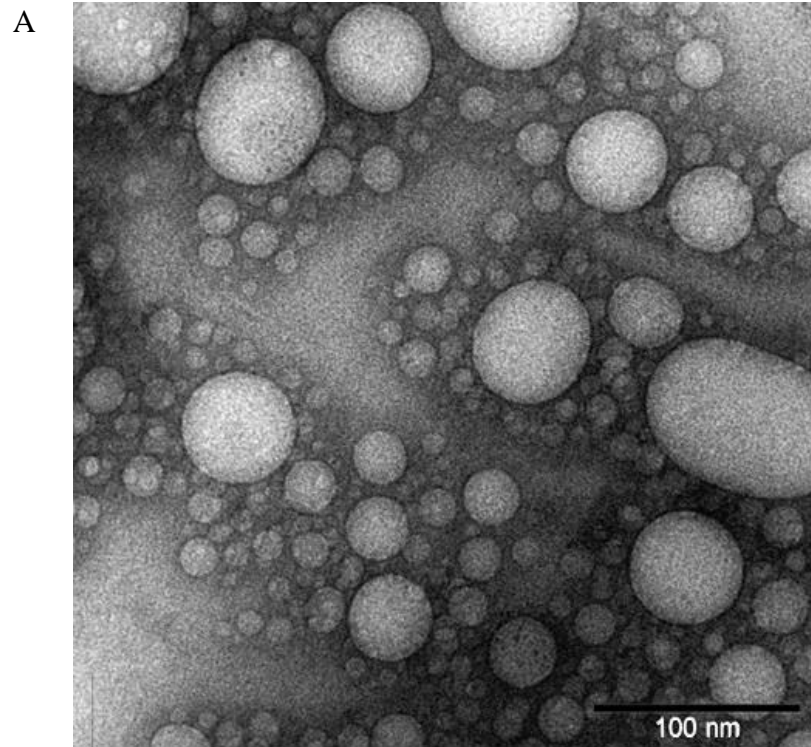
Figure 2-3: Transmission electron micrograph pictures of Tf-bearing (A) and control (B)

unilamellar liposomes loaded with plumbagin (Bar: 100 nm)

2.4.2.2 Transferrin-bearing polymeric nanoparticles

2.4.2.2.1 Synthesis of PLGA-PEG-MAL

The maleimide-functionalised PLGA-PEG block copolymer was synthesised by direct conjugation of PLGA-COOH and MAL-PEG5K-NH$_2$ (**Figure 2-4**). The yield of the final product was 63.3%.
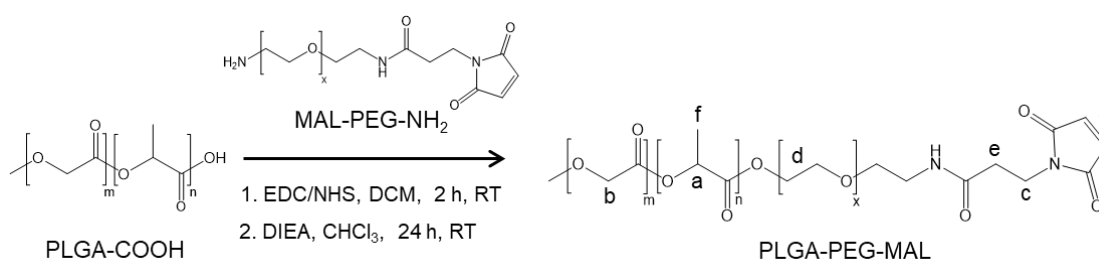
Figure 2-4: Schematic of PLGA-PEG-MAL synthesis

The ^{1}H-NMR confirmed the successful conjugation of PLGA-COOH to MAL-PEG-NH$_2$, as shown in **Figure 2-5**. The characteristic peaks of PLGA-PEG-MAL were as follows: ^{1}H-NMR (500 MHz, CDCl$_3$): δ 5.15 (m, (-O**CH**(CH$_3$)COO-)) (a), 4.71 (m, (-O**CH$_2$**COO-)) (b), 4.23 (-N**CH$_2$**CH$_2$-) (c), 3.57 (s, (-**CH$_2$CH$_2$**O-) (d), 2.45 (-NCH$_2$**CH$_2$**-CONH-) (e), 1.51 (-OCH(**CH$_3$**)COO-) (f). The characteristic peaks of methine protons (-**HC=CH**-) of maleimide group could be seen at 6.63 ppm (g).

To determine the conjugation efficiency between PEG molecule and PLGA molecule, PLGA-PEG ^{1}H-NMR was integrated using MestreNova®12.0.2 software (Mestrelab Research, Santiago de Compostela, Spain).
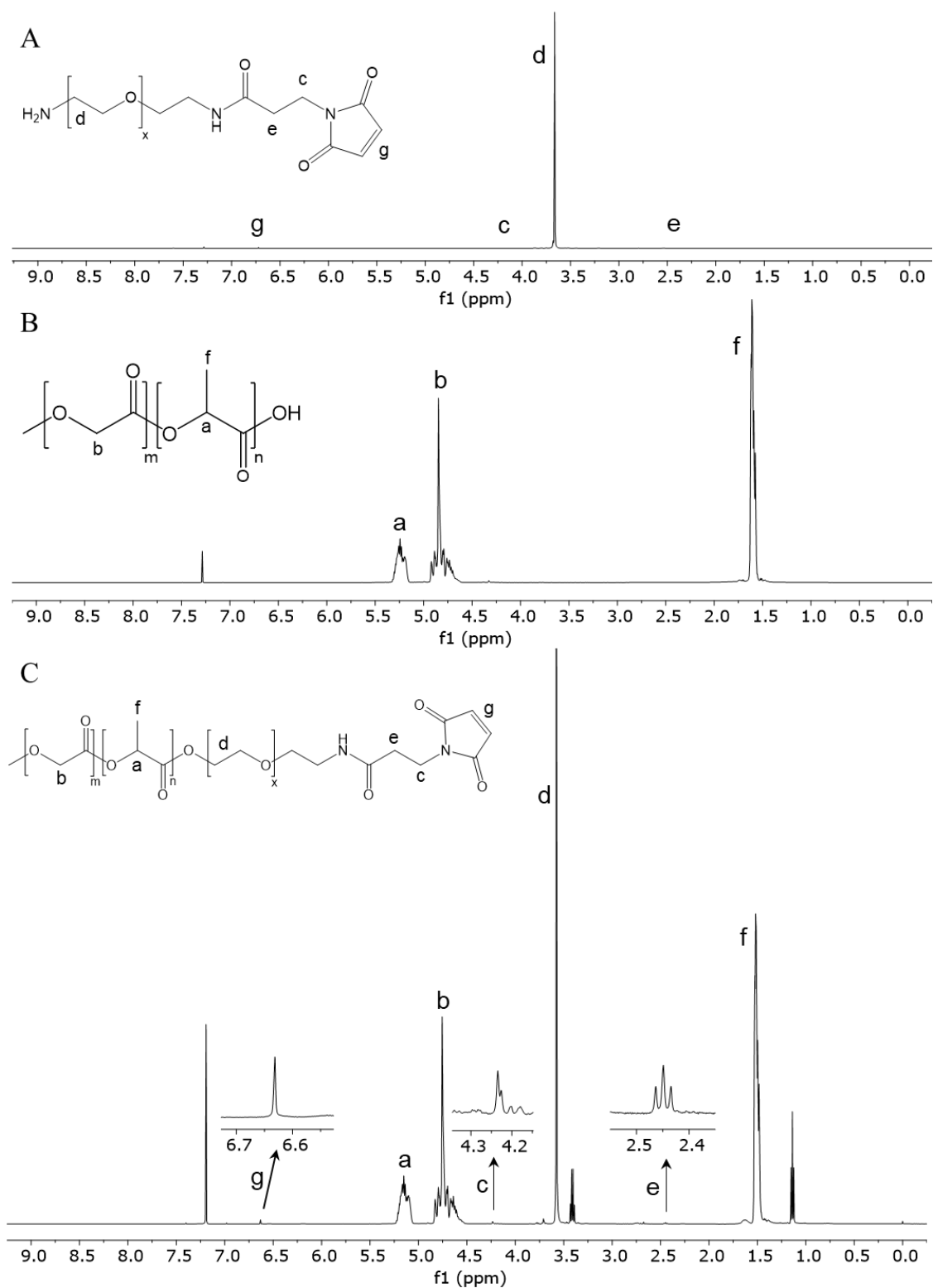
Figure 2-5: ^{1}H-NMR spectra of MAL-PEG5K-NH$_2$ (A), PLGA-COOH (B) and PLGA-PEG-MAL (C)

2.4.2.2.2 Nanoparticle preparation and optimisation

The PLGA-PEG nanoparticles entrapping plumbagin were prepared and optimised using three important parameters: particle size, zeta potential and entrapment efficiency. In this experiment, PLGA-PEG nanoparticles entrapping plumbagin were optimised by selecting acetone as the organic solvent and varying the volume ratio of water: organic solvent (1:1, 2:1, 3:1. 5:1 and 10:1), while fixing the concentration of polymer in organic solvent at 10 mg/mL and plumbagin loading at 10% w/w of PLGA-PEG polymer. As shown in **Figure 2-6**, the smallest particle size was obtained at the ratios of 2:1 (82.1 ± 0.4 nm) and 3:1 (82.4 ± 0.4 nm) with no significant difference between these two ratios, while the other ratios showed larger particle size (106.7 ± 1.1, 88.3 ± 0.2 and 91.8 ± 0.2 nm for 1:1, 5:1 and 10:1 ratio, respectively). The entrapment efficiency, on the other hand, decreased dramatically when increasing the volume ratio of water: organic solvent (57.8 ± 0.2% for 1:1 ratio, 53.1 ± 0.3% for 2:1 ratio, 48.8 ± 0.7% for 3:1 ratio, 39.9 ± 0.7% for 5:1 ratio and 26.4 ± 0.5% for 10:1 ratio). The nanoparticles exhibited similar negative surface charges at all water: organic solvent ratios (-25.5 ± 0.3 mV for 1:1 ratio, -26.2 ± 0.3 mV for 2:1 ratio, -27.5 ± 0.5 mV for 3:1 ratio, -27.5 ± 0.4 mV for 5:1 ratio and -27.1 ± 0.5 mV for 10:1 ratio).

From this result, the volume ratio of water: organic solvent of 2:1 was chosen due to the smallest particle obtained with high entrapment efficiency of plumbagin. Thus, the optimised formulation of plumbagin loaded PLGA-PEG nanoparticles was prepared at the water: acetone ratio of 2:1 with the concentration of polymer in organic solvent at 10 mg/mL and plumbagin loading at 10%.

Transferrin-bearing and control PLGA-PEG nanoparticles entrapping plumbagin were successfully prepared using nanoprecipitation method, as confirmed by TEM imaging (**Figure 2-7**).
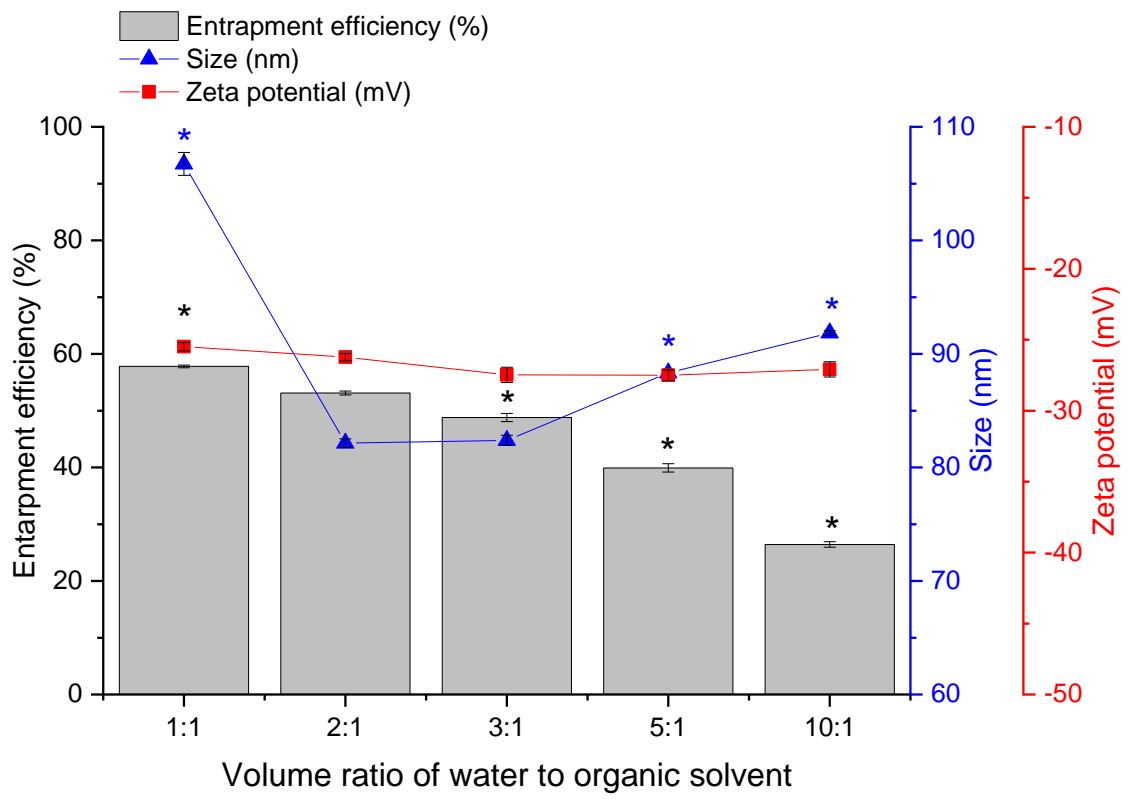
Figure 2-6: Optimisation of PLGA-PEG nanoparticles based on various volume ratios of water to organic solvent (1:1, 2:1, 3:1, 5:1 and 10:1) and plumbagin loading at 10% w/w of the polymer ($n=3$) (*: $p<0.05$ vs 2:1)
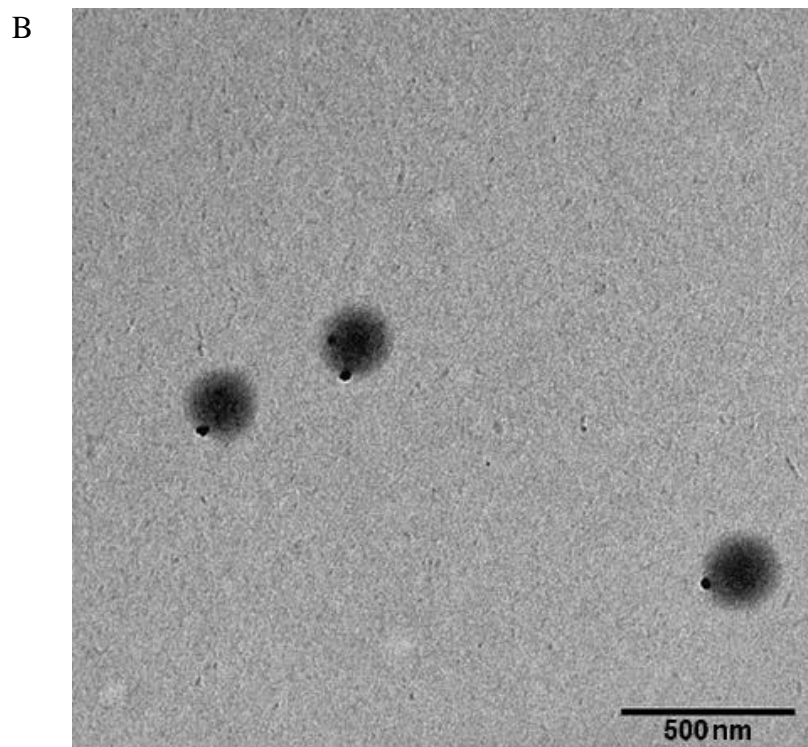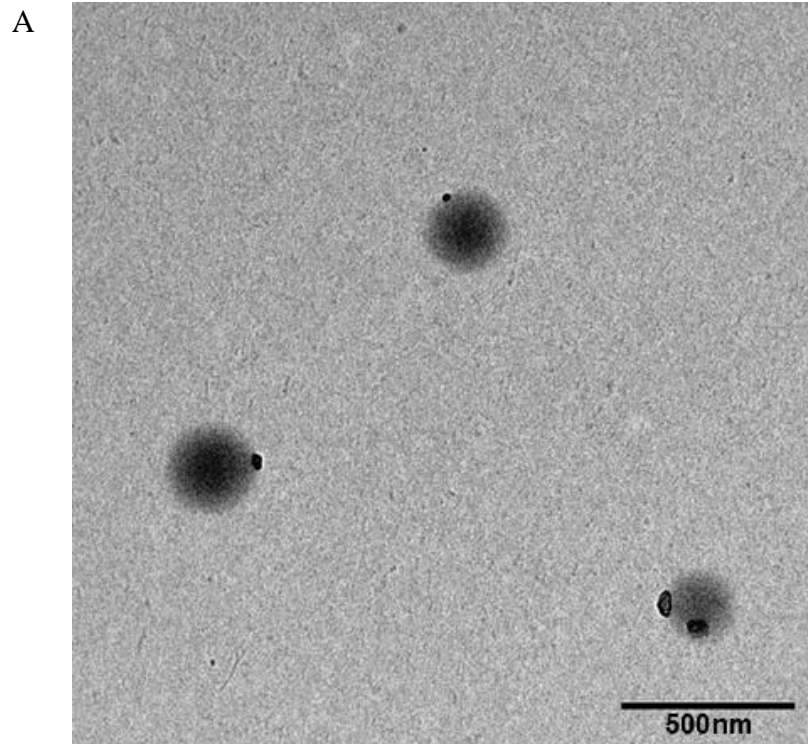
Figure 2-7: Transmission electron micrograph pictures of Tf-bearing (A) and control (B)

PLGA-PEG nanoparticles loaded with plumbagin (Bar: 500 nm)

2.4.2.3 Transferrin-bearing lipid-polymer hybrid nanoparticles

2.4.2.3.1 Nanoparticle preparation and optimisation

The lipid–polymer hybrid nanoparticles were first prepared with varying weight ratios of lipid to PLGA-COOH polymer. The lipid to polymer weight ratios of 1:10 and 1:5 resulted in nanoparticles having a desirable combination of particle size (143.8 ± 1.0 to 144.4 ± 1.1 nm) and zeta potential (-57.2 ± 0.3 to -58.9 ± 0.8 mV) (**Figure 2-8**). When increasing the weight ratio from 1:2.5 to 1:1, the nanoparticles became larger (169.0 ± 0.7 to 183.2 ± 0.9 nm) and were more negatively charged (-63.7 ± 0.4 to -68.0 ± 0.8 mV). The entrapment efficiency of plumbagin, on the other hand, did not change at all the tested lipid to polymer weight ratios (entrapment efficiency of ~40 %). From this result, the lipid to polymer weight ratio of 1:5 was chosen due to the smallest particle obtained for further studies.
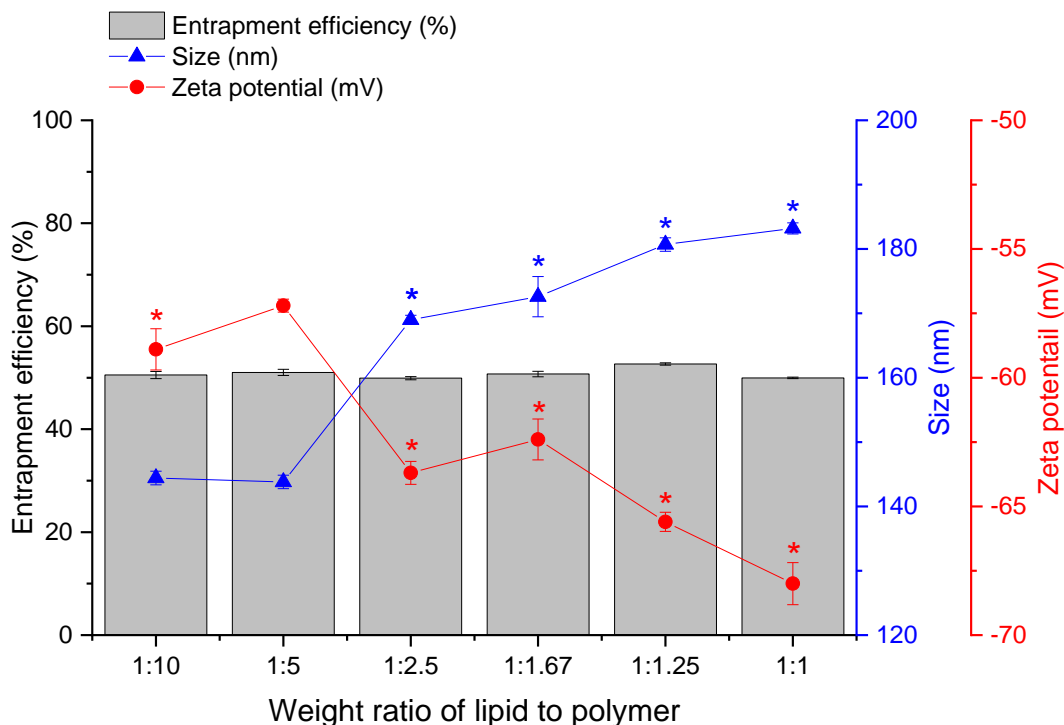
Figure 2-8: Optimisation of plumbagin loaded lipid-polymer hybrid nanoparticles based on the variation of lipid to PLGA weight ratios (*n*=3) (*: *p*<0.05 vs 1:5)

The nanoparticles were then further optimised by keeping the optimum lipid to polymer weight ratio obtained from the first step at 1:5 and varying the molar ratio of HSPC to DSPE-PEG2K-MAL. As shown in **Figure 2-9**, the HSPC to DSPE-PEG2K-MAL molar ratios of 90:10, 85:15, 80:20 and 70:30 resulted in nanoparticles having a desirable combination of particle size (143.1 ± 0.6 to 145.8 ± 0.5nm) and zeta potential (-57.2 ± 0.3 to -58.5 ± 1.4 mV), while the others ratios (60:40 and 50:50) showed an increase in both the particle size (151.4 to 157.0 ± 0.7 nm) and zeta potential (-53.0 ± 0.5 to -53.3 ± 0.4 mV). Similarly, the entrapment efficiency of plumbagin did not change when increasing the lipid to polymer weight ratio and the molar ratio of HSPC to DSPE-PEG2K-MAL (entrapment efficiency of 40-50 %).
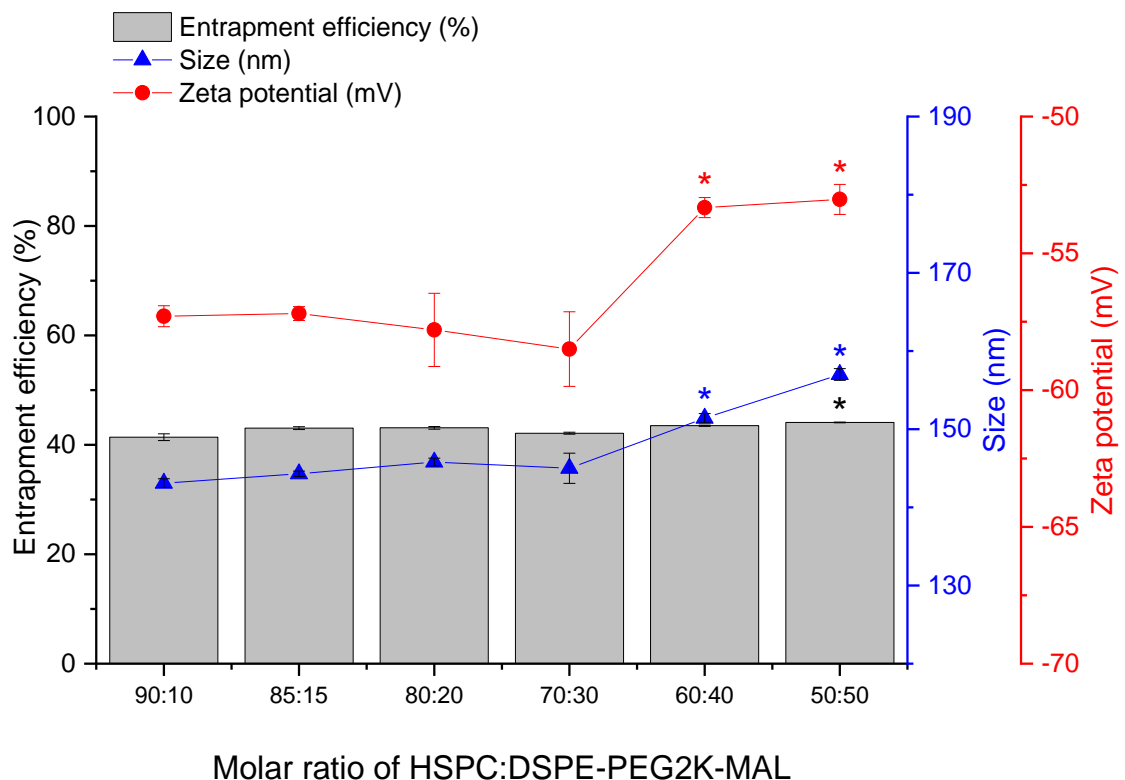
Figure 2-9: Optimisation of plumbagin loaded lipid-polymer hybrid nanoparticles by varying the molar ratio of HSPC to DSPE-PEG2K-MAL ($n=3$) (*: $p<0.05$ vs 70:30)

Thus, the optimum formulation of lipid–polymer hybrid nanoparticles obtained from the experiment were prepared at the weight ratio of lipid to polymer of 1:5 and the molar ratio of HSPC to DSPE-PEG2K-MAL of 70:30 with the concentration of polymer in organic solvent at 10 mg/mL, plumbagin loading at 10% of polymer weight and the ratio of water to organic solvent at 2:1.

Tf-bearing and control lipid–polymer hybrid nanoparticles entrapping plumbagin were successfully prepared using one-step nanoprecipitation method, where the PLGA polymer (in water-miscible organic solvent) and the aqueous lipid dispersion were mixed and formed by self-assembly, as shown in TEM pictures (**Figure 2-10**).
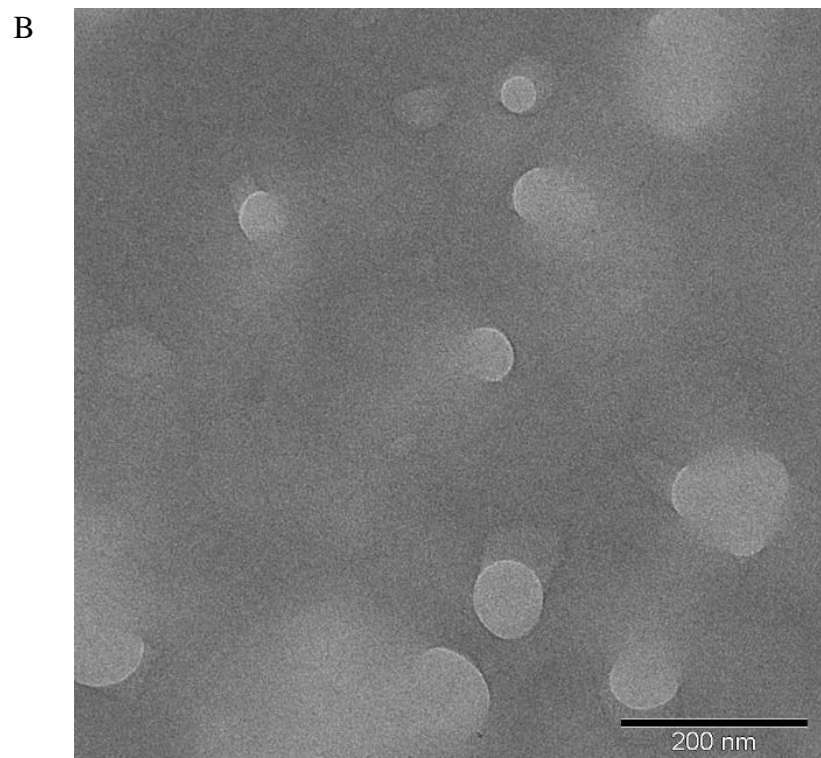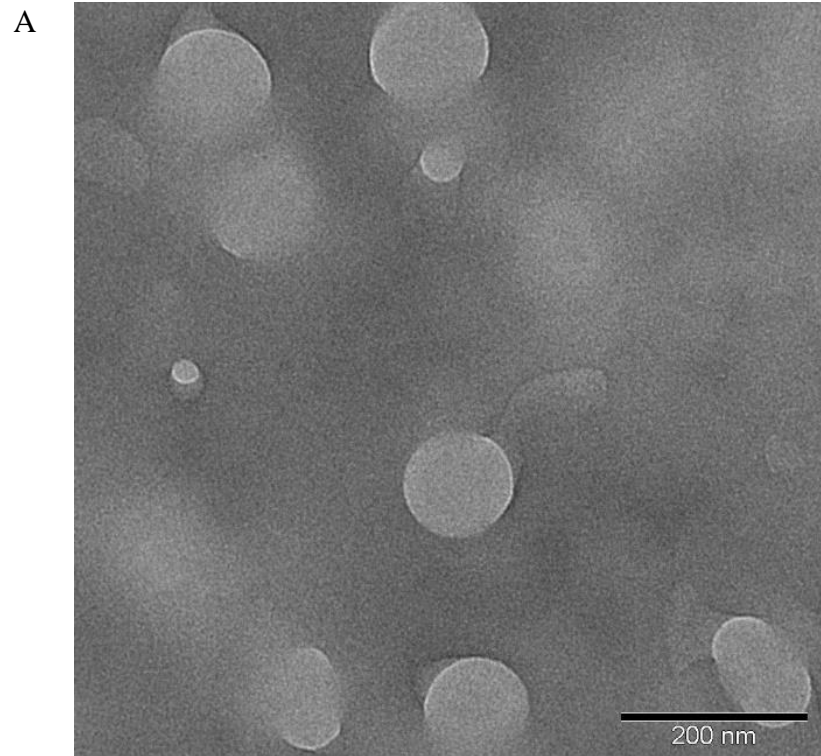
Figure 2-10: Transmission electron micrograph pictures of Tf-bearing (A) and control (B) lipid-polymer hybrid nanoparticles loaded with plumbagin (Bar: 200 nm)

2.4.3 Transferrin conjugation efficiency

Transferrin conjugation efficiency was determined by Lowry assay described in **section 2.3.7**. The amount of transferrin conjugated to the nanomedicines was calculated by correlating to BSA standard curves, as shown in **Table 2-2**. The amount of transferrin conjugated to the liposomes was 5.1 ± 0.1 mg (50.7 ± 0.5 % of the initial transferrin added or 159 µg Tf/mg of liposomes). Similar conjugation efficiency was observed in PLGA-PEG nanoparticles at a level of 5.8 ± 0.1 mg (58.2 ± 1.2 % of the initial transferrin added or 165 µg Tf/mg of nanoparticles). The amount of transferrin conjugated to the lipid-polymer hybrid nanoparticles was 7.2 ± 0.1 mg (72.2 ± 0.5% of the initial transferrin added or 240 µg Tf/mg of nanoparticles).

Table 2-2: Amount of transferrin conjugated to liposomes, polymeric nanoparticles and lipid-polymer hybrid nanoparticles (*n*=3)

Formulation	Amount of Tf conjugated (mg)	Conjugation efficiency (%)
Tf-LIP	5.1 ± 0.1	50.7 ± 0.5
Tf-PN	5.8 ± 0.1	58.2 ± 1.2
Tf-LPN	7.2 ± 0.1	72.2 ± 0.5

2.4.4 Drug entrapment efficiency

The entrapment efficiency of plumbagin within the liposomes was respectively 79.2 ± 0.3 % for Tf-LIP and 78.4 ± 0.4 % for control LIP, as shown in **Table 2-3**. This was higher than that obtained in PLGA-PEG nanoparticles (48.9 ± 2.6 % for Tf-PN and 59.3 ± 1.1 % for control PN) and lipid-polymer hybrid nanoparticles (48.0 ± 0.5 % for Tf-LPN and 56.5 ± 0.4 % for control LPN). However, in term of drug loading capacity (representing the amount of drug entrapped per unit of nanomedicines), all nanomedicine formulations had similar loading capacity.

Table 2-3: Entrapment efficiency of plumbagin in nanomedicine formulations (n=3)

Nanomedicine formulations	Entrapment efficiency (%)	Loading capacity (%)
Liposomes		
Tf-LIP	79.2 ± 0.3	4.47 ± 0.04
Control LIP	78.4 ± 0.4	4.43 ± 0.05
PLGA-PEG nanoparticles		
Tf-PN	48.9 ± 2.6	4.33 ± 0.06
Control PN	59.3 ± 1.1	5.98 ± 0.02
Lipid-polymer hybrid nanoparticles		
Tf-LPN	48.0 ± 0.5	4.00 ± 0.04
Control LPN	56.5 ± 0.4	4.71 ± 0.03

2.4.5 Size and zeta potential

The particle size and zeta potential measurements of the three nanomedicine formulations are summarised in **Table 2-4**.

As expected, the conjugation of Tf to the surface of the liposomes resulted in a larger average size of 113.5 ± 2.3 nm (polydispersity: 0.33 ± 0.01) than that of control liposomes (106.0 ± 1.5 nm, polydispersity: 0.32 ± 0.01). In addition, the zeta potential of liposomes was slightly decreased after conjugated with Tf in comparison with control liposomes (-18.4 ± 0.4 mV for Tf-LIP and -17.2 ± 0.1 mV for control LIP). This could be due to the negative charge of thiolated Tf (-22.1 ± 1.4 mV).

For PLGA-PEG nanoparticles, the conjugation of Tf to the surface of nanoparticles led to an increase in mean diameter size of Tf-PN (152.9 ± 0.6 nm, polydispersity: 0.20 ± 0.01) compared to control PN, which had an average size of 93.0 ± 0.3 nm (polydispersity: 0.11 ± 0.01). Both Tf-PN and control PN were bearing a negative surface charge, with zeta potential values of -34.3 ± 0.2 mV and -39.8 ± 0.9 mV respectively for Tf-PN and control PN. The significant increase in the zeta potential of Tf-PN is probably due to the shielding effect of transferrin on the surface of nanoparticles including some of the positively charged amino acids of transferrin as well as ferrous iron (Fe^{2+}) in the protein, which neutralized the negative charges of Tf-PN.

For lipid-polymer hybrid nanoparticles, the particle size of Tf-LPN was increased after conjugated with Tf (214.1 ± 1.5 nm, polydispersity: 0.17 ± 0.01) compared to that of control LPN (145.2 ± 0.6 nm, polydispersity: 0.16 ± 0.01). Furthermore, the presence of Tf on the surface of nanoparticles significantly increased the net surface charge of Tf-LPN (-46.6 ± 0.7 mV) in comparison with control LPN (-66.6 ± 0.6 mV) due to the impact of Tf, similar to Tf-PN.

87

Table 2-4: Size and zeta potential of liposomes, PLGA-PEG nanoparticles and lipid-polymer hybrid nanoparticles entrapping plumbagin ($n=3$)

Nanomedicine formulations	Particle Size (nm)	Polydispersity Index	Zeta Potential (mV)
Liposomes			
Tf-LIP	113.5 ± 2.3	0.33 ± 0.01	-18.4 ± 0.4
Control LIP	106.0 ± 1.5	0.32 ± 0.01	-17.2 ± 0.1
PLGA-PEG nanoparticles			
Tf-PN	152.9 ± 0.6	0.20 ± 0.01	-34.3 ± 0.2
Control PN	93.0 ± 0.3	0.11 ± 0.01	-39.8 ± 0.9
Lipid-polymer hybrid nanoparticles			
Tf-LPN	214.1 ± 1.5	0.17 ± 0.01	-46.6 ± 0.7
Control LPN	145.2 ± 0.6	0.16 ± 0.01	-66.6 ± 0.6

2.4.6 Stability of nanomedicines

Tf-bearing liposomes were found to be stable when stored at 4°C for at least 4 weeks. They displayed a slight decrease in size within 28 days (from 113.5 ± 2.3 nm at Day 0 to 102.8 ± 2.6 nm at Day 28 for size and 0.33 ± 0.01 at Day 0 to 0.28 ± 0.02 at Day 28 for polydispersity), unlike control liposomes, whose size slightly increased (from 106.0 ± 1.5 nm at Day 0 to 115.8 ± 2.4 nm at Day 28 for size and 0.32 ± 0.01 at Day 0 to 0.37 ± 0.02 at Day 28 for polydispersity). However, blank liposomes appeared to be less stable due to a significant increase in size observed during the experiment (from 115.9 ± 2.1 nm at Day 0 to 138.9 ± 4.4 nm at Day 28 for size and 0.30 ± 0.01 at Day 0 to 0.37 ± 0.01 at Day 28 for polydispersity) (**Figure 2-11A, 11B**). The zeta potential of all liposome formulations remained stable for 28 days (-18.4 ± 0.4 mV at Day 0 to -20.2 ± 0.8 mV at

Day 28 for Tf-LIP, -17.2 ± 0.1 mV at Day 0 to -18.6 ± 0.4 mV at Day 28 for control LIP

and -17.2 ± 0.2 mV at Day 0 to -19.0 ± 0.2 mV at Day 28 for blank LIP) (**Figure 2-11C**).

In term of drug leakage, the percentage of plumbagin retention in both Tf-bearing

liposomes and control liposomes remained stable, with a slight decrease of plumbagin

(less than 5%) over 4 weeks (from 79.1 ± 0.4% to 75.0 ± 0.9% for Tf-LIP and 78.5 ±

0.4% to 73.6 ± 0.9% for LIP) (**Figure 2-11D**).
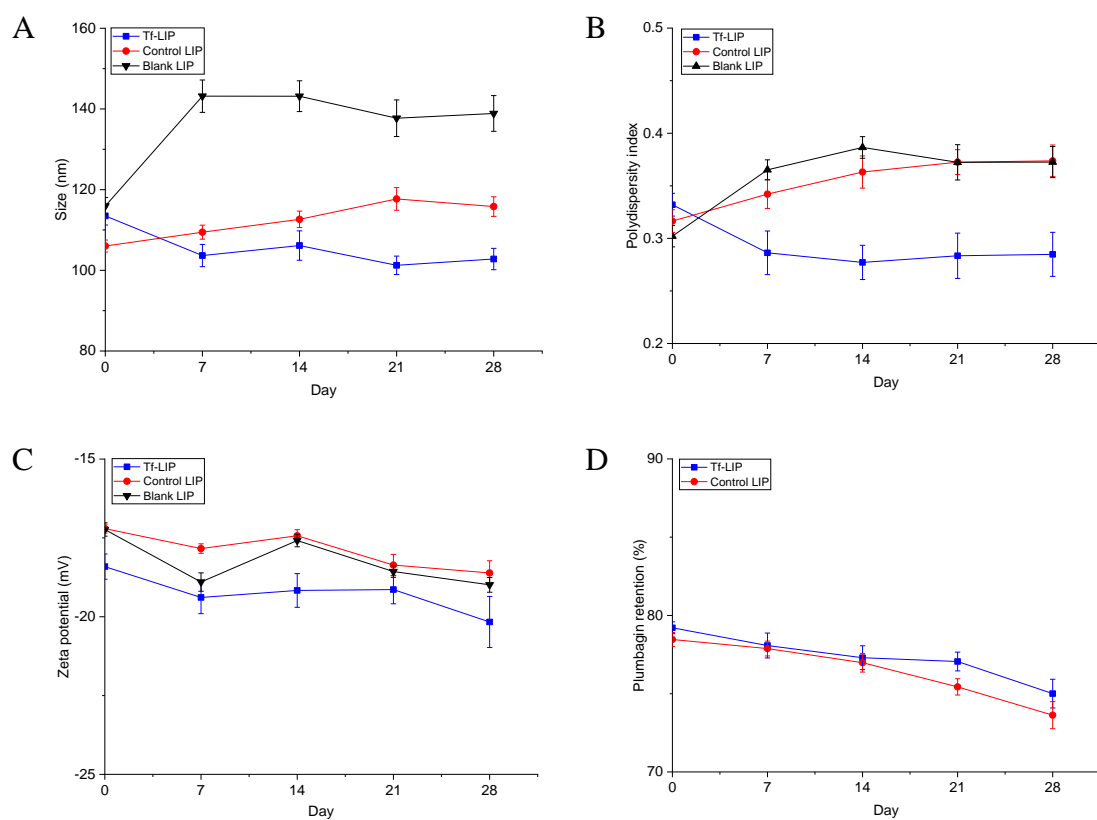
Figure 2-11: Size (A), polydispersity index (B), zeta potential (C) and percentage

retention (D) of plumbagin in Tf-bearing, control and blank liposomes after storage at 4

°C for 4 weeks (*n*=3)

For polymeric nanoparticles, all formulations of PLGA-PEG nanoparticles were found to be stable under storage condition at 4°C for at least 4 weeks. Tf-PN displayed a slight increase in size within 28 days (from 152.9 ± 0.6 nm at Day 0 to 163.1 ± 1.2 nm at Day 28 for size and 0.20 ± 0.01 at Day 0 to 0.21 ± 0.01 at Day 28 for polydispersity), while control PN (from 93.0 ± 0.3 nm at Day 0 to 94.9 ± 0.5 nm at Day 28 for size and 0.13 ± 0.00 at Day 0 to 0.14 ± 0.00 at Day 28 for polydispersity) and blank PN (from 83.7 ± 0.2 nm at Day 0 to 85.4 ± 0.5 nm at Day 28 for size and 0.12 ± 0.01 at Day 0 to 0.14 ± 0.01 at Day 28 for polydispersity) have almost a constant particle size over the duration of the experiment (**Figure 2-12A, 12B**). The zeta potential of all PLGA-PEG formulations showed an increase after 4 weeks but remained negatively charged (-34.3 ± 0.2 mV at Day 0 to -24.2 ± 0.3 mV at Day 28 for Tf-PN, -39.8 ± 0.9 mV at Day 0 to -28.4 ± 1.0 mV at Day 28 for control PN and -33.5 ± 0.5 mV at Day 0 to -26.5 ± 1.2 mV at Day 28 for blank PN) (**Figure 2-12C**). The percentage of plumbagin retention in Tf-PN and control PN was almost constant, with a slight decrease of plumbagin over 4 weeks (from $43.3 \pm 0.6\%$ to $40.9 \pm 0.4\%$ for Tf-PN and $59.8 \pm 0.2\%$ to $53.6 \pm 0.4\%$ for control PN) (**Figure 2-12D**).
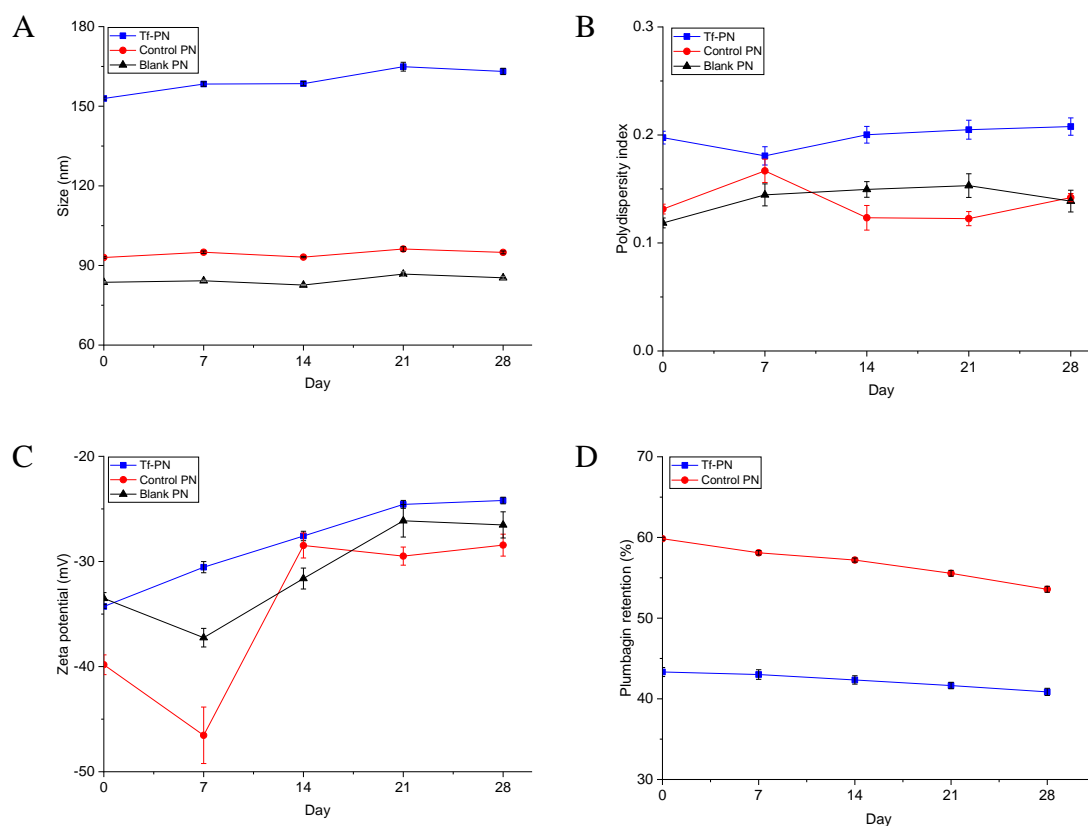
Figure 2-12: Size (A), polydispersity index (B), zeta potential (C) and percentage retention (D) of plumbagin in Tf-bearing, control and blank PLGA-PEG nanoparticles after storage at 4 °C for 4 weeks (*n*=3)

For the lipid-polymer hybrid nanoparticles, the particle size of Tf-LPN was found to increase over 4 weeks (from 214.1 ± 1.5 nm at Day 0 to 281.8 ± 3.7 nm at Day 28 for size and 0.17 ± 0.01 at Day 0 to 0.26 ± 0.01 at Day 28 for polydispersity), while control LPN (from 145.2 ± 0.6 nm at Day 0 to 143.1 ± 1.1 nm at Day 28 for size and 0.16 ± 0.01 at Day 0 to 0.13 ± 0.01 at Day 28 for polydispersity) and blank LPN (from 139.7 ± 0.4 nm at Day 0 to 138.7 ± 1.3 nm at Day 28 for size and 0.16 ± 0.01 at Day 0 to 0.14 ± 0.01 at Day 28 for polydispersity) have a constant particle size (**Figure 2-13A, 13B**). The zeta potential of all lipid-polymer hybrid formulations increased over the duration of the experiment (-46.6 ± 0.7 mV at Day 0 to -38.0 ± 0.2 mV at Day 28 for Tf-LPN, -66.6 ±

0.6 mV at Day 0 to -50.7 ± 0.6 mV at Day 28 for control LPN and -66.5 ± 0.3 mV at Day 0 to -47.2 ± 1.0 mV at Day 28 for blank LPN) (**Figure 2-13C**). The percentage of plumbagin retention in Tf-LPN slightly decreased over 4 weeks (from 48.0 ± 0.5% to 41.9 ± 0.5%), which was lower than that observed in control LPN (from 56.5 ± 0.4% at Day 0 to 44.1 ± 0.3% at Day 28) (**Figure 2-13D**).
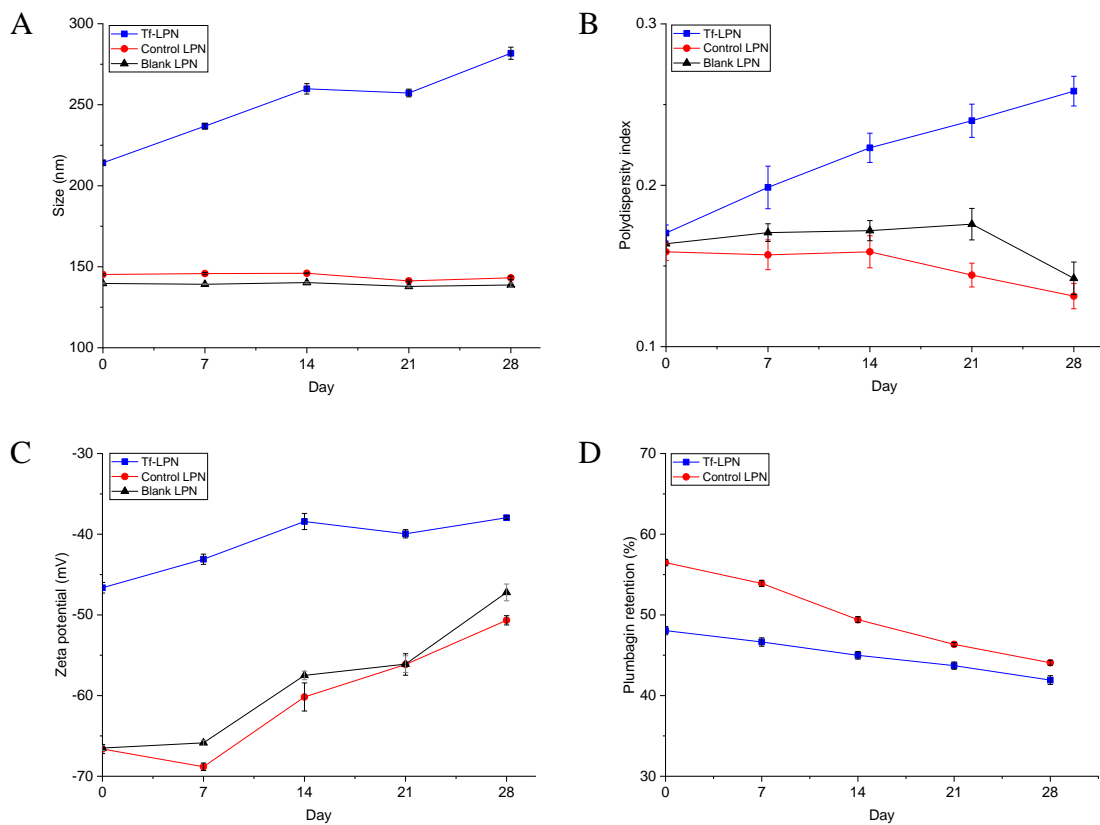
Figure 2-13: Size (A), polydispersity index (B), zeta potential (C) and percentage retention (D) of plumbagin in Tf-bearing, control and blank lipid-polymer hybrid nanoparticles after storage at 4 °C for 4 weeks (*n*=3)

2.4.7 Drug release profile

To confirm that plumbagin could be released from the delivery systems, the release profile of the drug was assessed by a dialysis technique at pH 5.5, 6.5 and 7.4, respectively mimicking the subcellular endosome, the tumour extracellular environment and the physiological pH in normal tissue and blood.

Tf-bearing and control liposomes showed similar release profile of plumbagin at all tested pHs, while plumbagin in solution diffused through the dialysis membrane to be completely released in 4 hours (**Figure 2-14**). An initial burst release of plumbagin (about 50 %) was observed in the first hour, followed by a sustained release of plumbagin with a maximum release to nearly 90-100 % in 10 hours. The conjugation of Tf to the surface of vesicles had a slight impact on the release profile of plumbagin at pH 7.4 (**Figure 2-14A**), with a percentage cumulative release of 88.3 ± 1.5 %, slightly lower than that observed at pH 6.5 (**Figure 2-14B**) and 5.5 (**Figure 2-14C**) during the first 10 hours (cumulative drug release of 96.99 ± 2.21 % at pH 6.5 and 95.53 ± 2.72 % at pH 5.5). The drug release from control liposomes also showed a similar profile and pH-independent trend (cumulative drug release of 96.51 ± 1.59 % at pH 7.4, 94.20 ± 1.85 % at pH 6.5 and 95.79 ± 1.12 % at pH 5.5, during the first 10 hours). In addition, it is worth mentioning that there is a decrease in the percentage cumulative release of plumbagin observed in our experiments at all tested pHs from 4 h for the plumbagin solution and from 10 h for the targeted and control liposomes. This can be explained by the fact that plumbagin can be evaporated from the solution once released from the liposomes.

A

B

C
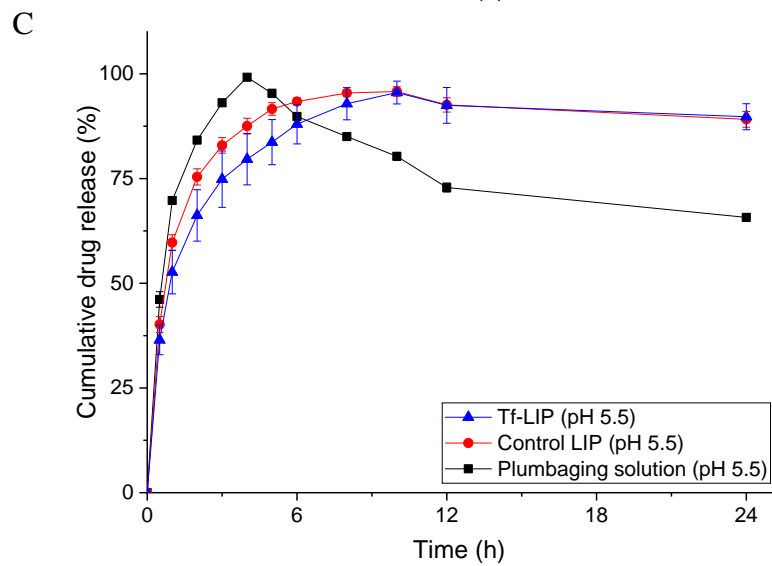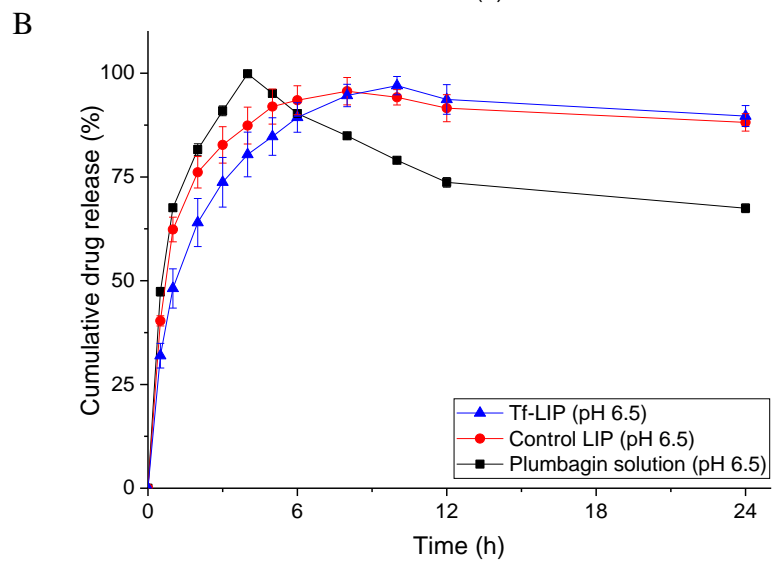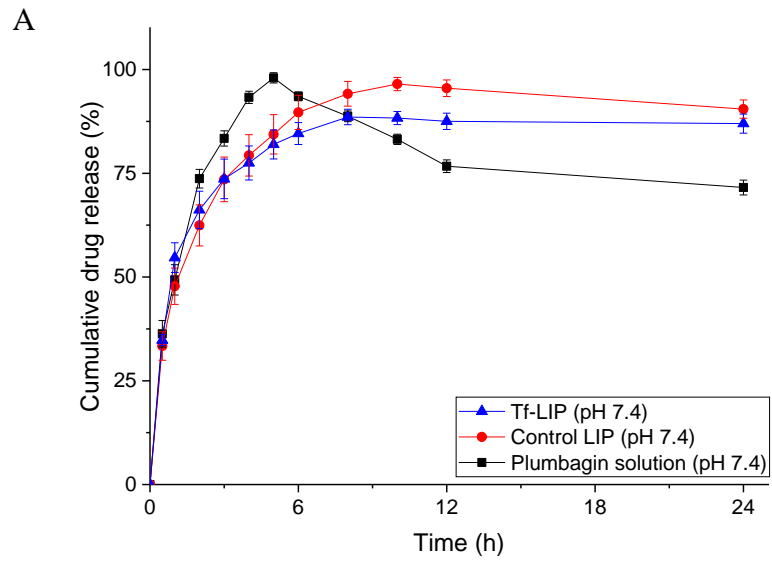
Figure 2-14: Drug release profile of plumbagin formulated as Tf-bearing and control liposomes or as free drug in phosphate buffer at pH 7.4 (A), 6.5 (B) and 5.5 (C) over 24 hours (n=3)

For polymeric nanoparticles, plumbagin was released from both Tf-PN and control PN in two phases with initial burst release in the first hour, followed by a sustained release of plumbagin in a pH-dependent manner over 24 hours (**Figure 2-15**). The conjugation of Tf to the surface of the nanoparticles also had an impact on the release profile of the drug. More precisely, at pH 7.4 (**Figure 2-15A**), plumbagin was initially burst released from Tf-PN with the cumulative drug release of 47.4 ± 0.9% at 1 hour, while 50.4 ± 1.0 % and 58.4 ± 0.4% of the drug was released from these nanoparticles respectively at pH 6.5 (**Figure 2-15B**) and 5.5 (**Figure 2-15C**) during the same period. Then, a steady release of plumbagin from Tf-PN was observed with a cumulative drug release of 85.4 ± 0.5% at pH 7.4, 91.4 ± 0.5% at pH 6.5 and 94.2 ± 0.9% at pH 5.5 at 24 hours. The drug release from the control PN followed a similar trend and pH-dependent manner but was faster than the targeted nanoparticles with a cumulative drug release of 90.1 ± 1.5% at pH 7.4, 93.3 ± 0.5% at pH 6.5, 97.3 ± 0.6% at pH 5.5 after 24 hours.
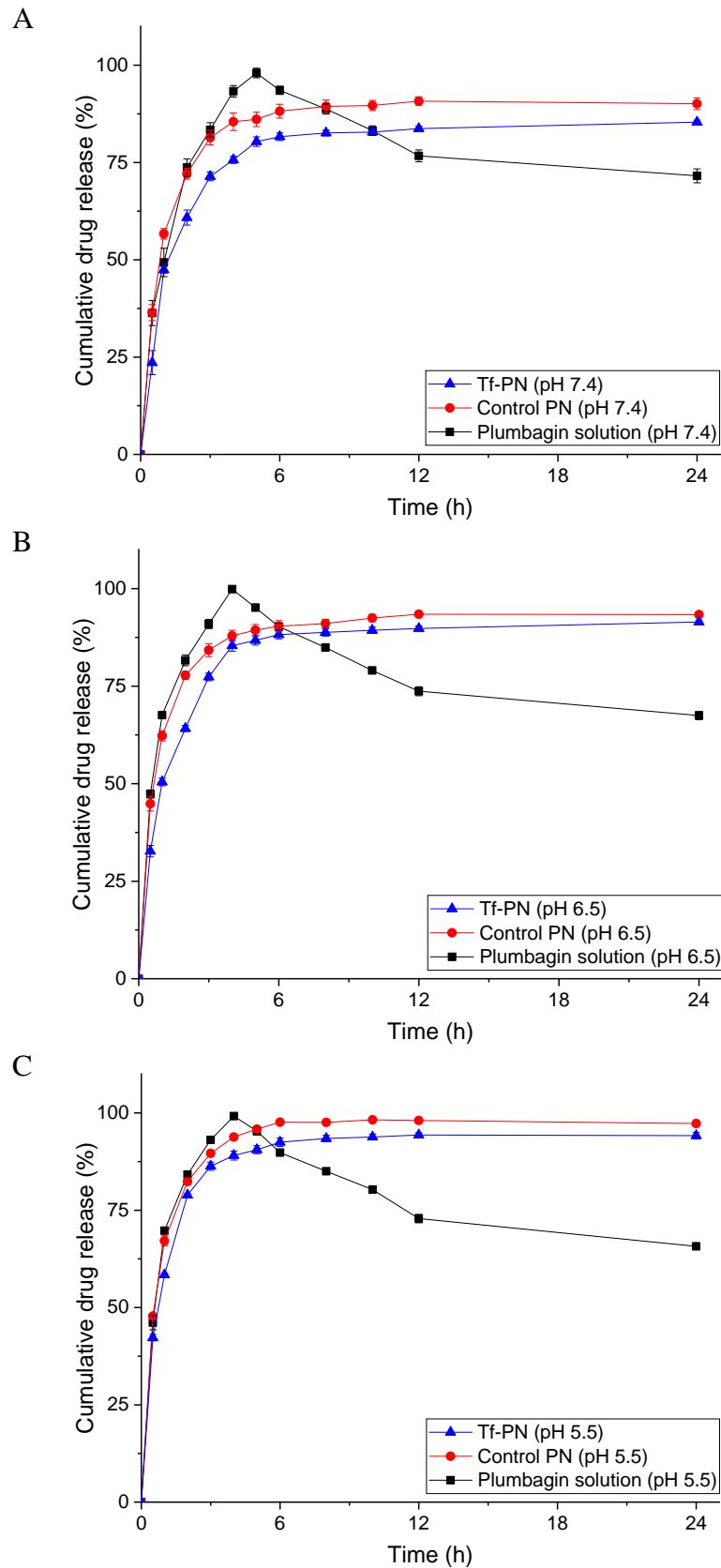
Figure 2-15: Drug release profile of plumbagin formulated as Tf-bearing and control PLGA-PEG nanoparticles or as free drug in phosphate buffer at pH 7.4 (A), 6.5 (B) and 5.5 (C) over 24 hours (*n*=3)

For lipid-polymer hybrid nanoparticle, both Tf-bearing and control lipid-polymer hybrid nanoparticles also exhibited a sustained release of plumbagin in a pH-dependent manner with an initial burst release (**Figure 2-16**). In addition, the conjugation of Tf to the nanoparticles slowed the release of the drug. Specifically, at pH 7.4 (**Figure 2-16A**), plumbagin was steadily released from the Tf-LPN with a cumulative drug release of 81.7 ± 1.4 % over a 24-hour period, while 87.2 ± 1.1 % and 95.4 ± 0.7 % of the drug was released from this nanoparticle respectively at pH 6.5 (**Figure 2-16B**) and 5.5 (**Figure 2-16C**) within the same period. The control LPN also exhibited a similar release trend of plumbagin with pH-dependent manner, but faster than that of Tf-LPN (cumulative drug release of 90.3 ± 1.0 % at pH 7.4, 95.1 ± 0.9 % at pH 6.5 and 98.9 ± 0.2 % at pH 5.5 within 24 hours).
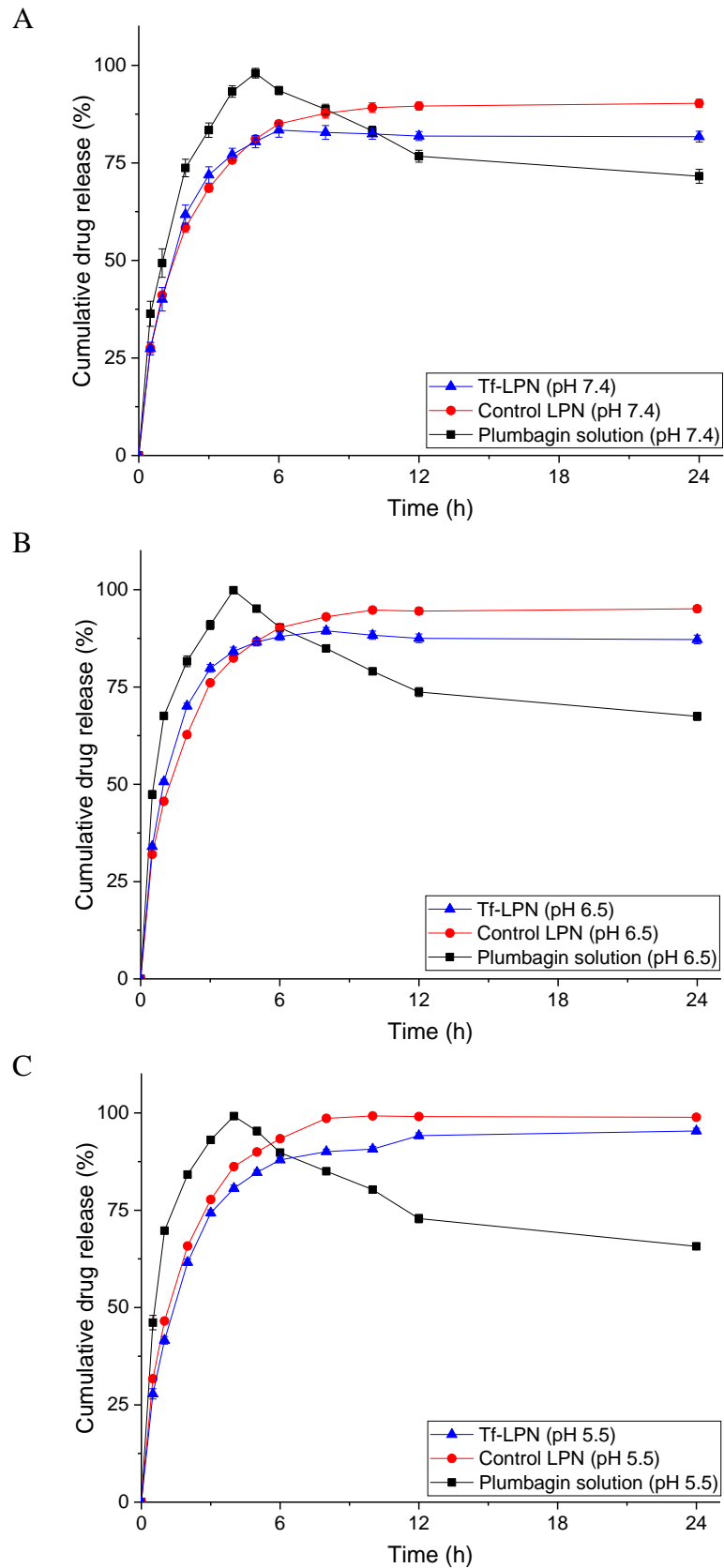
Figure 2-16: Drug release profile of plumbagin formulated as Tf-bearing and control lipid-polymer hybrid nanoparticles or as free drug in phosphate buffer at pH 7.4 (A), 6.5 (B) and 5.5 (C) over 24 hours (*n*=3)

2.5 Discussion

Plumbagin, a nature-derived naphthoquinone, has been reported to exert its anti-cancer effect in various types of cancer both *in vitro* and *in vivo*, for example breast, lung, prostate, cervical, liver, colon, brain and melanoma (Panichayupakaranant and Ahmad, 2016; Rajalakshmi et al., 2017; Checker et al., 2018). The therapeutic potential of plumbagin has however been limited so far, due to its poor solubility in water, lack of stability and low oral bioavailability, which limited its biopharmaceutical applications. Furthermore, plumbagin failed to specifically reach tumours at a therapeutic concentration due to its lack of tumour specificity and rapid elimination, with a short biological half-life.

To overcome this issue, we hypothesised that loading plumbagin into a tumour-targeted delivery system would enhance the specific delivery of plumbagin to cancer cells and increase the therapeutic efficacy both *in vitro* and *in vivo*, while at the same time reduce secondary effects to healthy tissues.

In this study, liposomes, polymeric nanoparticles and lipid-polymer hybrid nanoparticles were used as carriers of plumbagin. A liposomal formulation similar to that of Doxil® liposomes was selected, as it demonstrated long blood circulation half-life achieved by sterically stabilized liposomes with PEG (PEGylation) using DSPE-PEG2K (Čeh *et al*., 1997). PLGA-PEG block co-polymer was used in this study due to their physico-chemical properties such as biocompatibility, biodegradability, increasing drug solubility, enhancing drug bioavailability, protecting the drug from premature degradation and interaction with the biological environment and controlling drug release (Kumari *et al*., 2010; Makadia and Siegel, 2011; Li *et al*., 2018). Finally, plumbagin was entrapped in novel lipid-polymer hybrid nanoparticles as this delivery system combined characteristics of both PEGylated liposomes and polymeric nanoparticles. The PLGA

polymer was used to form the polymeric core of the hybrid nanoparticles which entrapped plumbagin, surrounded by a lipid monolayer consisting of HSPC and DSPE-PEG2K-MAL that provided a stealth effect (from PEG) as well as facilitating surface modification. In addition, all lipids and polymers used in this study have also been approved by the United States Food and Drug Administration (US FDA) and the European Medicines Agency (EMA) for use in humans (Barenholz, 2012; Sharma *et al*., 2016).

Using unmodified nanocarriers, however, may not be enough to improve tumour targeting of plumbagin, resulting from non-selective accumulation in other healthy tissues. Therefore, conjugation of nanocarriers with an active targeting ligand would be a promising way to improve tumour specificity and cellular uptake via receptor-mediated endocytosis. In this study, we selected Tf, an iron-transporting protein, as a targeting ligand whose receptors are overexpressed in most proliferating cells including cancer cells (Tortorella and Karagiannis, 2014). Our research group have previously prepared Tf-conjugated Span60/Solulan C24 niosomes entrapping the green tea polyphenol epigallocatechin gallate (EGCG) and tocotrienol that shared the same delivery issues as plumbagin. These targeted niosomes significantly increased the cellular uptake and anti-proliferative activity of the drugs in comparison with control niosomes and drug solution for all the tested cancer cell lines. This resulted in complete tumour suppression of respectively 40% and 60% of B16-F10 melanoma following intravenous injection of EGCG-loaded and tocotrienol-loaded vesicles over one month (Fu *et al*., 2009; Fu *et al*., 2011; Lemarié *et al*., 2013; Fu *et al*., 2014; Karim *et al*., 2017). In another study, systemic administration of Tf-modified polymeric nanoparticles loading resveratrol in rats bearing C6 glioma significantly decreased tumour volume and prolonged animal's lifespan compared to unmodified nanoparticles and free resveratrol (Gou *et al*., 2013), thus

highlighting the need of a tumour-targeted delivery system for delivering these compounds to their site of action.

For liposomes preparation, a stock solution of plumbagin was first prepared using DMSO prior vesicle preparation as it has poor solubility in water. The presence of DMSO also contributes to the increase of drug entrapment (Fu, 2010; Dhakar *et al.*, 2012; Shariat *et al.*, 2014). The lipids were heated at 75 °C above the phase transition temperature of phospholipids. Probe sonication was then used, as self-assembly of lipid bilayer is generally requires an input of energy (Uchegbu and Vyas, 1998; Gregoriadis, 2007). After preparation of control liposomes, transferrin was conjugated to the vesicles using the thiol–maleimide 'click' reaction described by Hermanson (2013) with some modifications (**Figure 2-17**). This method is one of the most widely used thiol-based bioconjugation techniques for grafting delivery systems with peptides, proteins or antibodies due to its high selectivity, rapid reaction (without heat or catalyst), compatibility with aqueous condition (Stenzel, 2013; Ponte *et al.*, 2016). In this study, transferrin was successfully conjugated to liposomes at the level of 50.7 ± 0.5 % of the initial Tf added, which was similar to our previous conjugation rate of around 50% obtained when using dimethylsuberimidate as a crosslinking agent (Dufès *et al.*, 2000; 2004). This result is also consistent with previous reports by Lopalco and colleagues (2018) when dopamine-loaded liposomes (HSPC:cholesterol at 7:3 molar ratio and 2.5 mol % of DSPE-PEG2K-COOH) was conjugated with transferrin (120 mg per mmol of lipid) using NHS/EDC coupling reagents (incubated for 12 h at 4 °C), resulting in a Tf conjugation efficiency of 48.8%. Jhaveri and colleagues (2018) reported slightly higher conjugation efficiency (60-70%) when preparing Tf-targeted resveratrol-loaded liposomes. In their study, a carbonate PEG derivative of DOPE (pNP-PEG3400-DOPE)

was synthesised and directly conjugated with Tf to obtain Tf-PEG3400-DOPE micelles, followed by post-insertion in the liposomes.
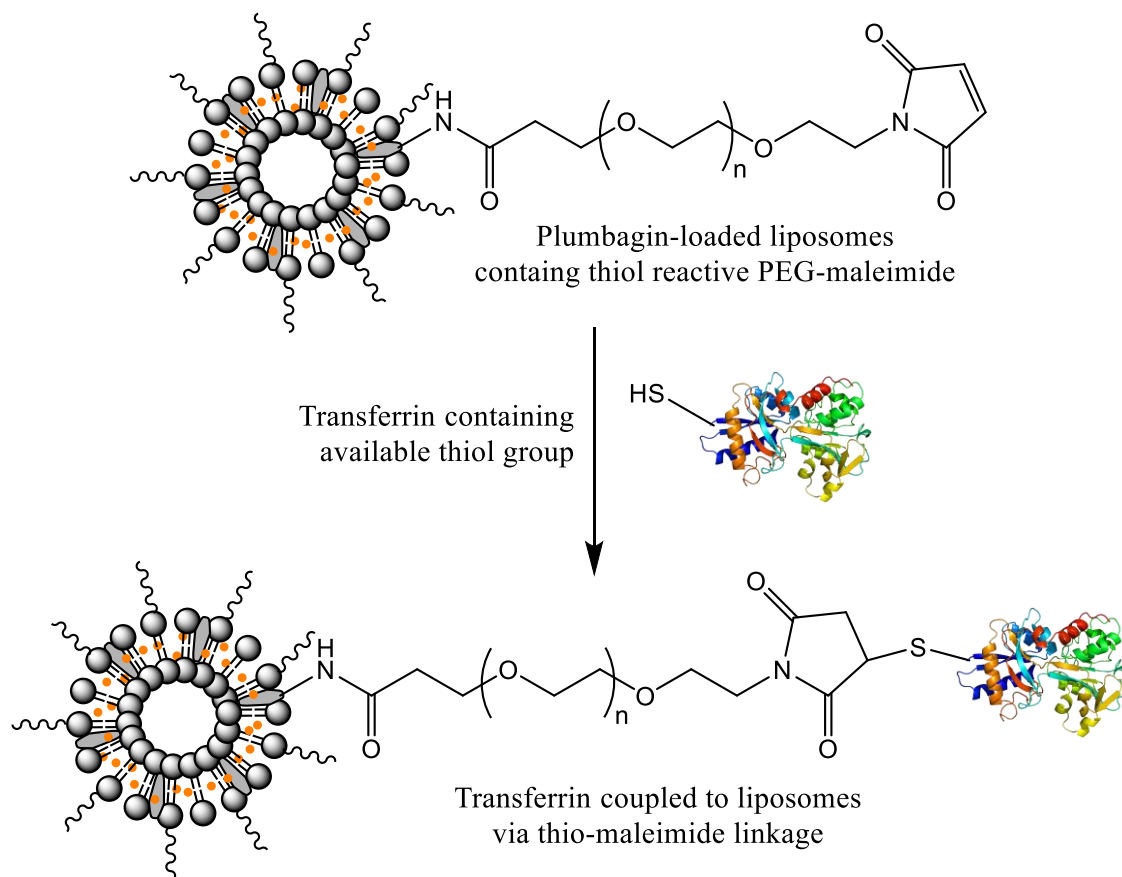
Figure 2-17: Conjugation reaction of Tf to the liposomes entrapping plumbagin. Cholesterol-PEG-maleimide is used to provide thiol-reactive groups (maleimide). Thiolated Tf can then be conjugated to this reactive intermediate to form covalent thioether bonds (adapted from Hermanson, 2013)

For preparation of PLGA-PEG nanoparticles entrapping plumbagin, nanoprecipitation method was selected, owing to its advantages over emulsification techniques, such as simple, rapid and surfactant-free preparation (Dinarvand *et al*., 2011; Almoustafa *et al*., 2017). Acetone was chosen as an organic solvent due to its low toxicity and low risk to human health (International conference on harmonisation of technical requirements for

registration of pharmaceuticals for human use (ICH) solvent classification: class III) (ICH, 2018) as well as its ease of removal (low boiling point, 56.2 °C) (Almoustafa *et al.*, 2017). For nanoparticle optimisation, we studied the effect of varying the volume ratio of water to organic solvent on the physical properties of PLGA-PEG nanoparticles. The smallest size of PLGA-PEG nanoparticles was obtained at low volume ratios of water: organic solvent of 2:1 and 3:1 and slightly increased when the ratios were ranging from 5:1 to 10:1. The largest size of PLGA-PEG nanoparticles was found at the volume ratio of water: organic solvent of 1:1. This could be due to poor phase separation between a polymer-rich phase (organic phase) and a polymer-poor phase (water phase) (Cheng *et al.*, 2007). By contrast, increasing the volume ratio of water: organic solvent caused significant decrease in the entrapment efficiency of plumbagin, which was similar to previous reports by Pan and colleagues (2017) when optimising aptamer-targeted PLGA-PEG nanoparticles entrapping plumbagin. After successful optimisation, PLGA-PEG nanoparticles were conjugated with Tf using the thiol–maleimide 'click' reaction, with a conjugation efficiency of 58.2 ± 1.2 % of the initial Tf added (equivalent to 165 μg of Tf per 1 mg of nanoparticles). This was higher than that was previously reported by Sahoo and Labhasetwar, who obtained a very low transferrin conjugation (only 2.9% w/w). In their study, PLGA nanoparticles entrapping paclitaxel (containing polyvinyl alcohol; PVA) were activated by an epoxy compound (a polyglycerol polyglycidyl ether; Denacol EX-512), followed by conjugation with transferrin at 37 °C for 2 h (Sahoo and Labhasetwar, 2005). In addition, Frasco and colleagues (2015) prepared transferrin-adsorbed PLGA nanoparticles entrapping bortezomib (PLGA, MW 24,000-38,000 Da) using physical adsorption method (incubation overnight with holo-Tf at room temperature), resulting in 49.7 μg of Tf adsorbed to nanoparticles (1 mg).

For the lipid-polymer hybrid nanoparticles, PLGA-COOH, a hydrophobic and biodegradable polymer, was used to form the polymeric core of the hybrid nanoparticles which entrapped plumbagin, surrounded by a lipid monolayer consisting of HSPC and DSPE-PEG2K-MAL that provided a stealth effect (from PEG) as well as facilitating surface modification (from MAL). The lipid-polymer hybrid nanoparticles were prepared by using one-step nanoprecipitation method, where the PLGA polymer (in water-miscible organic solvent) is mixed with the aqueous lipid dispersion in which they self-assembled. This method is more effective, requires less time and less energy, unlike the two-step method, where polymeric nanoparticles and lipid vesicles are prepared separately before being mixed (or ultrasonicated) and then homogenised (Hadinoto *et al*., 2013). For nanoparticle optimisation, based on the above information obtained from the PLGA-PEG nanoparticles, we also used acetone as an organic solvent, while fixing polymer concentration (10 mg/mL), plumbagin loading (10% w/w of polymer) and a volume ratio of water to acetone of 2:1. The optimal formulation of lipid-polymer hybrid nanoparticles was found at low lipid to polymer weight ratio (10-20%) which can be explained by the fact that, at this range, the entire surface of the PLGA-COOH polymer core was covered by the amount of lipids used (Zhang *et al*., 2008). On the contrary, at high lipid to polymer weight ratios, the excess HSPC and DSPE-PEG2K-MAL can spontaneously form liposomes, resulting in an increase of the overall measured size of lipid-polymer hybrid nanoparticles and lowering their zeta potential value. In addition, when keeping the lipid to polymer weight ratio at 20%, the increase of DSPE-PEG2K-MAL (40-50 mol%) also influenced both particle size and zeta potential of lipid-polymer hybrid nanoparticles, which might be due to the molecular conformations of PEG chains at different grafting densities (Zhan *et al*., 2012; Zhang *et al*., 2015b). At low density (10-30 mol%), the PEG chains formed a "mushroom" configuration which had low influence

on the particle size and zeta potential of lipid-polymer hybrid nanoparticles. However, at high density (40-50 mol%), PEG chains begin to stretch away from the surface and formed a "brush" structure, leading to an increase in the particle size as well as zeta potential due to shielding effect of PEG molecules. In the same manner, the conjugation of Tf to lipid-polymer hybrid nanoparticles was achieved by the thiol–maleimide 'click' reaction with a conjugation efficiency of 72.2 ± 0.5 % of the initial Tf added.

The encapsulation efficiency is one of the important parameters in the design of drug delivery systems. This parameter relies on several factors such as the types and compositions of nanocarrier, as well as the nature of drug load (Uchegbu *et al.*, 1998). Due to its lipophilic character, plumbagin can be entrapped mainly in the lipid bilayer of liposomes and the hydrophobic core of polymer-based nanoparticles. Our results indicated that all types of nanocarriers prepared in this study exhibited high entrapment efficiency of plumbagin, ranging from 45- 80 %. Plumbagin has previously been reported to be entrapped in various types of delivery systems. Our liposomes have higher entrapment efficiency of plumbagin than that was previously reported by Naresh and colleagues (1996), who developed plumbagin-loaded niosomes (cholesterol: span 60: dicetyl phosphate at molar ratio of 47.5:47.5:5), which were able to entrap 52% of plumbagin. A maximum entrapment efficiency of 66 % was found when entrapping plumbagin in liposomes (soybean phosphatidylcholine and cholesterol at molar ratio of 9:3) (Kumar *et al*., 2011). For PLGA-PEG nanomedicines, Pan and colleagues (2017) reported a lower entrapment efficiency than our polymeric nanoparticles (about 50-60% entrapment) when entrapping plumbagin in aptamer-targeted PLGA-PEG nanoparticles (PLGA, lactide: glycolide 50:50, MW ~17 kDa) with an entrapment efficiency of about 38 %. Plumbagin has also been entrapped in PLGA microspheres (PLGA, lactide: glycolide 50:50, MW 54 kDa) with 70% entrapment (Singh *et al*., 1996), higher than that

of our PLGA-PEG formulation. This variation in plumbagin entrapment efficiency observed in PLGA-based nanoparticles might be explained by the differences in the molecular weight of PLGA used for nanoparticle preparation. In general, higher molecular weight of the hydrophobic polymer chain shows a better drug loading (Zhang *et al*., 2014). However, it should be noted that the length of hydrophilic polymer chain (PEG segment), polymer concentration, drug to polymer ratio and preparation methods also affect the drug loading efficiency of polymeric nanoparticles (Zhang *et al*., 2014). To our knowledge, this is the first report for the preparation of Tf-bearing lipid-polymer hybrid nanoparticles entrapping plumbagin. We could not find any studies reporting the entrapment efficiency of plumbagin loaded lipid-polymer hybrid nanoparticles to allow a comparison with our results.

Particle size and morphology are also important characteristics of nanocarriers. They can affect several biological phenomena such as a recognition by the MPS, blood circulation time, biodistribution, extravasation through leaky vasculature, accumulation in tumours, targeted and cellular internalisation (Toy *et al.*, 2014; Blanco *et al.*, 2015). Small particles (less than 5 nm) are rapidly cleared from blood circulation by renal clearance, while large particles are rapidly recognised by the MPS. Particles larger than smallest blood capillaries (higher than 5 µm) can cause embolism (Müller *et al.*, 1998). Moreover, the vascular endothelium of tumours tends to become more permeable, allowing the extravasation of nanoparticles ranging from 400 to 600 nm (Yuan *et al.*, 1995). In term of morphology, spherical or ovoidal particles can be more rapidly internalised by the cells compared to elongated ellipsoids and worm-like particles (Herd *et al.*, 2013; Toy *et al.*, 2014). All Tf-bearing and control formulations in our study had spherical shape and displayed the required sizes (ranging from 93 to 216 nm) that should theoretically allow their extravasation through the leaky vasculature of most tumours via the EPR effect

(Yuan *et al*., 1995). In addition, the polydispersity index of all formulations was low (0.10 – 0.34), indicating a uniformly dispersed nanomedicine formulation with a narrow size distribution.

The surface charge of nanocarriers is also an important parameter that affects their stability, blood circulation time and selective accumulation in tumours. Negative (zeta potential less than -10 mV) and positive nanoparticles (zeta potential higher than 10 mV) exhibit high opsonisation with serum proteins compared to neutral particles (zeta potential within ±10 mV), resulting in rapid clearance by the RES and short circulation time (Ernsting *et al.*, 2013; Blanco *et al.*, 2015). Gessner *et al.* (2013) demonstaretd that positive nanoparticles tend to adsorb proteins with an isoelectric point (pI) lower than 5.5, such as albumin (pI = 4.7), while negative nanoparticles adsorb proteins with pI higher than 5.5, such as IgG (pI = 6.6-7.2). Moreover, it should be noted that the aggregates of positive nanoparticles and negatively charged serum proteins are often large, thus causing transient embolism in the lung capillaries (Li and Huang, 2008). In this study, zeta potential experiments have shown that all Tf-bearing and control nanomedicine formulations were bearing negative charges (between -17 mV and -67 mV). Therefore, these negatively charged nanoparticles would eventually reduce the risk of having electrostatic interactions between nanocarriers and negatively charged serum proteins, avoiding a rapid clearance by the MPS and prolonging blood circulation time (Ernsting *et al*., 2013; Blanco *et al*., 2015). In addition, the cellular internalisation is known to depend on the net surface charge of nanoparticles. Although positively charged nanoparticles have been shown to improve internalisation in many cancer cells (by interaction with negatively charged cell membrane), they also have a higher rate of non-specific uptake in normal cells (Blanco *et al*., 2015). Thus, the negative surface charge on the Tf-bearing nanomedicines in our study would enhance a specific delivery of

plumbagin to cancer cells, while minimising non-specific uptake of nanomedicines by healthy cells. The zeta potential is also related to the stability of a colloidal system. Colloidal dispersions with zeta potentials of more than ±30 mV and ±20-30 mV, ±10-20 mV and ±0-10 mV, are commonly classified as highly stable, moderately stable, relatively stable and highly unstable, respectively (Bhattacharjee, 2016). Our nanocarriers therefore have the required colloidal stability for being efficient delivery systems of plumbagin.

The physico-chemical stability of drug delivery systems is one of the essential parameters that affect their quality, safety and therapeutic efficacy. For liposome formulations, the changes in size, zeta potential and drug leakage ability of Tf-bearing and control liposomes was minimal when they were stored at low temperature, unlike blank liposomes, whose size significantly increased over time. This may be attributed to the presence of plumbagin in the lipid bilayer of the liposomes, thus increasing membrane rigidity while maintaining the negative surface charge and preventing liposome agglomeration. A similar observation was recently reported by Tsermentseli and colleagues (2018) regarding the entrapment of shikoni, another natural naphthoquinone compound, in PEGylated liposomes made of DOPC, DSPG and DSPE-mPEG2K. The authors reported that the drug-loaded liposomes also displayed a higher stability in size and zeta potential than that of empty liposomes when stored over 28 days at 4°C.

For polymeric and hybrid nanoparticles, although the deterioration in size and drug leakage ability of Tf-bearing and control formulations was low, the zeta potential of all nanoparticles was found to increase. This may be due to the hydrolytic degradation of PLGA to acidic oligomers and monomers of both lactic acid and glycolic acid, thus causing a pH drop and zeta potential increase of the nanoparticle formulations. This observation was previously reported by Hirsjärvi, regarding the effect of pH on the

stability of poly(lactic acid) (PLA) nanoparticles. When the pH of PLA nanoparticles is titrated to acidic values (from pH 7 to pH 2) by adding hydrochloric acid, the zeta potential of these nanoparticles increased (from -30 mV to -10 mV) (Hirsjärvi, 2008). Simon and colleagues (2016) recently reported a similar trend when the PLGA nanoparticles were exposed to gastric pH (pH 2), the zeta potential became close to neutral (raised from -36 mV to 0.35 mV).

Drug release profile is one the most noticeable parameters in the development of controlled release systems, which determines the concentration of the drug at the targeted sites as well as its therapeutic efficacy upon administration (Maherani *et al*., 2013). In this study, the release profile of plumbagin-loaded nanomedicines was determined using a dialysis method in phosphate buffer at three different pHs (7.4, 6.5 and 5.5). This release experiment indicated that plumbagin could be efficiently released from the targeted liposomal formulation in a sustained manner within 10 hours. However, its release was faster than expected and not pH-optimal yet, and should therefore be further optimised. The release of plumbagin from Tf-bearing liposomes followed a similar trend as previously described from plumbagin-loaded liposomes (made of phosphatidylcholine, cholesterol at a 9:1 molar ratio), with 100% cumulative drug release being observed within 12 hours at pH 7.4 (Kumar *et al*., 2011).

Plumbagin was released from polymeric and hybrid nanoparticles in a sustained manner with initial burst release. In general, polymer-based nanoparticles can release their entrapped drug using four basic mechanisms: (i) diffusion through water-filled pores, (ii) diffusion through the polymer matrix, (iii) osmotic pumping and (iv) erosion of the matrix (Karmaly *et al*., 2016). Although drug release may occur by any or all of these mechanisms (Pawar *et al*., 2016), the diffusion of drug through water-filled pores is the most common mechanism (Fredenberg *et al*., 2011). A pore-forming process, highly

dependent on the hydrophilicity of polymers, occurs immediately after water absorption by polymer-based nanoparticles. Thus, the initial burst release observed in our polymer-based nanoparticles may be due to the presence of PEG, which facilitates water absorption and accelerates the diffusion of plumbagin entrapped in the outer layer of polymer core through water pores. In addition, it is worth mentioning that low molecular weight compounds (i.e. plumbagin, MW of 188.17 g/mol) also have a high propensity for burst release due to osmotic pressure (Karmaly *et al.*, 2016). The following sustained release of plumbagin from polymer-based nanoparticles may occur by diffusion of the drug entrapped in polymeric core through water-filled pores. Pan and colleagues (2017) described a similar release of plumbagin. In their study, plumbagin was also rapidly released (66% in PBS pH 7.4) from aptamer-targeted PEG-PLGA nanoparticles in the first 2 hours, then its cumulative release increased constantly to 87% after 24 hours. In our study, Tf-bearing polymeric and hybrid nanoparticles showed slower release of plumbagin than their control counterparts. This may be due to the ability of Tf conjugated to the surface of nanoparticles to reduce water absorption by the nanoparticles, therefore slowing the rate of plumbagin diffusion through water-filled pores. Similar to our results, the release of docetaxel from Tf-targeted TPGS micelles (in PBS pH 7.4 containing 0.1% w/v Tween 80) was significantly slower than non-targeted micelles (Muthu *et al.*, 2015). Moreover, plumbagin was released from polymeric and hybrid nanoparticles in a pH-dependent manner. This may be particularly beneficial because plumbagin will be slowly released from the nanoparticles at the physiological pH (pH 7.4) after intravenous injection, minimising any secondary side effects on normal tissue. Once the nanoparticles reach the acidic tumour microenvironment (pH 5.5-6.5), they will rapidly release plumbagin, allowing it to exert its therapeutic effect.

CHAPTER 3

In vitro cell culture evaluation of tumour-targeted

nanomedicines entrapping plumbagin

3.1 Introduction

In recent years, cell culture has become one of the most important techniques used for drug discovery and development in the pre-clinical stage, since the first cancer cell line, HeLa, was introduced in the late nineteenth century (Ravi *et al*., 2015; Jaroch *et al*., 2018). The main features of cell culture are the ease to control the physiochemical environment (i.e. pH and temperature), the flexibility of experimental designs as well as the repeatability and reproducibility of measurements (Ravi *et al*., 2015; Amelian *et al*., 2017). By carefully selecting suitable cell lines and experimental conditions, cell-based assays can provide fundamental information which can be used to predict possible *in vivo* outcomes such as therapeutic activity, bioavailability and toxicity (Kura *et al*., 2014; Amelian *et al*., 2017; Gordon *et al*., 2018). In the field of drug delivery systems, cell culture is used as a baseline test to evaluate nanomedicines for their biological efficacy, cellular accumulation and internalisation of drugs and safety (Kura *et al*., 2014).

In this study, the main purpose of using tumour-targeted nanomedicines is to increase the specific delivery of plumbagin upon cellular internalisation at the target site where they can exert their therapeutic effects in specific subcellular compartments such as cytosol, mitochondria or nucleus (Sriraman *et al.*, 2014). Therefore, investigating the cellular uptake and internalisation mechanism of nanomedicines entrapping plumbagin will confirm the hypothesis that conjugating nanocarriers with a targeting ligand would enhance the uptake of plumbagin by the targeted cells.

Although low molecular weight drugs or hydrophobic drugs, like plumbagin, are able to enter the cells by simple diffusion (Blanco *et al.*, 2015), the uptake of nanoparticles requires an active transport called endocytosis, which is classified into two major pathways, phagocytosis and pinocytosis (Kou *et al.*, 2013). Phagocytosis is a process by which phagocytic cells (i.e. macrophages, neutrophils, monocytes and dendritic cells)

engulf large particles (larger than 0.5 µm) including nanoparticle-opsonin complexes (Rosales and Uribe, 2017). Pinocytosis is a process allowing the uptake of fluids, solutes as well as nanoparticles. It can be further divided into four sub-pathways: clathrin-dependent endocytosis, caveolae-dependent endocytosis, clathrin/caveolae-independent endocytosis and macropinocytosis (**Figure 3-1**) (Sahay *et al.*, 2010; Ernsting *et al.*, 2013).
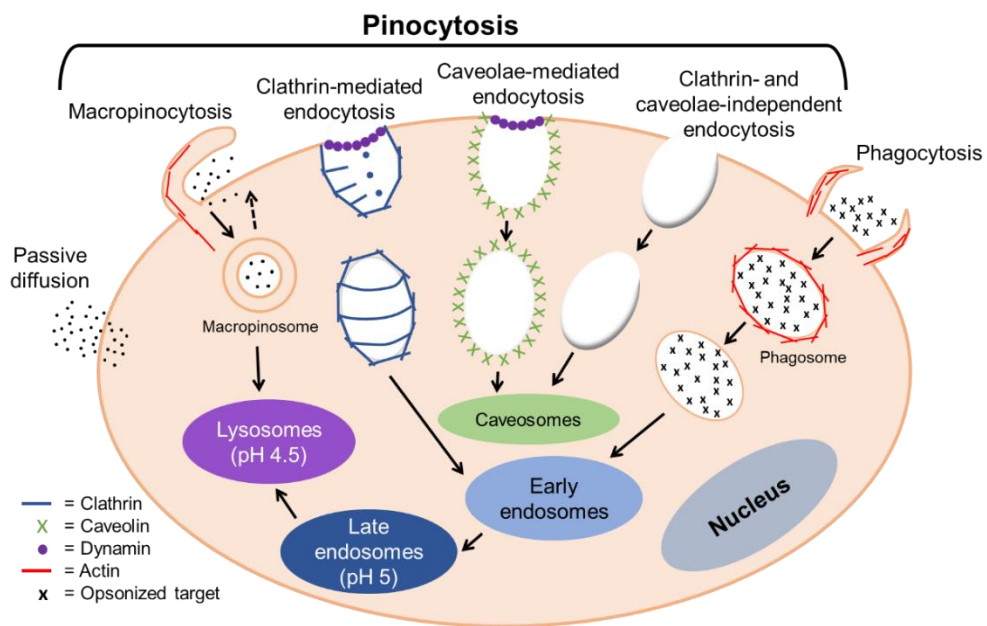
Figure 3-1: Summary of cellular internalisation pathways of nanocarriers (adapted from Panariti *et al.*, 2012)

Several inhibitors have been used to investigate the cellular uptake mechanisms of nanocarriers. Chlorpromazine is a common blocker of clathrin-mediated endocytosis, the main uptake mechanism of most nanocarriers, which causes the depletion of clathrin and adaptor proteins required for the formation of clathrin-coated pits (Herd *et al*., 2013). Filipin, a mixture of four isomeric polyene macrolides isolated from *Streptomyces filipinensis*, is used to inhibit caveolae-mediated endocytosis by binding caveolae-rich cholesterol, thus causing malfunction of caveolae (Schnitzer et al., 1994). Another

blocker, colchicine, inhibits macropinocytosis, a non-specific process for internalisation of fluids and large particles (> 200 nm) by inhibiting the polymerisation of microtubules, thereby preventing membrane ruffling (Herd *et al.*, 2013).

In vitro cytotoxic assays are widely used to monitor the cell response following treatment with test substances, generally using colorimetric, fluorimetric or bioluminescent techniques (Amelian *et al.*, 2017). MTT assay, a tetrazolium-based assay using 3-(4,5-dimethylthiazol-2-yl)-2,5-diphenyl-tetrazolium bromide (MTT), is a colorimetric technique used to determine the cytotoxic effect of drugs by measuring the percentage of cell viability. The principle of MTT assay is based on the mitochondrial activity of living cells that can convert MTT, a yellow, water-soluble tetrazolium salt, into insoluble purple formazan product (**Figure 3-2**). The formazan crystals can be dissolved in DMSO, ethanol, methanol, acidified isopropanol, and their absorbance can be measured at a wavelength of 570 nm (Lui *et al.*, 1997; Meerloo *et al.*, 2011; Stockert et al., 2012).
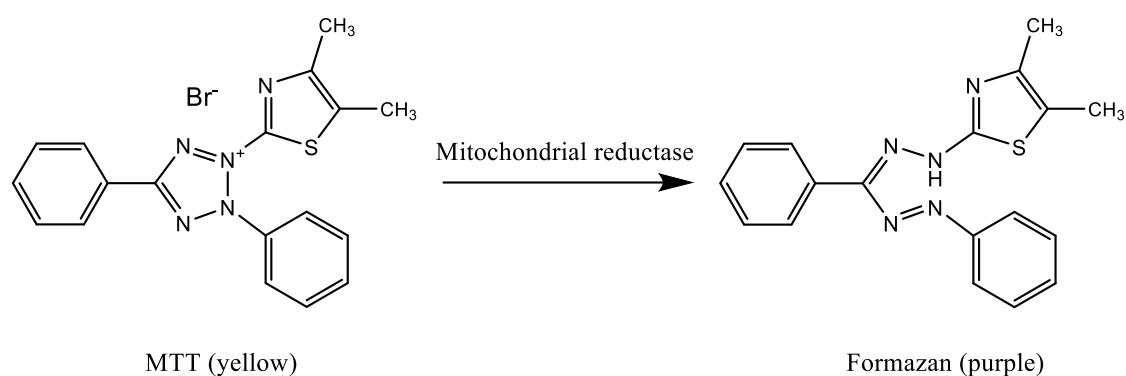
Figure 3-2: Reduction of 3-(4,5-dimethylthiazol-2-yl)-2,5-diphenyl-tetrazolium bromide (MTT) in living cells by mitochondrial reductase to form the insoluble formazan product

Apoptosis is a form of programmed cell death that plays a critical role in regulating the development, homeostasis and function of multicellular organisms (Zimmermann *et al.*, 2001). Cells that undergo this process demonstrate morphological changes such as cell

114

shrinkage, chromatin and cytoplasmic condensation, nuclear fragmentation and finally formation of small membrane-bound fragments (known as apoptotic bodies), which are removed by phagocytosis. Importantly, the intracellular constituents are not released into the extracellular environment, therefore reducing the inflammatory response on neighbouring cells (Zhang *et al*., 2018).

By contrast, necrosis is a mode of cell death in which the cells suffer an acute injury, resulting in the loss of membrane integrity, organelle swelling and rupture of plasma membrane. This leads to the release of intracellular components that can cause an inflammatory response and damage surrounding cells (**Figure 3-3**) (Duprez *et al*., 2009). Although most cytotoxic drugs are considered to mediate cell death mainly through apoptosis, it has been reported that some compounds may not only cause apoptosis but other forms of cell death such as necrosis and autophagy (Mansilla *et al.*, 2012). As mentioned in Chapter 1, apoptosis induction is one of the mechanisms associated with the anti-cancer activity of plumbagin. Therefore, investigating mechanisms mediating cell death using apoptosis assay will confirm that apoptosis is the mechanism responsible for the anti-cancer effect of nanomedicines entrapping plumbagin.

Several methods have been developed to characterise apoptotic cells based on morphological changes, DNA fragmentation, DNA loss or membrane changes. Annexin V FITC/ propidium iodide double staining assay is one of the most common techniques for the detection of apoptotic cells using flow cytometry. The principle of the assay is based on the differences in plasma membrane integrity and permeability of viable, apoptotic and necrotic cells (Rieger *et al*., 2011). In the early stages of apoptosis, the alteration of plasma membrane results in the translocation of phosphatidylserine from the inner side to the outer layer in which Annexin V, a Ca^{2+} dependent phospholipid-binding protein, binds specifically to phosphatidylserine due to its high affinity (Demchenko,

2013). On the other hand, Annexin V does not stain viable cells as this protein is not able to penetrate the intact phospholipid bilayer. In conjunction with Annexin V, propidium iodide, a membrane-impermeable nucleic acid stain, is used to discriminate between necrotic and apoptotic cells. This dye is generally excluded from both viable cells and early apoptotic cells due to the intact plasma membrane, whereas late apoptotic and necrotic cells lost their plasma and nuclear membrane integrity, allowing propidium iodide to penetrate through the plasma membrane then bind to nucleic acids (Rieger *et al*., 2011).
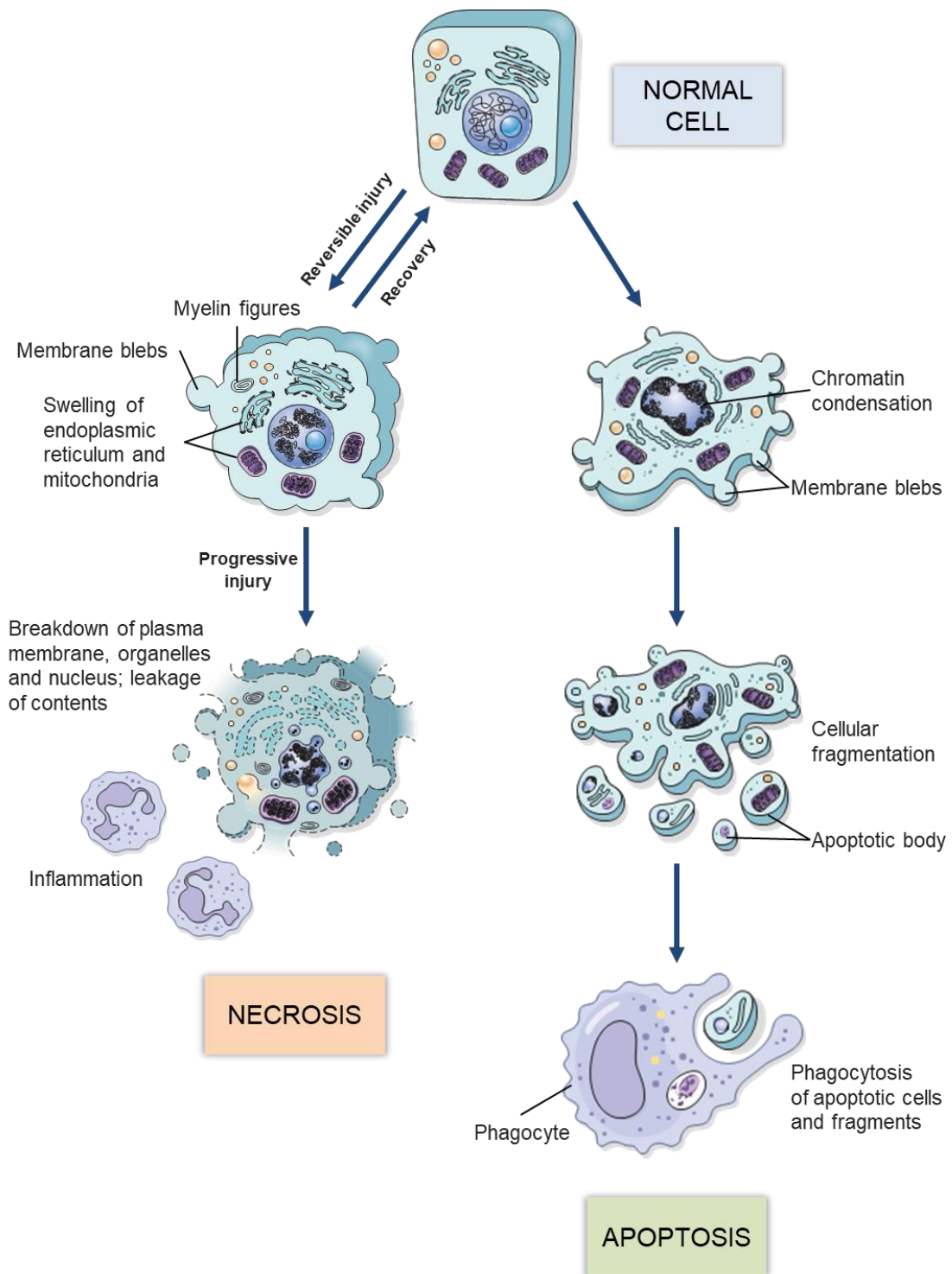
Figure 3-3: Schematic illustration of the morphological changes of cells in necrosis and apoptosis (adapted from Kumar *et al.*, 2010)

3.2 Aim and Objectives

In Chapter 2, we demonstrated the successful entrapment of plumbagin in three novel transferrin-bearing nanomedicines, namely liposomes, polymeric nanoparticles and lipid-polymer hybrid nanoparticles. We hypothesise that the entrapment of plumbagin within these novel nanomedicines conjugated with transferrin, whose receptors are overexpressed on many cancer cells, would increase the specific delivery of plumbagin to cancer cells, thereby enhancing its therapeutic efficacy.

In this chapter, these transferrin-bearing nanomedicines will be investigated for their ability to increase the cellular uptake and uptake mechanism of plumbagin formulations. We will also investigate the anti-proliferative and apoptotic efficacies of plumbagin entrapped in these novel transferrin-bearing nanomedicines.

3.3 Materials and methods

3.3.1 Materials

Materials	Supplier
3-(4,5-dimethylthiazol-2-yl)-2,5-diphenyl-tetrazolium bromide (MTT)	Sigma-Aldrich, UK
Accutase® cell detachment solution	BD Biosciences, USA
Alexa Fluor® 647 dye	Invitrogen, UK
BD Pharmingen® FITC Annexin V apoptosis detection kit I	BD Biosciences, USA
Chlorpromazine	Sigma-Aldrich, UK
Colchicine	Sigma-Aldrich, UK
Coumarin-6	Sigma-Aldrich, UK
Dimethyl sulfoxide (DMSO)	Sigma-Aldrich, UK
Dulbecco's Modified Eagle's Medium (DMEM)	Invitrogen, UK
Filipin complex from *Streptomyces filipinensis*	Sigma-Aldrich, UK
Foetal bovine serum (FBS)	Invitrogen, UK
Formaldehyde solution	Sigma-Aldrich, UK
Holo-transferrin, human (Tf)	Sigma-Aldrich, UK
Human epidermoid carcinoma (A431)	European and American Collection of Cell Cultures (ECACC)
Human glioblastoma (T98G)	European and American Collection of Cell Cultures (ECACC)

L-Glutamine	Invitrogen, UK
Methanol	Sigma-Aldrich, UK
Mouse melanoma (B16-F10-luc-G5)	American Type Culture Collection (ATCC)
N-(3-Dimethylaminopropyl)-*N′*-ethylcarbodiimide (EDC)	Sigma-Aldrich, UK
Penicillin-Streptomycin	Invitrogen, UK
Phosphate buffer saline (PBS)	Sigma-Aldrich, UK
Roswell Park Memorial Institute (RPMI)-1640 medium	Invitrogen, UK
Plumbagin (5-hydroxy-2-methyl-1,4-naphthoquinone)	Sigma-Aldrich, UK
TPP® Tissue Culture 96-Well Plates	Sigma-Aldrich, UK
TPP® Tissue Culture 6-Well Plates	Sigma-Aldrich, UK
Triton X-100	Sigma-Aldrich, UK
TrypLE® Express	Invitrogen, UK
Vectashield® mounting medium containing 4',6-diamidino-2-phenylindole (DAPI)	Vector Laboratories, UK

3.3.2 Cell lines

Three cell lines were used to investigate the activity of plumbagin entrapped in transferrin-bearing nanomedicines, control nanomedicines or free in solution. A431 human epidermoid carcinoma is derived from an epidermal carcinoma of the skin tissue of an 85-year old woman (ECACC). A431 cells were previously reported to overexpress transferrin receptors (Dufès, 2011; Daniels *et al*., 2012). Moreover, this cell line has been used to investigate the efficacy of transferrin-targeted delivery systems, such as polymeric chitosan vesicles, niosomes and dendrimers (Dufès *et al*., 2004; Fu *et al.*, 2009; Koppu *et al*., 2010), which makes it a desirable cell line to evaluate the targeting efficacy of our new transferrin-bearing formulations.

T98G glioblastoma is derived from a glioblastoma multiforme tumour from a 61-year old Caucasian man (ECACC). This cell line was included in this study as it also overexpresses transferrin receptors (Daniels *et al*., 2012).

B16-F10-luc-G5 mouse melanoma, a mixture of spindle-shaped and epithelial-like cells derived from the skin of C57BL/6J mouse (ATCC), was used in this study. Like A431 and T98G cells, this cell line also expresses high level of transferrin receptors. Moreover, it has already been used for *in vitro* and *in vivo* evaluation of transferrin-bearing niosomes (Fu *et al.*, 2011; Perche and Torchilin, 2013).

3.3.3 Cell culture

B16-F10-luc-G5, A431 and T98G cell lines were grown as monolayer cultures in either Roswell Park Memorial Institute (RPMI)-1640 medium (for B16-F10-luc-G5 cells) or in Dulbecco's Modified Eagle's Medium (DMEM) (for A431 and T98G cells) supplemented with 10% (v/v) foetal bovine serum, 1% (v/v) L-glutamine and 0.5% (v/v)

penicillin-streptomycin. Cells were cultured at 37°C in an incubator with a humid atmosphere of 5% carbon dioxide.

3.3.4 Cellular uptake

3.3.4.1 Quantification of cellular accumulation of plumbagin

Intracellular accumulation of plumbagin formulated as Tf- bearing nanomedicines, control nanomedicines or free in solution was quantified by spectrophotometry. Cells were seeded at a density of 2 x 10^5 cells/well in 6-well plates and grown at 37 °C for 72 hours before being treated with plumbagin (10 µg/well), either entrapped in Tf- bearing nanomedicines, control nanomedicines or free in solution. After 3 hours' treatment, the cells were harvested using TrypLE® Express. Subsequently, culture medium (500 µL) was added to the cell suspension to stop the trypsinisation reaction. Cells were then centrifuged at 2,000 rpm (370 g) for 5 min using an IEC Micromax® centrifuge (ThermoFisher Scientific, Waltham, MA). The cell pellets were washed twice with cold PBS (3 mL) before being lysed with 5% Triton-X (1 mL/sample) and incubated for another 24 hours at 37 °C. After incubation, cell lysates were centrifuged at 10,000 rpm (9,300 g) for 15 min using an IEC Micromax® centrifuge (ThermoFisher Scientific, Waltham, MA). The amount of plumbagin in the surfactant was quantified by spectrophotometry (λ_{max}: 420 nm), using a FlexStation 3® multi-mode microplate reader (Molecular Devices, Sunnyvale, CA), and calculated by correlating absorbance with standard calibration curve of plumbagin.

3.3.4.2 Preparation of transferrin-targeted nanomedicines entrapping coumarin-6

To further confirm the cellular uptake of nanomedicines, plumbagin was replaced with coumarin-6 as a fluorescent lipophilic drug model for quantitative and qualitative

measurements of drug cellular uptake in B16-F10 cells using flow cytometry and confocal microscopy. Coumarin-6 loaded transferrin-bearing and control liposomes, PLGA-PEG nanoparticles and lipid-polymer hybrid nanoparticles were prepared (fixing theoretical loading of coumarin-6 at 0.2% of total lipids weight (for liposomes) and polymer weight (for PLGA-PEG nanoparticles and lipid-polymer hybrid nanoparticles)) and characterised in the same manner as described in **section 2.3**, for formulations entrapping plumbagin.

3.3.4.3 Confocal microscopy

The cellular uptake of coumarin-6 formulated as Tf-bearing nanomedicines, control nanomedicines or free in solution was qualitatively assessed using confocal microscopy. B16-F10 cells were seeded at a density of 1×10^5 cells/well on coverslips in 6-well plates and were grown for 24 hours at 37 °C. They were treated with coumarin-6 (1 µg/well), either entrapped in Tf-bearing nanomedicines, control nanomedicines or free in solution. After 2 hours' incubation, the medium was removed, and cells were washed twice with cold PBS (3 mL) before being fixed with 2 mL formaldehyde solution (3.7 % in PBS) for 10 minutes at 25 °C. They were then washed twice with cold PBS (3 mL) and incubated at 25 °C with 3 mL Triton-X100 solution (0.1%) for 5 min, before a further incubation with 3 mL bovine serum albumin (1% w/v in PBS) for 30 min at 37 °C to reduce the non-specific binding. Cells were then stained with Alexa Fluor® 647 dye (one unit of dye diluted in 200 µL of PBS), incubated for 20 min at 25 °C, before a final wash with 3 mL cold PBS. Upon staining of the nuclei with Vectashield® mounting medium containing DAPI, the cells were examined using a Leica TCS SP5 confocal microscope (Wetzlar, Germany). DAPI (which stained the cell nuclei) was excited with the 405 nm laser line (emission bandwidth: 415-491 nm), while Alexa Fluor® 647 (which stained the cell

cytoplasm) was excited with the 633 nm laser line (emission bandwidth: 645-710 nm), and coumarin-6 was excited with the 505 nm laser line (emission bandwidth: 515-558 nm).

3.3.4.4 Cellular uptake of transferrin-bearing nanomedicines entrapping coumarin-6

The cellular uptake of coumarin-6 formulated as Tf- bearing nanomedicines, control nanomedicines or free in solution, was quantified by flow cytometry. To do so, B16-F10 cells were seeded at a density of 1×10^5 cells/well and grown at 37 °C for 24 hours before being treated with coumarin-6 (50 ng/well) entrapped in Tf-bearing nanomedicines, control nanomedicines or free in solution. After 2 hours' incubation, cells were then washed twice with cold PBS (3 mL) and trypsinised using TrypLE® Express (250 µL). Subsequently, RPMI-1640 medium (500 µL) was added to the cell suspension to stop the trypsinisation reaction. The mean fluorescence intensity (MFI) of coumarin-6 taken up by the cells was quantified by flow cytometry using a FACSCanto® flow cytometer (BD Biosciences, San Jose, CA) with a fluorescein isothiocyanate (FITC) filter (Ex_{max}: 494 nm / Em_{max}: 520nm). Ten thousand cells (gated events) were counted for each sample.

3.3.4.5 Mechanisms of cellular uptake

The mechanisms involved in the cellular uptake of coumarin-6 entrapped in Tf-bearing nanomedicines and control nanomedicines were investigated using various uptake inhibitors. To do so, B16-F10 cells were seeded in 6-well plates at a density of 2×10^5 cells/well and incubated for 24 hours at 37 °C. Cells were then pre-incubated with transferrin (50 µM), chlorpromazine (20 µg/mL), filipin (4 µg/mL) and colchicine (40 µg/mL) at 37 °C for 30 min. After incubation, the treatment was removed and replaced with fresh medium containing 50 ng/mL of coumarin-6 (either entrapped in Tf-bearing

and control nanomedicines) and the same concentration of each inhibitor (except chlorpromazine, added at a concentration of 5 µg/mL) for a further 2-hour incubation at 37 °C. After incubation, cells were then washed twice with cold PBS (3 mL) and harvested using TrypLE® Express (250 µL). Subsequently, RPMI-1640 medium (500 µL) was added to the cell suspension to stop the trypsinisation reaction. The mean fluorescence intensity (MFI) of coumarin-6 taken up by the cells was quantified by flow cytometry using a FACSCanto® flow cytometer (BD Biosciences, San Jose, CA) with a fluorescein isothiocyanate (FITC) filter (Ex_{max}: 494 nm / Em_{max}: 520nm). Ten thousand cells (gated events) were counted for each sample. The results were expressed as percentage of cellular uptake relative to treated cells without inhibitor (100% relative cellular uptake).

3.3.5 Anti-proliferative assay

The MTT assay was used to evaluate the anti-proliferative activity of plumbagin either entrapped in Tf-bearing nanomedicines, control nanomedicines, or free in solution, as well as blank nanomedicines. Cells were seeded in 96-well plates at a density of 5,000 cells/well and were incubated for 24 hours in an atmosphere of 37 °C, 5% CO_2 to allow for cells attachment. They were then treated with plumbagin entrapped in Tf-bearing nanomedicines, control nanomedicines, or free in solution, at final drug concentrations ranging from 7.81×10^{-3} to 10 µg/mL. Cells were then incubated for selected exposure time of 24 hours. At the end of treatment period, 50 µL of MTT solution (0.5 % w/v in PBS) was added in each well. After 4 hours' incubation (with protection from light), the treatments were removed, and 200 µL of DMSO was then added in each well to dissolve the formazan product. The optical density of the formazan solution was measured at an absorbance at 570 nm using Multiskan Ascent microplate reader (Thermo Labsystems,

Beverly, MA) and calculated as the percentage cell viability compared with the non-treated cells. Dose-response curves were fitted to obtain the growth inhibitory concentration for 50% of cell population (IC_{50}) by plotting percentage of cell viability versus logarithm of concentration of treatment using OriginPro 9.0 software (OriginLab Corporation, Northampton, MA).

3.3.6 Apoptosis assay

The number of apoptotic cells following treatment with plumbagin formulated as Tf-bearing nanomedicines, control nanomedicines or free drug was determined using BD Pharmingen® FITC Annexin V apoptosis detection kit I (BD Biosciences, Franklin Lakes, NJ), as described in the manufacturer's instructions. Cells were seeded in 6-well plates at a density of 2 x 10^5 cells per well and grown for 24 hours before being treated with plumbagin (1 µg/well), either entrapped in Tf-bearing nanomedicines, control nanomedicines or free in solution. After 4 hours' treatment at 37 °C, cells were harvested using Accutase® cell detachment solution (500 µL). Subsequently, culture medium (500 µL) was added to the cell suspension to stop the enzyme reaction before being centrifuged at 2,000 rpm (370 g) for 5 min using an IEC Micromax® centrifuge (ThermoFisher Scientific, Waltham, MA). The cell pellets were resuspended in 200 µL 1X Annexin V Binding Buffer (10X of the buffer containing 0.1 M HEPES/NaOH (pH 7.4), 1.4 M NaCl and 25 mM $CaCl_2$). Cell suspension (100 µL) was then transferred to a 5 mL culture tube, followed by 5 µL of annexin V-FITC labeling reagent and 5 µL of propidium iodide. After incubation for 15 minutes in the dark at 20 °C, 400 µL of 1X Annexin V Binding Buffer was added to each tube before analysis of apoptosis using a FACSCanto® flow cytometer (BD Biosciences, Franklin Lakes, NJ). Ten thousand cells (gated events) were counted for each sample. The results were reported as percentages of specific cell

populations as followed: propidium iodide -positively and FITC-negatively stained cells indicate necrosis (upper left, Q1), propidium iodide and FITC double-stained cells demonstrate late apoptosis (upper right, Q2), propidium iodide and FITC double-negative (unstained) are live cells (lower left, Q3) and FITC-positively and propidium iodide -negatively stained cells indicate early apoptosis (lower right, Q4).

3.3.7 Statistical analysis

Results were expressed as means ± standard error of the mean. Statistical significance was assessed by one-way analysis of variance and Tukey multiple comparison post-test using OriginPro 9.0 software (OriginLab Corporation, Northampton, MA). Differences were considered statistically significant for *p*-values lower than 0.05.

3.4 Results

3.4.1 Preparation of transferrin-targeted nanomedicines entrapping coumarin-6

The specific wavelength of coumarin-6 (Cu-6) was determined using an Agilent Varian Cary Eclipse® spectrofluorometer (Agilent Technologies, Santa Clara, CA). The spectrum of coumarin-6 obtained from a fluorescence scan indicated two excitation peaks, a small one at a wavelength of 300-305 nm and the highest peak at a wavelength of 460-465 nm (**Figure 3-4A**). Thus, the emission spectrum of coumarin-6 was measured using the maximum excitation at 463 nm. The maximum emission occurred at a wavelength of 508-515 nm (**Figure 3-4B**). As a result, determination of coumarin-6 was performed at an excitation wavelength of 463 nm and an emission wavelength of 510 nm. To measure the entrapment efficiency, coumarin-6 was first prepared at 7 concentrations in isopropanol (2, 5, 10, 25, 50, 100 and 150 ng/mL) and analysed by fluorescence quantification at the specific λ_{ex} and λ_{em} wavelengths obtained above. As shown in **Figure 3-5**, the standard calibration of coumarin-6 was linear for the concentrations range used, which could be described by the regression equation: $Y = 4.85959X + 1.55967$ with a coefficient of determination (R-square, R^2) of 0.99078.
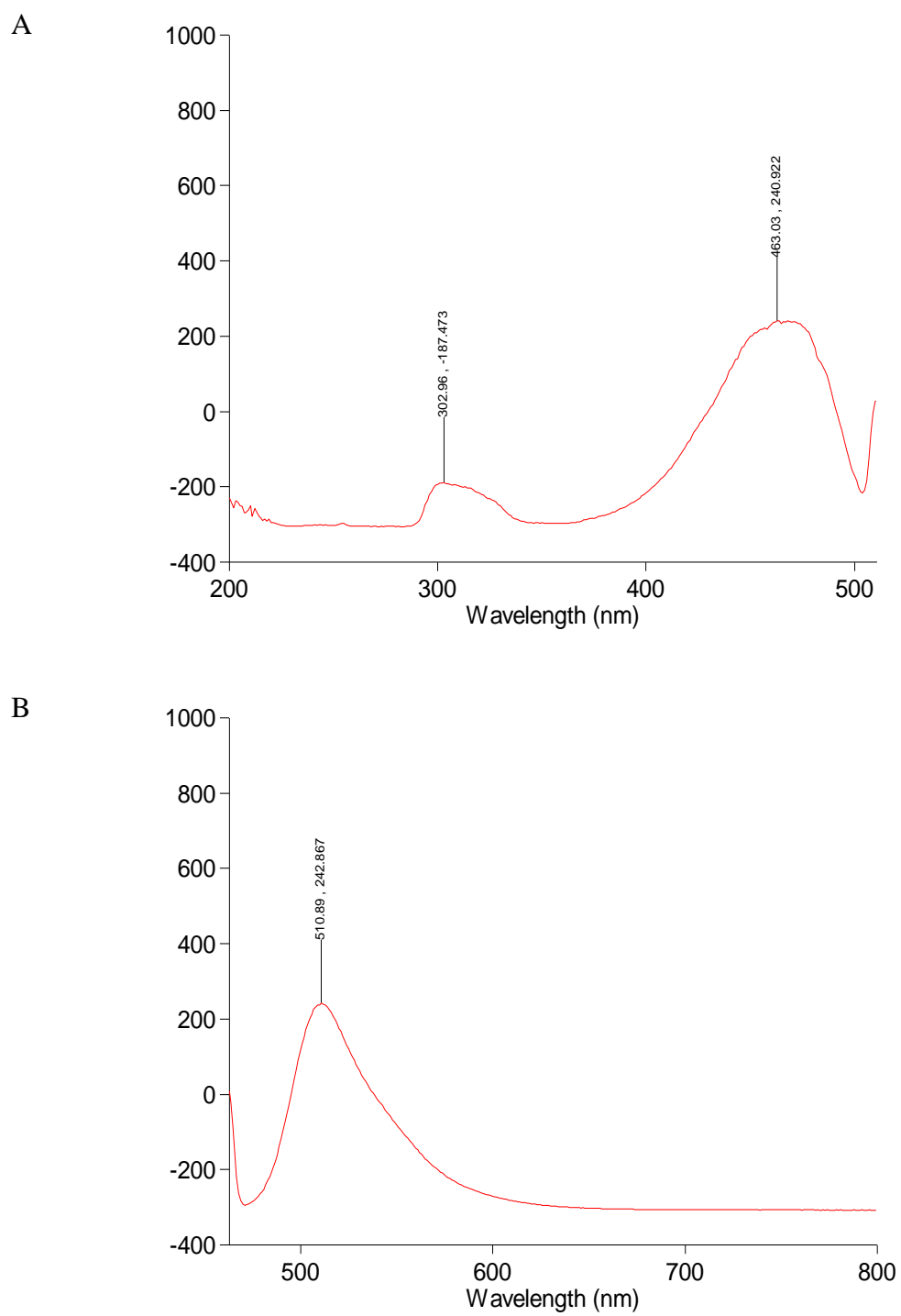
Figure 3-4: Excitation wavelength (A) and emission wavelength (B) obtained using fluorescence scan of coumarin-6 solution, prepared at 50 ng/mL in isopropanol
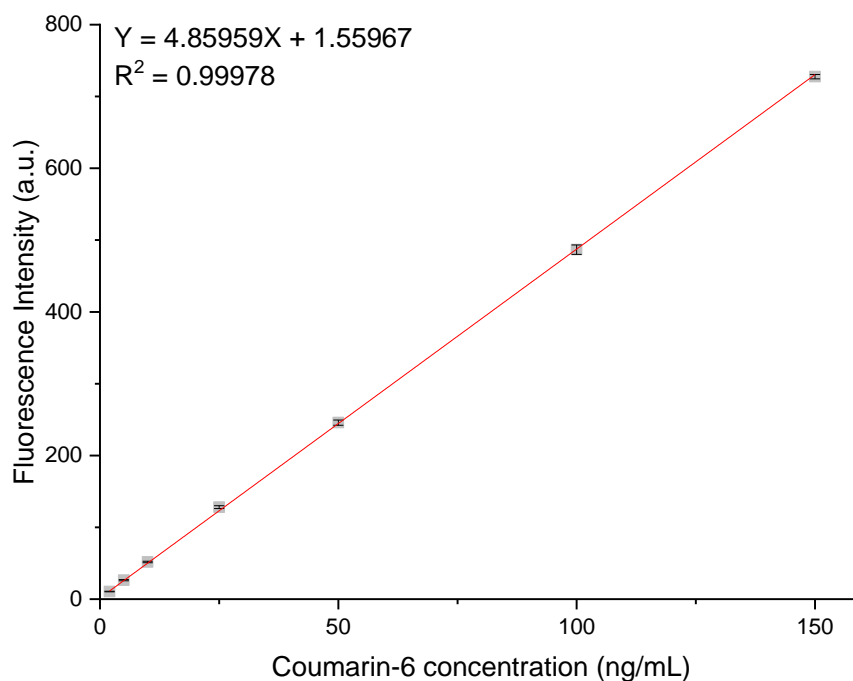
Figure 3-5: Standard calibration curve of coumarin-6. The fluorescence intensity in arbitrary unit (a.u.) was obtained from serial dilutions of coumarin-6 stock solution (1 mg/mL) in isopropanol (*n*=3) (error bars smaller than symbols)

For the purpose of qualitative and quantitative cellular uptake studies of nanomedicines using flow cytometry and confocal microscopy, coumarin-6 was used as a fluorescent lipophilic drug model because plumbagin does not contain a fluorophore that can emit light upon excitation. Coumarin-6 loaded liposomes, polymeric and lipid-polymer hybrid nanoparticles were prepared and characterised for entrapment efficiency, size and zeta potential measurements. As shown in **Table 3-1**, all nanomedicines formulations displayed relatively high entrapment efficiency of coumarin-6 (about 40-86% entrapment depending on nanomedicine formulations), with a similar trend of size and zeta potential as in nanomedicines entrapping plumbagin.

Table 3-1: Entrapment efficiency, size and zeta potential of liposomes, PLGA-PEG nanoparticles and lipid-polymer hybrid nanoparticles entrapping coumarin-6 ($n=3$)

Nanomedicine formulations	Entrapment efficiency (%)	Particle Size (nm)	Polydispersity Index	Zeta Potential (mV)
Liposomes				
Tf-LIP	86.6 ± 1.2	103.1 ± 0.8	0.12 ± 0.02	-22.0 ± 0.8
Control LIP	86.2 ± 1.4	100.9 ± 0.5	0.10 ± 0.00	-13.1 ± 0.2
PLGA-PEG nanoparticles				
Tf-PN	42.9 ± 0.3	138.7 ± 0.7	0.18 ± 0.01	-33.6 ± 0.5
Control PN	51.4 ± 0.2	98.7 ± 1.5	0.11 ± 0.01	-40.9 ± 1.3
Lipid-polymer hybrid nanoparticles				
Tf-LPN	40.9 ± 0.6	222.4 ± 3.1	0.22 ± 0.01	-37.6 ± 0.2
Control LPN	47.6 ± 0.7	139.1 ± 0.5	0.18 ± 0.01	-49.9 ± 0.3

The entrapment efficiency of coumarin-6 within the liposomes (86.6 ± 1.2 % for Tf-LIP and 86.2 ± 1.4 % for control LIP) was higher than that of PLGA-PEG nanoparticles (42.9 ± 0.3 % for Tf-PN and 51.4 ± 0.2 % for control PN) and lipid-polymer hybrid nanoparticles (40.9 ± 0.6 % for Tf-LPN and 47.6 ± 0.7 % for control LPN). This result might be explained by the vesicular structure of liposomes that can entrap coumarin-6 within the lipid bilayer. The similar entrapment efficiency of coumarin-6 between PLGA-PEG nanoparticles and lipid-polymer hybrid nanoparticles can be explained by the fact that both formulations used the same theoretical loading of coumarin-6 at 0.2% of polymer weight.

As expected, the conjugation of Tf to the surface of the three nanomedicine formulations entrapping coumarin-6 led to an increase in mean diameter size of Tf-bearing nanomedicines (103.1 ± 0.8 nm for Tf-LIP, 138.7 ± 0.7 nm for Tf-PN and 222.4 ± 3.1 nm for Tf-LPN) compared to control nanomedicines (100.9 ± 0.5 nm for control LIP, 98.7 ± 1.5 nm for control PN and 139.1 ± 0.5 nm for control LPN). Furthermore, the polydispersity index of all formulations was low (0.10 – 0.22), indicating a uniformly dispersed nanomedicine formulation with a narrow size distribution.

In addition, the zeta potential of all nanomedicines entrapping coumarin-6 were bearing a negative surface charge, ranging from -13.1 ± 0.2 mV to -49.9 ± 0.3 mV.

These results therefore demonstrated that the entrapment of coumarin-6 in the three nanomedicines did not change their physico-chemical properties, such as the particle size and surface charge, compared with the original formulations entrapping plumbagin.

3.4.2 Cellular uptake

3.4.2.1 Qualitative and quantitative analysis

3.4.2.1.1 Transferrin-bearing liposomes

The intracellular accumulation of plumbagin either formulated as Tf-bearing and control liposomes or free in solution was investigated in the three tested cell lines (**Figure 3-6**). As expected, the entrapment of plumbagin in Tf-bearing liposomes significantly increased plumbagin uptake by the cells in comparison with control liposomes and plumbagin solution. In B16-F10 cells, the amount of plumbagin accumulated in the cells treated with Tf-bearing liposomes was 1.6-fold and 2.4-fold higher than that of control liposomes and free drug, respectively (1.66 ± 0.04 μg for Tf-LIP, 1.02 ± 0.15 μg for control LIP and 0.70 ± 0.17 μg for plumbagin solution). In A431 cells, it was 1.5-fold and 2.1-fold for Tf-LIP in comparison with control liposomes and plumbagin solution,

respectively (1.97 ± 0.25 µg for Tf-LIP, 1.35 ± 0.15 µg for control LIP and 0.92 ± 0.07 µg for free plumbagin). The highest intracellular amount of plumbagin was found in T98G cells incubated with Tf-bearing liposomes which was significantly higher than that observed after being treated with control liposomes and free plumbagin respectively by 1.4-fold and 2.1-fold (3.02 ± 0.20 µg for Tf-LIP, 2.15 ± 0.14 µg for control LIP and 1.43 ± 0.05 µg for free plumbagin).
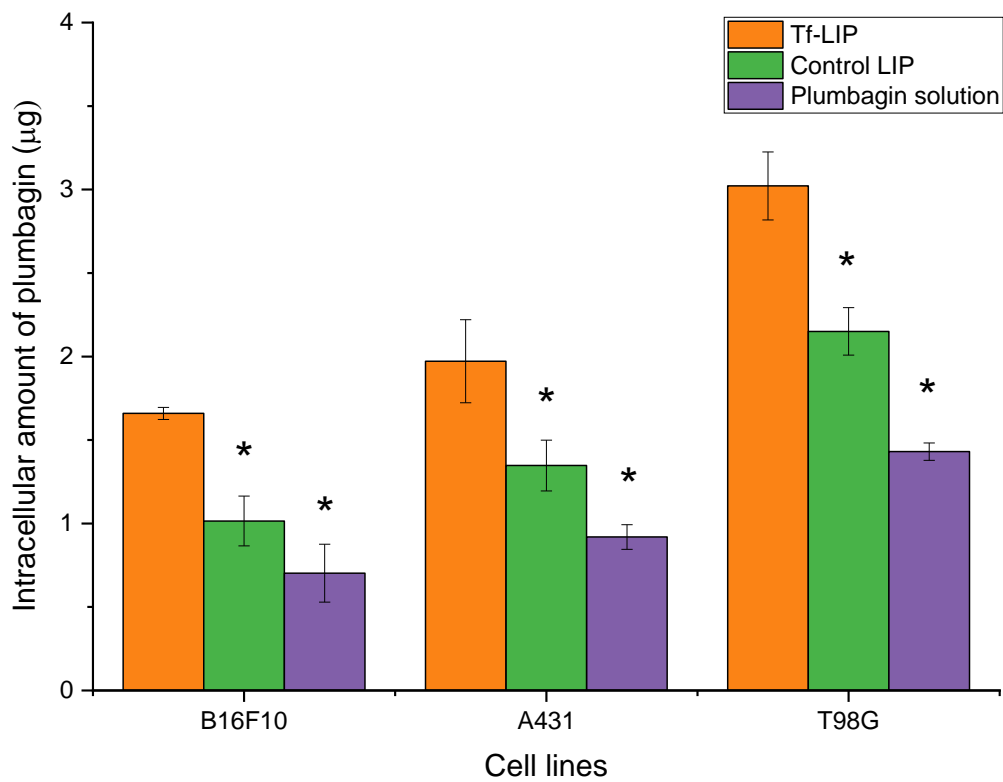
Figure 3-6: Cellular uptake of plumbagin (10 µg/well) either formulated as Tf-bearing liposomes (orange), control liposomes (green) or as free drug in solution (purple), in B16-F10, A431 and T98G cell lines (*n*=5) (*: *p*<0.05 vs Tf-LIP)

The cellular uptake of liposomes entrapping coumarin-6 was qualitatively analysed by confocal microscopy in B16-F10 cells (**Figure 3-7**). As expected, Tf-bearing liposomes led to a higher cellular uptake of coumarin-6 compared to that observed in control liposomes. Cells treated with coumarin-6 solution showed coumarin-6-derived fluorescence in the cytoplasm, probably due to the non-specific diffusion of the drug. In addition, coumarin-6-derived fluorescence was only disseminated in the cytoplasm following all treatments, with no visible co-localisation within the nucleus after 2 h incubation with the treatments.
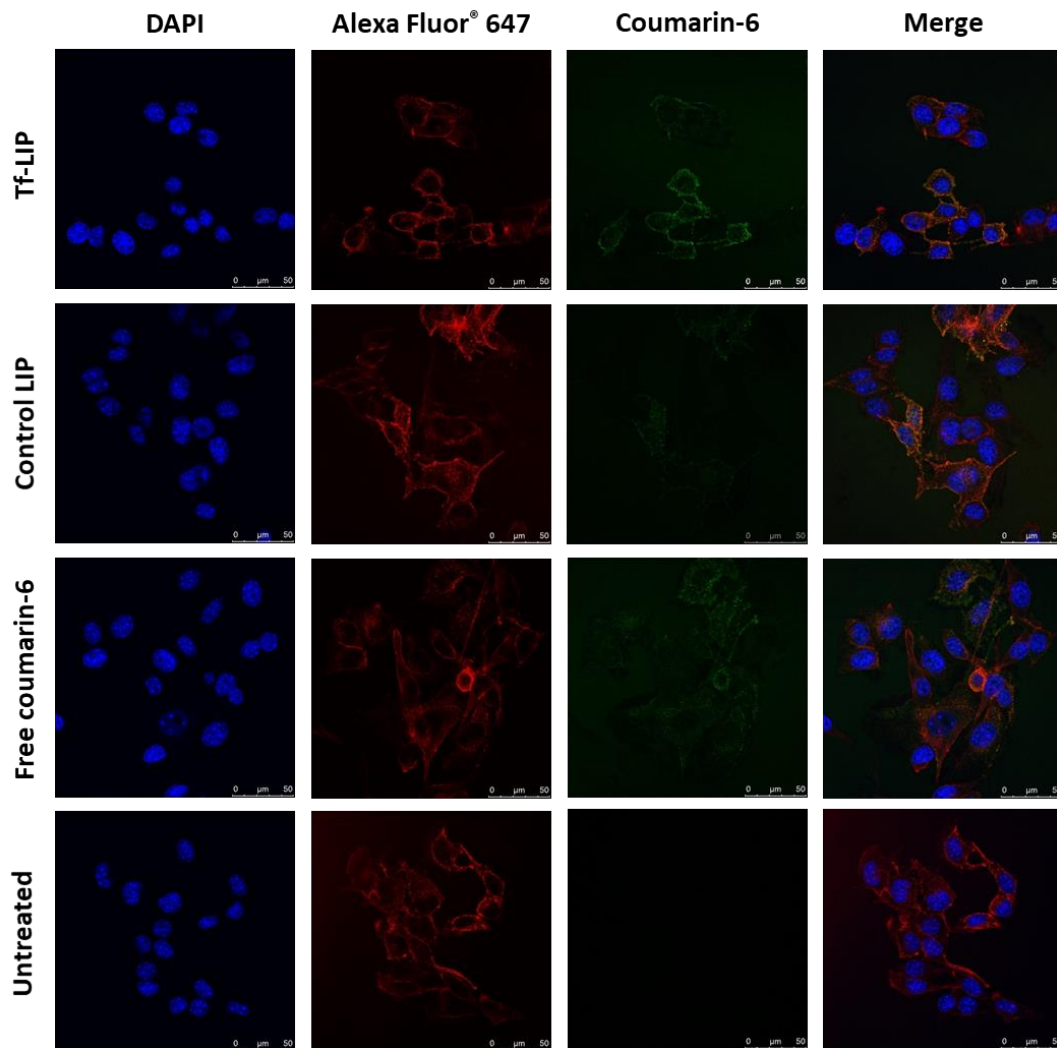
Figure 3-7: Confocal microscopy imaging of B16-F10 cells, showing the cellular uptake of coumarin-6 entrapped in Tf-bearing liposomes, control liposomes or as solution

Coumarin-6 uptake was also quantitatively confirmed by flow cytometry (**Figure 3-8**). The conjugation of transferrin to the liposomes significantly increased coumarin-6 uptake (mean fluorescence intensity (MFI) of 5673 ± 49 a.u.) compared to control liposomes (MFI of 4779 ± 48 a.u.). However, the highest uptake was observed following treatment with coumarin-6 solution (MFI of 6567 ± 79 a.u.), which might occur by passive diffusion due to its low molecular weight (350.43 g/mol).
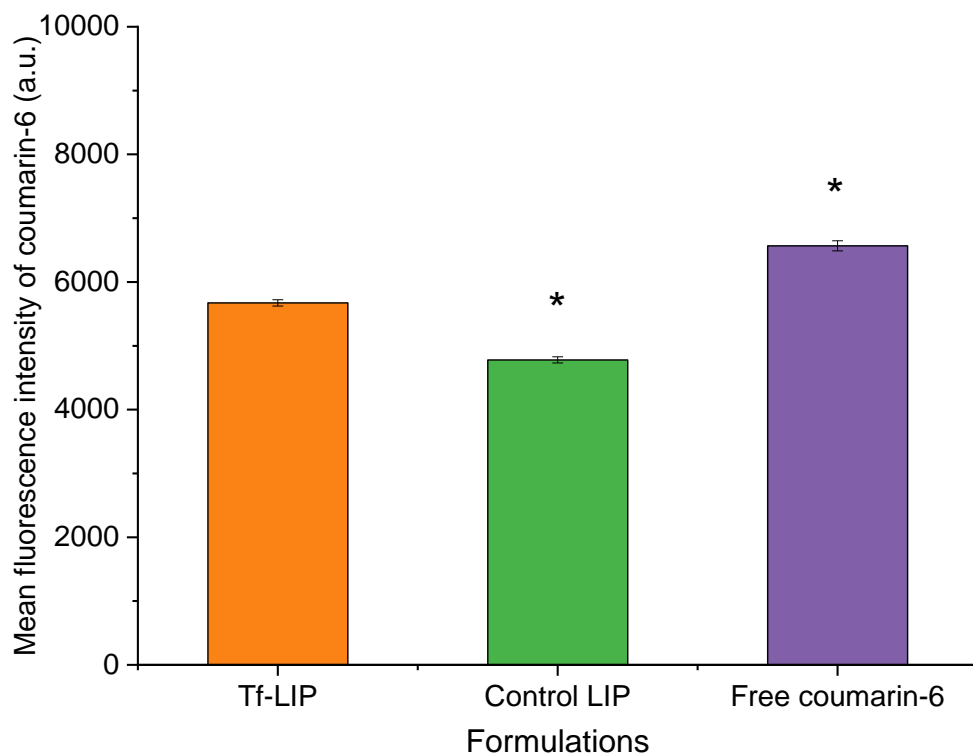
Figure 3-8: Flow cytometry quantification of the cellular uptake of coumarin-6 entrapped in Tf-bearing liposomes, control liposomes or as solution in B16-F10 cells (*n*=3) (*: *p*<0.05 vs Tf-LIP)

3.4.2.1.2 Transferrin-bearing PLGA-PEG nanoparticles

The entrapment of plumbagin in Tf-bearing PLGA-PEG nanoparticles significantly improved plumbagin uptake compared to that of control nanoparticles in all the tested cell lines (**Figure 3-9**), respectively by 1.3-fold in B16-F10 cells (2.83 ± 0.16 mg for Tf-PN and 2.18 ± 0.05 mg for control PN) and A431 cells (3.11 ± 0.13 mg for Tf-PN and 2.40 ± 0.05 mg for control PN), and 1.5-fold in T98G cells (3.65 ± 0.10 mg for Tf-PN and 2.43 ± 0.06 mg for control PN). It was more than 4-fold higher than that of free plumbagin for B16-F10 cells (0.70 ± 0.17 mg), 3.4-fold higher for A431 cells (0.92 ± 0.07 mg) and 2.6-fold higher for T98G cells (1.43 ± 0.05 mg).
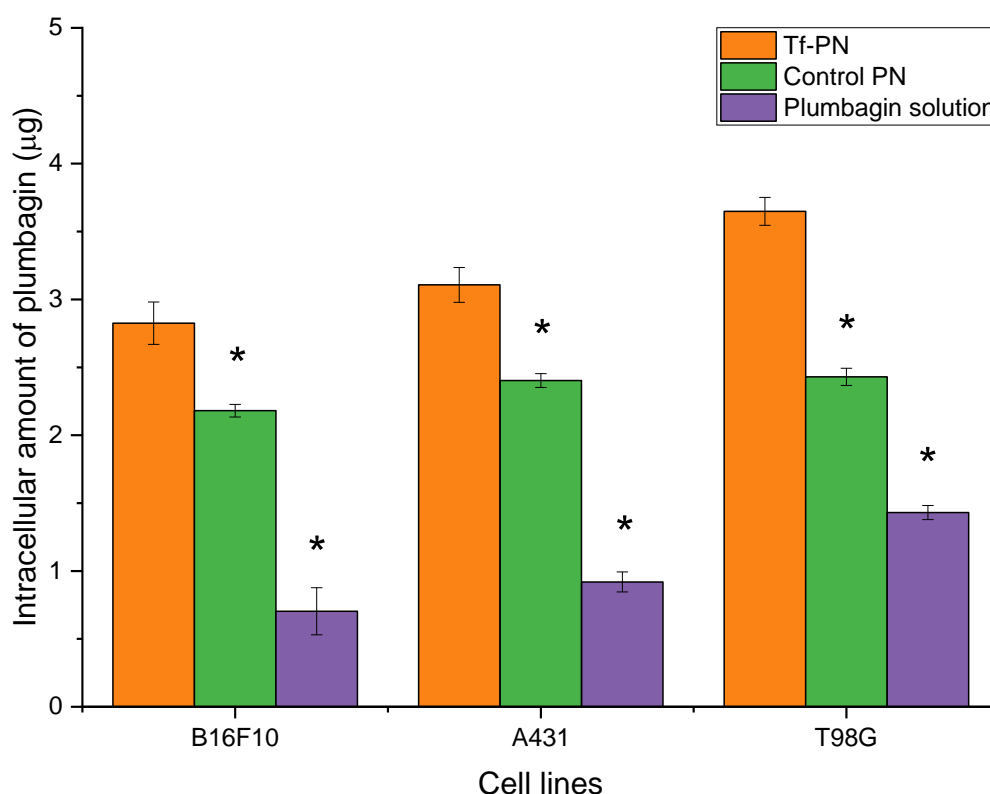
Figure 3-9: Cellular uptake of plumbagin (10 µg/well) either formulated as Tf-bearing (orange) and control PLGA-PEG nanoparticles (green) or as free drug in solution (purple), in B16-F10, A431 and T98G cell lines (*n*=5) (*: *p*<0.05 vs Tf-PN)

Confocal microscopy confirmed the cellular uptake of coumarin-6, which was disseminated in the cytoplasm of B16-F10 cells, with no visible co-localisation within the nucleus (**Figure 3-10**). As expected, the intensity of coumarin-6-derived fluorescence appeared to be more pronounced in the cells treated with Tf-bearing PLGA-PEG nanoparticles than that of control nanoparticles and free coumarin-6.
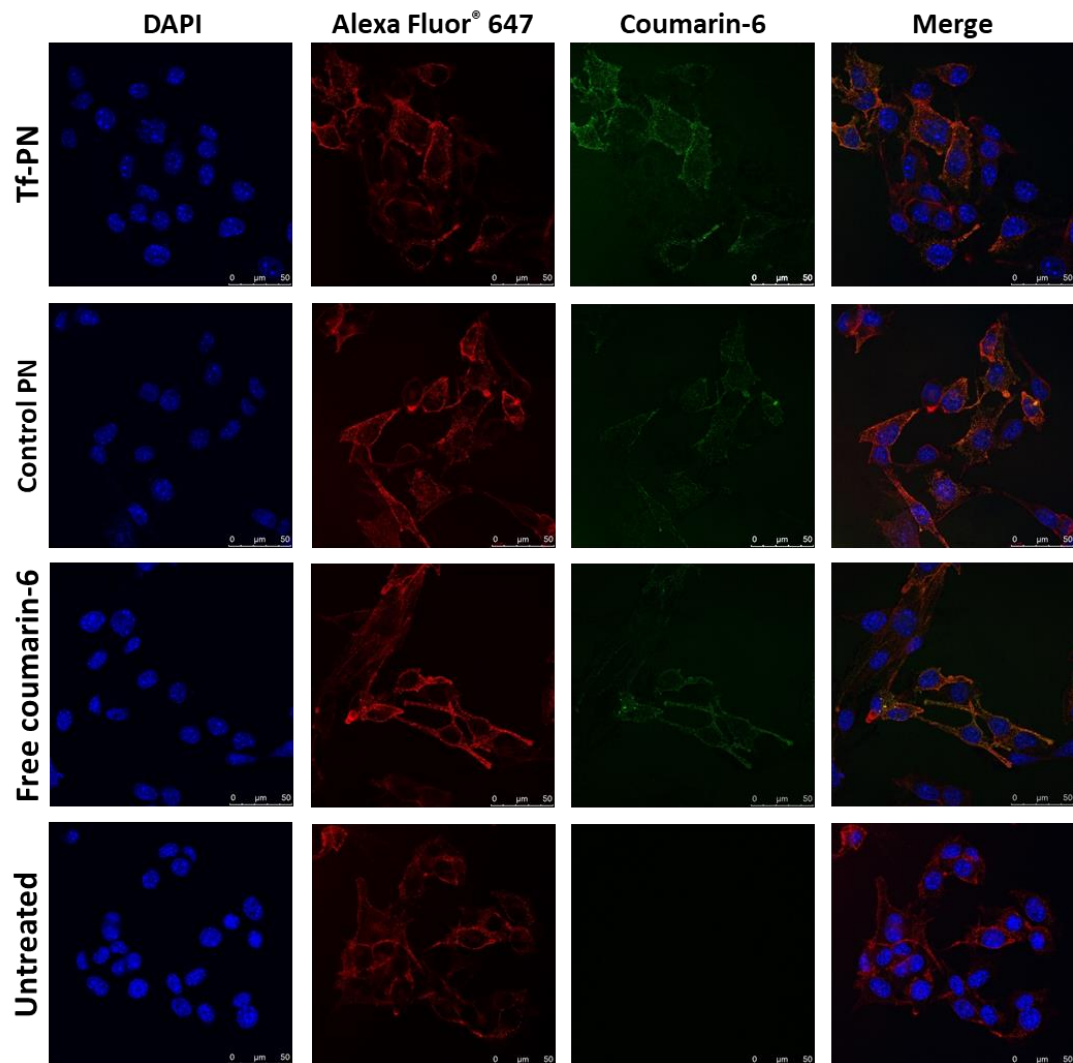
Figure 3-10: Confocal microscopy imaging of B16-F10 cells, showing the cellular uptake of coumarin-6 entrapped in Tf-bearing and control PLGA-PEG nanoparticles or as solution

Similarly, the highest uptake in B16-F10 cells was observed following treatment with coumarin-6 entrapped in Tf-bearing PLGA-PEG nanoparticles (MFI of 8690 ± 129), which was 1.1-fold and 1.3-fold higher than that observed in the cells treated with control nanoparticles (MFI of 7883 ± 86) and free coumarin-6 (MFI of 6567 ± 79) (**Figure 3-11**).
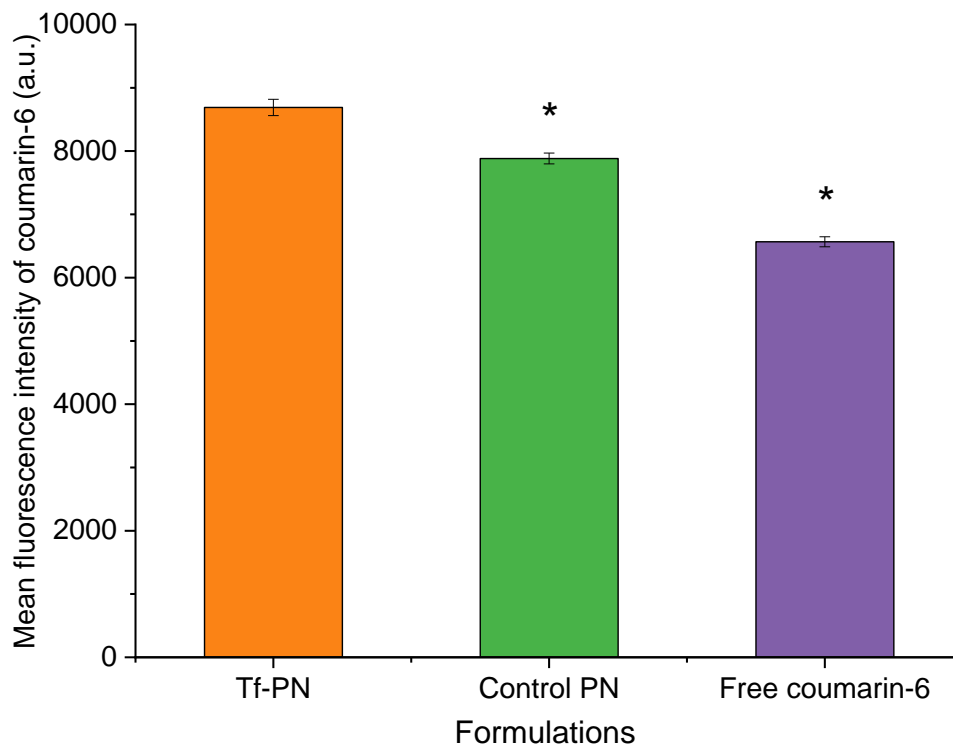
Figure 3-11: Flow cytometry quantification of the cellular uptake of coumarin-6 entrapped in Tf-bearing and control PLGA-PEG nanoparticles or as solution in B16-F10 cells (*n*=3) (*: *p*<0.05 vs Tf-PN)

3.4.2.1.3 Transferrin-bearing lipid-polymer hybrid nanoparticles

The cellular uptake of plumbagin in B16-F10 cells treated with Tf-bearing lipid-polymer hybrid nanoparticles was higher than that of control lipid-polymer hybrid nanoparticles and free drug, respectively by 1.6-fold and 2.1-fold (1.44 ± 0.06 μg for Tf-LPN, 0.92 ± 0.13 μg for control LPN and 0.70 ± 0.17 μg for plumbagin solution) (**Figure 3-12**). In A431 cells, it was 1.3-fold and 2.7-fold for Tf-bearing lipid-polymer hybrid nanoparticles in comparison with control nanoparticles and drug solution, respectively (2.46 ± 0.04 μg for Tf-LPN, 1.95 ± 0.05 μg for control LPN and 0.92 ± 0.07 μg for free plumbagin). In T98G cells, treatment of this cell line with Tf-bearing lipid-polymer hybrid nanoparticles resulted in the highest cellular uptake of plumbagin, which was significantly higher than that observed after treatment with unconjugated nanoparticles and free plumbagin respectively by 1.3-fold and 2-fold (2.80 ± 0.21 μg for Tf-LPN, 2.24 ± 0.13 μg for control LPN and 1.43 ± 0.05 μg for free plumbagin).
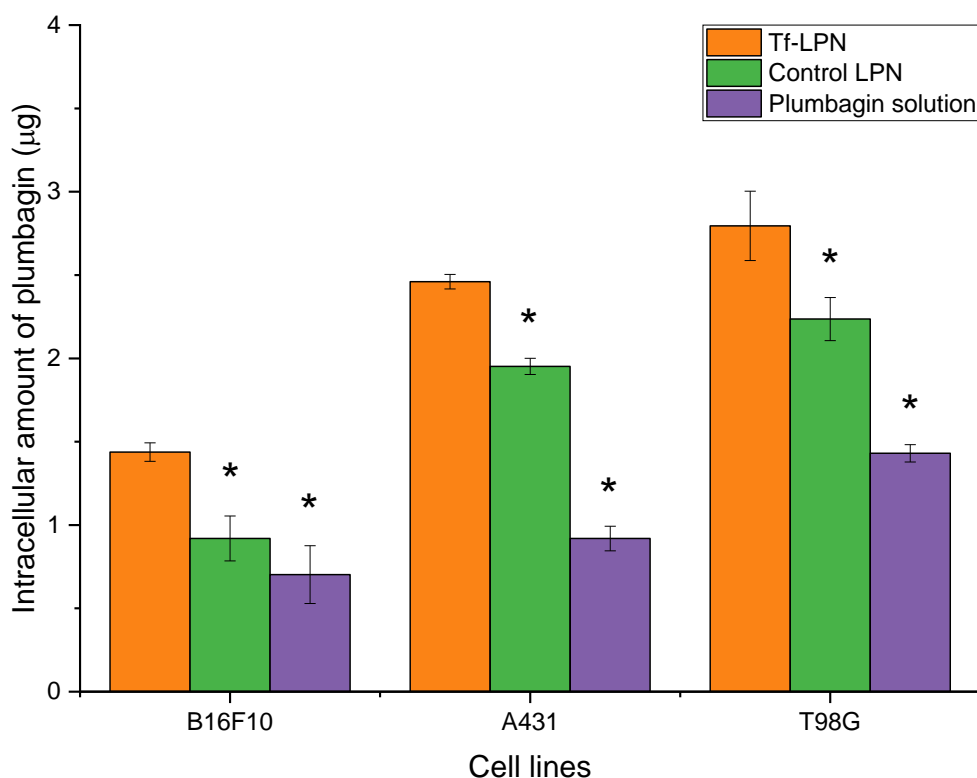
Figure 3-12: Cellular uptake of plumbagin (10 µg/well) either formulated as Tf-bearing (orange) and control lipid-polymer hybrid nanoparticles (green) or as free drug in solution (purple), in B16-F10, A431 and T98G cell lines (*n*=5) (*: *p*<0.05 vs Tf-LPN)

For confocal microscopy, the cellular uptake of coumarin-6 entrapped in lipid-polymer hybrid nanoparticles followed a similar trend as previously described in liposomes and PLGA-PEG nanoparticles. Tf-bearing lipid-polymer hybrid nanoparticles led to a higher cellular uptake of coumarin-6 compared to that observed in control nanoparticles (**Figure 3-13**). Cells treated with coumarin-6 solution showed coumarin-6-derived fluorescence in the cytoplasm, probably due to the non-specific diffusion of the drug. Coumarin-6-derived fluorescence was disseminated in the cytoplasm of B16-F10 cells following all treatments, with no visible co-localisation within the nucleus.
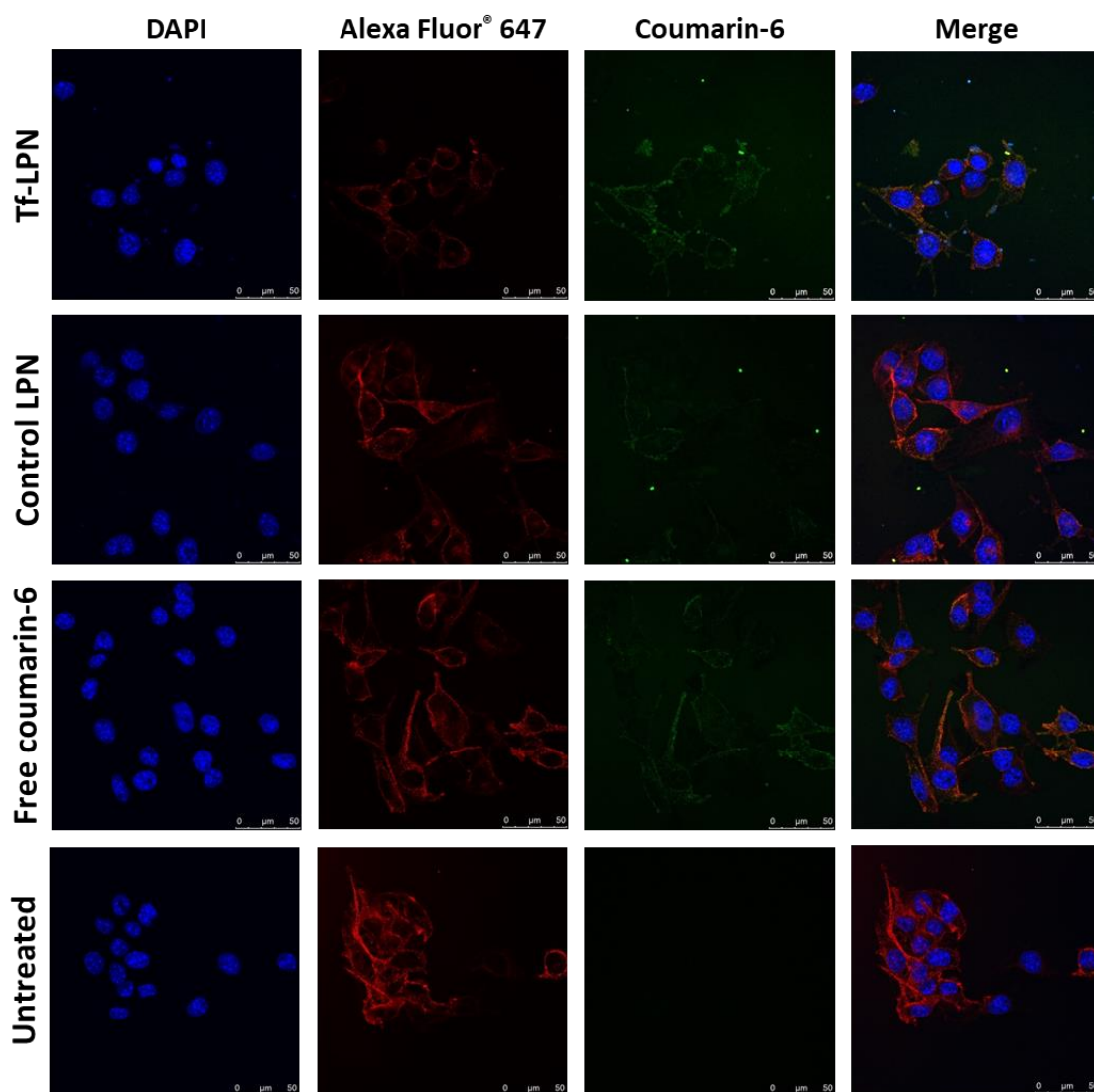
Figure 3-13: Confocal microscopy imaging of B16-F10 cells, showing the cellular uptake of coumarin-6 entrapped in Tf-bearing and control lipid-polymer hybrid nanoparticles or as solution

The quantitative analysis by the flow cytometry found that the conjugation of Tf to the nanoparticles significantly increased coumarin-6 uptake (MFI of 5784 ± 121 a.u.) by 1.6-fold compared to control nanoparticles (MFI of 3576 ± 123 a.u.) (**Figure 3-14**). The highest uptake was observed following treatment with coumarin-6 solution (MFI of 6567 ± 79 a.u.), similar to that observed in liposomes formulation.
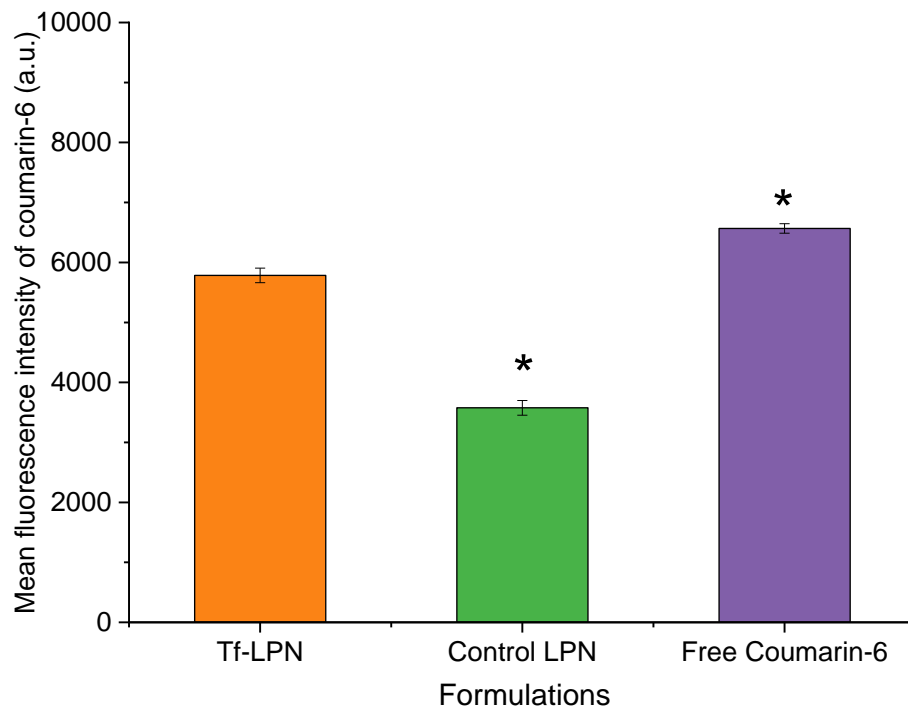
Figure 3-14: Flow cytometry quantification of the cellular uptake of coumarin-6 entrapped in Tf-bearing and control lipid-polymer hybrid nanoparticles or as solution in B16-F10 cells (*n*=3) (*: *p*<0.05 vs Tf-LPN)

3.4.2.2 Mechanisms of cellular uptake

3.4.2.2.1 Transferrin-bearing liposomes

Free transferrin, chlorpromazine, filipin and colchicine were used to inhibit transferrin receptor-mediated, clathrin-mediated, caveolae-mediated and macropinocytosis-mediated endocytosis, respectively (Cheng *et al*., 2014).

Unexpectedly, the cellular uptake of Tf-bearing vesicles loaded with coumarin-6 was not inhibited by free transferrin in B16-F10 cells, indicating that there was no competition between free transferrin and Tf-bearing vesicles at the studied experimental conditions (**Figure 3-15**).

Pre-treatment of B16-F10 cells with chlorpromazine significantly decreased the cellular uptake of coumarin-6 entrapped in Tf-bearing liposomes, which was 16% lower than that observed without pre-treatment and 9.7% lower than that observed with control liposomes (respectively $84.3 \pm 1.7\%$ and $94.0 \pm 0.4\%$ cellular uptake following treatment with Tf-LIP and control LIP, with the relative cellular uptake without inhibitor set at 100%).

The cellular uptake of coumarin-6 entrapped in Tf-bearing liposomes was also partially inhibited by filipin, unlike control liposomes. It decreased to $92.5 \pm 1.7\%$ compared to that measured in cells without pre-treatment, indicating that Tf-bearing liposomes were taken up by caveolae-mediated endocytosis through caveosomes.

Colchicine, however, did not inhibit the cellular uptake of Tf-bearing and control liposomes, meaning that macropinocytosis-mediated endocytosis pathway was not involved in the cellular internalisation of these liposomes.
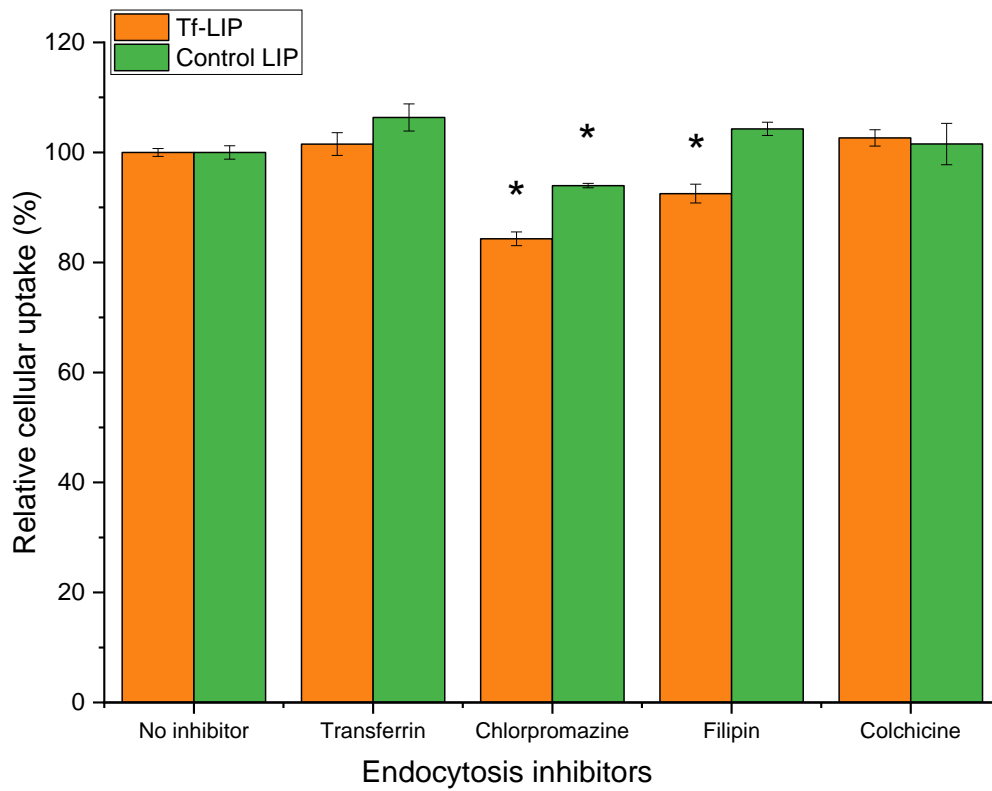
Figure 3-15: Relative cellular uptake of coumarin-6 entrapped in Tf-bearing liposomes (orange) or control liposomes (green), in the presence of endocytosis inhibitors, in B16-F10 cells (*n*=3) (*: *p*<0.05 vs No inhibitor)

3.4.2.2.2 Transferrin-bearing PLGA-PEG nanoparticles

Pre-treatment of B16-F10 cells with 50 μM of free transferrin significantly decreased the cellular uptake of Tf-bearing PLGA-PEG nanoparticles loaded with coumarin-6, which was 10% lower than that observed without pre-treatment (relative cellular uptake of 90.2 ± 1.0 % following treatment with Tf-PN, with the relative cellular uptake without inhibitor set at 100%) (**Figure 3-16**). This result indicated a competition between Tf-nanoparticles and free Tf for binding to Tf receptors, suggesting that the internalisation of Tf-bearing PLGA-PEG nanoparticles is partly due to Tf receptors-mediated endocytosis.

In this study, chlorpromazine, a cationic amphiphilic drug that prevents clathrin-coated pits assembly at the plasma membrane surface (Chen *et al*., 2018), caused the most significant inhibition in both Tf-bearing and control PLGA-PEG nanoparticles loaded with coumarin-6 (decrease of relative cellular uptake to 84.1 ± 0.4% for Tf-PN and 85.7 ± 4.7% for control PN), confirming that clathrin-mediated endocytosis is a major pathway for the internalisation of these nanoparticles.

Following pre-incubation with filipin, the cellular uptake of coumarin-6 entrapped in Tf-bearing PLGA-PEG nanoparticles decreased to 90.4 ± 1.6%, indicating that Tf-nanoparticles was partially taken up by caveolae-mediated endocytosis.

By contrast, colchicine did not inhibit the cellular uptake of coumarin-6 loaded Tf-bearing and control PLGA-PEG nanoparticles, suggesting that macropinocytosis-mediated endocytosis was not responsible for the cellular uptake of these nanoparticles.
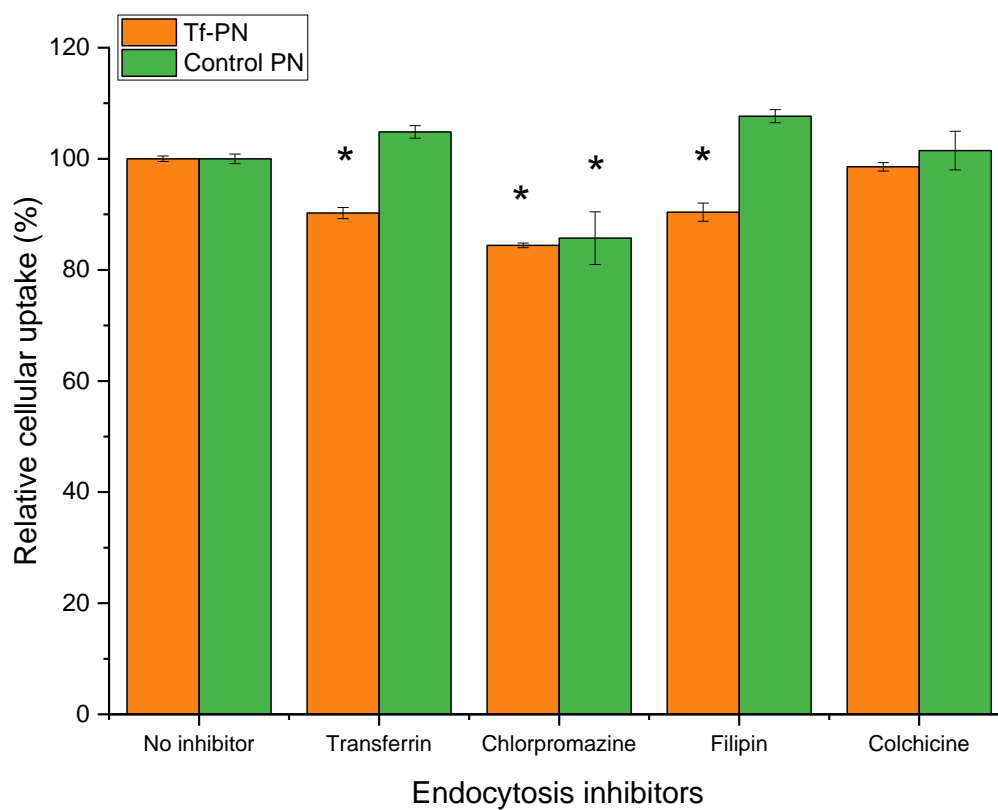
Figure 3-16: Relative cellular uptake of coumarin-6 entrapped in Tf-bearing PLGA-PEG nanoparticles (orange) or control PLGA-PEG nanoparticles (green), in the presence of endocytosis inhibitors, in B16-F10 cells (n=3) (*: $p<0.05$ vs No inhibitor)

3.4.2.2.3 Transferrin-bearing lipid-polymer hybrid nanoparticles

As expected, pre-treatment of B16-F10 cells with 50 µM of free transferrin caused a significant cellular uptake inhibition of Tf-bearing lipid-polymer hybrid nanoparticles entrapping coumarin-6, with a relative cellular uptake of 79.8 ± 0.9 % compared to that observed in the cells without pre-treatment (relative cellular uptake set as 100 %) (**Figure 3-17**). This result confirmed the involvement of Tf receptors-mediated endocytosis for the internalisation of Tf-bearing lipid-polymer hybrid nanoparticles.

Pre-treatment of the cells with chlorpromazine significantly decreased the cellular uptake for both the targeted and control nanoparticles (respectively 79.7 ± 3.1 % and 86.9 ± 1.3 %), indicating that clathrin-mediated endocytosis is a major pathway for internalisation of these nanoparticles.

The cellular uptake of coumarin-6 entrapped in Tf-bearing lipid-polymer hybrid nanoparticles was weakly inhibited by filipin, which decreased to 92.2 ± 3.0 % compared with cells without pre-treatment, meaning that caveolae-mediated endocytosis was partially responsible for the cellular uptake of Tf-bearing lipid-polymer hybrid nanoparticles.

By contrast, colchicine only caused some weak cellular uptake inhibition following treatment with control nanoparticles, with a relative cellular uptake of 93.9 ± 3.0 %, suggesting that macropinocytosis-mediated endocytosis was involved for the cellular uptake of control lipid-polymer hybrid nanoparticles.
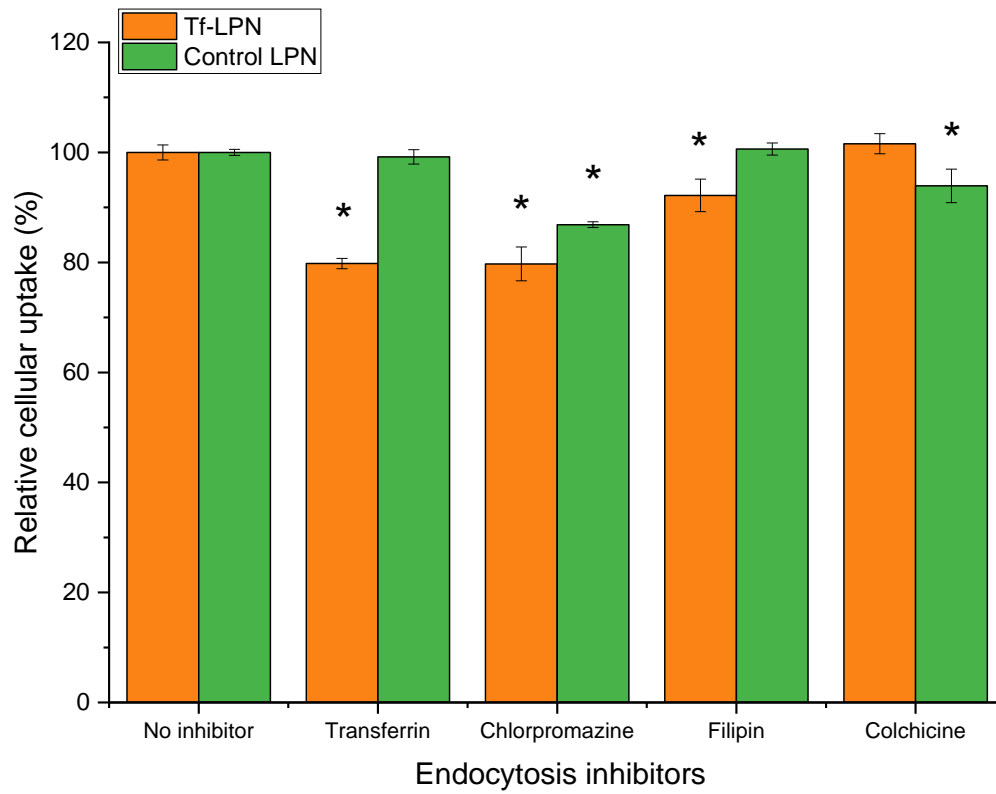
Figure 3-17: Relative cellular uptake of coumarin-6 entrapped in Tf-bearing lipid-polymer hybrid nanoparticles (orange) or control lipid-polymer hybrid nanoparticles (green), in the presence of endocytosis inhibitors, in B16-F10 cells ($n=3$) (*: $p<0.05$ vs No inhibitor)

3.4.3 Anti-proliferative activity

3.4.3.1 Transferrin-bearing liposomes

In this study, an MTT assay was used to examine the anti-proliferative activity of plumbagin either entrapped in Tf-bearing and control liposomes or as a free drug.

The entrapment of plumbagin in liposome formulations significantly improved the anti-proliferative activity of plumbagin, compared with the free solution, by at least 1.5-fold (**Table 3-2, Figure 3-18**). The conjugation of transferrin to the liposomes further increased plumbagin anti-proliferative efficacy, by 2.3-fold for B16-F10 cells, 4.3-fold for A431 cells and 4.2-fold for T98G cells, compared to that of plumbagin solution following 24 hours' treatment. These results correlated well with the improved cellular uptake of the drug following treatment with the targeted liposomes.

Plumbagin loaded in Tf-bearing liposomes exhibited the highest anti-proliferative efficacy against B16-F10 cells (IC$_{50}$: 0.22 ± 0.01 µg/mL), followed by A431 cells (IC$_{50}$: 0.41 ± 0.01 µg/mL). However, Tf-bearing liposomes entrapping plumbagin only exerted a limited anti-proliferative effect in T98G cells (IC$_{50}$: 1.47 ± 0.27 µg/mL). Although the highest plumbagin uptake was found in T98G cells after treatment with plumbagin loaded in Tf-bearing liposomes, improved anti-proliferative activities were found in B16-F10 and A431 cells, probably because T98G cells are more resistant to plumbagin than the two other cell lines.

3.4.3.2 Transferrin-bearing PLGA-PEG nanoparticles

The entrapment of plumbagin in PLGA-PEG nanoparticles led to a significant increase of *in vitro* anti-proliferative activity of plumbagin (**Table 3-2**, **Figure 3-19**). Moreover, the targeting of the nanoparticles with transferrin further improved plumbagin therapeutic efficacy. In B16-F10 cells, the increase was 2.1-fold for Tf-bearing PLGA-PEG nanoparticles and 1.6-fold for control nanoparticles compared to plumbagin solution (IC$_{50}$: 0.24 $\pm$ 0.01 µg/mL for Tf-PN, 0.34 $\pm$ 0.01 µg/mL for control PN and 0.51 $\pm$ 0.02 µg/mL for plumbagin solution). For A431 cells, both Tf-bearing PLGA-PEG nanoparticles and control nanoparticles only exerted a limited therapeutic improvement on this cell line (IC$_{50}$: 1.47 $\pm$ 0.21 µg/mL for Tf-PN, 1.61 $\pm$ 0.28 µg/mL for control PN and 1.78 $\pm$ 0.20 µg/mL for plumbagin solution). In T98G cells, the increase was at its highest, by 2.8-fold for Tf-bearing PLGA-PEG nanoparticles and 3-fold for control nanoparticles compared to that of free plumbagin (IC$_{50}$: 2.18 $\pm$ 0.51 µg/mL for Tf-PN, 2.03 $\pm$ 0.58 µg/mL for control PN and 6.19 $\pm$ 0.20 µg/mL for plumbagin solution). However, there was no significant difference in the IC$_{50}$ between Tf-bearing and control PLGA-PEG nanoparticles in T98G cells. By contrast, blank PLGA-PEG nanoparticles did not exert cytotoxicity to any of the cell lines at the tested conditions, demonstrating the safety of PLGA-PEG-MAL polymer at the tested experimental conditions.

3.4.3.3 Transferrin-bearing lipid-polymer hybrid nanoparticles

The *in vitro* anti-proliferative activity of plumbagin was significantly improved when formulated in lipid-polymer hybrid nanoparticles on the tested cell lines (**Table 3-2**, **Figure 3-20**). In addition, the conjugation of transferrin to the nanoparticles further improved plumbagin therapeutic efficacy when compared to the free drug. In B16-F10 cells, the anti-proliferative efficacy of plumbagin loaded Tf-bearing lipid-polymer hybrid

nanoparticles was higher than that of control nanoparticles and drug solution respectively by 1.6-fold and 3.2-fold (IC$_{50}$: 0.16 ± 0.02 µg/mL for Tf-LPN, 0.26 ± 0.01 µg/mL for control LPN and 0.51 ± 0.02 µg/mL for plumbagin solution). In A431 cells, Tf-bearing lipid-polymer hybrid nanoparticles significantly enhanced the therapeutic efficacy of plumbagin by 1.4-fold and 2.8-fold when compared with control nanoparticles and free plumbagin, respectively (IC$_{50}$: 0.63 ± 0.03 µg/mL for Tf-LPN, 0.86 ± 0.03 µg/mL for control LPN and 1.78 ± 0.20 µg/mL for plumbagin solution). In T98G cells, the efficacy was 3.0-fold for Tf-bearing lipid-polymer hybrid nanoparticles and 2.6-fold for control nanoparticles in comparison with plumbagin solution. However, there was no significant difference between Tf-bearing and control lipid-polymer hybrid nanoparticles (IC$_{50}$: 2.03 ± 0.15 µg/mL for Tf-LPN, 2.40 ± 0.49 µg/mL for control LPN and 6.19 ± 0.20 µg/mL for plumbagin solution). By contrast, blank lipid-polymer hybrid nanoparticles did not exert any cytotoxicity to the cell lines at the tested concentrations, similarly to liposomes and polymeric nanoparticles.

Table 3-2: Anti-proliferative activity of plumbagin entrapped in Tf-bearing and control formulations, or free in solution, expressed as IC_{50} values, in B16-F10, A431 and T98G cells, following 24 h treatment (*n*=15) (n.d.: not determined)

Cell lines	IC_{50} (µg/ml) [Mean ± SEM]		
	B16F10	**A431**	**T98G**
Plumbagin solution	0.51 ± 0.02	1.78 ± 0.19	6.19 ± 0.19
Liposomes			
Tf-LIP	0.22 ± 0.01	0.41 ± 0.01	1.47 ± 0.27
Control LIP	0.31 ± 0.03	0.63 ± 0.02	2.04 ± 0.35
Blank LIP	n.d.	n.d.	n.d.
PLGA-PEG nanoparticles			
Tf-PN	0.24 ± 0.01	1.47 ± 0.21	2.18 ± 0.51
Control PN	0.32 ± 0.01	1.61 ± 0.28	2.03 ± 0.58
Blank PN	n.d.	n.d.	n.d.
Lipid-polymer hybrid nanoparticles			
Tf-LPN	0.16 ± 0.02	0.63 ± 0.03	2.03 ± 0.15
Control LPN	0.26 ± 0.01	0.86 ± 0.03	2.40 ± 0.49
Blank LPN	n.d.	n.d.	n.d.
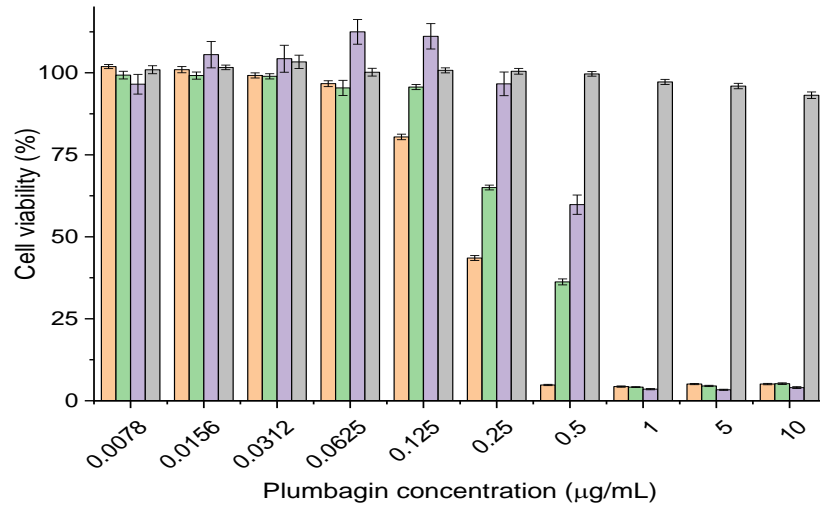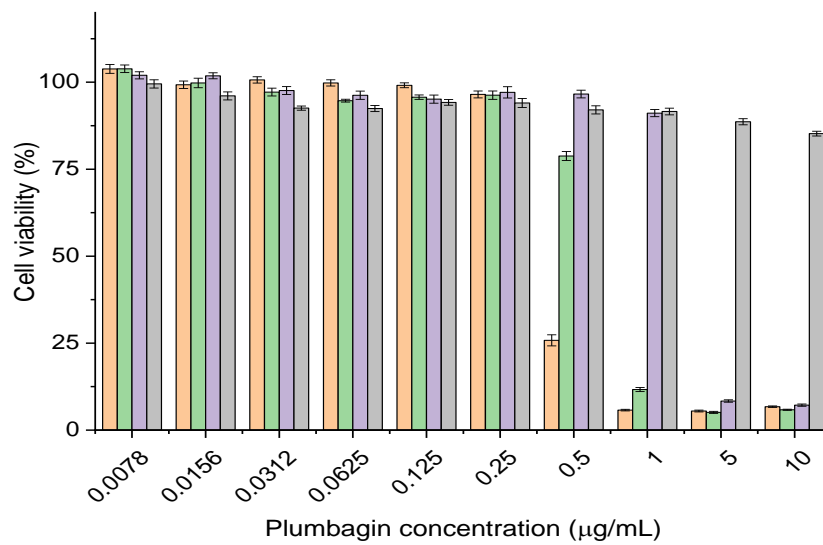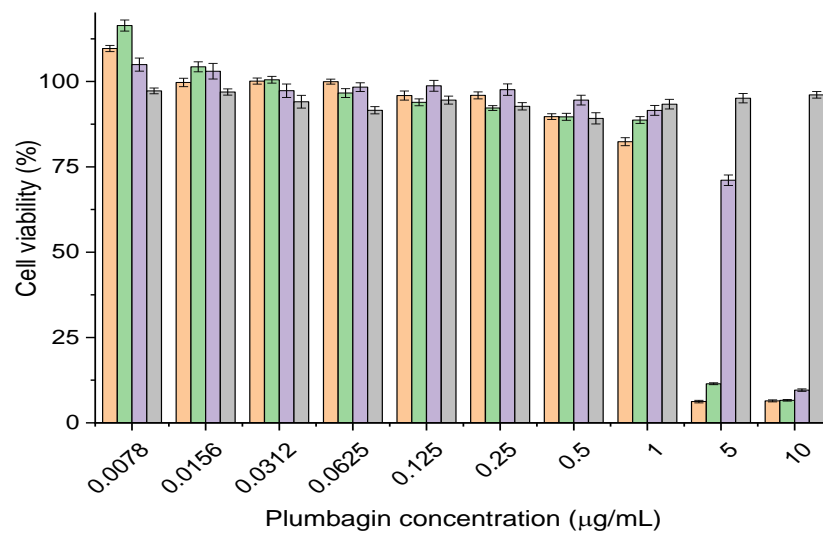
Figure 3-18: Anti-proliferative effect of plumbagin entrapped in Tf-bearing liposomes (orange), control liposomes (green) or free in solution (purple), on B16-F10, A431 and T98G cells, following 24 h treatment (control: blank liposomes (grey)) (n=15)
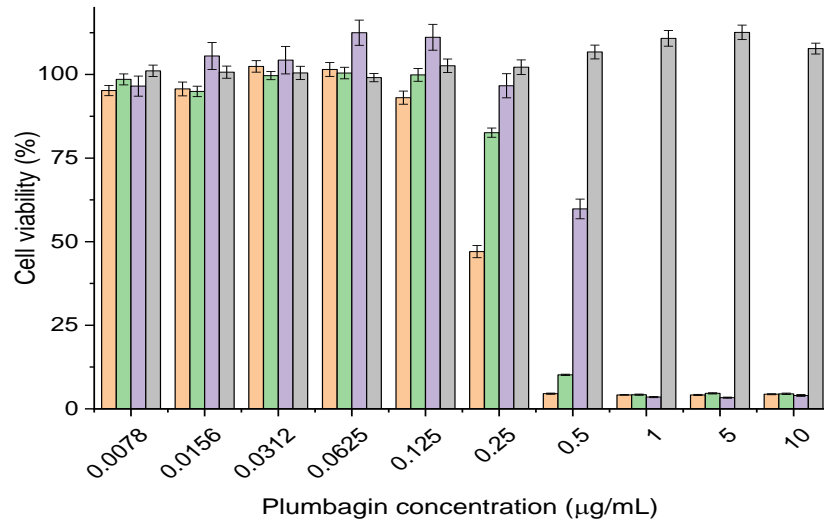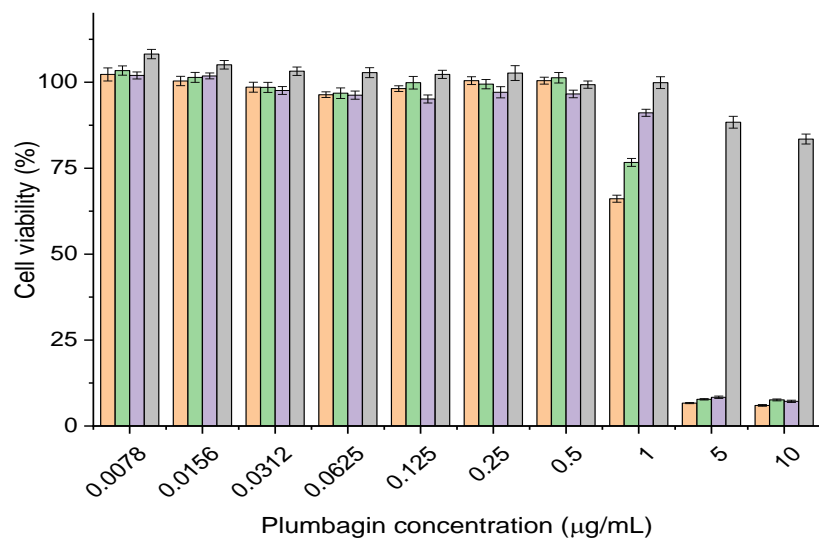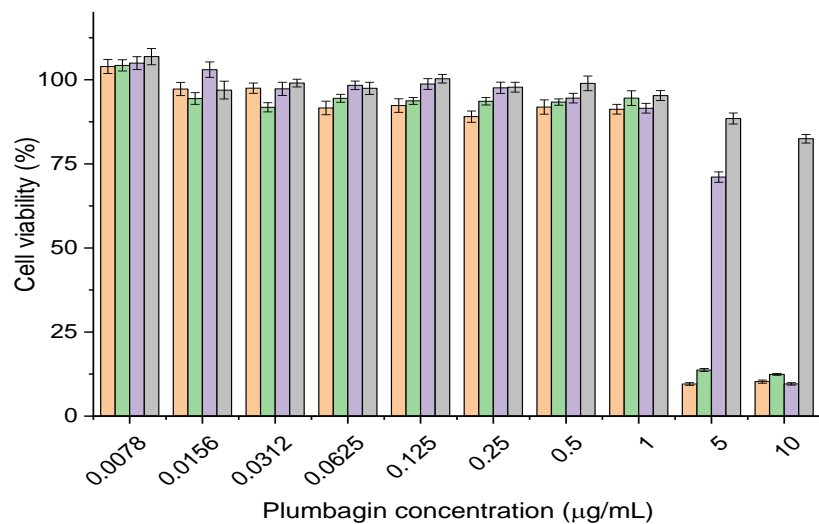
Figure 3-19: Anti-proliferative effect of plumbagin entrapped in Tf-bearing (orange) and control (green) PLGA-PEG nanoparticles or free in solution (purple), on B16-F10, A431 and T98G cells, following 24 h treatment (control: blank nanoparticles (grey)) (*n*=15)
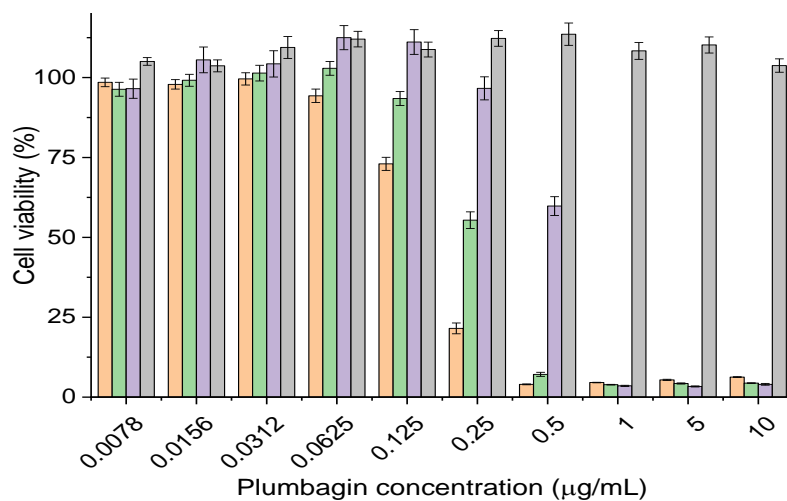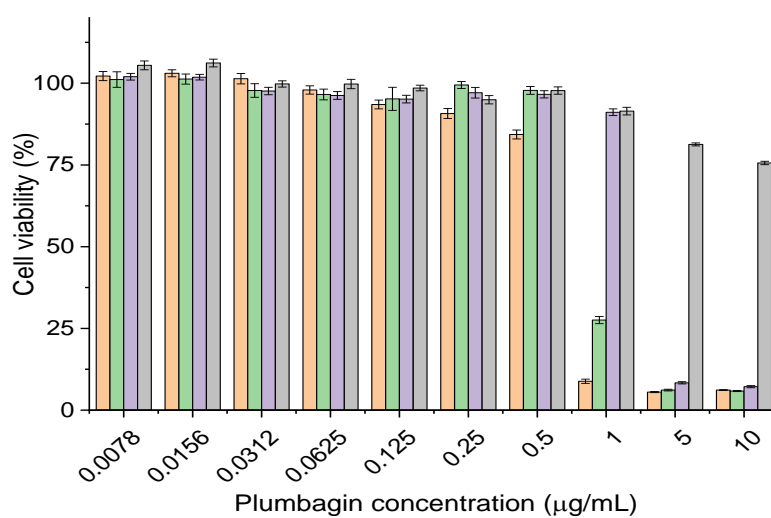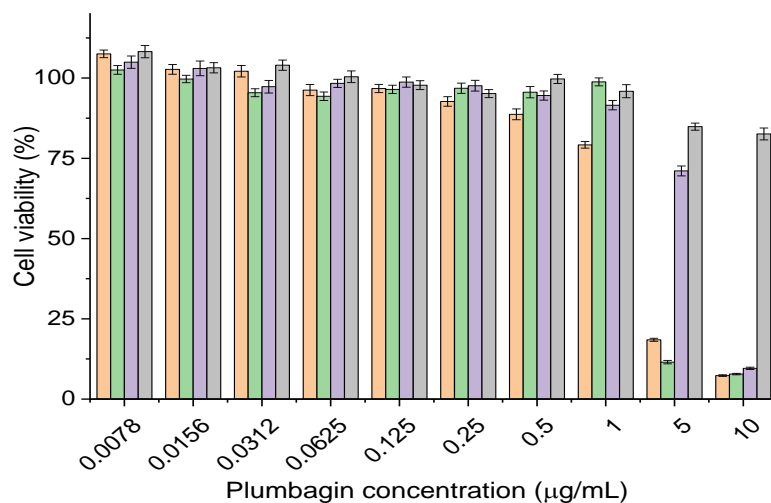
Figure 3-20: Anti-proliferative effect of plumbagin entrapped in Tf-bearing (orange) and control (green) lipid-polymer hybrid nanoparticles or free in solution (purple), on B16-F10, A431 and T98G cells, following 24 h treatment (control: blank nanoparticles (grey)) (*n*=15)

3.4.4 Cellular apoptosis

3.4.4.1 Transferrin-bearing liposomes

Tf-bearing liposomes entrapping plumbagin (1 µg/mL, 5.3 µM) significantly led to higher cellular apoptosis in B16-F10 cells compared to that of control liposomes and free plumbagin, with 88.4 ± 0.4 % of cells being in apoptosis following treatment with Tf-bearing liposomes, compared with 82.0 ± 1.5 % apoptotic cells following treatment with control liposomes. By contrast, only 27.5 ± 1.0 % of cells were apoptotic when treated with free plumbagin (**Figure 3-21 and 3-22**). In A431 cells, the apoptosis effect of Tf-bearing liposomes (total apoptosis of 43.3 ± 3.5 % cells) was lower than that observed with B16-F10 cells, but was still 1.9-fold higher than that observed following treatment with control liposomes (total apoptosis of 22.4 ± 3.5 % cells). Free plumbagin only exerted a limited apoptosis effect on this cell line at the tested conditions (7.9 ± 0.9 % apoptotic cells following treatment with free plumbagin). In T98G cells, the apoptosis effect of Tf-bearing liposomes was further reduced compared to that of the 2 other cell lines, but was still significantly higher ($p<0.05$) than that observed following treatment with control liposomes and free drug in solution (total apoptosis of 24.9 ± 0.8 % cells following treatment with Tf- bearing liposomes, 18.5 ± 1.0 % cells for control liposomes and 17.1 ± 1.5 % cells for free plumbagin). This result correlated well with those obtained from the anti-proliferative assay, showing that Tf-bearing liposomes entrapping plumbagin exhibited the highest anti-proliferative effect on B16-F10 cells followed by A431 and T98G cells.
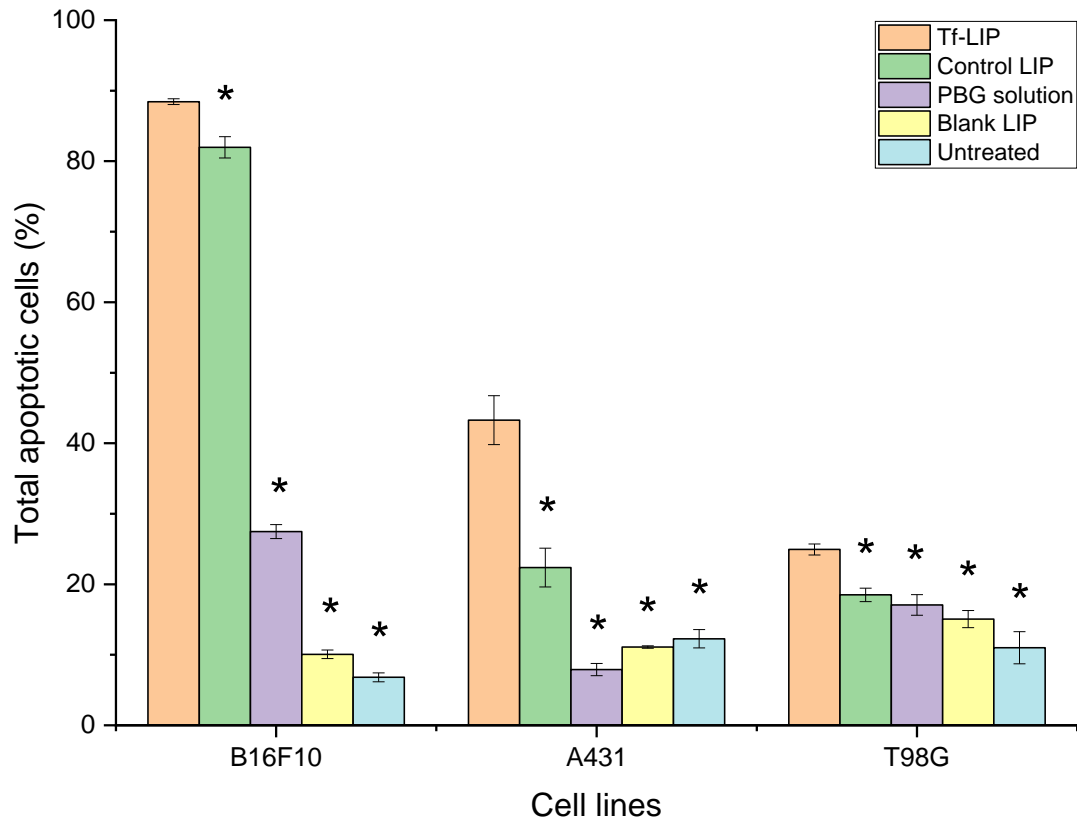
Figure 3-21: Apoptosis effect of plumbagin (1 µg) entrapped in Tf-bearing liposomes, control liposomes or free in solution on B16-F10, A431 and T98G cells following 4 h treatment, expressed as percentage of total apoptotic cells (early apoptosis + late apoptosis) (n=3) (*: $p<0.05$ vs Tf-LIP)
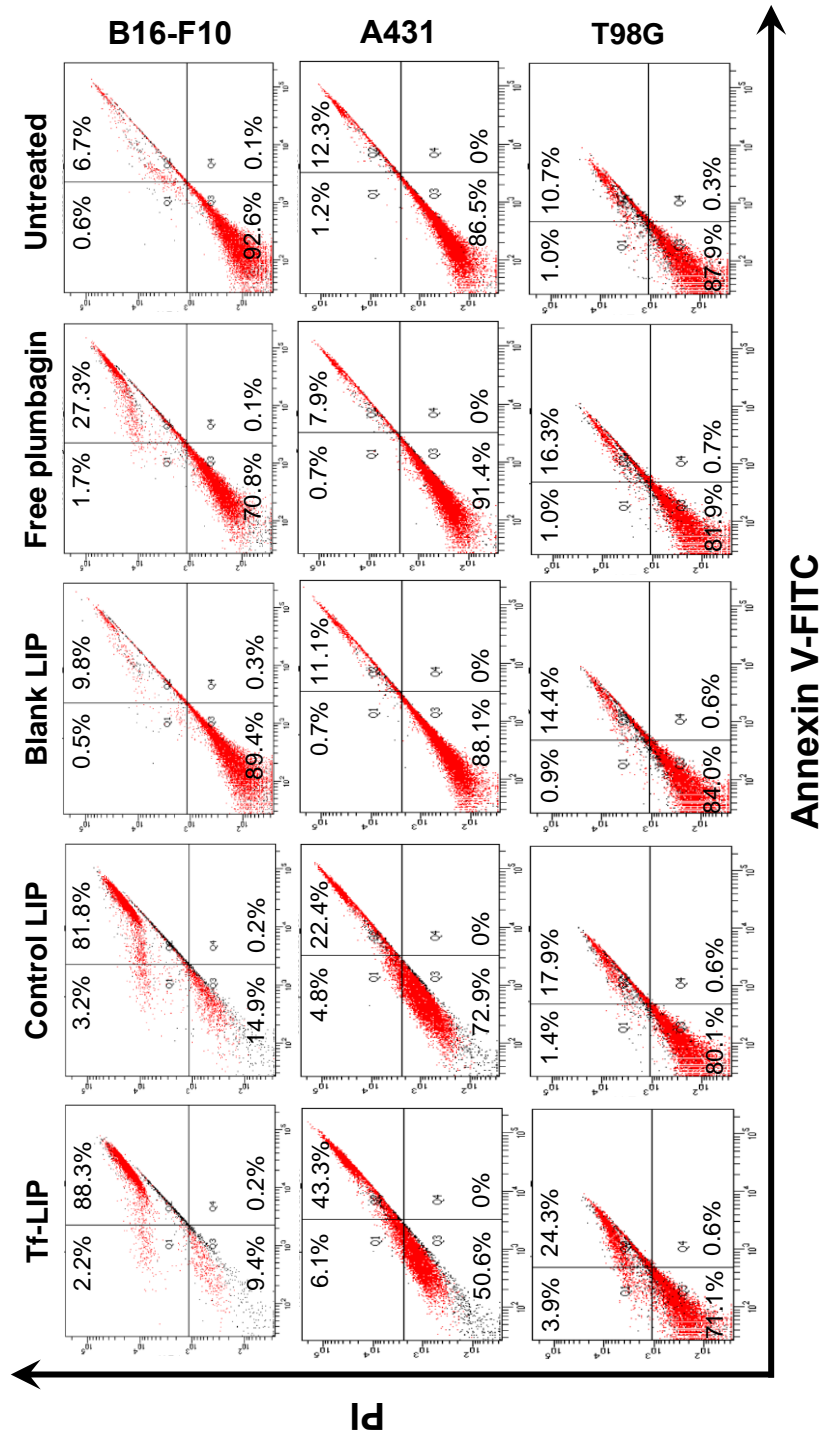
Figure 3-22: Analysis of apoptosis by FITC Annexin V/PI double-staining assay on B16-F10, A431 and T98G cells treated with plumbagin (1 µg) entrapped in Tf-bearing liposomes, control liposomes or free in solution after 4 h treatment. Flow cytometric scatter plots show the percentage of four specific cell populations, necrosis (upper left, Q1), late apoptosis (upper right, Q2), live (lower left, Q3) and early apoptosis (lower right, Q4)

3.4.4.2 Transferrin-bearing PLGA-PEG nanoparticles

The conjugation of transferrin to plumbagin loaded PLGA-PEG nanoparticles led to a significant increase in cellular apoptosis on B16-F10 cells compared to that of unconjugated nanoparticles and free plumbagin (**Figures 3-23 and 3-24**), with a total percentage of apoptotic cells respectively of 78.8 ± 1.4 % for Tf-bearing PLGA-PEG nanoparticles, 72.3 ± 0.8 % for control nanoparticles and 27.5 ± 1.0 % for free plumbagin. For A431 cells, Tf-bearing PLGA-PEG nanoparticles exhibited higher apoptosis activity than free plumbagin which did not exert any apoptosis on this cell line at the tested conditions. Its efficacy was not higher than that of control nanoparticles (total apoptosis of 27.2 ± 1.2 % for Tf-PN, 25.4 ± 0.8 % for control PN and 7.9 ± 0.9 % for free plumbagin). By contrast, in T98G cells, only free plumbagin solution induced apoptosis, while both Tf-bearing and control PLGA-PEG nanoparticles did not exert apoptosis at the tested conditions (total apoptosis of 7.7 ± 0.6 % for Tf-PN, 7.2 ± 0.5 % for control PN and 17.1 ± 1.5% for free plumbagin).
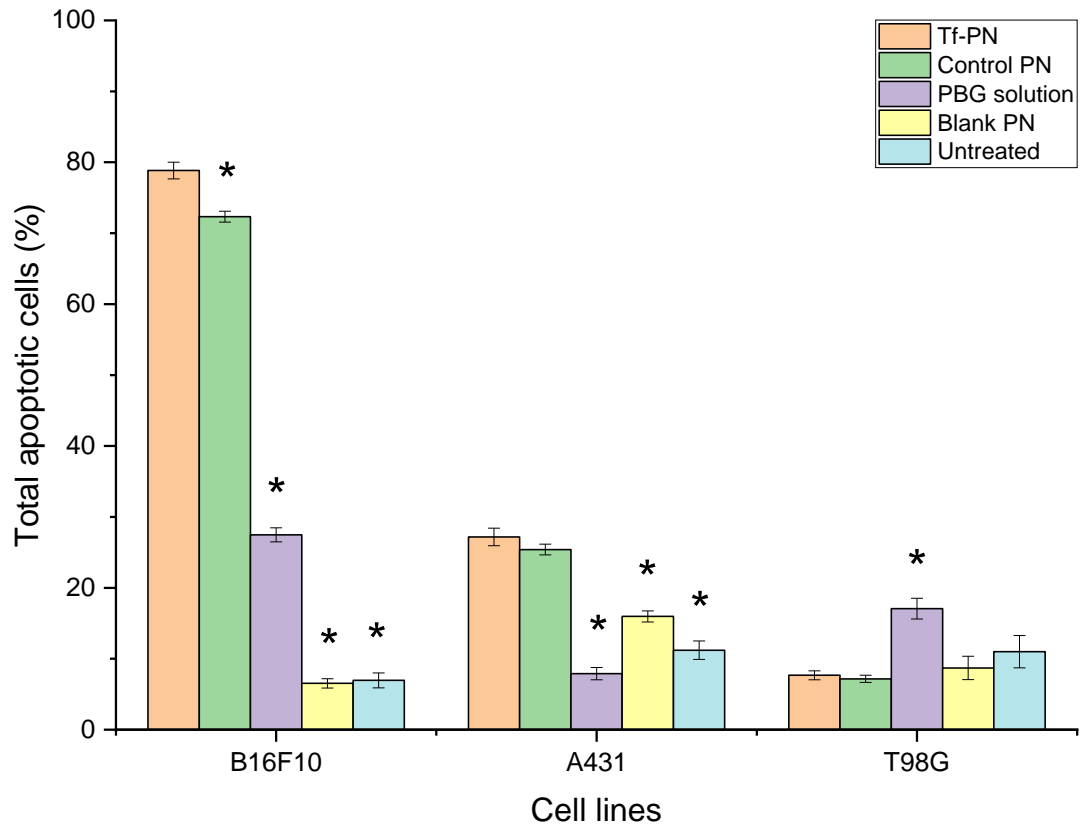
Figure 3-23: Apoptosis effect of plumbagin (1 µg) entrapped in Tf-bearing and control PLGA-PEG nanoparticles or free in solution on B16-F10, A431 and T98G cells following 4 h treatment, expressed as percentage of total apoptotic cells (early apoptosis + late apoptosis) (n=3) (*: p<0.05 vs Tf-PN)
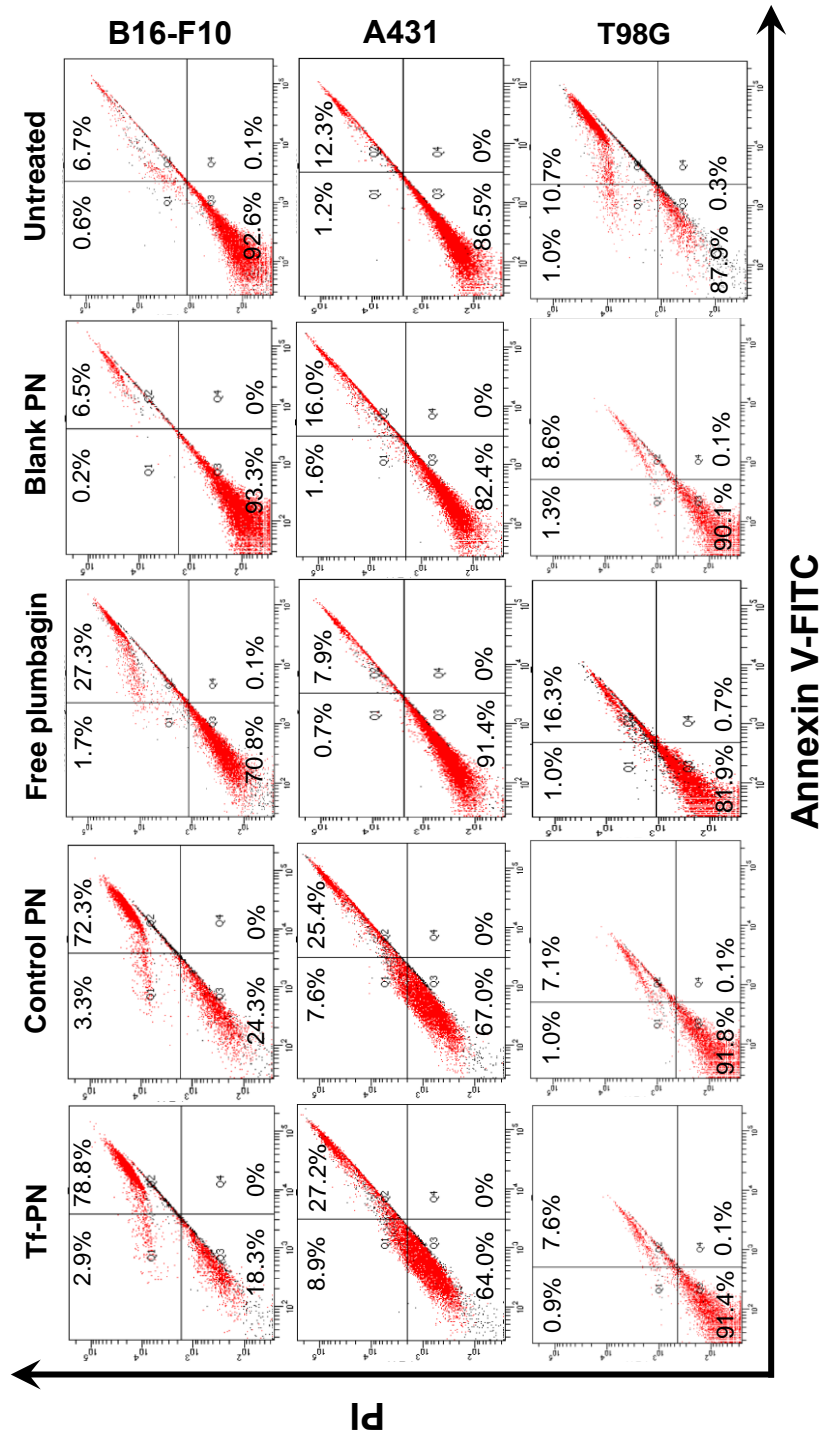
Figure 3-24: Analysis of apoptosis by FITC Annexin V/PI double-staining assay on B16-F10, A431 and T98G cells treated with plumbagin (1 μg) entrapped in Tf-bearing and control PLGA-PEG nanoparticles or free in solution after 4 h treatment. Flow cytometric scatter plots show the percentage of four specific cell populations, necrosis (upper left, Q1), late apoptosis (upper right, Q2), live (lower left, Q3) and early apoptosis (lower right, Q4)

3.4.4.3 Transferrin-bearing lipid-polymer hybrid nanoparticles

Tf conjugation on plumbagin-loaded lipid-polymer hybrid nanoparticles significantly led to the highest cellular apoptosis in B16-F10 cells (**Figure 3-25 and 3-26**), with 89.2 ± 0.4 % of cells being apoptotic as a result of their treatment. By contrast, 80.5 ± 0.6 % and 27.5 ± 1.0 % of cells were apoptotic when treated with the control nanoparticles or the plumbagin solution, respectively.

In A431 cells, the apoptosis effect of the targeted formulation was much lower than in B16-F10 cells (total apoptosis of 20.3 ± 1.1 %). Control nanoparticles and plumbagin solution only exerted a limited apoptosis on this cell line at the tested conditions (total apoptosis of 13.2 ± 0.3 % for control LPN, 7.9 ± 0.9% for plumbagin solution), similar to the 11.4 ± 0.3 % apoptosis obtained when treated with the blank nanoparticles.

In T98G cells, the apoptosis effect of Tf-bearing lipid-polymer hybrid nanoparticles (total apoptosis of 21.0 ± 0.4 % cells) was similar to that observed with A431 cells following treatment with the same formulation, but was not statistically different from that observed with control nanoparticles or drug solution (total apoptosis respectively of 17.6 ± 1.5 % and 17.1 ± 1.5 %).
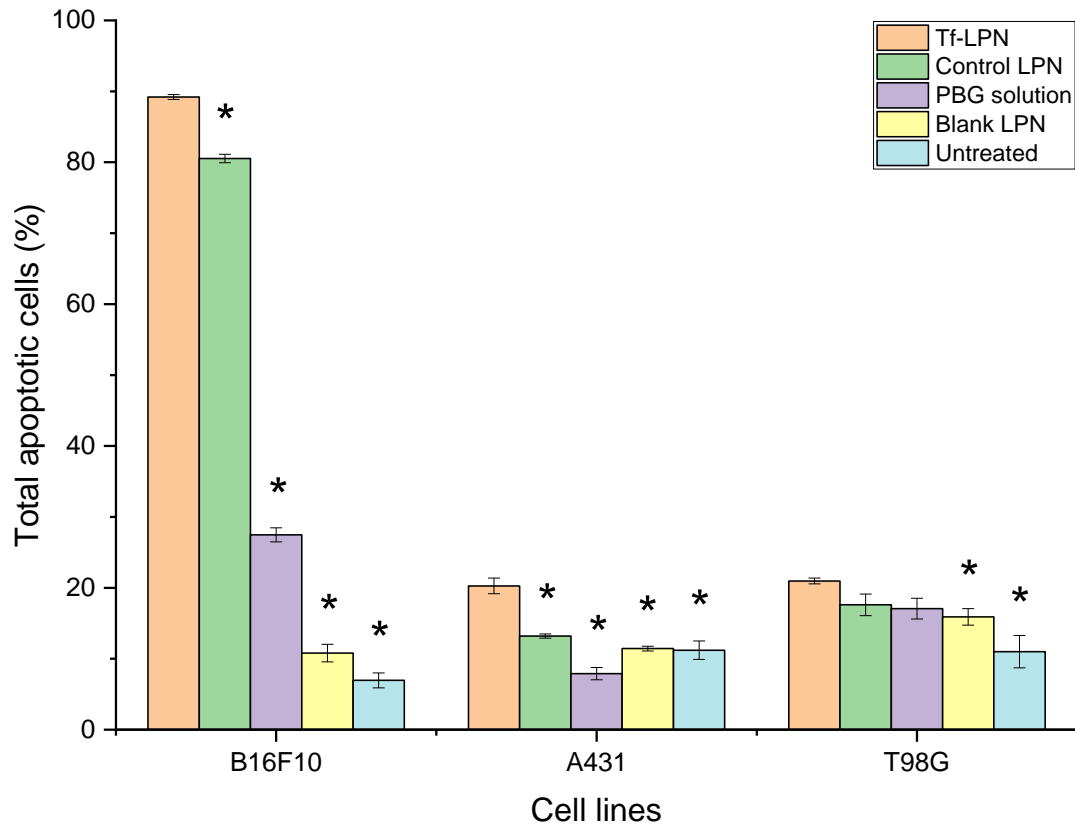
Figure 3-25: Apoptosis effect of plumbagin (1 µg) entrapped in Tf-bearing and control lipid-polymer hybrid nanoparticles or free in solution on B16-F10, A431 and T98G cells following 4 h treatment, expressed as percentage of total apoptotic cells (early apoptosis + late apoptosis) ($n=3$) (*: $p<0.05$ vs Tf-LPN)
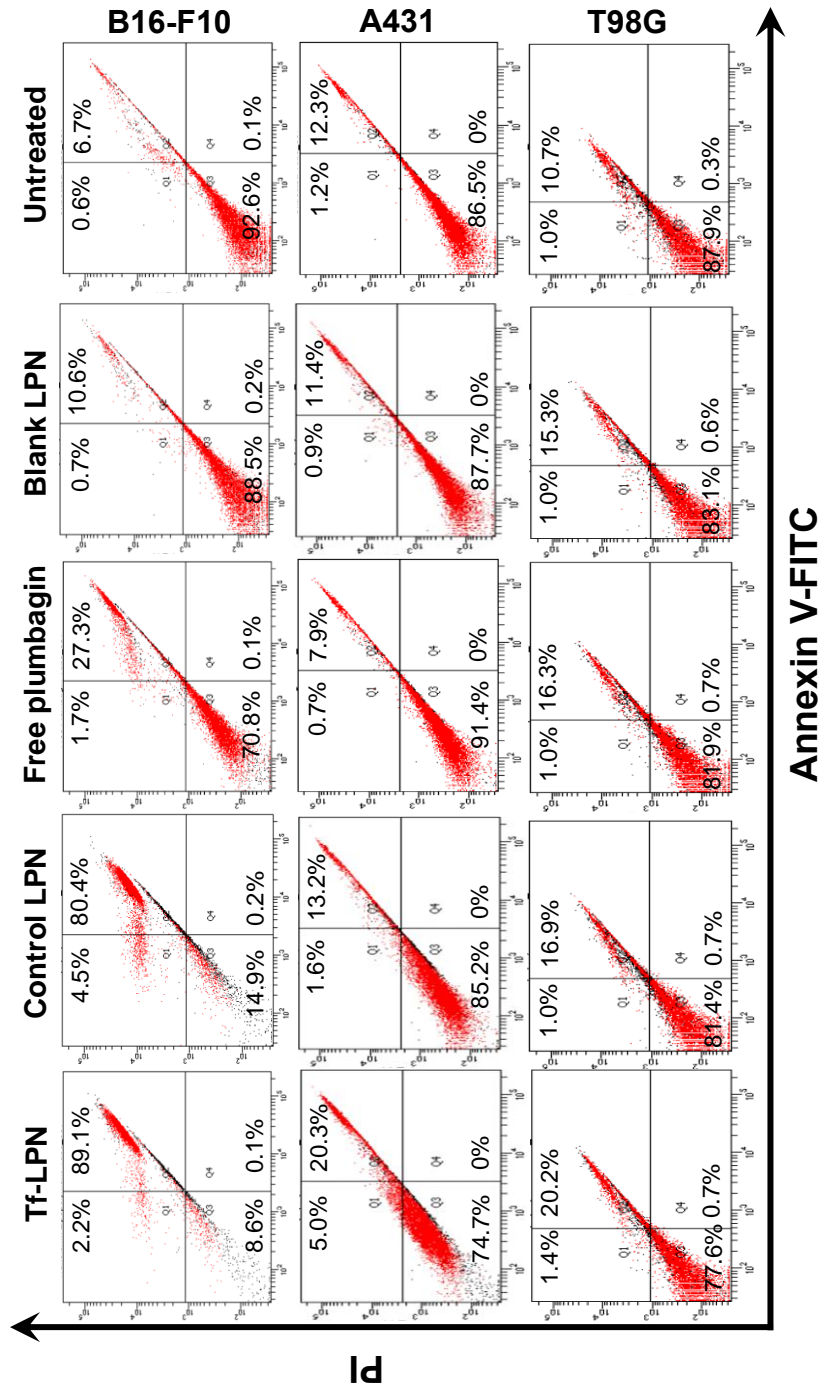
Figure 3-26: Analysis of apoptosis by FITC Annexin V/PI double-staining assay on B16-F10, A431 and T98G cells treated with plumbagin (1 µg) entrapped in Tf-bearing and control lipid-polymer hybrid nanoparticles or free in solution after 4 h treatment. Flow cytometric scatter plots show the percentage of four specific cell populations, necrosis (upper left, Q1), late apoptosis (upper right, Q2), live (lower left, Q3) and early apoptosis (lower right, Q4)

3.5 Discussion

The possibility of using plumbagin for cancer treatment is limited by the inability of this compound to specifically reach tumours at a therapeutic concentration following intravenous injection, resulting from short biological half-life and rapid elimination. To overcome this issue, we hypothesise that loading plumbagin into a tumour-targeted delivery system would enhance the specific delivery of plumbagin to cancer cells and increase its therapeutic efficacy.

In Chapter 2, we successfully prepared transferrin-bearing liposomes, PLGA-PEG nanoparticles and lipid-polymer hybrid nanoparticles entrapping plumbagin, and demonstrated that these tumour-targeted formulations have suitable physico-chemical properties for being efficient delivery systems for plumbagin. Thereafter, it is necessary to investigate the capability of these delivery systems to enhance the specific delivery of plumbagin to cancer cells and enhancement of its therapeutic efficacy.

For the PEGylated liposomes, cellular uptake studies demonstrated that Tf-bearing liposomes led to higher cellular accumulation of plumbagin in comparison with control liposomes and plumbagin solution. A similar result was obtained when replacing plumbagin with coumarin-6 as a lipophilic fluorescent drug model. These results were similar to that previously reported by our group when using Tf-bearing Solulan C24 / Span 60-based vesicles as drug carriers for tocotrienol and epigallocatechin gallate (Fu *et al*., 2009; Lemarié *et al*., 2013). This outcome was also reported by Jhaveri and colleagues (2018), who showed that the cellular uptake of resveratrol, a polyphenol compound found in grape seed, was increased in U87MG human glioblastoma cells following treatment with Tf-bearing liposomes compared to control liposomes. Among the three tested cancer cell lines, T98G cells exhibited the highest cellular uptake of plumbagin after treatment with transferrin-bearing vesicles. This might be explained by

the high level of transferrin receptors on the surface of T98G cells compared to B16-F10 and A431 cell lines (Bausch-Fluck *et al*., 2015).

The cellular uptake of Tf-bearing liposomes was not inhibited following pre-treatment with free transferrin. This result was observed for a fixed set of experimental conditions, but may have been different following optimisation (e.g. using various amounts of Tf, various durations of incubation). The explanation for this result might be the elasticity of vesicles. Guo and colleagues (2018) demonstrated that the vesicles that have high elasticity such as liposomes, can enter cells predominantly by fusion with the cell membrane, which is not affected by endocytosis inhibition. The cellular uptake of Tf-bearing liposomes was partially inhibited by chlorpromazine and filipin, while control liposomes were partially inhibited by chlorpromazine only. Both chlorpromazine and filipin are pinocytosis inhibitors: chlorpromazine has been reported to inhibit clathrin-mediated endocytosis, which is a major pathway for the internalisation of various nanomedicines (Chen *et al*., 2018), whereas filipin blocks the caveolae-mediated process, a clathrin-independent endocytosis (Gao *et al*., 2013). These results therefore confirm the involvement of clathrin-mediated endocytosis, which is a requisite for Tf receptor-mediated endocytosis, and caveolae-mediated endocytosis in the internalisation of Tf-bearing liposomes. This result is in agreement with previous reports showing that clathrin-mediated endocytosis is the main mechanism of nanomedicine internalisation (Li *et al*., 2012b; Gao *et al*., 2013; Alshehri *et al*., 2018). For instance, cellular uptake of Tf/TAT-liposomes containing doxorubicin in B16 cells was decreased by 20 % after pre-treatment with chlorpromazine (20 µg/ml for 2 hours) (Yuan *et al*., 2016).

The entrapment of plumbagin within liposomes increased its anti-proliferative activity by at least 1.5-fold compared with free drug. Furthermore, the conjugation of transferrin to liposomes further improved the IC_{50} values, showing approximately up to 4.3-fold,

166

compared to that of plumbagin solution. Although the highest plumbagin uptake was found in T98G cells after treatment with Tf-bearing liposomes loading plumbagin, improved anti-proliferative activities were found in B16-F10 and A431 cells, probably because T98G cells are more resistant to plumbagin than the two other cell lines. T98G cell line is a glioblastoma multiforme (GBM), known to be one of the most malignant and aggressive forms of brain cancer due to its high resistance to chemotherapy (Kriel *et al*., 2018). Glioblastomas have recently been reported to be resistant to the alkylating agent temozolomide (TMZ) (Munoz *et al*., 2014), and may also be resistant to the alkylating properties of plumbagin (Klotz *et al*., 2014), therefore limiting its therapeutic efficacy on T98G cells. Several delivery systems have previously been reported to improve the therapeutic efficacy of plumbagin. For example, silver caged nanoparticles containing plumbagin 2.5 µM (0.47 µg/mL) reduced the cell viability of A431 epidermoid carcinoma cells by 80% while free plumbagin at the same concentration reduced cell viability by only 20% (Duraipandy *et al*., 2014). In another work, Phospholipid-Tween® 80 mixed micelles containing plumbagin improved its *in vitro* anti-proliferative activity on MCF-7 cells by 2.1-fold (Bothiraja *et al*., 2013). The cytotoxicity of plumbagin-loaded nanoemulsion (composed of oleic acid and polysorbate 80) on PTEN-P2 murine prostate cancer cells was enhanced by 1.4-fold in comparison with free plumbagin (Chrastina *et al*., 2018). In comparison, our Tf-bearing vesicles entrapping plumbagin might inhibit cancer cells proliferation more efficiently than with non-targeted delivery systems, due to transferrin active targeting.

The entrapment of plumbagin in Tf-bearing liposomes also increased apoptosis in the three tested cancer cell lines, unlike drug solution. This improvement correlated well with anti-proliferative results, showing that Tf-bearing liposomes exhibited the highest apoptosis on B16-F10 cells followed by A431 and T98G cells. Our results were in

agreement with previous reports by Duraipandy and colleagues (2014), who demonstrated that the treatment with plumbagin entrapped in silver nanocages led to the apoptosis of A431 cells, unlike free drug solution. In another work, silver nanoparticles entrapping plumbagin was reported to induce apoptosis in Hela cells, unlike free plumbagin (Appadurai and Rathinasamy, 2015).

The entrapment of plumbagin in PLGA-PEG nanoparticles significantly improved the cellular accumulation of plumbagin compared to free drug. It was further improved when conjugating these nanoparticles with transferrin. These results were comparable with the cellular uptake of PLGA-PEG nanoparticles entrapping coumarin-6. Our data are in line with the flow cytometry results of Zhao and colleagues (2014), who found that the uptake of paclitaxel loaded in poly(γ-glutamic acid-maleimide-co-L-lactide)-1,2-dipalmitoyl-sn-glycero-3-phosphoethanolamine copolymer (γ-PGA-MAL-PLA-DPPE) nanoparticles modified with transferrin was significantly enhanced by more than 2.13-fold and 1.32-fold respectively in C666-1 and HeLa cells compared with unmodified nanoparticles. Tf-conjugated poly(lactide)-D-α-tocopheryl polyethylene glycol succinate diblock copolymer (PLA-TPGS) nanoparticles were also found to increase the uptake of coumarin-6 in a time-dependent manner compared with unmodified nanoparticles in C6 glioma cells (Gan and Feng, 2010). In another study, entrapping resveratrol within Tf modified polyethylene glycol-poly lactic acid (PEG-PLA) nanoparticles also increased its cellular uptake by C6 glioma cells (Guo *et al*., 2013), confirming the potential of transferrin for tumour targeting.

The study investigating the mechanisms of cellular uptake indicated that there was a competition between Tf-bearing PLGA-PEG nanoparticles and free Tf for binding to Tf receptors, confirming that the internalisation of Tf-bearing nanoparticles is partly due to Tf receptors-mediated endocytosis. Numerous studies have reported similar findings

where the presence of free Tf reduced cellular uptake of transferrin-conjugated nanoparticles in various cancer cell lines (Chang *et al.*, 2009; Zhang *et al.*, 2012; Jhaveri *et al.*, 2018). Clathrin-mediated endocytosis is well known for its role as the main mechanism for internalisation of most nanocarriers (Gao *et al.*, 2013; Oh and Park, 2014). As expected, chlorpromazine was found to have the maximum inhibitory effect on the cellular uptake of Tf-bearing and control PLGA-PEG nanoparticles (around 15 % reduction). Caveolae-mediated endocytosis was also found to be one of the internalisation mechanisms for Tf-bearing PLGA-PEG nanoparticles, as their cellular uptake was inhibited by filipin.

Treatment of the cells with Tf-bearing PLGA-PEG nanoparticles entrapping plumbagin resulted in an enhanced anti-proliferative activity on the three tested cell lines in comparison with free plumbagin. These results were in accordance with these previous reports, which demonstrated that the therapeutic efficacy of plumbagin is improved by entrapment in drug delivery systems. For example, folic acid-conjugated TPGS nanomicelles containing plumbagin improved its anti-proliferative activity on MCF-7 cells (IC$_{50}$ of $3.2 \pm 0.4\,\mu$g/mL) by 2.4-fold and 4.1-fold in comparison with unconjugated nanomicelles (IC$_{50}$ of $7.8 \pm 0.8\,\mu$g/mL) and free drug (IC$_{50}$ of $13.5 \pm 1.31\,\mu$g/mL) (Pawar *et al.*, 2016). Pan and colleagues (2017) have demonstrated that aptamer-targeted PLGA-PEG nanoparticles increased the cytotoxicity of plumbagin on LNCaP prostate cancer cells by 2.2-fold (IC$_{50}$ of $4.78 \pm 0.83\,\mu$M) compared with non-targeted nanoparticles (IC$_{50}$ of $10.33 \pm 2.48\,\mu$M), while blank PLGA-PEG nanoparticles showed low toxicity, following a similar trend as in our experiments.

Consistent with anti-proliferative studies, flow cytometric analysis revealed that the treatment of the cells with plumbagin entrapped in Tf-bearing lipid-polymer hybrid nanoparticles led to an increase in the percentage of total apoptotic cells of B16-F10 and

A431 cells, unlike those treated with drug solution. However, in T98G cells, Tf-bearing lipid-polymer hybrid nanoparticles entrapping plumbagin did not cause apoptosis at the tested experimental conditions. T98G cells, known to be highly resistant to alkylating agents such as temozolomide, the frontline treatment for glioblastoma multiforme (Keiel *et al*., 2010), might also resist the alkylating properties of plumbagin (Klotz *et al*., 2010), as mentioned above.

Lipid-polymer hybrid nanoparticles, cellular uptake studies demonstrated that the conjugation of Tf to lipid-polymer hybrid nanoparticles significantly increased plumbagin uptake in comparison with control nanoparticles and plumbagin solution on the three tested cell lines. Our data are in line with the finding of Guo and colleagues (2015) who found that the use of Tf as a targeting ligand on lipid-polymer hybrid nanoparticles entrapping doxorubicin improved the cellular uptake of doxorubicin by 2.8 times compared with non-targeted nanoparticles on A549 cells. This outcome was also reported by Zheng and colleagues (2010), who showed that Tf-conjugated lipid-polymer hybrid nanoparticles entrapping calcein was more efficiently taken up by SKBR-3 cells compared with the non-targeted formulation.

The cellular uptake of Tf-bearing lipid-polymer hybrid nanoparticles was partially inhibited by free Tf, chlorpromazine and filipin, while control nanoparticles was partially inhibited by chlorpromazine and colchicine. Pre-treatment of B16-F10 cells with free Tf led to competition between Tf-bearing lipid-polymer hybrid nanoparticles and free Tf, suggesting that the internalisation of Tf-bearing lipid-polymer hybrid nanoparticles is partly due to Tf receptors-mediated endocytosis. This result is in agreement with previous data obtained by Zheng and colleagues (2010), who revealed that the cellular uptake of Tf-conjugated lipid-polymer hybrid nanoparticles carrying the aromatase inhibitor, 7α-(4-amino)phenylthio-1,4-androstadiene-3,17-dione, was reduced by the excess free Tf in

the culture media. Chlorpromazine is a common blocker of clathrin-mediated endocytosis, while filipin is known to block the caveolae-mediated endocytosis.

Our study has shown that the cellular uptake of Tf-bearing lipid-polymer hybrid nanoparticles was blocked by these inhibitors. This result therefore confirms the involvement of clathrin-mediated and caveolae-mediated endocytosis in the internalisation of Tf-bearing lipid-polymer hybrid nanoparticles. Colchicine had a minimal inhibitory effect on control lipid-polymer hybrid nanoparticles, meaning that macropinocytosis, a non-specific process to internalise fluids and particles together (Oh and Park, 2014) was involved in the internalisation of this nanoparticles. Although clathrin-mediated endocytosis pathway mainly participated in the uptake of both Tf-bearing and control lipid-polymer hybrid nanoparticles, it should be noted that the conjugation of Tf to the surface of control nanoparticles also modified the cellular uptake pathway from clathrin-mediated endocytosis and macropinocytosis to caveolae-mediated endocytosis. This could have a significant impact on the therapeutic efficacy of Tf-bearing lipid-polymer hybrid nanoparticles, as the caveosome is a neutral pH endocytic compartment, thus partially avoiding the degradation of the drug by the acidic pH of endosomes and lysosomes in the clathrin-mediated endocytosis pathway (Xiang *et al*., 2012; Gao *et al*., 2013).

The conjugation of Tf to lipid-polymer hybrid nanoparticles increased the anti-proliferative activity of plumbagin in the three tested cancer cell lines. These results may be attributed to the enhanced cellular uptake when treated with plumbagin formulated as Tf-bearing lipid-polymer hybrid nanoparticles. The entrapment of plumbagin in various delivery systems has previously been reported to improve its therapeutic efficacy. For instance, micelles entrapping plumbagin improved its anti-proliferative activity on MCF-7 cells by 2.1-fold compared with free drug (Bothiraja *et al*., 2013). In another study,

Pawar and colleagues (2016) have demonstrated that loading plumbagin into folic acid conjugated D-α-tocopheryl polyethylene glycol 1000 succinate nanomicelles was able to improve its anti-proliferative activity on MCF-7 cells in comparison with unconjugated formulation and free drug respectively by 2.4-fold and 4.1-fold, in line with our results. The entrapment of plumbagin in Tf-bearing lipid-polymer hybrid nanoparticles also increased apoptosis in B16-F10 and A431 cell lines, unlike drug solution. This effect was more pronounced on B16-F10 than on A431 cells, probably due to an increased sensitivity of B16-F10 cells toward plumbagin-mediated apoptosis.

By comparing the cellular uptake of Tf-bearing nanomedicines entrapping plumbagin, we can conclude that Tf-bearing PLGA-PEG nanoparticles exhibited higher cellular uptake of plumbagin than Tf-bearing liposomes and lipid-polymer hybrid nanoparticles in all the tested cell lines. This result is in agreement with findings in literature showing that rigid nanoparticles normally have a higher cellular uptake/membrane-bound than their flexible counterparts (Anselmo *et al.*, 2015; Zhang *et al.*, 2015a). For example, a cellular uptake study in SKOV3 2D cell monolayers and 3D tumour spheroids model demonstrated that the cellular uptake of folate-modified PEG-PLGA NPs was much higher than that of folate-modified PEGylated liposomes (Wang *et al*., 2018). Similar observation was also reported by Hui and colleagues (2018), who showed that the uptake of rigid silica nanocapsules (Young's moduli of 9.7 GPa) by RAW264.7 murine macrophages was significantly higher than the flexible silica nanocapsules (Young's moduli of 704 kPa).

However, this trend was not followed when assessing the anti-proliferative and apoptosis activity of the formulations. The highest therapeutic efficacy in A431 and T98G cells were achieved with Tf-bearing liposome treatment, followed by Tf-bearing lipid-polymer hybrid nanoparticles, and then PLGA-PEG nanoparticles. In B16-F10 cells, however, the

anti‑proliferative efficacy of Tf-bearing lipid-polymer hybrid nanoparticles was higher than the two other Tf-bearing plumbagin formulations. The potent anti‑proliferative and apoptosis activity of Tf-bearing liposomes over the other two formulations may be explained as follows: 1) The lipid bilayer of Tf-LIP (or lipid shell of Tf-LPN) may enhance the ability to adhere to the cell membrane due to the similar nature of the lipids and the cell membrane (Li *et al.*, 2017a). 2) The Tf-LIP have higher elasticity than Tf-LPN and Tf-PN, allowing them to enter the cells via two pathways, namely fusion and endocytosis. On the other hand, Tf-LPN and Tf-PN can enter the cell via endocytosis only (Guo *et al*., 2018). 3) The release of plumbagin from the Tf-LIP is faster than the Tf-PN and Tf-LPN, thereby releasing a faster amount of drug in the cells.

A similar observation was recently reported by Qu and colleagues (2016) comparing temozolomide-loaded nanostructured lipid carriers, solid lipid nanoparticles and polymeric nanoparticles for glioblastoma therapy. The authors reported that temozolomide-loaded nanostructured lipid carriers exhibited significantly higher cytotoxicity in U87MG glioblastoma cells than the two other formulations.

In summary, the results obtained from cellular uptake assays confirmed the advantages of using drug delivery systems conjugated to transferrin, which significantly increased the cellular accumulation of plumbagin in cancer cells overexpressing Tf receptors. Although free plumbagin enters the cell by passive diffusion due to its low molecular weight, Tf-modified nanomedicines entrapping plumbagin are taken up by endocytosis, a comparatively slower process but highly specific, resulting in an improvement in the therapeutic efficacy of plumbagin.

CHAPTER 4

In vivo **evaluation of tumour-targeted nanomedicines**

entrapping plumbagin

4.1 Introduction

Although cell culture systems have been proven to be indispensable for a wide range of experiments in assessing the biological response of cancer cells to drug delivery systems, they are insufficient to provide a full understanding of the therapeutic efficacy and eventual toxicity of systemically administered delivery systems. This is mainly due to the complexity of biological processes and the tumour microenvironment that the drug delivery systems would face following intravenous administration (Klinghammer *et al*., 2017). Therefore, the use of animal models remains an important component of the development process for drug delivery systems (Barré-Sinoussi and Montagutelli, 2015). In cancer research, the animal models (usually mice) are used with the aim of predicting the impact of a treatment in pre-clinical stage, whether it is the therapeutic efficacy or the toxicity of any promising anti-cancer compounds (Morton and Houghton, 2007). One of the most widely used models to generate tumours is based on the transplantation of cancer cells into immunocompromised animals (syngeneic or xenogeneic). Another animal model used for studying cancer is the genetically engineered mouse (GEM) model with a specific cancer genotype (Richmond and Su, 2008).

The discovery of nude athymic (nu/nu) mice that are T-cell deficient, enabled the possibility of tumour xenografting either subcutaneously or orthotopically (into the tissue type in which they originated) (Morton and Houghton, 2007). In fact, orthotopic models have been demonstrated to be more predictive of a clinical response than subcutaneous models as they reflect the organ environment in which the tumour grows, with the potential for distant metastasis formation. However, the major challenge of this model is the difficulty of following tumour growth unless using magnetic resonance imaging (MRI) and micro-imaging techniques. Moreover, the development of orthotopic models is a lengthy process which requires advanced surgical skills (Richmond and Su, 2008;

Ruggeri *et al*., 2014). These reasons make the subcutaneous xenograft models a popular alternative option for assessing the therapeutic response to treatments, due to the ease of model reproducibility and tumour growth monitoring (by calliper measurement) and cost effectiveness (Ruggeri *et al*., 2014; Klinghammer *et al*., 2017). One major concern regarding these models is the validity of predictive values when estimating the clinical performance. The main reason behind this concern is the use of immortalised cell lines which have been subcultured for a period of time (Morton and Houghton, 2007). Nevertheless, according to a retrospective analysis of most chemotherapeutic agents by the National Cancer Institute (NCI), about 33% of their therapeutic activity performed using subcutaneous xenograft models was found to correlate well with their clinical outcome (Takimoto and Wick, 2012). This indicated that the xenograft tumours actually share a number of characteristics with the original tumours, enough to make them good models to assess the therapeutic efficacy of a nanomedicine.

Among the imaging modalities used *in vivo*, bioluminescence imaging (BLI) has become one of the most common techniques used to detect light emission from cells or tissues in small living animals (Sato *et al*., 2004). Bioluminescence imaging is gaining preference over other imaging techniques (i.e. fluorescence) because the absence of endogenous bioluminescent reactions in mammalian tissue enhances background-free imaging conditions, resulting in higher image resolution. In addition, this type of optical imaging is easy to operate and facilitates real-time visualisation without animal sacrifice, allowing for continuous monitoring on disease progression of a single animal and reducing errors resulting from inter-animal variations (Close *et al*., 2011).

The principle of this imaging technique is based on a natural phenomenon called bioluminescence, which occurs in several non-mammalian species having a bioluminescence reporter gene, such as the North American firefly (*Photinus pyralis*).

Luciferase enzyme produced from the firefly luciferase gene (*luc*) is able to catalyse the oxidation of D-luciferin substrate with the help of ATP-Mg^{2+} and oxygen to form oxyluciferin and emit yellow-green light at a wavelength of 562 nm. The light emission can be detected using sensitive charged coupled device (CCD) cameras which take a photographic image of the subject followed by a bioluminescent one. The acquisition time required to take the images can range from a few seconds to several minutes depending on signal strength. A specific software can be used to display the image in a pseudo-coloured format which correlate to luminescence quantification (**Figure 4-1**) (Close *et al*., 2011).

To date, some commercial cell lines have been genetically engineered to carry a luciferase reporter gene, mainly firefly *luc* gene (Close *et al*., 2011). In addition, no sightings or toxic effects related to multiple injections of D-luciferin substrate have been reported so far (Aswendt *et al*., 2017).

Several factors may affect the information obtained from bioluminescence imaging. First, the rate of luciferase reaction depends on ATP, oxygen and luciferin. If the target cells or tissues lack any of these components, light emission detected may not reflect the true activity of luciferase. Another factor is the depth of target tissues, which is known to decrease the intensity of photons by approximately 10-fold for each centimeter depth. Therefore, the process of data collection and analysis has to be approached with caution, and validation for each specific experiment is necessary (Sadikot and Blackwell, 2005).
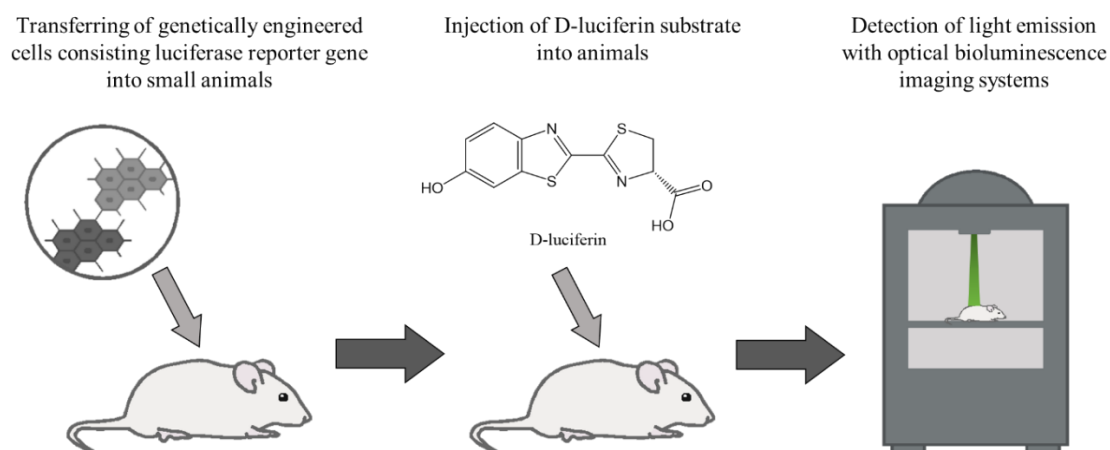
Figure 4-1: Schematic illustration of the *in vivo* bioluminescence imaging technique in small animals (adapted from Mezzanotte *et al.*, 2017)

4.2 Aim and Objectives

In Chapter 3, *in vitro* experiments demonstrated that the entrapment of plumbagin within these novel transferrin-bearing nanomedicines, namely liposomes, polymeric nanoparticles and lipid-polymer hybrid nanoparticles, led to an increase in plumbagin uptake by cancer cells, improved the anti-proliferative efficacy and apoptosis activity in the three tested cell lines, especially in B16-F10 cells, compared to that observed with the drug solution.

In this chapter, the *in vivo* therapeutic efficacy and toxicity of these three transferrin-bearing nanomedicines entrapping plumbagin will be investigated after intravenous administration using a murine B16-F10-luc-G5 xenograft model. Assessment of tumoricidal activity is based on tumour growth and animal survival, while the animal weight is monitored daily as a surrogate marker of toxicity of the treatments.

4.3 Materials and methods

4.3.1 Materials

Materials	Supplier
Foetal bovine serum (FBS)	Invitrogen, UK
Glucose	Sigma-Aldrich, UK
L-Glutamine	Invitrogen, UK
Luciferase assay reagent	Promega, UK
Mouse melanoma (B16-F10-luc-G5)	ATCC
Penicillin-Streptomycin	Invitrogen, UK
Phosphate buffer saline (PBS)	Sigma-Aldrich, UK
Roswell Park Memorial Institute (RPMI)-1640 medium	Invitrogen, UK
Plumbagin (5-hydroxy-2-methyl-1,4-naphthoquinone)	Sigma-Aldrich, UK
TrypLE® Express	Invitrogen, UK

4.3.2 Cell culture

B16-F10-luc-G5 cells were grown as monolayer cultures in RPMI- 1640 medium supplemented with 10% (v/v) foetal bovine serum, 1% (v/v) L-glutamine and 0.5% (v/v) penicillin-streptomycin. Cells were cultured in an incubator at 37°C with a humid atmosphere of 5% carbon dioxide.

4.3.3 Animals

Female immunodeficient BALB/c mice were selected for the *in vivo* experiments. They were kept at 19 to 23 ºC with 12-hour light-dark cycle and fed with a conventional mice diet and water. The experiments were approved by the local ethics committee and performed in accordance with the UK Home Office regulations

4.3.4 *In vivo* tumoricidal activity

To investigate *in vivo* tumoricidal activity of plumbagin formulations, B16-F10-luc-G5 cells in exponential growth were subcutaneously implanted to both flanks of female immunodeficient BALB/c mice (1×10^6 cells per flank). Once tumours became palpable and reached a diameter of 5 mm, the animals were randomised into groups of five. They were treated with plumbagin formulated as Tf-bearing and control formulations or drug solution, by intravenous tail vein injection (2 mg/kg of body weight per injection) once every 2 days for 10 days. The weight of the animal was measured daily to monitor the toxicity of the treatments. The tumour volume was also determined by calliper measurements and calculated as in the following equation:

$$\text{Tumour volume} = d^3 \times \frac{\pi}{6}$$

Where d: tumour diameter measured by calliper.

The results were expressed as relative tumour volume according to the following equation:

$$\text{Rel. Vol}_{tx} = \frac{\text{Vol}_{tx}}{\text{Vol}_{t0}}$$

Where Rel. Vol_{tx}: relative tumour volume; Vol_{tx}: tumour volume on the day of treatment; Vol_{t0}: initial tumour volume on the first day of the experiment.

Tumour responses were classified in accordance with Response Evaluation Criteria in Solid Tumours (RECIST) guidelines (Eisenhauer *et al.*, 2009). Progressive disease is defined as an increase in relative tumour volume higher than 1.2-fold, stable disease as a

relative volume between 0.7 and 1.2 of starting volume, partial response as a measurable tumour with a volume reduction more than 30% (0 to 0.7-fold) and complete response as the absence of any tumour. Any animal that lost more than 20% of its initial body weight or its tumours reaching the maximum allowed size of 10 mm, would have to be euthanised.

4.3.5 Bioluminescence imaging

Tumour growth or regression of mice treated with plumbagin formulations was assessed by bioluminescence imaging, using an IVIS Spectrum (Caliper Life Sciences, Hopkinton, MA). Briefly, mice bearing subcutaneous B16-F10-luc-G5 tumours were intravenously injected with plumbagin formulations as described in **section 4.3.4**. On Days 1, 3, 5, 7, 9 of the experiment, mice were intraperitoneally injected with the luciferase substrate, D-luciferin (150 mg/kg body weight), followed by inhalational anaesthesia with isoflurane. After 10 minutes, the light emitted from the bioluminescent tumours was detected for 2 min using Living Image® software. The resulting images were displayed as a pseudo-colour overlay onto a grey scale image of the animal. Identical illumination settings were used for all the acquired images.

4.3.6 Statistical analysis

Results were expressed as means ± standard error of the mean. Statistical significance was assessed by one-way analysis of variance and Tukey multiple comparison post-test using OriginPro 9.0 software (OriginLab Corporation, Northampton, MA). Differences were considered statistically significant for p-values lower than 0.05.

4.4 Results

4.4.1 Transferrin-bearing liposomes

4.4.1.1 *In vivo* tumoricidal activity

The intravenous injection of plumbagin entrapped in Tf-bearing and control liposomes led to a high variability of responses to treatment within the same group of mice and an overall reduced tumour growth compared to plumbagin solution treatment (**Figure 4-2**). For these 2 treatments, some tumours kept regressing while others started growing. At Day 6, mice bearing growing tumours had to be euthanised due to their tumours reaching the maximum allowed size. The remaining mice, whose tumours were regressing or had completely disappeared, were kept until the end of the study (Day 10). On the contrary, tumours treated with plumbagin solution or blank liposomes grew steadily at a growth rate close to that observed for untreated tumours.
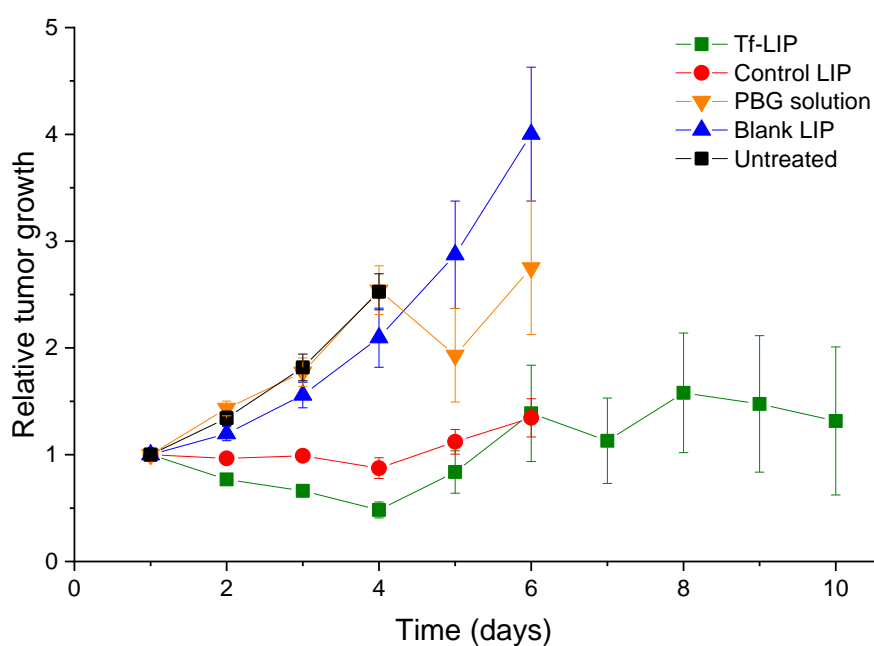
Figure 4-2: Tumour growth studies in a murine B16-F10-luc-G5 xenograft model after intravenous administration of plumbagin (2 mg/kg of body weight/injection) entrapped in Tf-bearing liposomes (■, dark green) and control liposomes (●, red), or free in solution (▼, orange), blank liposomes (▲, blue) (■, black: untreated) (*n*=10)

No apparent signs of toxicity or animal weight loss were observed during the experiment, thus showing the good tolerability of all the treatments by the animals (**Figure 4-3**).
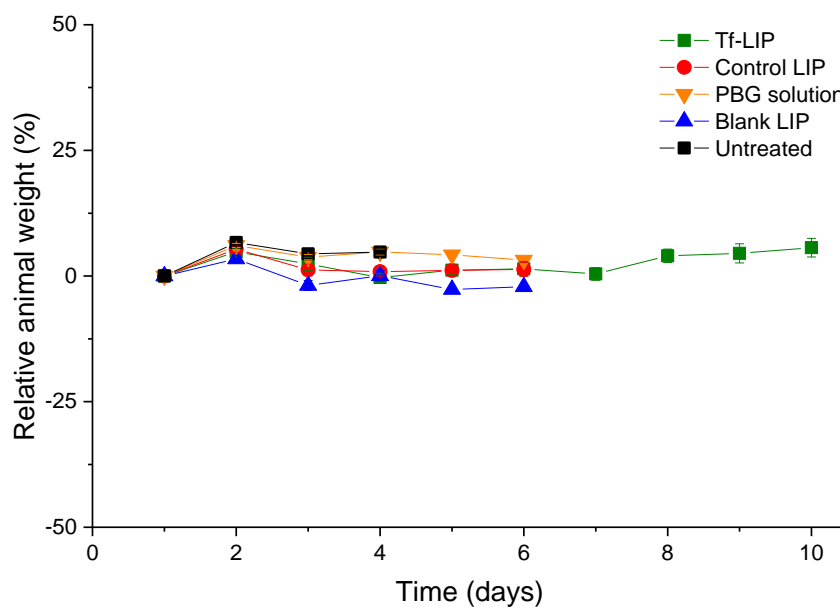
Figure 4-3: Percentage variation in animal body weight throughout the treatment period with plumbagin either entrapped in Tf-bearing liposomes (■, dark green) and control liposomes (●, red), or free in solution (▼, orange), blank liposomes (▲, blue) (■, black: untreated) (*n=5*)

On the last day of the experiment, 10% of the tumours treated with Tf-bearing liposomes entrapping plumbagin completely disappeared, while another 10% of tumours showed a partial response (**Figure 4-4**). Following treatment with control liposomes, 20% of the tumours were regressing, and 20% were stable. However, it should be noted that all the mice treated with this formulation had to be euthanised at Day 6 due to their tumours reaching the maximum allowed size (10 mm), unlike those of Tf-bearing liposomes. By contrast, all the tumours treated with plumbagin solution, blank liposomes or left untreated were progressive.
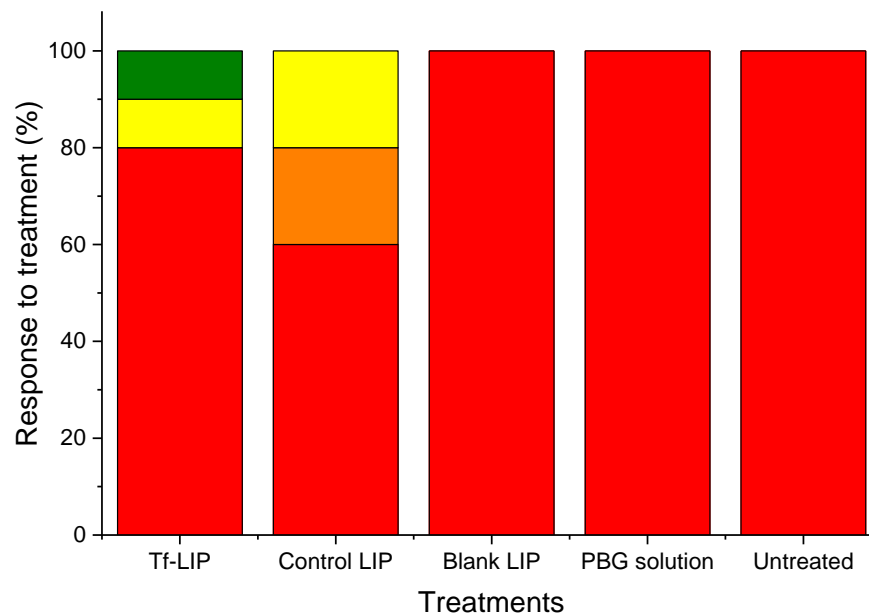
Figure 4-4: Overall tumour response at the end of the study after treatment with plumbagin either entrapped in Tf-bearing liposomes, control liposomes, or free in solution, blank liposomes, and untreated tumours (red: progressive response, orange: stable response, yellow: partial response, green: complete response)

The improved therapeutic efficacy observed following treatment with Tf-bearing liposomes entrapping plumbagin resulted in an extended survival of the mice by 6 days compared to untreated tumours (**Figure 4-5**).
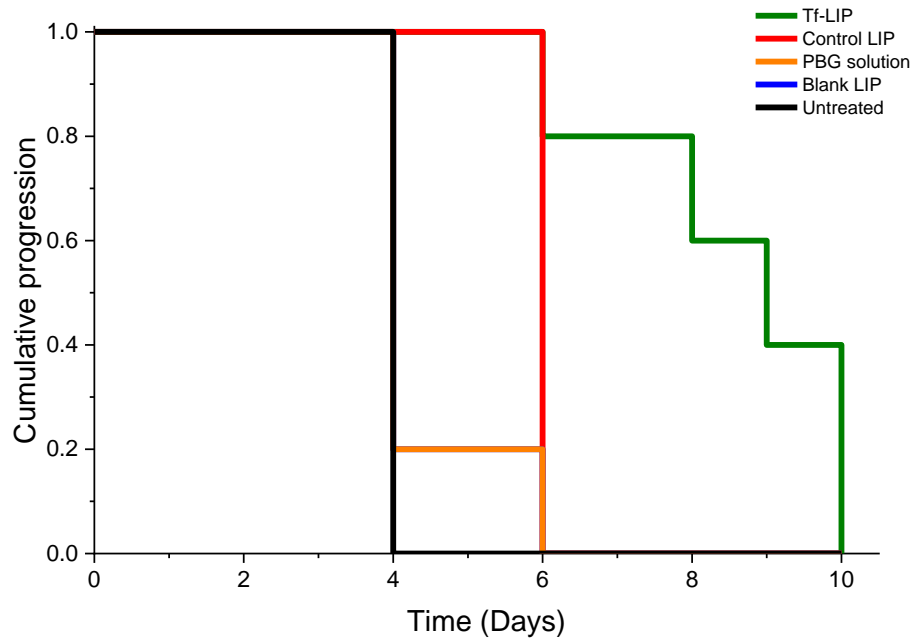
Figure 4-5: Time to disease progression where animals were removed from the experiment once their tumour reached 10 mm diameter (Tf-bearing liposomes (dark green), control liposomes (red), plumbagin solution (orange), blank liposomes (blue) and untreated tumours (black))

4.4.1.2 Bioluminescence imaging

The therapeutic effect resulting from treatment with liposomes entrapping plumbagin was also qualitatively confirmed by bioluminescence imaging on mice bearing subcutaneous B16-F10-luc tumours (**Figure 4-6**). Luciferase expression in the tumours treated with the Tf-bearing and control liposomes decreased from Day 1 to Day 3, but increased again on Day 5. By contrast, all the other treatments led to a steady increase of luciferase expression in the growing tumours.
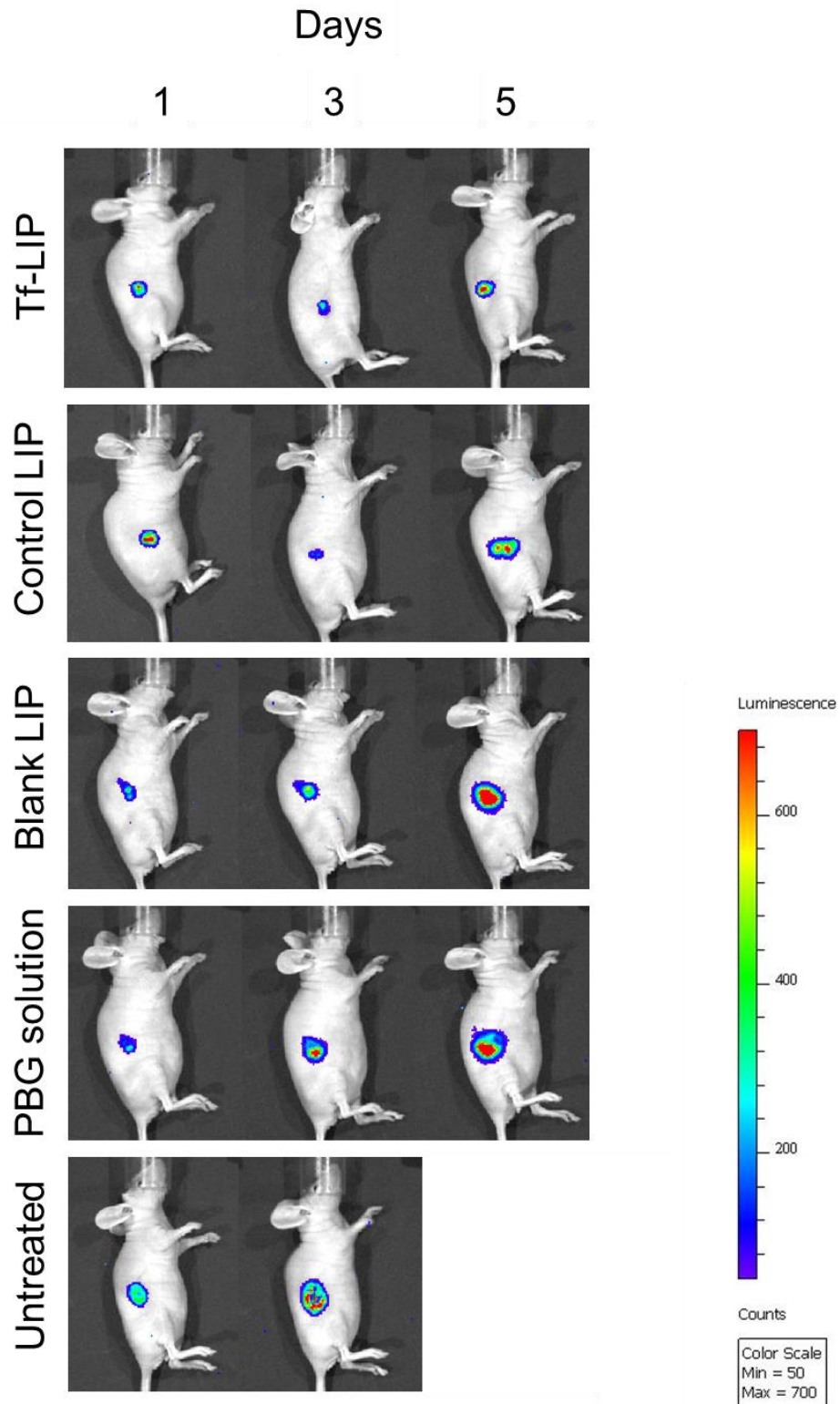
Figure 4-6: Bioluminescence imaging of the tumoricidal activity of plumbagin entrapped in Tf-bearing liposomes, control liposomes, or as drug solution in a B16-F10-luc-G5 tumour model (Controls: blank liposomes and untreated tumours). The scale indicates surface radiance (photons/s/cm^2/steradian)

4.4.2 Transferrin-bearing polymeric nanoparticles

4.4.2.1 *In vivo* tumoricidal activity

Mice treated with plumbagin entrapped in Tf-bearing and control PLGA-PEG nanoparticles showed a variability of responses to treatment within the same group (**Figure 4-7**). Tumours treated with Tf-bearing PLGA-PEG nanoparticles showed an immediate response within 24 hours after the first treatment with continuous regression until Day 5, where the tumours showed an eventual regrowth. Forty percent of the tumours kept regressing after receiving the final dose, while the others stopped responding to the treatment after Day 6 and had to be sacrificed. The intravenous injection of plumbagin entrapped in control PLGA-PEG nanoparticles only slowed the growth rate of tumour and all of them had to be removed from the study after 6 days. On the other hand, mice treated with plumbagin solution or blank nanoparticles had a growth rate similar to untreated tumours.
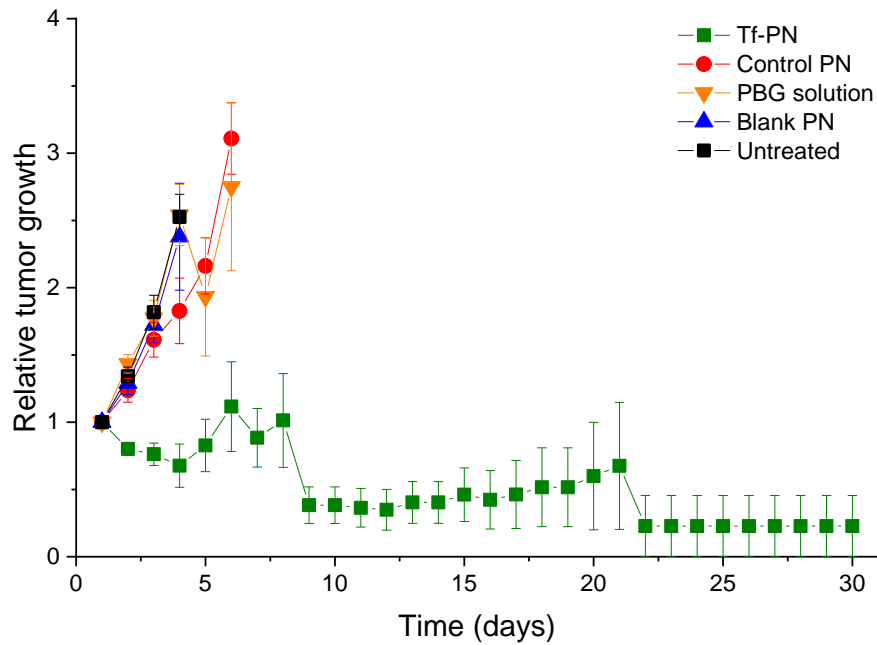
Figure 4-7: Tumour growth studies in a murine B16-F10-luc-G5 xenograft model after intravenous administration of plumbagin (2 mg/kg of body weight/injection) entrapped in Tf-bearing PLGA-PEG nanoparticles (■, dark green) and control nanoparticles (●, red), or free in solution (▼, orange), blank nanoparticles (▲, blue) (■, black: untreated) (*n*=10)

Mice showed a good tolerability to all treatments, as there were no significant variations in animal body weight or apparent signs of toxicity observed during the experiments (**Figure 4-8**).
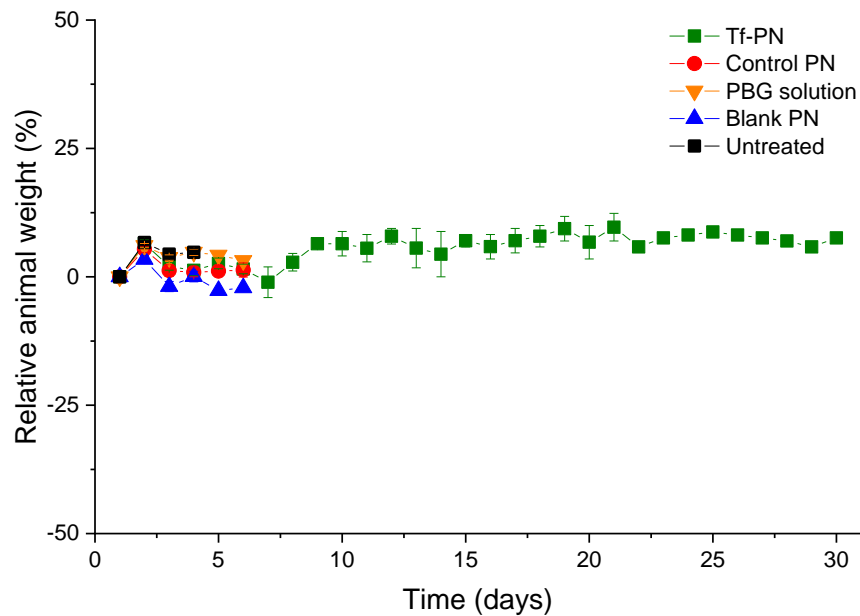
Figure 4-8: Percentage variation in animal body weight throughout the treatment period with plumbagin either entrapped in Tf-bearing PLGA-PEG nanoparticles (■, dark green) and control nanoparticles (●, red), or free in solution (▼, orange), blank nanoparticles (▲, blue) (■, black: untreated) ($n=5$)

On the last day of the experiment, 10% of the tumours completely disappeared after treatment with Tf-bearing PLGA-PEG nanoparticles, while 30% of tumours had a partial response and another 10% were stable (**Figure 4-9**). Tumours treated with control PLGA-PEG nanoparticles had 20% of regression and 20% were stable. On the contrary, all the tumours treated with plumbagin solution, blank nanoparticles or left untreated were 100% progressive.
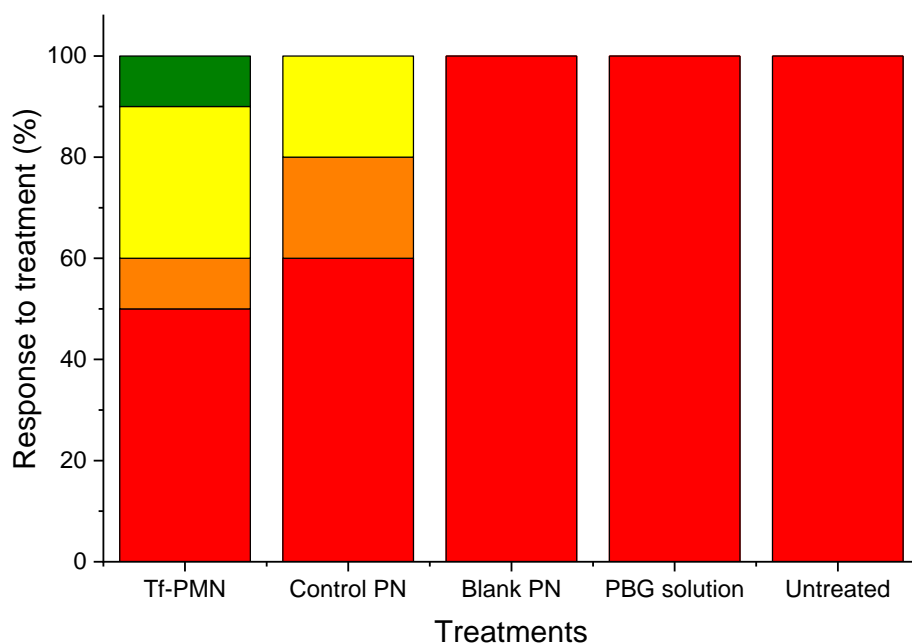
Figure 4-9: Overall tumour response at the end of the study after treatment with plumbagin either entrapped in Tf-bearing PLGA-PEG nanoparticles, control nanoparticles, or free in solution, blank nanoparticles, and untreated tumours (red: progressive response, orange: stable response, yellow: partial response, green: complete response)

The average survival rate in two animals treated with Tf-bearing PLGA-PEG nanoparticles was significantly improved by 17 days compared to those of the untreated animals, with one animal surviving until the end of the experiment at Day 30 (**Figure 4-10**). On the other hand, treatment with both control PLGA-PEG nanoparticles and plumbagin only extended mice survival by 2 days compared with untreated animals.
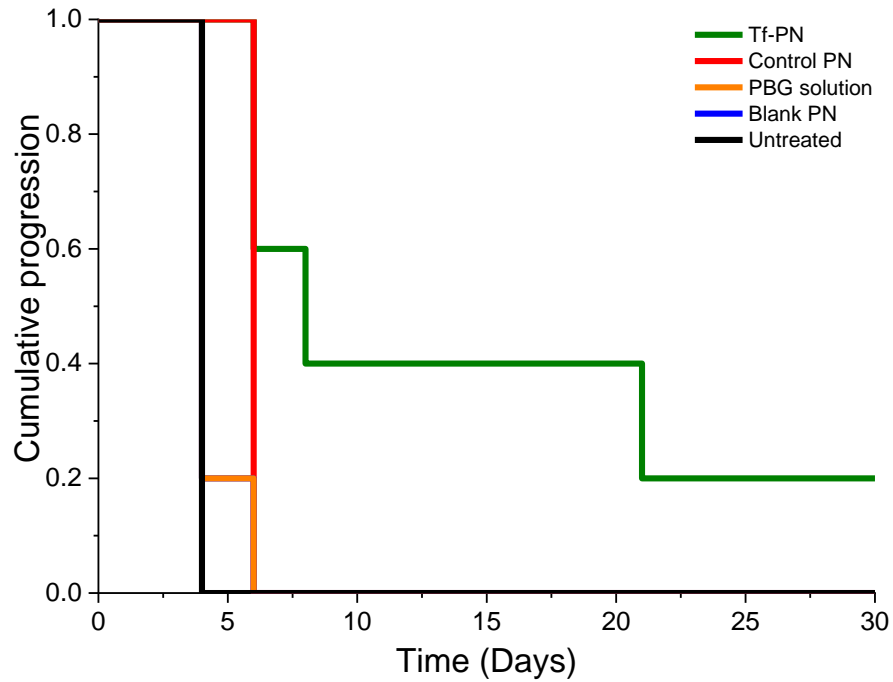
Figure 4-10: Time to disease progression where animals were removed from the experiment once their tumour reached 10 mm diameter (Tf-bearing PLGA-PEG nanoparticles (dark green), control nanoparticles (red), plumbagin solution (orange), blank nanoparticles (blue) and untreated tumours (black))

4.4.2.2 Bioluminescence imaging

Bioluminescence images showed that luciferase expression in the tumours treated with plumbagin entrapped in Tf-bearing PLGA-PEG nanoparticles was much lower than that observed in other treatments (**Figure 4-11**).
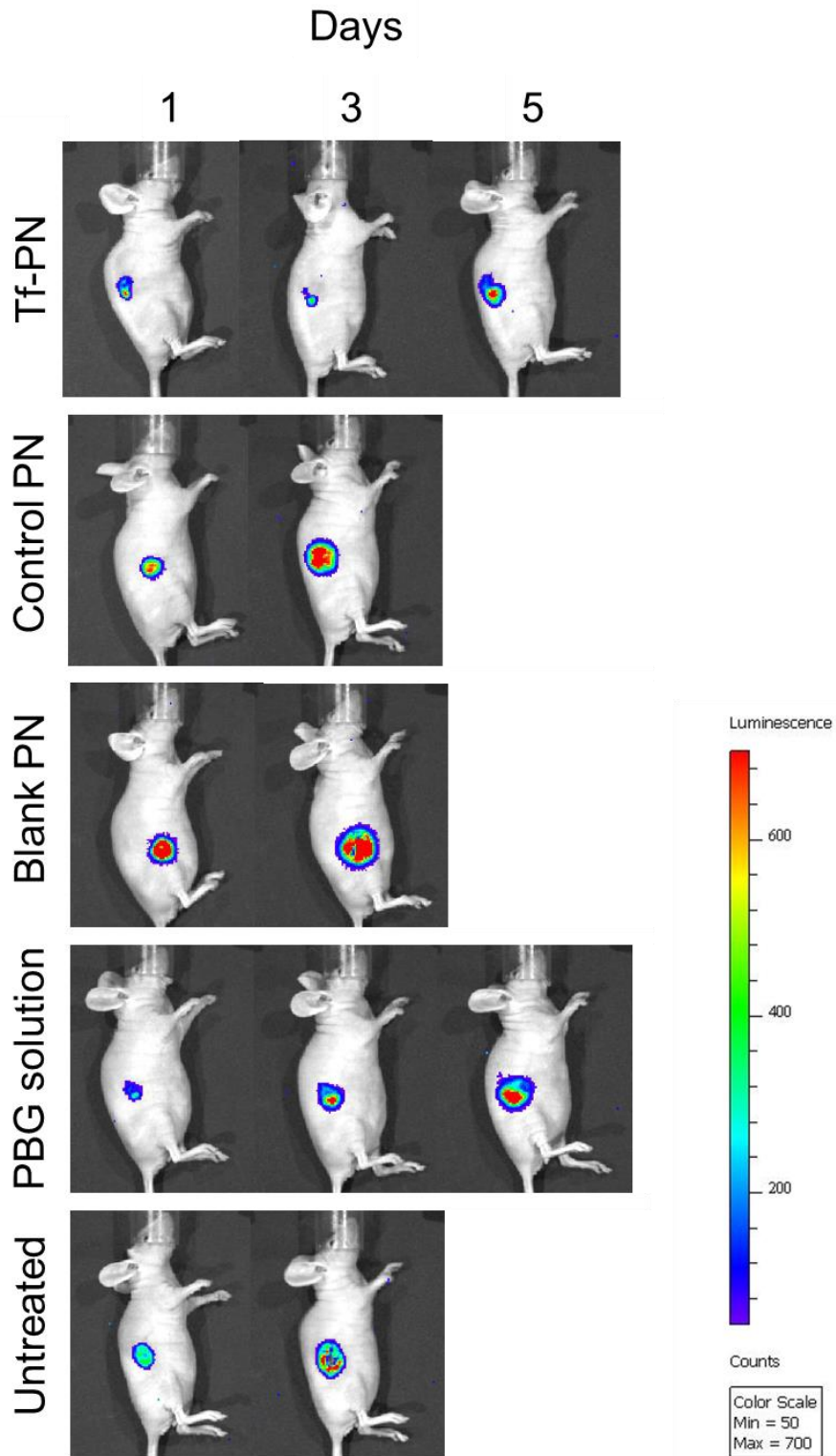
Figure 4-11: Bioluminescence imaging of the tumoricidal activity of plumbagin entrapped in Tf-bearing and control PLGA-PEG nanoparticles or as drug solution in a B16-F10-luc-G5 tumour model (Controls: blank nanoparticles and untreated tumours). The scale indicates surface radiance (photons/s/cm^2/steradian)

4.4.3 Transferrin-bearing lipid-polymer hybrid nanoparticles

4.4.3.1 *In vivo* tumoricidal activity

The intravenous injection of plumbagin entrapped in Tf-bearing lipid-polymer hybrid nanoparticles led to an overall decrease in B16-F10 tumour growth. This effect occurred within 24 h and was maintained for the whole duration of the experiment. From Day 6, some of the mice bearing growing tumours had to be euthanised due to their tumours reaching the maximum allowed size. By contrast, tumours treated with plumbagin solution, blank nanoparticles or left untreated kept growing (**Figure 4-12**).
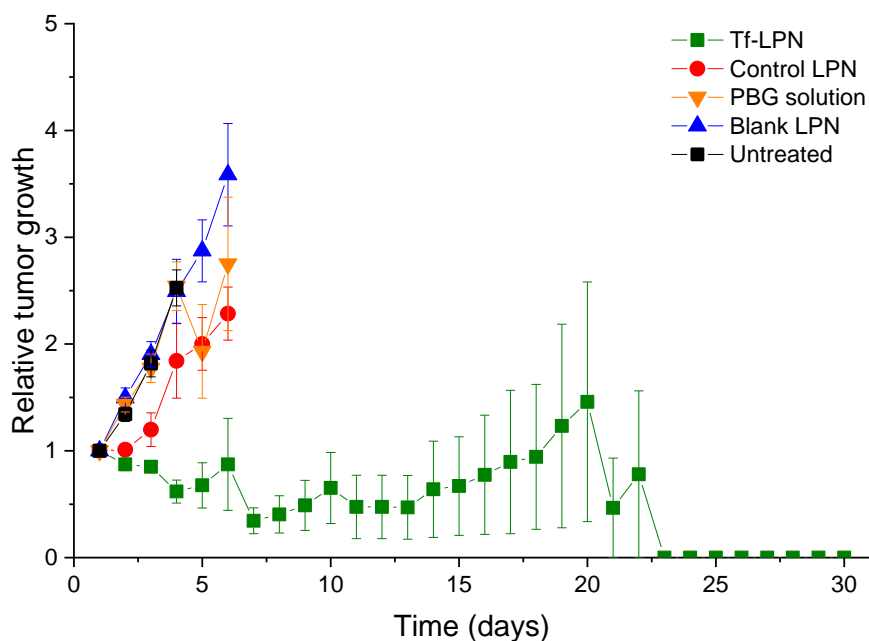
Figure 4-12: Tumour growth studies in a murine B16-F10-luc-G5 xenograft model after intravenous administration of plumbagin (2 mg/kg of body weight/injection) entrapped in Tf-bearing lipid-polymer hybrid nanoparticles (■, dark green) and control nanoparticles (●, red), or free in solution (▼, orange), blank nanoparticles (▲, blue) (■, black: untreated) (*n*=10)

No significant variations of animal body weight or apparent signs of toxicity were observed during the experiment, thus demonstrating the good tolerability of all the treatments by the mice (**Figure 4-13**).
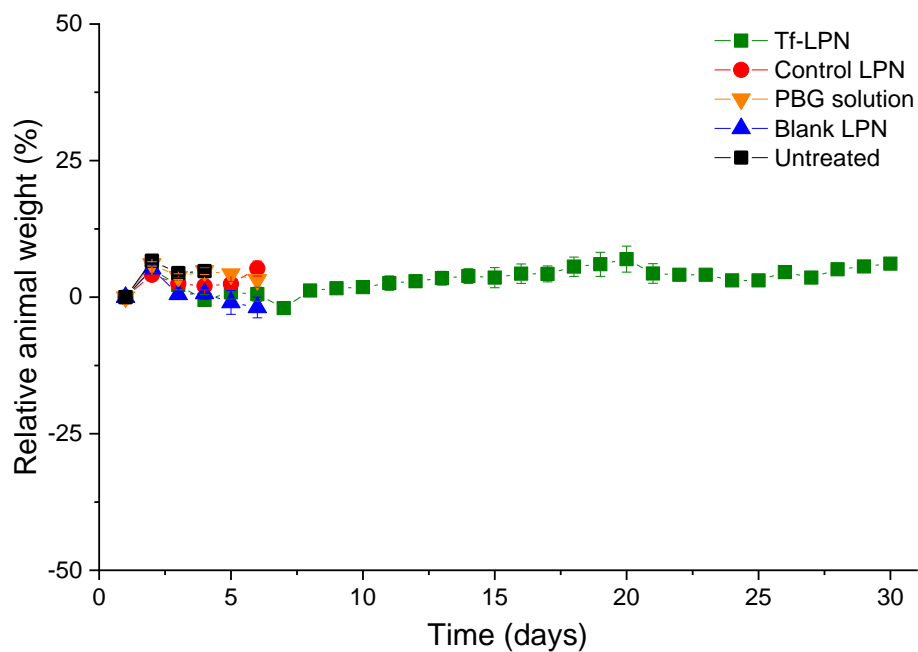
Figure 4-13: Percentage variation in animal body weight throughout the treatment period with plumbagin either entrapped in Tf-bearing lipid-polymer hybrid nanoparticles (■, dark green) and control nanoparticles (●, red), or free in solution (▼, orange), blank nanoparticles (▲, blue) (■, black: untreated) (*n*=5)

On the last day of the experiment, 40% of tumours treated with Tf-bearing lipid-polymer hybrid nanoparticles entrapping plumbagin completely disappeared, while another 10% of tumours showed a partial response and 10% were stable (**Figure 4-14**). By contrast, all the tumours treated with control nanoparticles, plumbagin solution, blank nanoparticles or left untreated, were progressive.
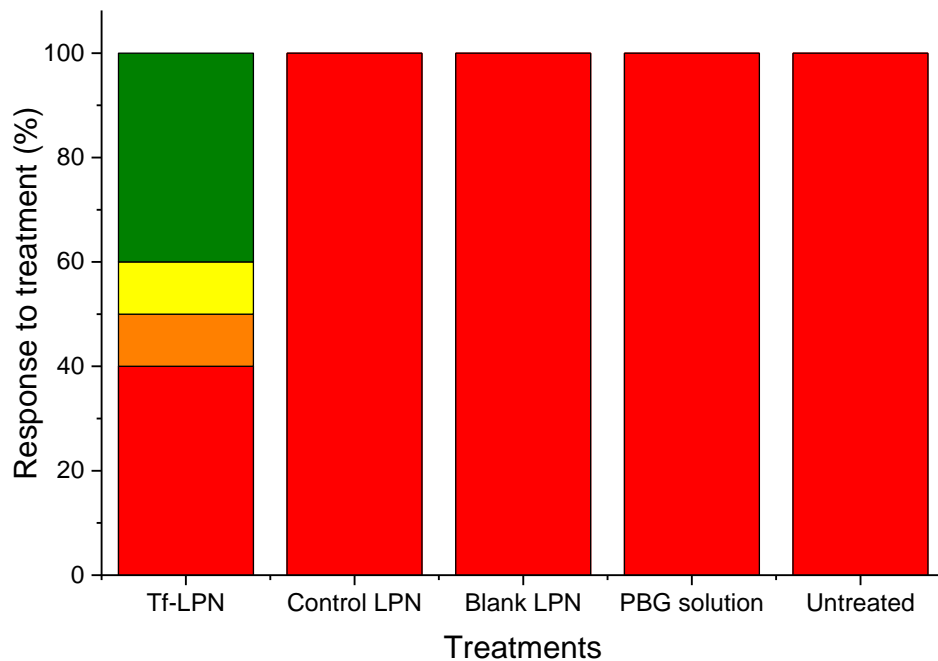
Figure 4-14: Overall tumour response at the end of the study after treatment with plumbagin either entrapped in Tf-bearing lipid-polymer hybrid nanoparticles, control nanoparticles, or free in solution, blank nanoparticles, and untreated tumours (red: progressive response, orange: stable response, yellow: partial response, green: complete response)

The improved therapeutic efficacy observed as a result of the treatment with Tf-bearing lipid-polymer hybrid nanoparticles entrapping plumbagin led to an extended survival of the mice compared to untreated tumours (**Figure 4-15**). Although two animals had to be sacrificed at Day 6 and Day 10 due to tumour enlargement, the remaining animals in the group maintained a slow rate of tumour growth and survived until Day 20 and Day 22, and one animal survived until the end of the experiment. By contrast, treatment with both control nanoparticles and plumbagin solution only extended mice survival by 2 days compared with untreated animals, thus emphasising the crucial need of a targeted delivery system for the systemic delivery of plumbagin to tumours.
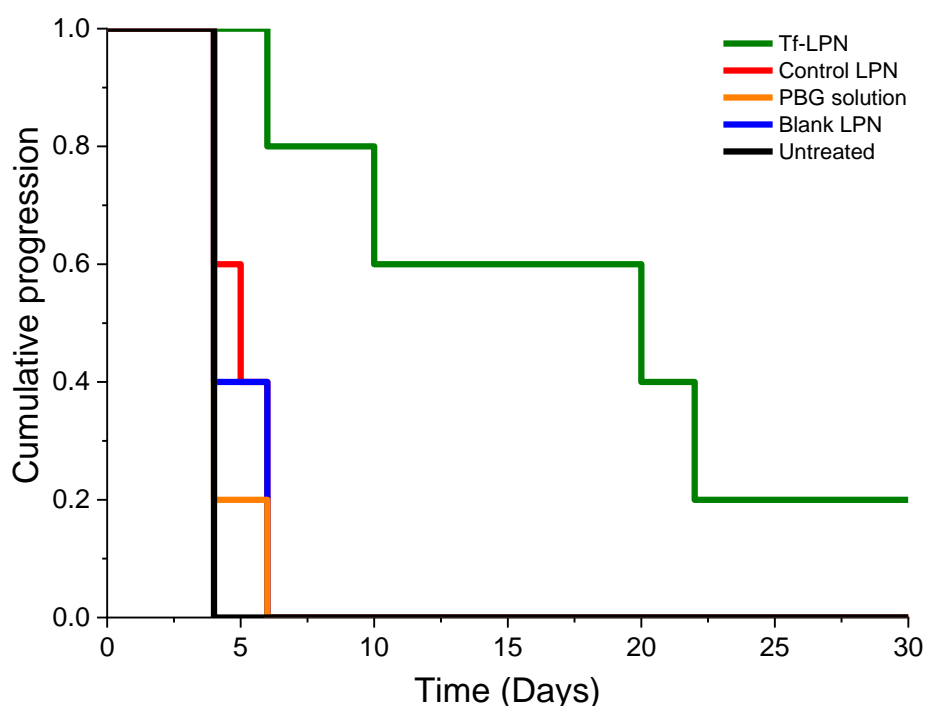
Figure 4-15: Time to disease progression where animals were removed from the experiment once their tumour reached 10 mm diameter (Tf-bearing lipid-polymer hybrid nanoparticles (dark green), control nanoparticles (red), plumbagin solution (orange), blank nanoparticles (blue) and untreated tumours (black))

4.4.3.2 Bioluminescence imaging

Bioluminescence imaging demonstrated that luciferase expression in the tumours treated with plumbagin entrapped in Tf-bearing lipid-polymer hybrid nanoparticles decreased from Day 1 to Day 3, then slightly increased on Day 5 (**Figure 4-16**). On the contrary, tumours treated with all the other treatments showed a steady increase of luciferase expression.
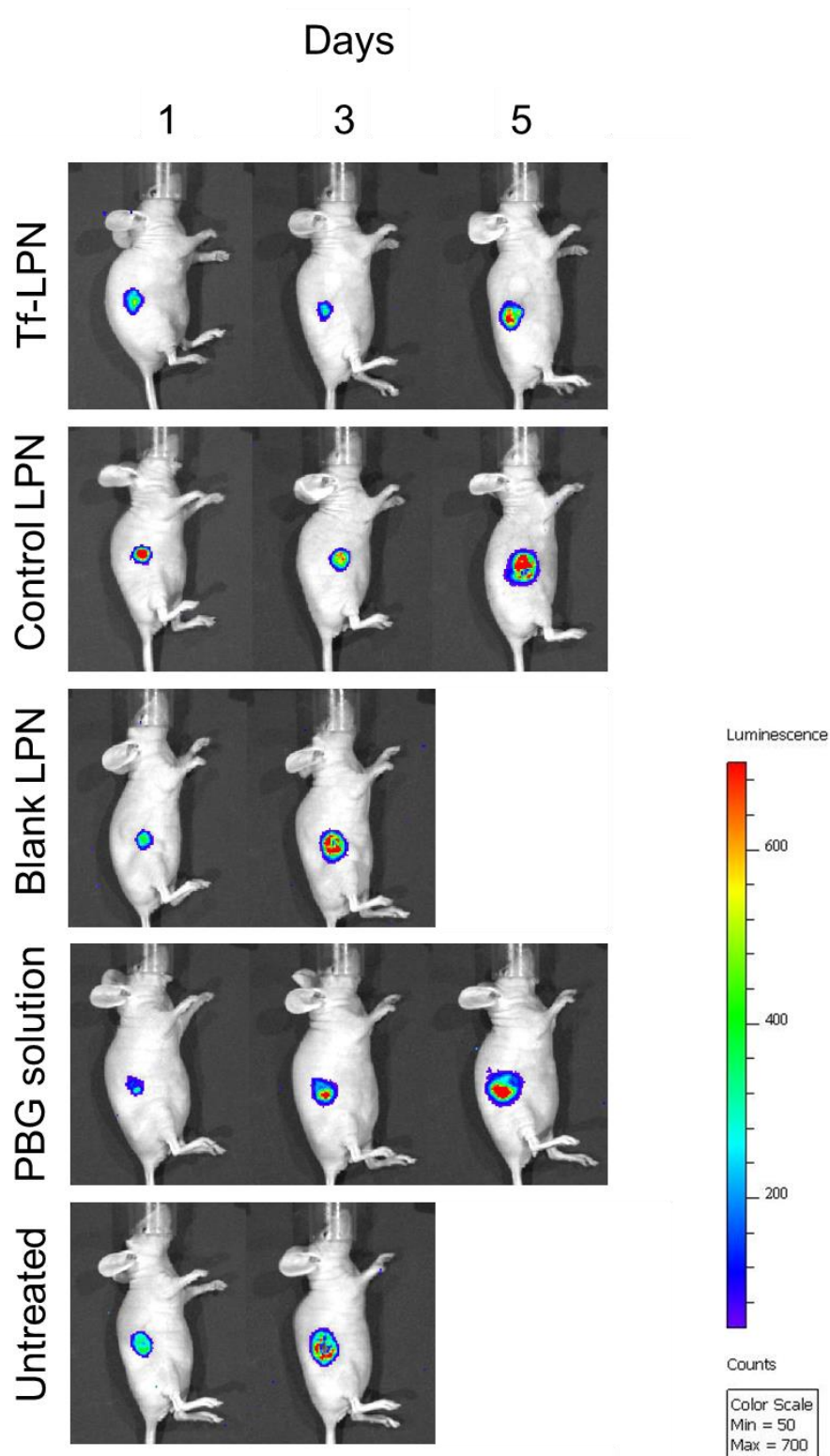
Figure 4-16: Bioluminescence imaging of the tumoricidal activity of plumbagin entrapped in Tf-bearing and control lipid-polymer hybrid nanoparticles or as drug solution in a B16-F10-luc-G5 tumour model (Controls: blank nanoparticles and untreated tumours). The scale indicates surface radiance (photons/s/cm^2/steradian)

4.5 Discussion

We have demonstrated for the first time that the intravenous administration of plumbagin entrapped in a tumour-targeted delivery system to mice bearing tumours was able to lead to tumour regression and even complete tumour suppression in some cases as well as extend survival rate of the animals.

Transferrin-bearing lipid-polymer hybrid nanoparticles entrapping plumbagin showed the best *in vivo* tumoricidal activity with 40% complete disappearance of B16-F10 tumours after treatment. Complete tumour eradication was also detected in 10% of B16-F10 tumours after intravenous administration of plumbagin entrapped in Tf-bearing liposomes and Tf-bearing PLGA-PEG nanoparticles. Tf-bearing PLGA-PEG nanoparticles exhibited a better therapeutic efficacy than Tf-bearing liposomes, because they significantly improved the average survival of animals (extended by 17 days compared to untreated animals) compared with Tf-bearing liposomes (which only extended animal survival by 6 days compared to untreated animals).

Control nanomedicines entrapping plumbagin only exerted a limited therapeutic efficacy on tumours, which supports the need of transferrin conjugation to increase the targeting efficacy to tumours. No therapeutic effect was observed in animals treated with plumbagin solution, because of its unability to reach the tumours due to its short half-life with rapid elimination after intravenous administration. The mice injected with blank nanomedicines did not show any visible toxicity of the nanocarriers.

Other studies have previously demonstrated the ability of plumbagin entrapped in various delivery systems to slow down the growth of tumours, rather than the tumour regression or suppression observed in some instances in our experiments. The intravenous administration of plumbagin loaded in niosomes (3-6 mg/kg) has been reported to slowdown the growth of sarcoma-180 and Ehrlich ascites tumours in BALB/c mice

compared to that observed with the drug solution (Naresh *et al.*, 1996). In addition, plumbagin entrapped in temperature-sensitive liposomes (6 mg/kg with localised hyperthermia treatment at 43°C) (Tiwari *et al.*, 2002) or in PEGylated liposomes (2 mg/kg) (Kumar *et al.*, 2011) also exhibited a significant anti-tumour effect in C57BL/6J mice bearing B16F1 melanoma model by slowing tumour growth, unlike plumbagin solution. Similar therapeutic effects were also observed when using another route of administration. The subcutaneous injection of plumbagin entrapped in PLGA microspheres (10 mg/kg) to BALB/c mice resulted in a significant decrease in tumour growth volume of sarcoma-180 tumours compared to free plumbagin (volume-doubling times (VDT) respectively of 14.3 ± 1.5 days and 7.2 ± 0.9 days) (Singh *et al.*, 1996). In another study, the intramuscular administration of plumbagin entrapped in chitosan-based microspheres (6 mg/kg) to C57BL/6J mice increased the animals' lifespan by 30% compared to free plumbagin (which increased the lifespan by 20%) (Rayabandla *et al.*, 2010).

The most striking effects of the tumour-targeted nanomedicines entrapping plumbagin was the induction of tumour regression within one day after the start of the treatment and the disappearance of the tumours for some animals. In addition, these effects occurred using doses of 2 mg/kg, lower than reported in most other studies, and without apparent toxicity. These therapeutic systems were able to act on subcutaneous tumours after systemic administration and should therefore have the potential to target multiple metastatic nodules disseminated throughout the body. Although a high variability of response and short animals' lifespan were observed, the therapeutic effect of tumour-targeted nanomedicines entrapping plumbagin was promising (especially Tf-bearing lipid-polymer hybrid nanoparticles) and strongly encourages the further improvement of these well tolerated delivery systems, by using a higher dose, slowing the release rate of

the drug from the carriers, increasing the frequency of the treatment (from every 2 days to every day) and extending the length of the treatment, which should hopefully lead to an optimised therapeutic effect.

Comparing the tumoricidal activity among the three Tf-bearing nanomedicines entrapping plumbagin developed in this study, Tf-bearing lipid-polymer hybrid nanoparticles exhibited the highest potent anti-tumour activity, followed by Tf-bearing PLGA-PEG nanoparticles and Tf-bearing liposomes for the treatment of B16-F10 tumours. This result correlated well with the *in vitro* anti-proliferative activity and cellular apoptosis findings, as B16-F10 cells responded well to treatment with Tf-bearing lipid-polymer hybrid nanoparticles (IC_{50} of 0.16 µg/mL with 89.2 % of cells being apoptotic), which was higher than Tf-bearing liposomes (IC_{50} of 0.22 µg/mL with 88.4 % of cells being apoptotic) and Tf-bearing PLGA-PEG nanoparticles (IC_{50} of 0.24 µg/mL with 78.8 % of cells being apoptotic).

The strongest anti-tumour effect of Tf-bearing lipid-polymer hybrid nanoparticles over the two other formulations may be explained as follows: 1) the lipid layer enhances the affinity of the delivery system to the lipid cell membrane, and thus increases the delivery of plumbagin to the tumours. 2) The polymeric core of the LPN provides a good stability in blood stream after intravenous administration compared to liposomes. 3) The unique structure of the LPN delayed plumbagin release more than the LIP and PN formulations, thereby prolonging blood circulation half-life and increasing plumbagin accumulation in tumours (Li *et al.*, 2017a; 2017b).

A similar observation was recently reported by Zhang and colleagues (2019) regarding a comparison of nanostructured lipid carriers, polymeric nanoparticles, and lipid-polymer hybrid nanoparticles for cisplatin delivery. The authors reported that cisplatin-loaded lipid-polymer hybrid nanoparticles exhibit the highest plasma concentration-time curve

(AUC) of drug and the longest half-life, with the strongest anti-tumour effect in BALB/c mice bearing SKOV3 ovarian cancer, compared with polymeric nanoparticles and nanostructured lipid carriers. This outcome was also reported by Li and co-workers (2017a), who showed that lipid-polymer hybrid nanoparticles loading cisplatin and curcumin displayed higher anti-tumour activity compared to polymeric nanoparticles tested in BALB/c mice bearing HeLa cervical cancer.

In summary, transferrin-bearing liposomes, PLGA-PEG nanoparticles and lipid-polymer hybrid nanoparticles were successful in improving the anti-cancer effect of plumbagin, with 40% and 10% of complete tumour suppression at the end of the study without any visible signs of toxicity. They also increased the survival rate of the animals by around 26 days, compared with free plumbagin, in the case of the Tf-bearing lipid-polymer hybrid nanoparticles. These therapeutic effects therefore make transferrin-bearing nanomedicines entrapping plumbagin, especially Tf-bearing lipid-polymer hybrid nanoparticles, highly promising formulations for cancer therapy.

CHAPTER 5

Conclusion and future works

5.1 Conclusion

Cancer remains one of the leading causes of death and continues to rapidly grow worldwide (Bray *et al*., 2018). Despite recent advances in knowledge of cancer cell biology and molecular targets over the past three decades, the translation into effective therapies able to increase the long-term survival of patients is still disappointing, with a high rate of failure approaching 95% (Prasad *et al*., 2016; Ocaña *et al*., 2018). The development of new effective anti-cancer strategies is hampered by several factors, including tumour heterogeneity and complexity, selection of pre-clinical models (both *in vitro* and *in vivo*) and costs (Hait, 2010; Ocaña *et al*., 2018).

Natural products are important sources for the discovery of new anti-cancer agents. It has been reported that approximately 55% of current anti-cancer drugs used in clinic were derived from natural sources such as paclitaxel, doxorubicin, vincristine, flavopiridol and homoharringtonine (Peyressatre *et al*., 2015; Newman *et al*., 2016; Seca and Pinto, 2018). Moreover, several nature-derived compounds, such as soy isoflavones, curcumin, aspirin, epigallocatechin gallate and vitamin E, are currently on the clinical pipeline for chemotherapy and chemoprevention (Cragg *et al*., 2016).

Plumbagin is a natural naphthoquinone which has been isolated mainly from the roots of Plumbaginaceae plants. It has been reported to have promising anti-cancer potential efficacy in many types of cancer, mediated through modulation of cellular redox and alteration of cell signalling pathways, then resulting in cell growth inhibition and cell death (Checker, 2018). However, plumbagin has some limitations which significantly hampered its biopharmaceutical applications such as its toxic side effects in animal models and poor solubility in water. Besides, the therapeutic concentration of plumbagin at tumour targets was not sufficient to cause regression due to its lack of tumour

specificity and rapid elimination (Kumar *et al*., 2011; Hafeez *et al*., 2013; Pawar *et al*., 2016).

In this thesis, therefore, we aimed to formulate plumbagin in liposomes, polymeric nanoparticles and lipid-polymer hybrid nanoparticles, to improve its water solubility and to sustain its release over a period of time. Additionally, we proposed to modify the surface of nanocarriers for specific delivery of plumbagin to cancer cells and further enhance its therapeutic efficacy by conjugation with the tumour-targeting ligand transferrin, whose receptors are overexpressed on many cancers (Daniels *et al*., 2012).

In terms of formulation, we successfully developed three transferrin-bearing nanocarriers entrapping plumbagin, Tf-LIP, Tf-PN and Tf-LPN. These formulations were prepared by probe sonication (for Tf-LIP) or nanoprecipitation (for Tf-PN and Tf-LPN) and were conjugated with transferrin using the thiol–maleimide 'click' reaction, with high percentage of drug entrapment (45–80%) and high Tf conjugation efficiency (50–70%). The optimal nanocarriers entrapping plumbagin had mean diameter sizes less than 115 nm, 155 nm and 210 nm respectively for LIP, PN and LPN, and displayed negative charges for all formulations. Drug release study exhibited that all transferrin-bearing formulations were able to release plumbagin in a sustained manner over 10 hours for Tf-LIP, and over 24 hours for Tf-PN and Tf-LPN. Moreover, they were found to be stable under storage condition at 4°C for at least 4 weeks, with minimal leakage of plumbagin (less than 5%).

In vitro evaluation showed that the cellular accumulation of plumbagin in all the tested cell lines (B16-F10, A413 and T98G cells) was enhanced by up to 2.4, 3.4 and 2.7-fold after treatment with Tf-LIP, Tf-PN and Tf-LPN respectively, compared to that of non-targeted formulations and plumbagin solution. This resulted in a significant improvement in the anti-proliferative activity of plumbagin by up to 4.3-fold for Tf-LIP, 2.8-fold for

Tf-PN and 3.2-fold for Tf-LPN in comparison with free plumbagin. Similarly, the results obtained from apoptosis assay showed an increase in the percentage of total apoptotic cells of B16-F10 and A431 cells when treating with plumbagin formulated as transferrin-bearing nanocarriers compared to plumbagin solution, by up to 5.5, 3.4 and 3.2-fold for Tf-LIP, Tf-PN and Tf-LPN respectively.

In vivo, the intravenous administration of novel tumour-targeted delivery systems entrapping plumbagin resulted in complete tumour eradication for 40% (for Tf-LPN) and 10% (for Tf-LIP and Tf-PN) of B16-F10 tumours. To our knowledge, this is the first time that intravenously administered targeted plumbagin was shown to lead to complete tumour disappearance. In addition, the animals did not display any visible signs of toxicity. Nevertheless, the most remarkable effect of these tumour-targeted nanocarriers entrapping plumbagin was their ability to induce tumour regression within one day after treatment, which occurred even using a low dose of plumbagin of 2 mg/kg. By contrast, tumours treated with non-targeted formulations, plumbagin solution or left untreated were mostly progressive.

In conclusion, these results are promising and support the use of these tumour-targeted delivery systems to further improve stability, therapeutic efficacy and tumour specificity of plumbagin, especially when formulated as lipid-polymer hybrid nanoparticles.

5.2 Future works

In this study, three novel transferrin-targeted nanocarriers have been developed, characterised and evaluated *in vitro* and *in vivo* as potential delivery systems for enhancing the specific delivery of plumbagin to cancer cells, as well as improving its therapeutic efficacy. The results obtained from this thesis provide a proof of principle that the entrapment of plumbagin in a tumour-targeted delivery system is a highly promising strategy for cancer treatment that might be applicable to future work.

Our current formulations may not be suitable for long-term storage due to the risk of plumbagin leakage, as well as the intrinsic instability of lipid-based vesicles (oxidation of lipids) and PLGA-based nanoparticles (hydrolysis of PLGA). To overcome this potential problem, lyophilisation of nanomedicines may increase the stability of the formulations, facilitating transportation and improving product shelf-life.

In vitro, other cancer cell lines such as breast cancer cells (e.g. MCF-7 and MDA-MB-231), lung cancer cells (e.g. A541 and L9981), liver cancer cells (e.g. HepG2 and Huh7) and prostate cancer cells (e.g. PC-3 and LNCaP) may be investigated, based on the overexpression of transferrin receptors on their surface membrane. Moreover, in order to prove the hypothesis that the loading of plumbagin in a tumour-targeted delivery system would reduce secondary effects on healthy tissues, it will be necessary to assess the cytotoxicity of Tf-bearing nanomedicines entrapping plumbagin in normal cell lines such as WS1 skin fibroblast cells, MRC-5 lung fibroblast cells, HL-7702 hepatic cells and HK-2 renal epithelial cell.

In vivo, our studies showed that the intravenous administration of tumour-targeted nanomedicines entrapping plumbagin at low dose (2 mg/kg) significantly caused tumour eradication and regression in mice xenograft B16-F10 tumour models. Even though we observed some variability of responses and short animals' lifespan in some mice, the dose

of plumbagin (2 mg/kg) used in our study was low compared to other previous studies (6-10 mg/kg) (Singh *et al*., 2002; Tiwari *et al*., 2002). Thus, for therapeutic improvement, the next *in vivo* step would be to further investigate the maximum tolerance dose of plumbagin formulations and to increase the frequency of administration of the treatment, as well as to investigate the eventual toxicity on organs and tissues by histopathological examination.

Moreover, a deeper understanding of the pharmacokinetics and biodistribution of the novel transferrin-targeted nanocarriers entrapping plumbagin following intravenous injection will be required.

Another interesting point to pursue is the use of combinational therapy by using co-administration of plumbagin with other drugs that can synergistically improve the overall therapeutic efficacy, while reducing the dose and side effects of each drug. This possibility has been examined by Gowda and colleagues (2017) who developed plumbagin co-encapsulated with celecoxib (plumbagin: celecoxib at 1:20 molar ratio) in liposomes called CelePlum-777. *In vitro*, these liposomes (at the concentration of plumbagin 5 μM and celecoxib 100 μM) were able to decrease the cell viability of UACC 903 and 1205 LU metastatic melanoma cell lines by about 80% compared to that of both drugs individually entrapped in liposomes, suggesting a synergistic effect.

In addition, co-administration of plumbagin and gene therapy would be possible to improve the therapeutic efficacy of plumbagin. For example, Xu and co-workers (2016) made polymeric nanoparticles for co-delivery of paclitaxel and plasmid DNA encoding pigment epithelium-derived factor (PEDF). This combination was able to improve anti-cancer effect in a subcutaneous C26 murine colon adenocarcinoma by reducing the tumour vessel formation and promoting tumour cell apoptosis.

References

ABEDINPOUR, P. , BARON, V. T., CHRASTINA, A., WELSH, J. & BORGSTRöM, P. 2013. The combination of plumbagin with androgen withdrawal causes profound regression of prostate tumors *in vivo*. *The Prostate,* 73**,** 489-499.

AHMAD, A., BANERJEE, S., WANG, Z., KONG, D. & SARKAR, F. H. 2008. Plumbagin-induced apoptosis of human breast cancer cells is mediated by inactivation of NF-κB and Bcl-2. *Journal of Cellular Biochemistry,* 105**,** 1461-1471.

ALEXIS, F., PRIDGEN, E. M., LANGER, R. & FAROKHZAD, O. C. 2010. Nanoparticle technologies for cancer therapy. *In:* SCHÄFER-KORTING, M. (ed.) *Drug Delivery.* Berlin, Heidelberg: Springer Berlin Heidelberg.

ALMOUSTAFA, H. A., ALSHAWSH, M. A. & CHIK, Z. 2017. Technical aspects of preparing PEG-PLGA nanoparticles as carrier for chemotherapeutic agents by nanoprecipitation method. *International Journal of Pharmaceutics,* 533**,** 275-284.

ALSHEHRI, A., GRABOWSKA, A. & STOLNIK, S. 2018. Pathways of cellular internalisation of liposomes delivered siRNA and effects on siRNA engagement with target mRNA and silencing in cancer cells. *Scientific Reports,* 8**,** 3748.

AMELIAN, A., WASILEWSKA, K., MEGIAS, D. & WINNICKA, K. 2017. Application of standard cell cultures and 3D *in vitro* tissue models as an effective tool in drug design and development. *Pharmacological Reports,* 69**,** 861-870.

ANABOUSI, S., BAKOWSKY, U., SCHNEIDER, M., HUWER, H., LEHR, C. M. & EHRHARDT, C. 2006. *In vitro* assessment of transferrin-conjugated liposomes as drug delivery systems for inhalation therapy of lung cancer. *European Journal of Pharmaceutical Sciences,* 29**,** 367-374.

ANDERSON, M. & OMRI, A. 2004. The effect of different lipid components on the *in vitro* stability and release kinetics of liposome formulations. *Drug Delivery*, 11, 33-39.

ANSELMO, A. C. & MITRAGOTRI, S. 2014. An overview of clinical and commercial impact of drug delivery systems. *Journal of Controlled Release,* 190**,** 15-28.

APPADURAI, P. & RATHINASAMY, K. 2015. Plumbagin-silver nanoparticle formulations enhance the cellular uptake of plumbagin and its antiproliferative activities. *IET Nanobiotechnology,* 9**,** 264-272.

ARRUEBO, M., VILABOA, N., SÁEZ-GUTIERREZ, B., LAMBEA, J., TRES, A., VALLADARES, M. & GONZáLEZ-FERNáNDEZ, A. 2011. Assessment of the evolution of cancer treatment therapies. *Cancers,* 3**,** 3279-3330.

ASWENDT, M., COLLMANN, F. M. & HOEHN, M. 2017. Neurobiological insights from bioluminescence imaging. *Oncotarget,* 8**,** 69198-69199.

BAMRUNGSAP, S., ZHAO, Z., CHEN, T., WANG, L., LI, C., FU, T. & TAN, W. 2012. Nanotechnology in therapeutics: a focus on nanoparticles as a drug delivery system. *Nanomedicine,* 7**,** 1253-1271.

BANGHAM, A. D. & HORNE, R. W. 1964. Negative staining of phospholipids and their structural modification by surface-active agents as observed in the electron microscope. *Journal of Molecular Biology*, 8, 660-668.

BANGHAM, A. D., STANDISH, M. M. & WATKINS, J. C. 1965. Diffusion of univalent ions across the lamellae of swollen phospholipids. *Journal of Molecular Biology*, 13, 238-252.

BARENHOLZ, Y. 2012. Doxil® — The first FDA-approved nano-drug: Lessons learned. *Journal of Controlled Release,* 160**,** 117-134.

BARENHOLZ, Y. & PEER, D. 2012. Liposomes and other assemblies as drugs and nano-drugs: From basic and translational research to the clinics. *Journal of Controlled Release,* 160**,** 115-116.

BARRÉ-SINOUSSI, F. & MONTAGUTELLI, X. 2015. Animal models are essential to biological research: issues and perspectives. *Future Science OA,* 1**,** FSO63-FSO63.

BARUA, S. & MITRAGOTRI, S. 2014. Challenges associated with penetration of nanoparticles across cell and tissue barriers: A review of current status and future prospects. *Nano Today,* 9**,** 223-243.

BAUSCH-FLUCK, D., HOFMANN, A., BOCK, T., FREI, A. P., CERCIELLO, F., JACOBS, A., MOEST, H., OMASITS, U., GUNDRY, R. L., YOON, C., SCHIESS, R., SCHMIDT, A., MIRKOWSKA, P., HARTLOVA, A., VAN EYK, J. E., BOURQUIN, J. P., AEBERSOLD, R., BOHELER, K. R., ZANDSTRA, P. & WOLLSCHEID, B. 2015. A mass spectrometric-derived cell surface protein atlas. *PLoS One,* 10**,** e0121314.

BAZAK, R., HOURI, M., ACHY, S. E., HUSSEIN, W. & REFAAT, T. 2014. Passive targeting of nanoparticles to cancer: A comprehensive review of the literature. *Molecular and Clinical Oncology,* 2**,** 904-908.

BERTRAND, N., WU, J., XU, X., KAMALY, N. & FAROKHZAD, O. C. 2014. Cancer nanotechnology: The impact of passive and active targeting in the era of modern cancer biology. *Advanced Drug Delivery Reviews,* 66**,** 2-25.

BHATTACHARJEE, S. 2016. DLS and zeta potential – What they are and what they are not? *Journal of Controlled Release,* 235**,** 337-351.

BHOSLE, J. & HALL, G. 2009. Principles of cancer treatment by chemotherapy. *Surgery (Oxford),* 27**,** 173-177.

BLANCO, E., SHEN, H. & FERRARI, M. 2015. Principles of nanoparticle design for overcoming biological barriers to drug delivery. *Nature Biotechnology,* 33**,** 941-951.

BOTHIRAJA, C., KAPARE, H. S., PAWAR, A. P. & SHAIKH, K. S. 2013. Development of plumbagin-loaded phospholipid–Tween® 80 mixed micelles: formulation, optimization, effect on breast cancer cells and human blood/serum compatibility testing. *Therapeutic Delivery,* 4**,** 1247-1259.

BRAY, F., FERLAY, J., SOERJOMATARAM, I., SIEGEL, R. L., TORRE, L. A. & JEMAL, A. 2018. Global cancer statistics 2018: GLOBOCAN estimates of incidence and mortality worldwide for 36 cancers in 185 countries. *CA: A Cancer Journal for Clinicians,* 0**,** 3-31.

BRIUGLIA, M. L., ROTELLA, C., MCFARLANE, A. & LAMPROU, D. A. 2015. Influence of cholesterol on liposome stability and on *in vitro* drug release. *Drug Delivery and Translational Research,* 5**,** 231-242.

BRUNDAGE, M., FOXCROFT, S., MCGOWAN, T., GUTIERREZ, E., SHARPE, M. & WARDE, P. 2013. A survey of radiation treatment planning peer-review activities in a provincial radiation oncology programme: current practice and future directions. *British Medical Journal Open,* 3**,** e003241.

CAGEL, M., GROTZ, E., BERNABEU, E., MORETTON, M. A. & CHIAPPETTA, D. A. 2017. Doxorubicin: nanotechnological overviews from bench to bedside. *Drug Discovery Today,* 22**,** 270-281.

CALEY, A. & JONES, R. 2012. The principles of cancer treatment by chemotherapy. *Surgery (Oxford),* 30**,** 186-190.

CAO, Y. Y., YU, J., LIU, T. T., YANG, K. X., YANG, L. Y., CHEN, Q., SHI, F., HAO, J. J., CAI, Y., WANG, M. R., LU, W. H. & ZHANG, Y. 2018. Plumbagin inhibits the proliferation and survival of esophageal cancer cells by blocking STAT3-PLK1-AKT signaling. *Cell Death Discovery*, 9, 17.

ČEH, B., WINTERHALTER, M., FREDERIK, P. M., VALLNER, J. J. & LASIC, D. D. 1997. Stealth® liposomes: from theory to product. *Advanced Drug Delivery Reviews,* 24**,** 165-177.

CHAIRUNGSI, N., JUMPATONG, K., SUEBSAKWONG, P., SENGPRACHA, W., PHUTDHAWONG, W. & BUDDHASUKH, D. 2006. Electrocoagulation of quinone pigments. *Molecules (Basel, Switzerland),* 11**,** 514-522.

CHANG, J., JALLOULI, Y., KROUBI, M., YUAN, X. B., FENG, W., KANG, C. S., PU, P. Y. & BETBEDER, D. 2009. Characterization of endocytosis of transferrin-coated PLGA nanoparticles by the blood–brain barrier. *International Journal of Pharmaceutics,* 379**,** 285-292.

CHECKER, R., PATWARDHAN, R. S., SHARMA, D. & SANDUR, S. K. 2018. Chemopreventive and Anti-cancer Effects of Plumbagin: Novel Mechanism(s) via Modulation of Cellular Redox. *In:* BHARTI, A. C. & AGGARWAL, B. B. (eds.) *Role of Nutraceuticals in Cancer Chemosensitization.* 1 ed. Cambridge, MA, USA: Academic Press.

CHECKER, R., SHARMA, D., SANDUR, S. K., KHANAM, S. & PODUVAL, T. B. 2009. Anti-inflammatory effects of plumbagin are mediated by inhibition of NF-kappaB activation in lymphocytes. *International Immunopharmacology,* 9**,** 949-958.

CHEN, A., ZHOU, X., TANG, S., LIU, M. & WANG, X. 2016. Evaluation of the inhibition potential of plumbagin against cytochrome P450 using LC-MS/MS and cocktail approach. *Scientific Reports,* 6**,** 28482-28482.

CHEN, C. A., CHANG, H. H., KAO, C. Y., TSAI, T. H. & CHEN, Y. J. 2009. Plumbagin, isolated from *Plumbago zeylanica*, induces cell death through apoptosis in human pancreatic cancer cells. *Pancreatology,* 9**,** 797-809.

CHEN, F., ZHU, L., ZHANG, Y., KUMAR, D., CAO, G., HU, X., LIANG, Z., KUANG, S., XUE, R. & GONG, C. 2018. Clathrin-mediated endocytosis is a candidate entry sorting mechanism for *Bombyx mori* cypovirus. *Scientific Reports,* 8**,** 7268.

CHEN, M. B., ZHANG, Y., WEI, M. X., SHEN, W., WU, X. Y., YAO, C. & LU, P. H. 2013. Activation of AMP-activated protein kinase (AMPK) mediates plumbagin-induced apoptosis and growth inhibition in cultured human colon cancer cells. *Cellular Signalling,* 25**,** 1993-2002.

CHENG, J., TEPLY, B. A., SHERIFI, I., SUNG, J., LUTHER, G., GU, F. X., LEVY-NISSENBAUM, E., RADOVIC-MORENO, A. F., LANGER, R. & FAROKHZAD, O. C. 2007. Formulation of functionalized PLGA-PEG nanoparticles for *in vivo* targeted drug delivery. *Biomaterials,* 28**,** 869-876.

CHITTASUPHO, C. 2012. Multivalent ligand: design principle for targeted therapeutic delivery approach. *Therapeutic Delivery,* 3**,** 1171-87.

CHRASTINA, A., BARON, V. T., ABEDINPOUR, P., RONDEAU, G., WELSH, J. & BORGSTRöM, P. 2018. Plumbagin-loaded nanoemulsion drug delivery formulation and evaluation of antiproliferative effect on prostate cancer cells. *BioMed Research International,* 2018**,** 7.

CHU, H., YU, H., REN, D., ZHU, K. & HUANG, H. 2016. Plumbagin exerts protective effects in nucleus pulposus cells by attenuating hydrogen peroxide-induced oxidative stress, inflammation and apoptosis through NF-kappaB and Nrf-2. *International Journal of Molecular Medicine,* 37**,** 1669-76.

CLINICALTRIALS.GOV 2019, accessed 14 May 2019, <http:// clinicaltrials.gov>.

CLOSE, D. M., XU, T., SAYLER, G. S. & RIPP, S. 2010. *In vivo* bioluminescent imaging (BLI): noninvasive visualization and interrogation of biological processes in living animals. *Sensors (Basel, Switzerland),* 11**,** 180-206.

CRAGG, G. M. & PEZZUTO, J. M. 2016. Natural Products as a vital source for the discovery of cancer chemotherapeutic and chemopreventive agents. *Medical principles and practice: international journal of the Kuwait University, Health Science Centre,* 25 Suppl 2**,** 41-59.

DANHIER, F., ANSORENA, E., SILVA, J. M., COCO, R., LE BRETON, A. & PRÉAT, V. 2012. PLGA-based nanoparticles: An overview of biomedical applications. *Journal of Controlled Release,* 161**,** 505-522.

DANIELS, T. R., BERNABEU, E., RODRíGUEZ, J. A., PATEL, S., KOZMAN, M., CHIAPPETTA, D. A., HOLLER, E., LJUBIMOVA, J. Y., HELGUERA, G. & PENICHET, M. L. 2012. Transferrin receptors and the targeted delivery of therapeutic agents against cancer. *Biochimica et Biophysica Acta,* 1820**,** 291-317.

DANIELS, T. R., DELGADO, T., HELGUERA, G. & PENICHET, M. L. 2006a. The transferrin receptor part II: Targeted delivery of therapeutic agents into cancer cells. *Clinical Immunology,* 121**,** 159-176.

DANIELS, T. R., DELGADO, T., RODRIGUEZ, J. A., HELGUERA, G. & PENICHET, M. L. 2006b. The transferrin receptor part I: Biology and targeting with cytotoxic antibodies for the treatment of cancer. *Clinical Immunology,* 121**,** 144-158.

DEMCHENKO, A. P. 2013. Beyond annexin V: fluorescence response of cellular membranes to apoptosis. *Cytotechnology,* 65**,** 157-172.

DEMMA, J., HALLBERG, K. & HELLMAN, B. 2009. Genotoxicity of plumbagin and its effects on catechol and NQNO-induced DNA damage in mouse lymphoma cells. *Toxicology in Vitro,* 23**,** 266-271.

DESHPANDE, P. P., BISWAS, S. & TORCHILIN, V. P. 2013. Current trends in the use of liposomes for tumor targeting. *Nanomedicine (London, England),* 8**,** 1-32.

DHAKAR, R. C., MAURYA, S. D. & SALUJA, V. 2012. From formulation variables to drug entrapment efficiency of microspheres: A technical review. *Journal of Drug Delivery and Therapeutics,* 2**,** 128-133.

DHILLON, A. S., HAGAN, S., RATH, O. & KOLCH, W. 2007. MAP kinase signalling pathways in cancer. *Oncogene,* 26**,** 3279-3290.

DHINGRA, D. & BANSAL, S. 2015. Antidepressant-like activity of plumbagin in unstressed and stressed mice. *Pharmacological Reports,* 67**,** 1024-1032.

DINARVAND, R., SEPEHRI, N., MANOOCHEHRI, S., ROUHANI, H. & ATYABI, F. 2011. Polylactide-co-glycolide nanoparticles for controlled delivery of anti-cancer agents. *International Journal of Nanomedicine,* 6**,** 877-895.

DING, C., LI, L., YANG, T., FAN, X. & WU, G. 2016. Combined application of anti-VEGF and anti-EGFR attenuates the growth and angiogenesis of colorectal cancer mainly through suppressing AKT and ERK signaling in mice model. *BMC Cancer,* 16**,** 791-791.

DOESSEGGER, L. & BANHOLZER, M. L. 2015. Clinical development methodology for infusion-related reactions with monoclonal antibodies. *Clinical & Translational Immunology,* 4**,** e39.

DOVIZIO, M., TACCONELLI, S., SOSTRES, C., RICCIOTTI, E. & PATRIGNANI, P. 2012. Mechanistic and pharmacological issues of aspirin as an anti-cancer agent. *Pharmaceuticals,* 5**,** 1346-1371.

DUFÈS, C. 2011. Delivery of the vitamin E compound tocotrienol to cancer cells. *Therapeutic Delivery,* 2**,** 1385-9.

DUFÈS, C., MULLER, J. M., COUET, W., OLIVIER, J. C., UCHEGBU, I. F. & SCHÄTZLEIN, A. G. 2004. Anti-cancer drug delivery with transferrin targeted polymeric chitosan vesicles. *Pharmaceutical Research,* 21**,** 101-107.

DUFÈS, C., SCHÄTZLEIN, A. G., TETLEY, L., GRAY, A. I., WATSON, D. G., OLIVIER, J. C., COUET, W. & UCHEGBU, I. F. 2000. Niosomes and Polymeric Chitosan Based Vesicles Bearing Transferrin and Glucose Ligands for Drug Targeting. *Pharmaceutical Research,* 17**,** 1250-1258.

DUFÈS, C., UCHEGBU, I. F. & SCHÄTZLEIN, A. G. 2005. Dendrimers in gene delivery. *Advanced Drug Delivery Reviews,* 57**,** 2177-2202.

DUPREZ, L., WIRAWAN, E., BERGHE, T. V. & VANDENABEELE, P. 2009. Major cell death pathways at a glance. *Microbes and Infection,* 11**,** 1050-1062.

DURAIPANDY, N., LAKRA, R., KUNNAVAKKAM, V. S., SAMANTA, D., KORRAPATI, P. S. & KIRAN, M. S. 2014. Caging of plumbagin on silver nanoparticles imparts selectivity and sensitivity to plumbagin for targeted cancer cell apoptosis. *Metallomics,* 6**,** 2025-2033.

DURYMANOV, M. O., ROSENKRANZ, A. A. & SOBOLEV, A. S. 2015. Current approaches for improving intratumoral accumulation and distribution of nanomedicines. *Theranostics,* 5**,** 1007-1020.

DZOYEM, J. P., TANGMOUO, J. G., LONTSI, D., ETOA, F. X. & LOHOUE, P. J. 2007. *In vitro* antifungal activity of extract and plumbagin from the stem bark of *Diospyros crassiflora* Hiern (Ebenaceae). *Phytotherapy Research,* 21**,** 671-674.

EGUSQUIAGUIRRE, S. P., IGARTUA, M., HERNÁNDEZ, R. M. & PEDRAZ, J. L. 2012. Nanoparticle delivery systems for cancer therapy: advances in clinical and preclinical research. *Clinical and Translational Oncology,* 14**,** 83-93.

EISENHAUER, E. A. , THERASSE, P. , BOGAERTS, J. , SCHWARTZ, L. H. , SARGENT, D. , FORD, R., DANCEY, J., ARBUCK, S., GWYTHER, S., MOONEY, M., RUBINSTEIN, L., SHANKAR, L., DODD, L., KAPLAN, R., LACOMBE, D. & VERWEIJ, J. 2009. New response evaluation criteria in solid tumours: Revised RECIST guideline (version 1.1). *European Journal of Cancer,* 45**,** 228-247.

ELDHOSE, B., GUNAWAN, M., RAHMAN, M., LATHA, M. S. & NOTARIO, V. 2014. Plumbagin reduces human colon cancer cell survival by inducing cell cycle arrest and mitochondria-mediated apoptosis. *International Journal of Oncology,* 45**,** 1913-1920.

ERNSTING, M. J., MURAKAMI, M., ROY, A. & LI, S. D. 2013. Factors controlling the pharmacokinetics, biodistribution and intratumoral penetration of nanoparticles. *Journal of Controlled Release,* 172**,** 782-794.

FARAJI, A. H. & WIPF, P. 2009. Nanoparticles in cellular drug delivery. *Bioorganic & Medicinal Chemistry,* 17**,** 2950-2962.

FERNANDO, J. & JONES, R. 2015. The principles of cancer treatment by chemotherapy. *Surgery (Oxford),* 33**,** 131-135.

FRASCO, M. F., ALMEIDA, G. M., SANTOS, S. F., PEREIRA, M. D. C. & COELHO, M. A. N. 2015. Transferrin surface-modified PLGA nanoparticles-mediated delivery of a proteasome inhibitor to human pancreatic cancer cells. *Journal of Biomedical Materials Research Part A,* 103**,** 1476-1484.

FREDENBERG, S., WAHLGREN, M., RESLOW, M. & AXELSSON, A. 2011. The mechanisms of drug release in poly(lactic-co-glycolic acid)-based drug delivery systems—A review. *International Journal of Pharmaceutics,* 415**,** 34-52.

FU, J. Y. 2010. *Preparation and evaluation of tumour-targeted delivery systems for tocotrienol.* PhD, University of Strathclyde.

FU, J. Y., BLATCHFORD, D. R., TETLEY, L. & DUFÈS, C. 2009. Tumor regression after systemic administration of tocotrienol entrapped in tumor-targeted vesicles. *Journal of Controlled Release,* 140**,** 95-99.

FU, J. Y. & DUFÈS, C. 2014. Anti-cancer efficacy of intravenously administered tumor-targeted vesicles entrapping tocotrienol. *Pharmaceutical Nanotechnology,* 2**,** 172-181.

FU, J. Y., TAN, D. M. Y., ER, H. M., CHEN, Y. S. & NESARETNAM, K. 2016. Tumor-targeted niosome as novel carrier for intravenous administration of tocotrienol. *Asian Journal of Pharmaceutical Sciences,* 11**,** 79-80.

FU, J. Y., ZHANG, W., BLATCHFORD, D. R., TETLEY, L., MCCONNELL, G. & DUFÈS, C. 2011. Novel tocotrienol-entrapping vesicles can eradicate solid tumors after intravenous administration. *Journal of Controlled Release,* 154**,** 20-6.

GAN, C. W. & FENG, S. S. 2010. Transferrin-conjugated nanoparticles of poly(lactide)-d-α-tocopheryl polyethylene glycol succinate diblock copolymer for targeted drug delivery across the blood–brain barrier. *Biomaterials,* 31**,** 7748-7757.

GAO, H., YANG, Z., ZHANG, S., CAO, S., SHEN, S., PANG, Z. & JIANG, X. 2013. Ligand modified nanoparticles increases cell uptake, alters endocytosis and elevates glioma distribution and internalization. *Scientific Reports,* 3**,** 2534.

GESSNER, A., LIESKE, A., PAULKE, B. R. & MüLLER, R. H. 2003. Functional groups on polystyrene model nanoparticles: Influence on protein adsorption. *Journal of Biomedical Materials Research Part A,* 65A**,** 319-326.

GOMATHINAYAGAM, R., SOWMYALAKSHMI, S., MARDHATILLAH, F., KUMAR, R., AKBARSHA, M. A. & DAMODARAN, C. 2008. Anti-cancer mechanism of plumbagin, a natural compound, on non-small cell lung cancer cells. *Anticancer Research,* 28**,** 785-92.

GORDON, J. L., BROWN, M. A. & REYNOLDS, M. M. 2018. Cell-based methods for determination of efficacy for candidate therapeutics in the clinical management of cancer. *Diseases (Basel, Switzerland),* 6**,** 85.

GOWDA, R., KARDOS, G., SHARMA, A., SINGH, S. & ROBERTSON, G. P. 2017. Nanoparticle-based celecoxib and plumbagin for the synergistic treatment of melanoma. *Molecular Cancer Therapeutics,* 16**,** 440-452.

GREGORIADIS, G. 2007. *Liposome technology,* New York, Informa Healthcare.

GRISHAM, R., KY, B., TEWARI, K. S., CHAPLIN, D. J. & WALKER, J. 2018. Clinical trial experience with CA4P anti-cancer therapy: focus on efficacy, cardiovascular adverse events, and hypertension management. *Gynecologic Oncology Research and Practice,* 5**,** 1-1.

GROBMYER, S. R., IWAKUMA, N., SHARMA, P. & MOUDGIL, B. M. 2010. What Is Cancer Nanotechnology? *In:* GROBMYER, R. S. & MOUDGIL, M. B. (eds.) *Cancer Nanotechnology: Methods and Protocols.* Totowa, NJ: Humana Press.

GUO, P., LIU, D., SUBRAMANYAM, K., WANG, B., YANG, J., HUANG, J., AUGUSTE, D. T. & MOSES, M. A. 2018. Nanoparticle elasticity directs tumor uptake. *Nature Communications,* 9**,** 130.

GUO, W., LI, A., JIA, Z., YUAN, Y., DAI, H. & LI, H. 2013. Transferrin modified PEG-PLA-resveratrol conjugates: *In vitro* and *in vivo* studies for glioma. *European Journal of Pharmacology,* 718**,** 41-47.

GUO, Y., WANG, L., LV, P. & ZHANG, P. 2015. Transferrin-conjugated doxorubicin-loaded lipid-coated nanoparticles for the targeting and therapy of lung cancer. *Oncology Letters,* 9**,** 1065-1072.

GUPTA, A. C., MOHANTY, S., SAXENA, A., MAURYA, A. K. & BAWANKULE, D. U. 2018. Plumbagin, a vitamin K3 analogue ameliorate malaria pathogenesis by inhibiting oxidative stress and inflammation. *Inflammopharmacology,* 26**,** 983-991.

HADINOTO, K., SUNDARESAN, A. & CHEOW, W. S. 2013. Lipid–polymer hybrid nanoparticles as a new generation therapeutic delivery platform: A review. *European Journal of Pharmaceutics and Biopharmaceutics,* 85**,** 427-443.

HAFEEZ, B. B., JAMAL, M. S., FISCHER, J. W., MUSTAFA, A. & VERMA, A. K. 2012. Plumbagin, a plant derived natural agent inhibits the growth of pancreatic cancer cells in *in vitro* and *in vivo* via targeting EGFR, Stat3 and NF-κB signaling pathways. *International Journal of Cancer,* 131**,** 2175-2186.

HAFEEZ, B. B., ZHONG, W., FISCHER, J. W., MUSTAFA, A., SHI, X., MESKE, L., HONG, H., CAI, W., HAVIGHURST, T., KIM, K. & VERMA, A. K. 2013. Plumbagin, a medicinal plant (*Plumbago zeylanica*)-derived 1,4-naphthoquinone, inhibits growth and metastasis of human prostate cancer PC-3M-luciferase cells in an orthotopic xenograft mouse model. *Molecular Oncology,* 7**,** 428-439.

HAIT, W. N. 2010. Anti-cancer drug development: the grand challenges. *Nature Reviews Drug Discovery,* 9**,** 253.

HAIT, W. N., RUBIN, E. & BERTINO, J. R. 2015. Cancer Therapeutics. *In:* MENDELSOHN, J., GRAY, J. W., HOWLEY, P. M., ISRAEL, M. A. & THOMPSON, C. B. (eds.) *The Molecular Basis of Cancer (Fourth Edition).* Philadelphia: Elsevier.

HANAHAN, D. & WEINBERG, R. A. 2000. The hallmarks of cancer. *Cell*, 100, 57-70.

HANAHAN, D. & WEINBERG, R. A. 2011. Hallmarks of cancer: the next generation. *Cell*, 144, 646-674.

HARTMAN, K. B., WILSON, L. J. & ROSENBLUM, M. G. 2008. Detecting and treating cancer with nanotechnology. *Molecular Diagnosis & Therapy,* 12**,** 1-14.

HENGARTNER, M. O. 2000. The biochemistry of apoptosis. *Nature,* 407**,** 770-776.

HERD, H., DAUM, N., JONES, A. T., HUWER, H., GHANDEHARI, H. & LEHR, C. M. 2013. Nanoparticle geometry and surface orientation influence mode of cellular uptake. *ACS Nano,* 7**,** 1961-1973.

HERMANSON, G. T. 2013. Dendrimers and Dendrons. *Bioconjugate Techniques (Third edition).* Boston: Academic Press.

HERRERO, E. P. & MEDARDE, A. F. 2015. Advanced targeted therapies in cancer: Drug nanocarriers, the future of chemotherapy. *European Journal of Pharmaceutics and Biopharmaceutics,* 93**,** 52-79.

HIRSJÄRVI, S. 2008. *Preparation and characterization of poly(lactic acid) nanoparticles for pharmaceutical use.* PhD, University of Helsinki.

HO, R. J. Y. & CHIEN, J. 2014. Trends in translational medicine and drug targeting and delivery: new insights on an old concept-targeted drug delivery with antibody-drug conjugates for cancers. *Journal of Pharmaceutical Sciences,* 103**,** 71-77.

HOSHYAR, N., GRAY, S., HAN, H. & BAO, G. 2016. The effect of nanoparticle size on *in vivo* pharmacokinetics and cellular interaction. *Nanomedicine,* 11**,** 673-692.

HSIEH, Y. J., LIN, L. C. & TSAI, T. H. 2006. Measurement and pharmacokinetic study of plumbagin in a conscious freely moving rat using liquid chromatography/tandem mass spectrometry. *Journal of Chromatography B,* 844**,** 1-5.

HSU, Y. L., CHO, C. Y., KUO, P. L., HUANG, Y. T. & LIN, C. C. 2006. Plumbagin (5-hydroxy-2-methyl-1,4-naphthoquinone) induces apoptosis and cell cycle arrest in A549 cells through p53 accumulation via c-Jun NH2-terminal kinase-mediated phosphorylation at serine 15 *in vitro* and *in vivo. Journal of Pharmacology and Experimental Therapeutics,* 318**,** 484-94.

HUSSEINI, G. A. & PITT, W. G. 2008. Micelles and nanoparticles for ultrasonic drug and gene delivery. *Advanced Drug Delivery Reviews,* 60**,** 1137-1152.

INBARAJ, J. J. & CHIGNELL, C. F. 2004. Cytotoxic action of juglone and plumbagin: A mechanistic study using HaCaT keratinocytes. *Chemical Research in Toxicology,* 17**,** 55-62.

IQBAL, J., ABBASI, B. A., MAHMOOD, T., KANWAL, S., ALI, B., SHAH, S. A. & KHALIL, A. T. 2017. Plant-derived anti-cancer agents: A green anti-cancer approach. *Asian Pacific Journal of Tropical Biomedicine,* 7**,** 1129-1150.

JAISWAL, A., SABARWAL, A., NARAYAN MISHRA, J. P. & SINGH, R. P. 2018. Plumbagin induces ROS-mediated apoptosis and cell cycle arrest and inhibits EMT in human cervical carcinoma cells. *RSC Advances,* 8**,** 32022-32037.

JAROCH, K., JAROCH, A. & BOJKO, B. 2018. Cell cultures in drug discovery and development: The need of reliable *in vitro-in vivo* extrapolation for pharmacodynamics and pharmacokinetics assessment. *Journal of Pharmaceutical and Biomedical Analysis,* 147**,** 297-312.

JHAVERI, A., DESHPANDE, P., PATTNI, B. & TORCHILIN, V. 2018. Transferrin-targeted, resveratrol-loaded liposomes for the treatment of glioblastoma. *Journal of Controlled Release,* 277**,** 89-101.

JHAVERI, A. M. & TORCHILIN, V. P. 2014. Multifunctional polymeric micelles for delivery of drugs and siRNA. *Frontiers in Pharmacology,* 5.

KAKADIA, P. G. & CONWAY, B. R. 2014. Solid lipid nanoparticles: A potential approach for dermal drug delivery. *American Journal of Pharmacological Sciences,* 2**,** 1-7.

KALRA, J. & BALLY, M. B. 2013. Liposomes. *In:* UCHEGBU, I. F., SCHÄTZLEIN, A. G., CHENG, P. W. & LALATSA, A. (eds.) *Fundamentals of Pharmaceutical Nanoscience.* New York, NY: Springer New York.

KAMALY, N., YAMEEN, B., WU, J. & FAROKHZAD, O. C. 2016. Degradable controlled-release polymers and polymeric nanoparticles: Mechanisms of controlling drug release. *Chemical Reviews,* 116**,** 2602-2663.

KAPUR, A., BERES, T., RATHI, K., NAYAK, A. P., CZARNECKI, A., FELDER, M., GILLETTE, A., ERICKSEN, S. S., SAMPENE, E., SKALA, M. C., BARROILHET, L. & PATANKAR, M. S. 2018. Oxidative stress via inhibition of the mitochondrial electron transport and Nrf-2-mediated anti-oxidative response regulate the cytotoxic activity of plumbagin. *Scientific Reports,* 8**,** 1073-1073.

KARIM, R., SOMANI, S., AL ROBAIAN, M., MULLIN, M., AMOR, R., MCCONNELL, G. & DUFÈS, C. 2017. Tumor regression after intravenous administration of targeted vesicles entrapping the vitamin E α-tocotrienol. *Journal of Controlled Release,* 246**,** 79-87.

KAUR, T. & SLAVCEV, R. 2013. Solid lipid nanoparticles: Tuneable anti-cancer gene/drug delivery systems. *In:* WEI, M. (ed.) *Novel Gene Therapy Approaches.* InTech.

KAWIAK, A. & DOMACHOWSKA, A. 2016. Plumbagin suppresses the invasion of HER2-overexpressing breast cancer cells through inhibition of IKKα-mediated NF-κB activation. *PloS One,* 11**,** e0164064-e0164064.

KHAW, A. K., SAMENI, S., VENKATESAN, S., KALTHUR, G. & HANDE, M. P. 2015. Plumbagin alters telomere dynamics, induces DNA damage and cell death in human brain tumour cells. *Mutation Research/Genetic Toxicology and Environmental Mutagenesis,* 793**,** 86-95.

KHAWAR, I. A., KIM, J. H. & KUH, H. J. 2015. Improving drug delivery to solid tumors: Priming the tumor microenvironment. *Journal of Controlled Release,* 201**,** 78-89.

KLEMM, F. & JOYCE, J. A. 2015. Microenvironmental regulation of therapeutic response in cancer. *Trends in Cell Biology,* 25**,** 198-213.

KLINGHAMMER, K., WALTHER, W. & HOFFMANN, J. 2017. Choosing wisely – Preclinical test models in the era of precision medicine. *Cancer Treatment Reviews,* 55**,** 36-45.

KLOTZ, L. O., HOU, X. & JACOB, C. 2014. 1,4-Naphthoquinones: from oxidative damage to cellular and inter-cellular signaling. *Molecules (Basel, Switzerland),* 19**,** 14902-14918.

KOBAYASHI, T., ISHIDA, T., OKADA, Y., ISE, S., HARASHIMA, H. & KIWADA, H. 2007. Effect of transferrin receptor-targeted liposomal doxorubicin in P-glycoprotein-mediated drug resistant tumor cells. *International Journal of Pharmaceutics,* 329**,** 94-102.

KOHNO, M., TANIMURA, S. & OZAKI, K.-I. 2011. Targeting the extracellular signal-regulated kinase pathway in cancer therapy. *Biological and Pharmaceutical Bulletin,* 34**,** 1781-1784.

KOPPU, S., OH, Y. J., EDRADA-EBEL, R., BLATCHFORD, D. R., TETLEY, L., TATE, R. J. & DUFÈS, C. 2010. Tumor regression after systemic administration of a novel tumor-targeted gene delivery system carrying a therapeutic plasmid DNA. *Journal of Controlled Release,* 143**,** 215-221.

KOU, L., SUN, J., ZHAI, Y. & HE, Z. 2013. The endocytosis and intracellular fate of nanomedicines: Implication for rational design. *Asian Journal of Pharmaceutical Sciences,* 8**,** 1-10.

KRIEL, J., MÜLLER-NEDEBOCK, K., MAARMAN, G., MBIZANA, S., OJUKA, E., KLUMPERMAN, B. & LOOS, B. 2018. Coordinated autophagy modulation overcomes glioblastoma chemoresistance through disruption of mitochondrial bioenergetics. *Scientific Reports,* 8**,** 10348.

KRISHNASWAMY, M. & PURUSHOTHAMAN, K. K. 1980. Plumbagin: A study of its anti-cancer, antibacterial & antifungal properties. *Indian Journal of Experimental Biology,* 18**,** 876-7.

KUMAR, M. R. S., AITHAL, B. K., UDUPA, N., REDDY, M. S., RAAKESH, V., MURTHY, R. S., RAJU, D. P. & RAO, B. S. 2011. Formulation of plumbagin loaded long circulating PEGylated liposomes: *in vivo* evaluation in C57BL/6J mice bearing B16F1 melanoma. *Drug Delivery,* 18**,** 511-22.

KUMAR, V., ABBAS, A. K., FAUSTO, N. & ASTER, J. C. 2010. *Robbins and Cotran Pathologic Basis of Disease,* Philadelphia, PA, Elsevier.

KUMARI, A., YADAV, S. K. & YADAV, S. C. 2010. Biodegradable polymeric nanoparticles based drug delivery systems. *Colloids and Surfaces B: Biointerfaces,* 75**,** 1-18.

KURA, A. U., FAKURAZI, S., HUSSEIN, M. Z. & ARULSELVAN, P. 2014. Nanotechnology in drug delivery: the need for more cell culture based studies in screening. *Chemistry Central Journal,* 8**,** 46-46.

KWOK, K. K., VINCENT, E. C. & GIBSON, J. N. 2017. Antineoplastic drugs. *In:* DOWD, F. J., JOHNSON, B. S. & MARIOTTI, A. J. (eds.) *Pharmacology and Therapeutics for Dentistry (Seventh Edition).* Missouri: Elsevier.

LAI, L., LIU, J., ZHAI, D., LIN, Q., HE, L., DONG, Y., ZHANG, J., LU, B., CHEN, Y., YI, Z. & LIU, M. 2012. Plumbagin inhibits tumour angiogenesis and tumour growth through the Ras signalling pathway following activation of the VEGF receptor-2. *British Journal of Pharmacology,* 165**,** 1084-96.

LAMMERS, T., HENNINK, W. E. & STORM, G. 2008. Tumour-targeted nanomedicines: principles and practice. *British Journal of Cancer,* 99**,** 392-397.

LEE, C. C., MACKAY, J. A., FRECHET, J. M. J. & SZOKA, F. C. 2005. Designing dendrimers for biological applications. *Nature Biotechnology,* 23**,** 1517-1526.

LEE, C. H., JEON, Y. T., KIM, S. H. & SONG, Y. S. 2007. NF-κB as a potential molecular target for cancer therapy. *BioFactors,* 29**,** 19-35.

LEE, J. H., YEON, J. H., KIM, H., ROH, W., CHAE, J., PARK, H. O. & KIM, D. M. 2012. The natural anti-cancer agent plumbagin induces potent cytotoxicity in MCF-7 human breast cancer cells by inhibiting a PI-5 kinase for ROS generation. *PloS One,* 7**,** e45023-e45023.

LEE, S. Y. 2016. Temozolomide resistance in glioblastoma multiforme. *Genes & Diseases,* 3**,** 198-210.

LEMARIÉ, F., CHANG, C. W., BLATCHFORD, D. R., AMOR, R., NORRIS, G., TETLEY, L., MCCONNELL, G. & DUFÈS, C. 2013. Antitumor activity of the tea polyphenol epigallocatechin-3-gallate encapsulated in targeted vesicles after intravenous administration. *Nanomedicine (Lond),* 8**,** 181-92.

LI, C., GE, X. & WANG, L. 2017a. Construction and comparison of different nanocarriers for co-delivery of cisplatin and curcumin: A synergistic combination nanotherapy for cervical cancer. *Biomedicine & Pharmacotherapy,* 86**,** 628-636.

LI, H., TONG, Y., BAI, L., YE, L., ZHONG, L., DUAN, X. & ZHU, Y. 2018. Lactoferrin functionalized PEG-PLGA nanoparticles of shikonin for brain targeting therapy of glioma. *International Journal of Biological Macromolecules,* 107**,** 204-211.

LI, J., SHEN, L., LU, F. R., QIN, Y., CHEN, R., LI, J., LI, Y., ZHAN, H. Z. & HE, Y. Q. 2012a. Plumbagin inhibits cell growth and potentiates apoptosis in human gastric cancer cells *in vitro* through the NF-κB signaling pathway. *Acta pharmacologica Sinica,* 33**,** 242-249.

LI, Q., CAI, T., HUANG, Y., XIA, X., COLE, S. P. C. & CAI, Y. 2017b. A review of the structure, preparation, and application of NLCs, PNPs, and PLNs. *Nanomaterials (Basel, Switzerland),* 7**,** 122.

LI, S. D. & HUANG, L. 2008. Pharmacokinetics and biodistribution of nanoparticles. *Molecular Pharmaceutics,* 5**,** 496-504.

LI, W., SAUD, S. M., YOUNG, M. R., CHEN, G. & HUA, B. 2015. Targeting AMPK for cancer prevention and treatment. *Oncotarget,* 6**,** 7365-7378.

LI, X., DING, L., XU, Y., WANG, Y. & PING, Q. 2009. Targeted delivery of doxorubicin using stealth liposomes modified with transferrin. *International Journal of Pharmaceutics,* 373**,** 116-123.

LI, Y., WANG, J., WIENTJES, M. G. & AU, J. L. S. 2012b. Delivery of nanomedicines to extracellular and intracellular compartments of a solid tumor. *Advanced Drug Delivery Reviews,* 64**,** 29-39.

LI, Y. C., HE, S. M., HE, Z. X., LI, M., YANG, Y., PANG, J. X., ZHANG, X., CHOW, K., ZHOU, Q., DUAN, W., ZHOU, Z. W., YANG, T., HUANG, G. H., LIU, A., QIU, J. X., LIU, J. P. & ZHOU, S. F. 2014. Plumbagin induces apoptotic and autophagic cell death through inhibition of the PI3K/Akt/mTOR pathway in human non-small cell lung cancer cells. *Cancer Letters,* 344**,** 239-259.

LIN, C. H., JI, T., CHEN, C. F. & HOANG, B. H. 2014. Wnt signaling in osteosarcoma. *In:* KLEINERMAN, M. D. E. S. (ed.) *Current Advances in Osteosarcoma.* Cham: Springer International Publishing.

LIU, Y., CAI, Y., HE, C., CHEN, M. & LI, H. 2017. Anti-cancer properties and pharmaceutical applications of plumbagin: A review. *The American Journal of Chinese Medicine,* 45**,** 423-441.

LIU, Y., PETERSON, D. A., KIMURA, H. & SCHUBERT, D. 1997. Mechanism of cellular 3-(4,5-dimethylthiazol-2-yl)-2,5-diphenyltetrazolium bromide (MTT) reduction. *Journal of Neurochemistry,* 69**,** 581-593.

LOPALCO, A., CUTRIGNELLI, A., DENORA, N., LOPEDOTA, A., FRANCO, M. & LAQUINTANA, V. 2018. Transferrin functionalized liposomes loading dopamine HCl: Development and permeability studies across an *in vitro* model of human blood–brain barrier. *Nanomaterials,* 8**,** 178.

LOPEZ, D. R. S. & LALATSA, A. 2013. Active Targeting. *In:* UCHEGBU, I. F., SCHÄTZLEIN, A. G., CHENG, P. W. & LALATSA, A. (eds.) *Fundamentals of Pharmaceutical Nanoscience.* New York, NY: Springer New York.

LOWRY, O. H., ROSEBROUGH, N. J., FARR, A. L. & RANDALL, R. J. 1951. Protein measurement with the Folin phenol reagent. *The Journal of Biological Chemistry,* 193**,** 265-75.

LUO, P., WONG, Y. F., GE, L., ZHANG, Z. F., LIU, Y., LIU, L. & ZHOU, H. 2010. Anti-inflammatory and analgesic effect of plumbagin through inhibition of nuclear factor-κB activation. *Journal of Pharmacology and Experimental Therapeutics,* 335**,** 735.

MACGILLIVRAY, R. T., MENDEZ, E., SINHA, S. K., SUTTON, M. R., LINEBACK-ZINS, J. & BREW, K. 1982. The complete amino acid sequence of human serum transferrin. *Proceedings of the National Academy of Sciences of the United States of America,* 79**,** 2504-2508.

MAEDA, H. 1992. The tumor blood vessel as an ideal target for macromolecular anti-cancer agents. *Journal of Controlled Release,* 19**,** 315-324.

MAEDA, H., WU, J., SAWA, T., MATSUMURA, Y. & HORI, K. 2000. Tumor vascular permeability and the EPR effect in macromolecular therapeutics: a review. *Journal of Controlled Release,* 65**,** 271-284.

MAHERANI, B., ARAB-TEHRANY, E., KHEIROLOMOOM, A., GENY, D. & LINDER, M. 2013. Calcein release behavior from liposomal bilayer; influence of physicochemical/mechanical/structural properties of lipids. *Biochimie,* 95**,** 2018-2033.

MAKADIA, H. K. & SIEGEL, S. J. 2011. Poly lactic-co-glycolic acid (PLGA) as biodegradable controlled drugd carrier. *Polymers,* 3**,** 1377-1397.

MANSILLA, S., LLOVERA, L. & PORTUGAL, J. 2012. Chemotherapeutic targeting of cell death pathways. *Anti-Cancer Agents in Medicinal Chemistry,* 12**,** 226-38.

MARASINI, N., GHAFFAR, K. A., SKWARCZYNSKI, M. & TOTH, I. 2017. Chapter twelve - Liposomes as a vaccine delivery system. *In:* SKWARCZYNSKI, M. & TOTH, I. (eds.) *Micro and Nanotechnology in Vaccine Development.* William Andrew Publishing.

MARIANECCI, C., MARZIO, L., RINALDI, F., ESPOSITO, S. & CARAFA, M. 2013. Niosomes. *In:* UCHEGBU, I. F., SCHÄTZLEIN, A. G., CHENG, P. W. & LALATSA, A. (eds.) *Fundamentals of Pharmaceutical Nanoscience.* New York, NY: Springer New York.

MATSUMURA, Y. & MAEDA, H. 1986. A New concept for macromolecular therapeutics in cancer chemotherapy: Mechanism of tumoritropic accumulation of proteins and the antitumor agent smancs. *Cancer Research,* 46**,** 6387-6392.

MEERLOO, J. V., KASPERS, G. J. L. & CLOOS, J. 2011. Cell sensitity assays: The MTT assay. *In:* CREE, I. A. (ed.) *Cancer Cell Culture: Methods and Protocols.* Totowa, NJ: Humana Press.

MELO, A. M., JARDIM, M. L., DE SANTANA, C. F., LACET, Y., LOBO FILHO, J. & DE LIMA E IVAN LEONCIO, O. G. 1974. First observations on the topical use of primin, plumbagin and maytenin in patients with skin cancer. *Revista do Instituto de Antibioticos, Universidade Federal de Pernambuco,* 14**,** 9-16.

MEZZANOTTE, L., VAN 'T ROOT, M., KARATAS, H., GOUN, E. A. & LöWIK, C. W. G. M. 2017. *In vivo* molecular bioluminescence imaging: New tools and applications. *Trends in Biotechnology,* 35**,** 640-652.

MOGHASSEMI, S. & HADJIZADEH, A. 2014. Nano-niosomes as nanoscale drug delivery systems: An illustrated review. *Journal of Controlled Release,* 185**,** 22-36.

MOGHIMI, S. M., HUNTER, A. C. & MURRAY, J. C. 2001. Long-circulating and target-specific nanoparticles: theory to practice. *Pharmacological Reviews,* 53**,** 283-318.

MORTON, C. L. & HOUGHTON, P. J. 2007. Establishment of human tumor xenografts in immunodeficient mice. *Nature Protocols,* 2**,** 247.

MÜLLER, R. H., BENITA, S. & BÖHM, B. H. L. 1998. *Emulsions and Nanosuspensions for the Formulation of Poorly Soluble Drugs*, Medpharm.

MüLLER, R. H., MÄDER, K. & GOHLA, S. 2000. Solid lipid nanoparticles (SLN) for controlled drug delivery – a review of the state of the art. *European Journal of Pharmaceutics and Biopharmaceutics,* 50**,** 161-177.

MUNOZ, J. L., RODRIGUEZ-CRUZ, V., GRECO, S. J., RAMKISSOON, S. H., LIGON, K. L. & RAMESHWAR, P. 2014. Temozolomide resistance in glioblastoma cells occurs partly through epidermal growth factor receptor-mediated induction of connexin 43. *Cell Death & Disease,* 5**,** e1145.

MUTHU, M. S., KUTTY, R. V., LUO, Z., XIE, J. & FENG, S. S. 2015. Theranostic vitamin E TPGS micelles of transferrin conjugation for targeted co-delivery of docetaxel and ultra bright gold nanoclusters. *Biomaterials,* 39**,** 234-248.

NARESH, R. A. R., UDUPA, N. & DEVI, P. U. 1996. Niosomal plumbagin with reduced toxicity and improved anti-cancer activity in BALB/c mice. *Journal of Pharmacy and Pharmacology,* 48**,** 1128-1132.

NEWMAN, D. J. & CRAGG, G. M. 2016. Natural products as sources of new drugs from 1981 to 2014. *Journal of Natural Products,* 79**,** 629-661.

NIU, M., CAI, W., LIU, H., CHONG, Y., HU, W., GAO, S., SHI, Q., ZHOU, X., LIU, X. & YU, R. 2015. Plumbagin inhibits growth of gliomas *in vivo* via suppression of FOXM1 expression. *Journal of Pharmacological Sciences,* 128**,** 131-136.

OCAÑA, A., GARCÍA-ALONSO, S., AMIR, E. & PANDIELLA, A. 2018. Refining early antitumoral drug development. *Trends in Pharmacological Sciences,* 39**,** 922-925.

OH, N. & PARK, J. H. 2014. Endocytosis and exocytosis of nanoparticles in mammalian cells. *International Journal of Nanomedicine,* 9**,** 51-63.

OLUSANYA, T. O. B., HAJ AHMAD, R. R., IBEGBU, D. M., SMITH, J. R. & ELKORDY, A. A. 2018. Liposomal drug delivery systems and anti-cancer drugs. *Molecules (Basel, Switzerland),* 23**,** 907.

OOMMEN, E., SHENOY, B. D., UDUPA, N., KAMATH, R. & DEVI, P. U. 1999. Antitumour efficacy of cyclodextrin-complexed and niosome-encapsulated plumbagin in mice bearing melanoma B16F1. *Pharmacy and Pharmacology Communications,* 5**,** 281-285.

PADHYE, S., DANDAWATE, P., YUSUFI, M., AHMAD, A. & SARKAR, F. H. 2012. Perspectives on medicinal properties of plumbagin and its analogs. *Medicinal Research Reviews,* 32**,** 1131-1158.

PAI, S. A., MUNSHI, R. P., PANCHAL, F. H., GAUR, I. S., MESTRY, S. N., GURSAHANI, M. S. & JUVEKAR, A. R. 2019. Plumbagin reduces obesity and nonalcoholic fatty liver disease induced by fructose in rats through regulation of lipid metabolism, inflammation and oxidative stress. *Biomedicine & Pharmacotherapy,* 111**,** 686-694.

PAIVA, S. R. D., FIGUEIREDO, M. R., ARAGÃO, T. V. & KAPLAN, M. A. C. 2003. Antimicrobial activity *in vitro* of plumbagin isolated from Plumbago species. *Memórias do Instituto Oswaldo Cruz,* 98**,** 959-961.

PALUMBO, M. O., KAVAN, P., MILLER, W. H., JR., PANASCI, L., ASSOULINE, S., JOHNSON, N., COHEN, V., PATENAUDE, F., POLLAK, M., JAGOE, R. T. & BATIST, G. 2013. Systemic cancer therapy: achievements and challenges that lie ahead. *Frontiers in Pharmacology,* 4**,** 1-9.

PAN, M., LI, W., YANG, J., LI, Z., ZHAO, J., XIAO, Y., XING, Y., ZHANG, X. & JU, W. 2017. Plumbagin-loaded aptamer-targeted poly d,l-lactic-co-glycolic acid-b-polyethylene glycol nanoparticles for prostate cancer therapy. *Medicine,* 96**,** e7405.

PAN, S. T., QIN, Y., ZHOU, Z. W., HE, Z. X., ZHANG, X., YANG, T., YANG, Y. X., WANG, D., QIU, J. X. & ZHOU, S. F. 2015. Plumbagin induces G(2)/M arrest, apoptosis, and autophagy via p38 MAPK- and PI3K/Akt/mTOR-mediated pathways in human tongue squamous cell carcinoma cells. *Drug Design, Development and Therapy,* 9**,** 1601-1626.

PANARITI, A., MISEROCCHI, G. & RIVOLTA, I. 2012. The effect of nanoparticle uptake on cellular behavior: disrupting or enabling functions? *Nanotechnology, Science and Applications,* 5**,** 87-100.

PANICHAYUPAKARANANT, P. & AHMAD, M. I. 2016. Plumbagin and its role in chronic diseases. *In:* GUPTA, S. C., PRASAD, S. & AGGARWAL, B. B. (eds.) *Drug Discovery from Mother Nature.* Cham, Switzerland: Springer International Publishing.

PATRAVALE, V., DANDEKAR, P. & JAIN, R. 2012. *Nanoparticulate drug delivery: perspectives on the transition from laboratory to market*, Elsevier Science.

PATTNI, B. S. & TORCHILIN, V. P. 2015. Targeted drug delivery systems: strategies and challenges. *In:* DEVARAJAN, V. P. & JAIN, S. (eds.) *Targeted Drug Delivery: Concepts and Design.* Cham: Springer International Publishing.

PAWAR, A., PATEL, R., ARULMOZHI, S. & BOTHIRAJA, C. 2016. d-α-Tocopheryl polyethylene glycol 1000 succinate conjugated folic acid nanomicelles: towards enhanced bioavailability, stability, safety, prolonged drug release and synergized anti-cancer effect of plumbagin. *RSC Advances,* 6**,** 78106-78121.

PEER, D., KARP, J. M., HONG, S., FAROKHZAD, O. C., MARGALIT, R. & LANGER, R. 2007. Nanocarriers as an emerging platform for cancer therapy. *Nature Nanotechnology,* 2**,** 751-760.

PERCHE, F. & TORCHILIN, V. P. 2013. Recent Trends in Multifunctional Liposomal Nanocarriers for Enhanced Tumor Targeting. *Journal of Drug Delivery,* 2013**,** 32.

PEYRESSATRE, M., PRÉVEL, C., PELLERANO, M. & MORRIS, M. C. 2015. Targeting cyclin-dependent kinases in human cancers: from small molecules to Peptide inhibitors. *Cancers,* 7**,** 179-237.

PONTE, J. F., SUN, X., YODER, N. C., FISHKIN, N., LALEAU, R., COCCIA, J., LANIERI, L., BOGALHAS, M., WANG, L., WILHELM, S., WIDDISON, W., PINKAS, J., KEATING, T. A., CHARI, R., ERICKSON, H. K. & LAMBERT, J. M. 2016. Understanding how the stability of the thiol-maleimide linkage impacts the pharmacokinetics of lysine-linked antibody–maytansinoid conjugates. *Bioconjugate Chemistry,* 27**,** 1588-1598.

POWOLNY, A. A. & SINGH, S. V. 2008. Plumbagin-induced apoptosis in human prostate cancer cells is associated with modulation of cellular redox status and generation of reactive oxygen species. *Pharmaceutical Research,* 25**,** 2171-2180.

PRASAD, S., GUPTA, S. C. & AGGARWAL, B. B. 2016. Serendipity in cancer drug discovery: rational or coincidence? *Trends in Pharmacological Sciences,* 37**,** 435-450.

R.S, R., K.H, S., SOMASUNDARAM, V., S, S. K., NADHAN, R., NAIR, R. S. & SRINIVAS, P. 2016. Plumbagin, a naphthaquinone derivative induces apoptosis in BRCA 1/2 defective castrate resistant prostate cancer cells as well as prostate cancer stem-like cells. *Pharmacological Research,* 105**,** 134-145.

RAGHU, D. & KARUNAGARAN, D. 2014. Plumbagin downregulates Wnt signaling independent of p53 in human colorectal cancer cells. *Journal of Natural Products,* 77**,** 1130-1134.

RAJALAKSHMI, S., VYAWAHARE, N., PAWAR, A., MAHAPARALE, P. & CHELLAMPILLAI, B. 2018. Current development in novel drug delivery systems of bioactive molecule plumbagin. *Artificial Cells, Nanomedicine, and Biotechnology***,** 1-10.

RAO, J. P. & GECKELER, K. E. 2011. Polymer nanoparticles: Preparation techniques and size-control parameters. *Progress in Polymer Science,* 36**,** 887-913.

RAVI, M., PARAMESH, V., KAVIYA, S. R., ANURADHA, E. & SOLOMON, F. D. P. 2015. 3D cell culture systems: advantages and applications. *Journal of Cellular Physiology,* 230**,** 16-26.

RAYABANDLA, S. K. M., AITHAL, K., ANANDAM, A., SHAVI, G., NAYANABHIRAMA, U., ARUMUGAM, K., MUSMADE, P., BHAT, K. & BOLA SADASHIVA, S. R. 2010. Preparation, *in vitro* characterization, pharmacokinetic, and pharmacodynamic evaluation of chitosan-based plumbagin microspheres in mice bearing B16F1 melanoma. *Drug Delivery,* 17**,** 103-113.

RICCIOTTI, E. & FITZGERALD, G. A. 2011. Prostaglandins and Inflammation. *Arteriosclerosis, Thrombosis, and Vascular Biology,* 31**,** 986-1000.

RICHMOND, A. & SU, Y. 2008. Mouse xenograft models vs GEM models for human cancer therapeutics. *Disease Models & Mechanisms,* 1**,** 78-82.

RIEGER, A. M., NELSON, K. L., KONOWALCHUK, J. D. & BARREDA, D. R. 2011. Modified annexin V/propidium iodide apoptosis assay for accurate assessment of cell death. *Journal of Visualized Experiments: JoVE***,** 2597.

ROBERTS, P. J. & DER, C. J. 2007. Targeting the Raf-MEK-ERK mitogen-activated protein kinase cascade for the treatment of cancer. *Oncogene,* 26**,** 3291-3310.

RONDEVALDOVA, J., NOVY, P. & KOKOSKA, L. 2015. *In vitro* combinatory antimicrobial effect of plumbagin with oxacillin and tetracycline against *Staphylococcus aureus*. *Phytotherapy Research,* 29**,** 144-147.

ROSALES, C. & URIBE, Q. E. 2017. Phagocytosis: a fundamental process in immunity. *BioMed Research International,* 2017**,** 9042851-9042851.

RUGGERI, B. A., CAMP, F. & MIKNYOCZKI, S. 2014. Animal models of disease: pre-clinical animal models of cancer and their applications and utility in drug discovery. *Biochemical Pharmacology,* 87**,** 150-161.

SADIKOT, R. T. & BLACKWELL, T. S. 2005. Bioluminescence imaging. *Proceedings of the American Thoracic Society,* 2**,** 537-512.

SAHAY, G., ALAKHOVA, D. Y. & KABANOV, A. V. 2010. Endocytosis of nanomedicines. *Journal of Controlled Release,* 145**,** 182-195.

SAHIN, N. O. 2007. Niosomes as nanocarrier systems. *In:* MOZAFARI, M. R. (ed.) *Nanomaterials and Nanosystems for Biomedical Applications.* Dordrecht: Springer Netherlands.

SAHOO, S. K. & LABHASETWAR, V. 2005. Enhanced antiproliferative activity of transferrin-conjugated paclitaxel-loaded nanoparticles is mediated via sustained intracellular drug retention. *Molecular Pharmaceutics,* 2**,** 373-383.

SANDUR, S. K., ICHIKAWA, H., SETHI, G., AHN, K. S. & AGGARWAL, B. B. 2006. Plumbagin (5-hydroxy-2-methyl-1,4-naphthoquinone) suppresses NF-kappaB activation and NF-kappaB-regulated gene products through modulation of p65 and IkappaBalpha kinase activation, leading to potentiation of apoptosis induced by cytokine and chemotherapeutic agents. *Journal of Biological Chemistry,* 281**,** 17023-33.

SANTHAKUMARI, G., SARALAMMA, P. G. & RADHAKRISHNAN, N. 1980. Effect of plumbagin on cell growth & mitosis. *Indian Journal of Experimental Biology,* 18**,** 215-8.

SARALAMP, P., CHUAKUL, W., TEMSIRIRIRLKUL, R. & CLAYTON, T. 1996. *Medicinal plant in Thailand volume I,* Bangkok, Thailand., Department of Pharmaceutical Botany, Faculty of Pharmacy, Mahidol University.

SATO, A., KLAUNBERG, B. & TOLWANI, R. 2004. *In vivo* bioluminescence imaging. *Comparative Medicine,* 54**,** 631-634.

SCHÄTZLEIN, A. G. 2003. Targeting of synthetic gene delivery systems. *Journal of Biomedicine and Biotechnology,* 2003**,** 149-158.

SCHNITZER, J. E., OH, P., PINNEY, E. & ALLARD, J. 1994. Filipin-sensitive caveolae-mediated transport in endothelium: reduced transcytosis, scavenger endocytosis, and capillary permeability of select macromolecules. *The Journal of Cell Biology,* 127**,** 1217-1232.

SCHRÖR, K. 2009. *Acetylsalicylic acid*, Weinheim: Wiley-VCH; Chichester: John Wiley, distributor.

SCHWARTSMANN, G., DA ROCHA, A. B., BERLINCK, R. G. S. & JIMENO, J. 2001. Marine organisms as a source of new anti-cancer agents. *The Lancet Oncology,* 2**,** 221-225.

ŠEBESTíK, J., REINIŠ, M. & JEŽEK, J. 2012. Dendrimers in drug delivery. *Biomedical Applications of Peptide-, Glyco- and Glycopeptide Dendrimers, and Analogous Dendrimeric Structures.* Vienna: Springer Vienna.

SECA, A. M. L. & PINTO, D. C. G. A. 2018. Plant secondary metabolites as anti-cancer agents: successes in clinical trials and therapeutic application. *International Journal of Molecular Sciences,* 19**,** 263.

SENAPATI, S., MAHANTA, A. K., KUMAR, S. & MAITI, P. 2018. Controlled drug delivery vehicles for cancer treatment and their performance. *Signal Transduction and Targeted Therapy,* 3**,** 7.

SESHADRI, P., RAJARAM, A. & RAJARAM, R. 2011. Plumbagin and juglone induce caspase-3-dependent apoptosis involving the mitochondria through ROS generation in human peripheral blood lymphocytes. *Free Radical Biology and Medicine,* 51**,** 2090-2107.

SHAKER, D. S., SHAKER, M. A. & HANAFY, M. S. 2015. Cellular uptake, cytotoxicity and *in vivo* evaluation of tamoxifen citrate loaded niosomes. *International Journal of Pharmaceutics,* 493**,** 285-294.

SHANNON, A. M., BOUCHIER-HAYES, D. J., CONDRON, C. M. & TOOMEY, D. 2003. Tumour hypoxia, chemotherapeutic resistance and hypoxia-related therapies. *Cancer Treatment Reviews,* 29**,** 297-307.

SHARIAT, S., BADIEE, A., JAAFARI, M. R. & MORTAZAVI, S. A. 2014. Optimization of a method to prepare liposomes containing HER2/Neu- derived peptide as a vaccine delivery system for breast cancer. *Iranian Journal of Pharmaceutical Research: IJPR,* 13**,** 15-25.

SHARMA, S., PARMAR, A., KORI, S. & SANDHIR, R. 2016. PLGA-based nanoparticles: a new paradigm in biomedical applications. *TrAC Trends in Analytical Chemistry,* 80**,** 30-40.

SHAW, R. J. 2009. LKB1 and AMPK control of mTOR signalling and growth. *Acta Physiologica (Oxford, England),* 196**,** 65-80.

SHIH, Y. W., LEE, Y. C., WU, P. F., LEE, Y. B. & CHIANG, T. A. 2009. Plumbagin inhibits invasion and migration of liver cancer HepG2 cells by decreasing productions of matrix metalloproteinase-2 and urokinase- plasminogen activator. *Hepatology Research,* 39**,** 998-1009.

SHIMADA, H., YAMAOKA, Y., MORITA, R., MIZUNO, T., GOTOH, K., HIGUCHI, T., SHIRAISHI, T. & IMAMURA, Y. 2012. Possible mechanism of superoxide formation through redox cycling of plumbagin in pig heart. *Toxicology in Vitro,* 26**,** 252-257.

SIMON, L. C., STOUT, R. W. & SABLIOV, C. 2016. Bioavailability of orally delivered alpha-tocopherol by poly(lactic-co-glycolic) acid (PLGA) nanoparticles and chitosan covered PLGA nanoparticles in F344 rats. *Nanobiomedicine,* 3**,** 8-8.

SINGH, J., JAIN, K., MEHRA, N. K. & JAIN, N. K. 2016. Dendrimers in anticancer drug delivery: mechanism of interaction of drug and dendrimers. *Artificial Cells, Nanomedicine, and Biotechnology*, 44, 1626-34.

SINGH, U. V., BISHT, K. S., RAO, S., DEVI, P. U. & UDUPA, N. 1996. Plumbagin-loaded PLGA microspheres with reduced toxicity and enhanced antitumour efficacy in mice. *Pharmacy and Pharmacology Communications,* 2**,** 407-409.

SINHA, S., PAL, K., ELKHANANY, A., DUTTA, S., CAO, Y., MONDAL, G., IYER, S., SOMASUNDARAM, V., COUCH, F. J., SHRIDHAR, V., BHATTACHARYA, R., MUKHOPADHYAY, D. & SRINIVAS, P. 2013. Plumbagin inhibits tumorigenesis and angiogenesis of ovarian cancer cells *in vivo*. *International Journal of Cancer,* 132**,** 1201-1212.

SLINGERLAND, M., GUCHELAAR, H.J. & GELDERBLOM, H. 2012. Liposomal drug formulations in cancer therapy: 15 years along the road. *Drug Discovery Today,* 17**,** 160-166.

SOLOMON, R. & GABIZON, A. A. 2008. Clinical pharmacology of liposomal anthracyclines: focus on PEGylated liposomal doxorubicin. *Clinical Lymphoma and Myeloma,* 8**,** 21-32.

SOMASUNDARAM, V., HEMALATHA, S. K., PAL, K., SINHA, S., NAIR, A. S., MUKHOPADHYAY, D. & SRINIVAS, P. 2016. Selective mode of action of plumbagin through BRCA1 deficient breast cancer stem cells. *BMC cancer,* 16**,** 336-336.

SOUTO, E. B., FANGUEIRO, J. F. & MüLLER, R. H. 2013. Solid lipid nanoparticles (SLN™). *In:* UCHEGBU, I. F., SCHÄTZLEIN, A. G., CHENG, P. W. & LALATSA, A. (eds.) *Fundamentals of Pharmaceutical Nanoscience.* New York, NY: Springer New York.

SRINIVAS, G., ANNAB, L. A., GOPINATH, G., BANERJI, A. & SRINIVAS, P. 2004a. Antisense blocking of BRCA1 enhances sensitivity to plumbagin but not tamoxifen in BG-1 ovarian cancer cells. *Molecular Carcinogenesis,* 39**,** 15-25.

SRINIVAS, P., GOPINATH, G., BANERJI, A., DINAKAR, A. & SRINIVAS, G. 2004b. Plumbagin induces reactive oxygen species, which mediate apoptosis in human cervical cancer cells. *Molecular Carcinogenesis,* 40**,** 201-211.

SRINIVAS, P., PATRA, C. R., BHATTACHARYA, S. & MUKHOPADHYAY, D. 2011. Cytotoxicity of naphthoquinones and their capacity to generate reactive oxygen species is quenched when conjugated with gold nanoparticles. *International Journal of Nanomedicine,* 6**,** 2113-2122.

SRIRAMAN, S. K., ARYASOMAYAJULA, B. & TORCHILIN, V. P. 2014. Barriers to drug delivery in solid tumors. *Tissue Barriers,* 2**,** e29528.

STENZEL, M. H. 2013. Bioconjugation using thiols: old chemistry rediscovered to connect polymers with nature's building blocks. *ACS Macro Letters,* 2**,** 14-18.

STOCKERT, J. C., BLÁZQUEZ-CASTRO, A., CAÑETE, M., HOROBIN, R. W. & VILLANUEVA, Á. 2012. MTT assay for cell viability: intracellular localization of the formazan product is in lipid droplets. *Acta Histochemica,* 114**,** 785-796.

STREBHARDT, K. & ULLRICH, A. 2008. Paul Ehrlich's magic bullet concept: 100 years of progress. *Nature Reviews Cancer,* 8**,** 473-480.

SUBRAMANIYA, B. R., SRINIVASAN, G., SADULLAH, S. S. M., DAVIS, N., SUBHADARA, L. B. R., HALAGOWDER, D. & SIVASITAMBARAM, N. D. 2011. Apoptosis inducing effect of plumbagin on colonic cancer cells depends on expression of COX-2. *PloS One,* 6**,** e18695-e18695.

SUKKASEM, N., CHATUPHONPRASERT, W., TATIYA-APHIRADEE, N. & JARUKAMJORN, K. 2016. Imbalance of the antioxidative system by plumbagin and *Plumbago indica* L. extract induces hepatotoxicity in mice. *Journal of Intercultural Ethnopharmacology,* 5**,** 137-145.

SUMSAKUL, W. & NA-BANGCHANG, K. 2016. Permeability of plumbagin across human intestinal cell *in vitro. Archives of Pharmacal Research,* 39**,** 380-389.

SUMSAKUL, W., PLENGSURIYAKARN, T., CHAIJAROENKUL, W., VIYANANT, V., KARBWANG, J. & NA-BANGCHANG, K. 2014. Antimalarial activity of plumbagin *in vitro* and in animal models. *BMC Complementary and Alternative Medicine,* 14**,** 15.

SUMSAKUL, W., PLENGSURIYAKARN, T. & NA-BANGCHANG, K. 2016. Pharmacokinetics, toxicity, and cytochrome P450 modulatory activity of plumbagin. *BMC Pharmacology & Toxicology,* 17**,** 50.

SUN, T., ZHANG, Y. S., PANG, B., HYUN, D. C., YANG, M. & XIA, Y. 2014. Engineered nanoparticles for drug delivery in cancer therapy. *Angewandte Chemie International Edition,* 53**,** 12320-64.

SUN, Y. & SUN, Z. L. 2016. Transferrin-conjugated polymeric nanomedicine to enhance the anti-cancer efficacy of edelfosine in acute myeloid leukemia. *Biomedicine & Pharmacotherapy,* 83**,** 51-57.

SUZUKI, R., TAKIZAWA, T., KUWATA, Y., MUTOH, M., ISHIGURO, N., UTOGUCHI, N., SHINOHARA, A., ERIGUCHI, M., YANAGIE, H. & MARUYAMA, K. 2008. Effective anti-tumor activity of oxaliplatin encapsulated in transferrin–PEG-liposome. *International Journal of Pharmaceutics,* 346**,** 143-150.

TAKIMOTO, C. H. & WICK, M. J. 2012. Non-Clinical Drug Development. *In:* ATKINSON, A. J., HUANG, S.-M., LERTORA, J. J. L. & MARKEY, S. P. (eds.) *Principles of Clinical Pharmacology (Third Edition).* London: Academic Press.

TAMJIDI, F., SHAHEDI, M., VARSHOSAZ, J. & NASIRPOUR, A. 2013. Nanostructured lipid carriers (NLC): A potential delivery system for bioactive food molecules. *Innovative Food Science & Emerging Technologies,* 19**,** 29-43.

THANKI, K., KUSHWAH, V. & JAIN, S. 2015. Recent Advances in Tumor Targeting Approaches. *In:* DEVARAJAN, V. P. & JAIN, S. (eds.) *Targeted Drug Delivery: Concepts and Design.* Cham: Springer International Publishing.

THORN, C. F., OSHIRO, C., MARSH, S., HERNANDEZ-BOUSSARD, T., MCLEOD, H., KLEIN, T. E. & ALTMAN, R. B. 2011. Doxorubicin pathways: pharmacodynamics and adverse effects. *Pharmacogenetics and Genomics,* 21**,** 440-446.

TIWARI, S. B., PAI, R. M. & UDUPA, N. 2002. Temperature sensitive liposomes of plumbagin: characterization and *in vivo* evaluation in mice bearing melanoma B16F1. *Journal of Drug Targeting*, 10, 585-91.

TORCHILIN, V. P. 2006. *Nanoparticulates as Drug Carriers*, Imperial College Press.

TORCHILIN, V. P. 2010. Passive and active drug targeting: drug delivery to tumors as an example. *In:* SCHÄFER-KORTING, M. (ed.) *Drug Delivery.* Berlin, Heidelberg: Springer Berlin Heidelberg.

TORTORELLA, S. & KARAGIANNIS, T. C. 2014. Transferrin receptor-mediated endocytosis: a useful target for cancer therapy. *The Journal of Membrane Biology,* 247**,** 291-307.

TOY, R., PEIRIS, P. M., GHAGHADA, K. B. & KARATHANASIS, E. 2014. Shaping cancer nanomedicine: The effect of particle shape on the *in vivo* journey of nanoparticles. *Nanomedicine (London, England),* 9**,** 121-134.

TOZER, G. M., KANTHOU, C. & BAGULEY, B. C. 2005. Disrupting tumour blood vessels. *Nature Reviews Cancer,* 5**,** 423-435.

TSAI, M. J., CHANG, W. A., HUANG, M. S. & KUO, P. L. 2014. Tumor microenvironment: a new treatment target for cancer. *ISRN Biochemistry,* 2014**,** 1-9.

TSERMENTSELI, S., KONTOGIANNOPOULOS, K., PAPAGEORGIOU, V. & ASSIMOPOULOU, A. 2018. Comparative study of PEGylated and conventional liposomes as carriers for shikonin. *Fluids,* 3**,** 36.

UCHEGBU, I. F., DOUBLE, J. A., KELLAND, L. R., TURTON, J. A. & FLORENCE, A. T. 1996. The activity of doxorubicin niosomes against an ovarian cancer cell line and three in vivo mouse tumour models. *Journal of Drug Targeting,* 3**,** 399-409.

UCHEGBU, I. F., LALATSA, A. & WONG, D. 2013. Polymeric nanoparticles. *In:* UCHEGBU, I. F., SCHÄTZLEIN, A. G., CHENG, P. W. & LALATSA, A. (eds.) *Fundamentals of Pharmaceutical Nanoscience.* New York, NY: Springer New York.

UCHEGBU, I. F. & VYAS, S. P. 1998. Non-ionic surfactant based vesicles (niosomes) in drug delivery. *International Journal of Pharmaceutics,* 172**,** 33-70.

VASCONCELOS, A., VEGA, E., PéREZ, Y., GóMARA, M. J., GARCíA, M. L. & HARO, I. 2015. Conjugation of cell-penetrating peptides with poly(lactic-co-glycolic acid)-polyethylene glycol nanoparticles improves ocular drug delivery. *International Journal of Nanomedicine,* 10**,** 609-631.

VASUDEVAN, K. M., GURUMURTHY, S. & RANGNEKAR, V. M. 2004. Suppression of PTEN expression by NF-kappa B prevents apoptosis. *Molecular and cellular biology,* 24**,** 1007-1021.

VASUDEVARAO, M. D., MIZAR, P., KUMARI, S., MANDAL, S., SIDDHANTA, S., SWAMY, M. M. M., KAYPEE, S., KODIHALLI, R. C., BANERJEE, A., NARYANA, C., DASGUPTA, D. & KUNDU, T. K. 2014. Naphthoquinone-mediated inhibition of lysine acetyltransferase KAT3B/p300, basis for non-toxic inhibitor synthesis. *The Journal of Biological Chemistry,* 289**,** 7702-7717.

VENTOLA, C. L. 2017. Progress in Nanomedicine: Approved and Investigational Nanodrugs. *P & T: A Peer-Reviewed Journal for Formulary Management,* 42**,** 742-755.

VIDEIRA, M., ALMEIDA, A. J. & FABRA, À. 2012. Preclinical evaluation of a pulmonary delivered paclitaxel-loaded lipid nanocarrier antitumor effect. *Nanomedicine: Nanotechnology, Biology and Medicine,* 8**,** 1208-1215.

VIJAYAKUMAR, R., SENTHILVELAN, M., RAVINDRAN, R. & DEVI, R. S. 2006. *Plumbago zeylanica* action on blood coagulation profile with and without blood volume reduction. *Vascular Pharmacology,* 45**,** 86-90.

WAKASKAR, R. R. 2018. General overview of lipid–polymer hybrid nanoparticles, dendrimers, micelles, liposomes, spongosomes and cubosomes. *Journal of Drug Targeting,* 26**,** 311-318.

WANG, C. C. C., CHIANG, Y. M., SUNG, S. C., HSU, Y. L., CHANG, J. K. & KUO, P. L. 2008. Plumbagin induces cell cycle arrest and apoptosis through reactive oxygen species/c-Jun N-terminal kinase pathways in human melanoma A375.S2 cells. *Cancer Letters,* 259**,** 82-98.

WANG, F., WANG, Q., ZHOU, Z. W., YU, S. N., PAN, S. T., HE, Z. X., ZHANG, X., WANG, D., YANG, Y. X., YANG, T., SUN, T., LI, M., QIU, J. X. & ZHOU, S. F. 2015. Plumbagin induces cell cycle arrest and autophagy and suppresses epithelial to mesenchymal transition involving PI3K/Akt/mTOR-mediated pathway in human pancreatic cancer cells. *Drug Design, Development and Therapy,* 9**,** 537-560.

WANG, H. F., RAN, R., LIU, Y., HUI, Y., ZENG, B., CHEN, D., WEITZ, D. A. & ZHAO, C. X. 2018. Tumor-vasculature-on-a-chip for investigating nanoparticle extravasation and tumor accumulation. *ACS Nano,* 12**,** 11600-11609.

WANG, R., BILLONE, P. S. & MULLETT, W. M. 2013. Nanomedicine in action: an overview of cancer nanomedicine on the market and in clinical trials. *Journal of Nanomaterials,* 2013**,** 1-12.

WANG, S. X., WANG, J., SHAO, J. B., TANG, W. N. & ZHONG, J. Q. 2016. Plumbagin mediates cardioprotection against myocardial ischemia/reperfusion injury through Nrf-2 signaling. *Medical science monitor: International Medical Journal of Experimental and Clinical Research,* 22**,** 1250-1257.

WEI, Y., HUANG, M., LIU, X., YUAN, Z., PENG, Y., HUANG, Z., DUAN, X. & ZHAO, T. 2015. Anti-fibrotic effect of plumbagin on CCl_4-lesioned rats. *Cellular Physiology and Biochemistry,* 35**,** 1599-1608.

WEI, Y., YANG, Q., ZHANG, Y., ZHAO, T., LIU, X., ZHONG, J., MA, J., CHEN, Y., ZHAO, C. & LI, J. 2017. Plumbagin restrains hepatocellular carcinoma angiogenesis by suppressing the migration and invasion of tumor-derived vascular endothelial cells. *Oncotarget,* 8**,** 15230-15241.

WEISSIG, V., PETTINGER, T. K. & MURDOCK, N. 2014. Nanopharmaceuticals (part 1): products on the market. *International Journal of Nanomedicine,* 9**,** 4357-4373.

WICKI, A., WITZIGMANN, D., BALASUBRAMANIAN, V. & HUWYLER, J. 2015. Nanomedicine in cancer therapy: Challenges, opportunities, and clinical applications. *Journal of Controlled Release,* 200**,** 138-157.

WIDHALM, J. R. & RHODES, D. 2016. Biosynthesis and molecular actions of specialized 1,4-naphthoquinone natural products produced by horticultural plants. *Horticulture Research*, 3, 16046.

WISSING, S. A., KAYSER, O. & MüLLER, R. H. 2004. Solid lipid nanoparticles for parenteral drug delivery. *Advanced Drug Delivery Reviews,* 56**,** 1257-1272.

XIANG, S., TONG, H., SHI, Q., FERNANDES, J. C., JIN, T., DAI, K. & ZHANG, X. 2012. Uptake mechanisms of non-viral gene delivery. *Journal of Controlled Release,* 158**,** 371-378.

XU, B., XIA, S., WANG, F., JIN, Q., YU, T., HE, L., CHEN, Y., LIU, Y., LI, S., TAN, X., REN, K., YAO, S., ZENG, J. & SONG, X. 2016. Polymeric nanomedicine for combined gene/chemotherapy elicits enhanced tumor suppression. *Molecular Pharmaceutics,* 13**,** 663-676.

XUE, Y. L., MENG, X. Q., MA, L. J. & YUAN, Z. 2016. Plumbagin exhibits an anti-proliferative effect in human osteosarcoma cells by downregulating FHL2 and interfering with Wnt/β-catenin signalling. *Oncology letters,* 12**,** 1095-1100.

YAMEEN, B., CHOI, W. I., VILOS, C., SWAMI, A., SHI, J. & FAROKHZAD, O. C. 2014. Insight into nanoparticle cellular uptake and intracellular targeting. *Journal of Controlled Release,* 190**,** 485-499.

YAN, C. H., LI, F. & MA, Y. C. 2015. Plumbagin shows anti-cancer activity in human osteosarcoma (MG-63) cells via the inhibition of S-Phase checkpoints and down-regulation of c-myc. *International Journal of Clinical and Experimental Medicine,* 8**,** 14432-14439.

YAN, W., TU, B., LIU, Y. Y., WANG, T. Y., QIAO, H., ZHAI, Z. J., LI, H. W. & TANG, T. T. 2013. Suppressive effects of plumbagin on invasion and migration of breast cancer cells via the inhibition of STAT3 signaling and down-regulation of inflammatory cytokine expressions. *Bone Research,* 1**,** 362-70.

YEO, Y. 2013. *Nanoparticulate Drug Delivery Systems: Strategies, Technologies, and Applications*, Hoboken, New Jersey, John Wiley & Sons, Inc.

YU, T., XU, Y. Y., ZHANG, Y. Y., LI, K. Y., SHAO, Y. & LIU, G. 2018. Plumbagin suppresses the human large cell lung cancer cell lines by inhibiting IL-6/STAT3 signaling *in vitro. International Immunopharmacology,* 55**,** 290-296.

YUAN, F., DELLIAN, M., FUKUMURA, D., LEUNIG, M., BERK, D. A., TORCHILIN, V. P. & JAIN, R. K. 1995. Vascular permeability in a human tumor xenograft: molecular size dependence and cutoff size. *Cancer Research,* 55**,** 3752-6.

YUAN, M., QIU, Y., ZHANG, L., GAO, H. & HE, Q. 2016. Targeted delivery of transferrin and TAT co-modified liposomes encapsulating both paclitaxel and doxorubicin for melanoma. *Drug Delivery,* 23**,** 1171-1183.

ZHAI, G., WU, J., YU, B., GUO, C., YANG, X. & LEE, R. J. 2010. A transferrin receptor-targeted liposomal formulation for docetaxel. *Journal of Nanoscience and Nanotechnology,* 10**,** 5129-36.

ZHAN, X., TRAN, K. K. & SHEN, H. 2012. Effect of the poly(ethylene glycol) (PEG) density on the access and uptake of particles by antigen-presenting cells (APCs) after subcutaneous administration. *Molecular Pharmaceutics,* 9**,** 3442-3451.

ZHANG, K., TANG, X., ZHANG, J., LU, W., LIN, X., ZHANG, Y., TIAN, B., YANG, H. & HE, H. 2014. PEG–PLGA copolymers: Their structure and structure-influenced drug delivery applications. *Journal of Controlled Release,* 183**,** 77-86.

ZHANG, L., CHAN, J. M., GU, F. X., RHEE, J.W., WANG, A. Z., RADOVIC-MORENO, A. F., ALEXIS, F., LANGER, R. & FAROKHZAD, O. C. 2008. Self-assembled lipid−polymer hybrid nanoparticles: a robust drug delivery platform. *ACS Nano,* 2**,** 1696-1702.

ZHANG, L., FENG, Q., WANG, J., ZHANG, S., DING, B., WEI, Y., DONG, M., RYU, J. Y., YOON, T. Y., SHI, X., SUN, J. & JIANG, X. 2015a. Microfluidic synthesis of hybrid nanoparticles with controlled lipid layers: understanding flexibility-regulated cell–nanoparticle interaction. *ACS Nano,* 9**,** 9912-9921.

ZHANG, P., HU, L., YIN, Q., ZHANG, Z., FENG, L. & LI, Y. 2012. Transferrin-conjugated polyphosphoester hybrid micelle loading paclitaxel for brain-targeting delivery: Synthesis, preparation and *in vivo* evaluation. *Journal of Controlled Release,* 159**,** 429-434.

ZHANG, S., TANG, C. & YIN, C. 2015b. Effects of poly(ethylene glycol) grafting density on the tumor targeting efficacy of nanoparticles with ligand modification. *Drug Delivery,* 22**,** 182-190.

ZHANG, Y., CHEN, X., GUEYDAN, C. & HAN, J. 2018. Plasma membrane changes during programmed cell deaths. *Cell Research,* 28**,** 9-21.

ZHANG, Y., ZHANG, P. & ZHU, T. 2019. Ovarian carcinoma biological nanotherapy: Comparison of the advantages and drawbacks of lipid, polymeric, and hybrid nanoparticles for cisplatin delivery. *Biomedicine & Pharmacotherapy,* 109**,** 475-483.

ZHAO, C., LIU, X., LIU, J., YANG, Z., RONG, X., LI, M., LIANG, X. & WU, Y. 2014. Transferrin conjugated poly (γ-glutamic acid-maleimide-co-l-lactide)-1,2-dipalmitoylsn-glycero-3-phosphoethanolamine copolymer nanoparticles for targeting drug delivery. *Colloids and Surfaces B: Biointerfaces*, 123, 787-796.

ZHAO, N., WOODLE, M. C. & MIXSON, A. J. 2018. Advances in delivery systems for doxorubicin. *Journal of Nanomedicine & Nanotechnology,* 9**,** 519.

ZHENG, Y., YU, B., WEECHARANGSAN, W., PIAO, L., DARBY, M., MAO, Y., KOYNOVA, R., YANG, X., LI, H., XU, S., LEE, L. J., SUGIMOTO, Y., BRUEGGEMEIER, R. W. & LEE, R. J. 2010. Transferrin-conjugated lipid-coated PLGA nanoparticles for targeted delivery of aromatase inhibitor 7α-APTADD to breast cancer cells. *International Journal of Pharmaceutics,* 390**,** 234-241.

ZHOU, Z. W., LI, X. X., HE, Z. X., PAN, S. T., YANG, Y., ZHANG, X., CHOW, K., YANG, T., QIU, J. X., ZHOU, Q., TAN, J., WANG, D. & ZHOU, S. F. 2015. Induction of apoptosis and autophagy via sirtuin1- and PI3K/Akt/mTOR-mediated pathways by plumbagin in human prostate cancer cells. *Drug Design, Development and Therapy,* 9**,** 1511-1554.

ZIMMERMANN, K. C., BONZON, C. & GREEN, D. R. 2001. The machinery of programmed cell death. *Pharmacology & Therapeutics,* 92**,** 57-70.

Appendix I: List of Publications

1. Sakpakdeejaroen, I., Somani, S., Laskar, P., Mullin, M., and Dufès, C. 2019. Transferrin-targeted liposomes entrapping plumbagin for cancer therapy (in press Journal of Interdisciplinary Nanomedicine, DOI: 10.1002/jin2.56).

2. Sakpakdeejaroen, I., Somani, S., Laskar, P., Mullin, M., and Dufès, C. Tumor regression after intravenous administration of plumbagin entrapped in transferrin-conjugated, lipid–polymer hybrid nanoparticles (submitted for publication).

3. Sakpakdeejaroen, I., Somani, S., Laskar, P., Irving, C., Mullin, M., and Dufès, C. Development of transferrin-targeted poly(lactide-co-glycolide)-block-poly(ethylene glycol) nanoparticles entrapping plumbagin for cancer therapy (submitted for publication).

4. Sakpakdeejaroen, I., Somani, S., Mullin, M., and Dufès, C. 2019. Development of transferrin-bearing vesicles encapsulating aspirin for cancer therapy (in press in Journal of Liposome Research, DOI: 10.1080/08982104.2019.1614054).

Appendix II: Conference Abstracts

1. <u>Sakpakdeejaroen, I.</u>, Somani, S., and Dufès, C. Development of transferrin-bearing vesicles entrapping plumbagin for cancer therapy. 11th European and Global Summit for Clinical Nanomedicine, Targeted Delivery Precision Medicine - The Building Blocks to Personalized Medicine, Basel, Switzerland (September 2-5, 2018), Poster presentation.

2. <u>Sakpakdeejaroen, I.</u>, Somani, S., and Dufès, C. Development of plumbagin-loaded transferrin-conjugated lipid-coated polymeric nanoparticles for tumour-targeted delivery. The Conference of the Faculty of Medicine, Thammasat University, Pathumthani, Thailand (July 16-18, 2018), Poster presentation.

Others

1. Best poster presentation award, The Conference of the Faculty of Medicine, Thammasat University, Thailand, July 2018.

2. University of Strathclyde postgraduate travel award for poster presentation to attend European Foundation for Clinical Nanomedicine conference and exhibition 2018, Basel, Switzerland.